Carbon Dioxide Corrosion

Modelling and Experimental Work Applied to Natural Gas Pipelines

Philip Loldrup Fosbøl
2008

Carbon Dioxide Corrosion:
Modelling and Experimental Work
Applied to Natural Gas Pipelines

Philip Loldrup Fosbøl

Ph.D. Thesis

2008

IVC-SEP
Department of Chemical Engineering
Technical University of Denmark
DK-2800 Kongens Lyngby
Denmark

Front cover by Philip L. Fosbøl: Severe CO_2 attacked pipeline.
Handed in October 2007.
Defended at DTU building 101 room 1, 12th of February 2008 at 13:00.
Corrections and additions included in the manuscript after the defence.

Preface

This thesis is published as a partial fulfilment of the requirements for the Ph.D. degree at the Technical University of Denmark (DTU). The work was carried out in the research group IVC-SEP at the Department of Chemical Engineering under supervision of Kaj Thomsen and Erling H. Stenby. The project was started February 2004 and ended October 2007, interrupted by a two month leave for another project during 2006.

I would like to thank Erling H. Stenby for making this project possible, mainly the industrial contact, but also for the suggestions and comments during the years.

Especially Kaj Thomsen has helped me in all aspects of the theory and experimental work. I am grateful to the theory, database, programs, and library he has developed over the years. It is a core part of this project. Thank you for being patient and letting me have my own opinions. I look back at our fruitful discussions and hope to have even more in the future.

I acknowledge gratefully that Mærsk Oil and Gas A/S let me use their production data and internal knowledge unrestricted, but also the communication to the company through Kim Rasmussen and Steffen Fredberg Hansen.

I appreciate the weeks Hans Wesselingh stayed at DTU for teaching, where he introduced me to the Maxwell and Stefan diffusion theory. I recognise the importance of the few discussions Heinz Gamsjäger and I had during ISSP on *FeCO$_3$* and related solubility experiments.

In the IVC-SEP group I would like to thank the technical personal for helping me set up the equipment and sort out the difficulties, but also the four students who performed some of the experiments. I am very happy for the time that I spend with the colleagues in IVC-SEP and for the social part, let it continue.

I am thankful to Martin P. Breil and Kaj Thomsen who proof read parts of the thesis. Thank you Jan Kamyno Rasmussen for giving me useful guidance and support during the last months of writing. I am glad that all my friends and family understood the problems that I had. Last but not least I owe it to you Marie. Hanging in there, even in the most difficult times.

Hopefully this work will be used in the corrosion related research institutions at IFE and the Ohio University or any other scientific research group out there.

_____

Philip Loldrup Fosbøl,
Kongens Lyngby, October 2007

Summary

CO_2 corrosion is a general problem in the industry and it is expensive. The focus of this study is an oil gas production related problem. CO_2 corrosion is observed in offshore natural gas transportation pipelines. A general overview of the problem is presented in chapter 1. The chemical system consists mainly of CO_2-Na_2CO_3-$NaHCO_3$-MEG-H_2O. Sodium is injected in the pipelines as $NaOH$ in order to pH-stabilize the pipeline to avoid corrosion and MEG is injected in order to prevent gas hydrates.

There are a great number of models available in the literature which may predict CO_2 corrosion. These models are not very accurate and assume ideality in the main part of the equations. This thesis deals with aspect of improving the models to account for the non-ideality.

A general overview and extension of the theory behind electrochemical corrosion is presented in chapter 2 to 4. The theory deals with the basic thermodynamics of electrolytes in chapter 2, the general description and extension of electrolyte mass transport in chapter 3, and the electrochemical kinetics of corrosion in chapter 4. A literature overview of CO_2 corrosion is shown in chapter 5 and possible extensions of the models are discussed. A list of literature cited is given in chapter 6.

The literature review in chapter 5 shows how $FeCO_3$ plays a main part in the protection of steel. Especially the solubility of $FeCO_3$ is an important factor. Chapter 7 discusses and validates the thermodynamic properties of $FeCO_3$. The study shows that there is a discrepancy in the properties of $FeCO_3$. Sets of consistent thermodynamic properties of $FeCO_3$ are given.

A mixed solvent electrolyte model is regressed in chapter 8 for the CO_2-Na_2CO_3-$NaHCO_3$-MEG-H_2O system. Parameters of the extended UNIQUAC model is fitted to literature data of VLE, SLE, heat excess, and validated against heat capacity data. The model is also fitted to experimental data produced and shown in chapter 8 for SLE in the Na_2CO_3-$NaHCO_3$-MEG-H_2O system.

The application of the above model is shown in chapter 9. Here the thermodynamic correction factors are calculated. These show how the diffusion process in CO_2 corrosion models deviate from the ideal case. Conclusion and suggestion for future work are presented in chapter 10 and 11.

Resumé på Dansk

CO_2 korrosion er et udbredt og dyrt problem for industrien. I dette arbejde sættes fokus på et olie og gas relateret produktionsproblem, som findes i offshore naturgasrør. Problemet præsenteres kort i kapitel 1. Det kemiske system består af CO_2-Na_2CO_3-$NaHCO_3$-MEG-H_2O og natrium indføres i rørledningerne i form af $NaOH$ for a pH-stabilisere og på den måde forhindre korrosion. MEG tilføres for at undgå gashydratdannelse. I litteraturen findes et stort antal modeller som kan forudsige CO_2 korrosion. De er dog ikke præcise og idealitet er antaget i store dele af modellerne. Kapitlerne i denne tese gennemgår hvordan teorien og de eksisterende modeller kan forbedres for at kunne håndtere ikke-idealiteten i gas og væske fasen. Et overblik og en udvidelse af teorien bag elektrokemisk korrosion præsenteres i kapitel 2 til 4. Teorien for elektrolytters termodynamik præsenteres i kapitel 2, en udvidelse af teorien for elektrolytisk masse transport præsenteres i kapitel 3 og udvidelsen af elektrokemisk kinetik præsenteres i kapitel 4. Et resume over CO_2 relateret korrosions litteratur præsenteres i kapitel 5 og det diskuteres hvordan modeller kan forbedres. De anvendte referencer er givet i kapitel 6.

Diskussionen i kapitel 5 viser at $FeCO_3$ spiller en vigtig rolle for beskyttelsen mod korrosion og specielt $FeCO_3$'s opløselighed er en vigtig parameter. I kapitel 7 diskuteres og valideres de termodynamiske egenskaber for $FeCO_3$. Her vises at der er en stor usikkerhed i $FeCO_3$'s egenskaber. De tilgængelige egenskaber valideres og sæt af konsistente egenskaber gives.

En termodynamisk model for det blandede solvent system CO_2-Na_2CO_3-$NaHCO_3$-MEG-H_2O præsenteres i kapitel 8. Parametrene for den udvidede UNIQUAC model tilpasses litteratur data for gas-væske, fastof-væske, entalpi-excess og varmekapacitet. Modellen tilpasses også eksperimentelle fastof-væske ligevægts data for Na_2CO_3-$NaHCO_3$-MEG-H_2O systemet, som er blevet målt i dette studie og præsenteret i kapitel 8.

Den udvidede UNIQUAC models anvendelse vises i kapitel 9. Her præsenteres de beregnede termodynamiske faktorer. De viser hvordan diffusions processer i CO_2 korrosion afviger fra ideal diffusion og at man derfor bør tage højde for dette i korrosions modeller. Konklusionen og forslag til fremtidig arbejde gives i kapitlerne 10 og 11.

Table of content

1   Introduction

Process equipment is exposed to corrosion on a daily basis. Maintenance and repair cost make up a significant part of the economy. CorrosionCost.com estimates that $276 billion dollars/year is lost and spend in relation to corrosion only in the US which is 2.5% of the US gross national product. $12 billion dollars/year are related directly to the transportation lines of the oil and gas industry[1].

The focus of this project is the natural gas transportation lines between platforms in the North Sea. A crude separation of oil, gas, and water is carried out close to the wellhead on an unmanned platform. The produced natural gas is transported 10-20 km in 16" pipelines downstream for post-processing, see figure 1.
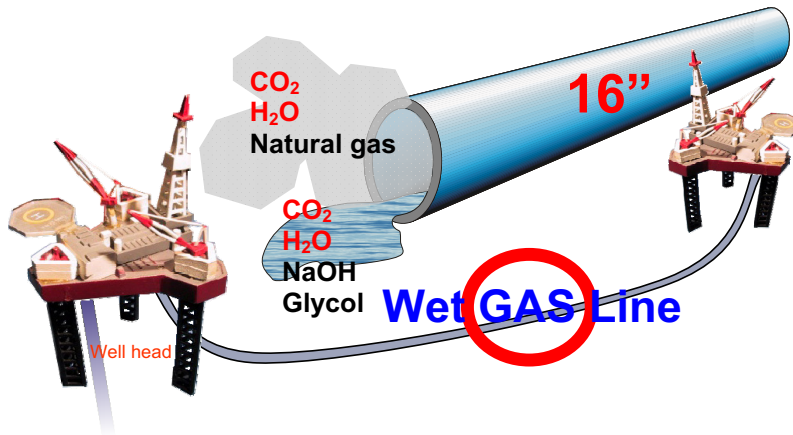
Figure 1: An overview of the gas transportation systems.

A pipeline transports on average 4 million m^3 natural gas/day. A breakdown will be costly. Unfortunately the oil industry often deal with the problems as they arise, instead of applying know-how and understanding of the system to prevent potential problems.

Table 1 shows a typical composition of the alloy used for the offshore pipelines. It is a mild carbon steel which indicate that the carbon content is relatively low. High carbon steels are up to 1 *wt%* carbon. A corrosion resistant alloy as e.g. duplex steel, has a high content of chromium and nickel. These types of steels are not used for gas transportations since it adds to the cost of pipeline and makes the gas production uneconomical.

Table 1: Composition of mild carbon steel, X65, used for pipelines.

X65	C	Si	Mn	S	P	Cr	Ni	V	Mo	Cu	Al	Sn
wt %	0.057	0.22	1.56	0.002	0.013	0.05	0.04	0.04	0.02	0.01	0.041	0.001

Table 2 lists a typical composition of the gas phase at the production site. The total pressure is 60 to 70 bar in the pipe inlet and the pressure drop is approximately 5 bar across the pipelines.

Table 2: Composition of a typical natural gas transported in pipelines in focus of this study.

Component	Composition (*mol%*)
Methane	88
Ethane	6
Propane	2
Butane	1
CO_2	1.6 (approx. 1 bar)
N_2	0.2
H_2O	0.1
Higher alkanes	Residual

Table 2 shows that small amounts of CO_2 is found in natural gas and it is corrosive like O_2. The CO_2 partial pressure is close to 1 bar. Produced natural gas is saturated with water and it is therefore also known as wet gas. The water condenses at the cold pipe wall during sub-sea transportation. Liquid mono ethylene glycol (*MEG*) or methanol is injected at the inlet to prevent gas hydrates. The concentration is 95 *wt%* in the inlet and approximate 30 *wt%* in the outlet due to dilution by the condensed water. CO_2 dissolves in the water-*MEG* liquid phase and the electrolytes will corrode the bottom of the pipeline. *pH* is increased at the production site by adding *NaOH*, *NaHCO$_3$* or a similar base in order to lower corrosion. The concentration is typically 10 *mol NaOH/kg* water in the inlet and 0.1 in the outlet. This shows that the liquid phase is not simple, it is thermodynamically non-ideal and it is a multi solvent electrolyte system.

Various protective corrosion products are produced, depending on the chemical environment. $FeCO_3(s)$ is formed as a corrosion product. It can protect against corrosion depending on *pH*, inhibitors and the bulk composition. Figure 2 shows the ideal solubility of $FeCO_3$ in water. When no *pH*-stabilizer of *NaOH* is added, then *pH* is approximately 5 and a high solubility of $FeCO_3$ is observed.
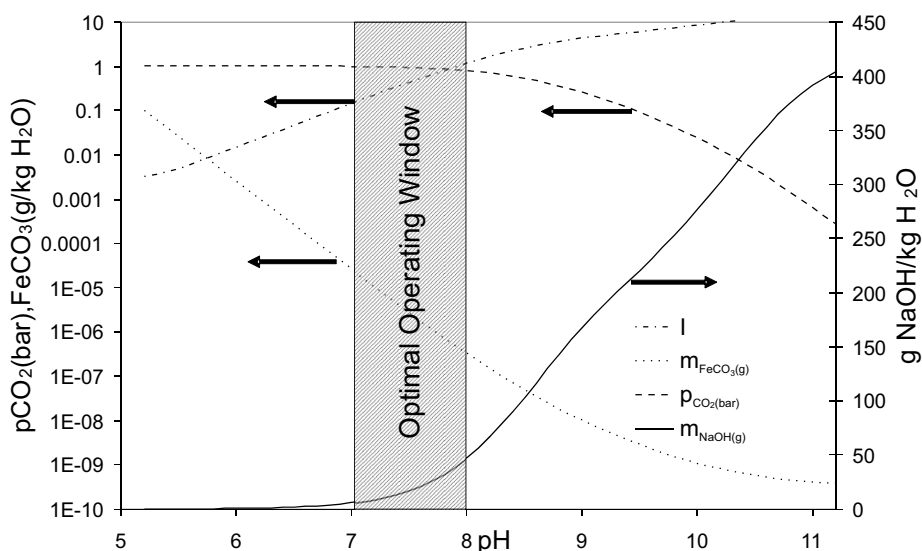
Figure 2: Ideal calculation of $FeCO_3$ solubility in water. The liquid composition at *pH* >8 is a hypothetical since *NaHCO$_3$* is most likely to precipitate. It was not included in the above calculations.

When small amounts of *NaOH* is added, *pH* increases fast and at an addition of approximately 25 *g NaOH/kg H₂O* the *pH* is 7.5. The solubility of *FeCO₃* decreases rapidly in the *pH* interval 5 to 7.5 from 0.1g/kg *H₂O* to 10^{-6}g/kg *H₂O*. It is important to notice that the partial pressure of *CO₂* stays almost constant in the interval *pH*=5 to 7.5 while above *pH*=8 significant amounts of *CO₂* is dissolved into the liquid phase. It neutralizes the *NaOH* and it is not effectively used for *pH*-stabilization. The operating window, shown in figure 2, gives the correct amount of *NaOH* to inject. This is done to prevent iron dissolution and to keep the use of *NaOH* down to an economical level but also to prevent dissolution of *CO₂* into the liquid phase. The ionic strength (*I*) is shown in the figure. It rises from approximately 0.005 up to 10 *mol/kg H₂O* in the shown *pH* interval. The high ionic strength may never be reached due to saturation by *NaHCO₃*, though it may approach 4 *mol/kg H₂O*.

Another way to avoid *CO₂* corrosion is to remove *CO₂* from the gas or dry it. This is not possible since the process is offshore and production platform is unmanned. Separation equipment is basically too expensive and highly cost-ineffective.

1.1   Corrosion definition

Different types of corrosion exist and the phenomenon is not a simple process. The reaction is typically an interaction between many mechanisms. Corrosion is generally defined as the irreversible deterioration of a substance or its properties because of a reaction with its environment. Some of the known types of corrosion are electrochemical corrosion caused by electron transfer, cracking caused by tensile stress, flow assisted corrosion caused by fluid flow, fretting caused by friction and rubbing and high temperature corrosion caused by alloy melting.

CO₂ corrosion is an electrochemical process which is discussed in this study and the remaining types of corrosion are subsequently not discussed.

1.2   Motivation and method

The motivation of this project has been to build a *CO₂* corrosion model in order to predict corrosion rates. A great number of these models are available in the open literature or as commercial products. Instead of reproducing their result the focus has been to improve the existing models and discuss the main assumption. The method has been to improve the thermodynamic description through experimental work and modelling. The model can be plugged into existing corrosion models in order to improve the description of the liquid phase. The protective corrosion product layers are discussed in order to present a reliable set of thermodynamic properties for these compounds.

2 Theory of electrolyte thermodynamics

2.1 Standard states and reference *(T°, P°)*

Thermodynamic properties like *G*, *H*, and *S,* etc. (Gibbs energy, enthalpy, and entropy) are always modelled relative to a well-defined origin. In electrolyte systems this implies modelling properties relative to the $H^+(aq)$ ion. Thermodynamic properties of $H^+(aq)$ are arbitrarily defined as 0 at $T°$=298.15K and $P°$=1 bar. The standard state properties at e.g. 313K and 1.5 bar are modelled relative to the defined properties at *(T°, P°)*. *(T°, P°)* are called the reference temperature and pressure. Most standard state tables give properties at *(T°, P°)* but other conditions are seen. This could for example be 350K and 2 bar, but the reference temperature and pressure are still 298.15K and 1 bar.
Some old tables use a *(T°, P°)* of 273.15K and 1 atm. This implies that the properties of the $H^+(aq)$ ion are arbitrarily set to 0 at this *(T°, P°)*. It is not difficult to use properties at other *(T°, P°)*, but the user must be aware. The final result is always independent of *(T°, P°)*, since all of the thermodynamic properties that we are interested in are basically changes from one state to another. The choice of *(T°, P°)* is not crucial. Databases which uses different *(T°, P°)* may not be combined without converting to the same *(T°, P°)*.
The standard state is an arbitrary well defined chemical state. It is chosen for convenience of the particular thermodynamic calculations. It is a well-defined chemical state which is used as an origin for the remaining calculations. The properties of the mixture are modelled relative to the defined standard state and it is a set point of the calculations. The final result is independent of the particular standard state. It can be chosen intelligently in order to facilitate the calculations. The temperature, pressure, and composition may change, but the type of standard state does not change.

There is a new defined standard state for every temperature and pressure in the system.

There is a great misunderstanding of the principles in the literature on standard states and reference *(T°, P°)*. Standard states are given at every *(T,P)*. Standard state properties are always listed relative to reference *(T°, P°)*. This is why properties at (T,P) are always calculated from well known values at *(T°, P°)*.

A standard state of ideal gas is typically used for gas phases. In standard state property tables this is indicated by (g). The standard state Gibbs energy of formation, $\Delta_f G^{\circ ig}$, at a reference temperature 298.15K and 1 bar, is the Gibbs energy a compound would have, if it were an ideal gas. The "non-ideality" arises if the mixture suddenly does not behave as an ideal gas.
Liquids do not behave as ideal gasses and therefore other types of standard states are used. Three schemes are typically applied, one which assumes the liquid phase is a very non-ideal gas phase, second a standard state which uses pure liquid properties and third a standard state which uses the properties in a well-defined mixture. The

third standard state is typically used for components which can not exist as a pure component, e.g. ions.

2.2 The thermodynamic framework

From the first law of thermodynamics for a closed system, the following is true for the internal energy, U:

$$dU = TdS - Pdv \tag{1}$$

where v is molar volume of the system. The enthalpy and Gibbs energy per mol are defined by:

$$H \equiv U + Pv \tag{2}$$

$$G \equiv H - TS \tag{3}$$

differentiation of the above gives the following relations:

$$dH \equiv dU + Pdv + vdP \tag{4}$$

$$dG \equiv dH - TdS - SdT \tag{5}$$

By substitution (4) into (5) and (1) into (4) reveals dG given by:

$$dG = vdP - SdT \tag{6}$$

Equation (6) reduces to the following, at constant T:

$$dG = vdP \quad \text{(constant } T\text{)} \tag{7}$$

For the "ideal" system v is substituted by RT/P and the above is therefore:

$$dG = RT\frac{dP}{P} = RTd\ln P \quad \text{(constant } T\text{)} \tag{8}$$

Fluids are not ideal and in the real mixture, the pressure P is given by an observed total pressure, f, the fugacity. By assuming that the equation for a non-ideal solution looks like (8). A relation can be defined between the total fugacity and the total molar Gibbs energy, G, in *J/mol* by:

$$dG \equiv RTd\ln f \tag{9}$$

Every component in the mixture contributes to the total Gibbs energy. The fractions that they provide are the derivative of the total Gibbs energy with composition:

$$\mu_i \equiv \overline{G}_i = \left(\frac{dnG}{dn_i}\right)_{T,P,n_{i\neq j}} \tag{10}$$

this quantity is defined as the partial molar Gibbs energy, $\bar{G}_i$, also called the chemical potential, μ_i. Similar to equation (9), it may be assumed that the "real pressure" of a component i in a mixture of more than one component also follows a relation equivalent to (9):

$$d\bar{G}_i \equiv RTd\ln \hat{f}_i^{\pi} \tag{11}$$

The hat signifies the mixture and the fugacity of component i in phase π, $\hat{f}_i^{\pi}$, is not a partial molar property like the chemical potential but a definition given by (11). Substituting (10) in (11) for the partial Gibbs energy shows that:

$$d\mu_i = RTd\ln \hat{f}_i^{\pi} \tag{12}$$

Integration over the chemical potential and the fugacity from a well defined standard state to the state of the system gives:

$$\mu_i = \mu_i^{\Theta_k s_l} + RT\ln \frac{\hat{f}_i^{\pi}}{\hat{f}_i^{\Theta_k s_l}} \tag{13}$$

$\mu_i^{\Theta_k s_l}$ and $\hat{f}_i^{\Theta_k s_l}$ represent the chemical potential and the solution fugacity in the arbitrary standard state Θ with a concentration scale of s. s can be mol fraction scale x also called *rational* scale, *molal* scale b (designated by superscript m) and *molar* scale c. The indices k and l indicates the standard state type k and concentration scale type, l. This sub-indexing of scale and standard state is used since different types can be chosen for the same component in the varying phases.

An equation that converts from one standard state to another is derived from (12) similar to (13). An integration of (12) from a standard state Θ_1 of a scale s_1 to a standard state Θ_2 of a scale s_2 shows:

$$\mu_i^{\Theta_2 s} - \mu_i^{\Theta_1 s} = RT\ln \frac{\hat{f}_i^{\Theta_2 s}}{\hat{f}_i^{\Theta_1 s}} \tag{14}$$

Appendix A.3 shows how to convert the chemical potential between standard state types.

2.3   Activity

Equation (13) may be written in terms of the activity of component i in phase π, $a_{i,\pi}^{\Theta_k s_l}$:

$$\mu_i = \mu_i^{\Theta_k s_l} + RT\ln a_{i,\pi}^{\Theta_k s_l} \tag{15}$$

The activity is defined as the deviation of the fugacity from the standard state fugacity in the liquid phase:

$$a_i^{\Theta s}\left(T,P,\mathbf{n}\right) = \frac{\hat{f}_i^{L}\left(T,P,\mathbf{n}\right)}{f_i^{\Theta s}\left(T,P,\mathbf{n}\right)} = \gamma_i^{\Theta s}\left(T,P,\mathbf{n}\right)s_i \big/ s_i^{\Theta} \qquad (16)$$

which indicate that the activity is 1 in the standard state, $f_i^{\Theta s}$. $a_i^{\Theta s}$ is also related to the activity coefficient $\gamma_i^{\Theta s}$ and the concentration scale s_i, where s_i^{Θ} is the constant concentration in the standard state as shown by (16). $\left(T,P,\mathbf{n}\right)$ signifies the variable is a function of temperature, pressure, and composition. $f_i^{\Theta s}$ is shown to be a function of composition even though it in most thermodynamic frameworks is solely a function of T and P. Appendix A.1 shows the relation between different types of activity coefficients. A component expresses ideal behaviour, when $\gamma_i^{\Theta s}\left(T,P,\mathbf{n}\right) \approx 1$ and the activity of a component which behaves ideally is therefore:

$$a_i^{\Theta s,id}\left(T,P,\mathbf{n}\right) = s_i \big/ s_i^{\Theta} \quad \text{(ideal)} \qquad (17)$$

where *id* indicates ideality. Equation (16) shows that activity is $a_i^{\Theta s}=1$ when the solution fugacity, $\hat{f}_i^{L}\left(T,P,\mathbf{n}\right)$, is identical to the standard state fugacity, $f_i^{\Theta s}\left(T,P,\mathbf{n}\right)$. Equation (17) shows that $a_i^{\Theta s,id} \approx 1$ if a component behaves ideal and $s_i \approx s_i^{\Theta}$. The concentration relative to the standard state concentration is defined by:

$$s_{i,r} = s_i \big/ s_i^{\Theta} \qquad (18)$$

denoted by subscript *r*.

2.4 Standard states and concentration scales

The symbol Θ in equation (13) signifies an arbitrary standard state. There are two well know standard states, the symmetrical and the unsymmetrical standard state. There are other types of standard states. Recently a mixed-solvent electrolyte standard state is being applied in the open literature[2].
The *symmetrical standard state* is denoted by a superscript °. The symmetrical standard state fugacity, $f_i^{\circ s}$, is defined by:

$$\lim_{x_i \to 1} \frac{\hat{f}_i\, s_i^{\Theta}}{s_i} = f_i^{\circ s} \qquad (19)$$

$$\lim_{x_i \to 1} \gamma_i^{\circ s} = 1 \qquad (20)$$

The symmetrical standard state concentration is purity. This indicates that s_i^{Θ} on a mol fraction scale is $s_i^{\Theta} = x_i^{\Theta} = 1$ but at molal scale it is $s_i^{\Theta} = b_i^{\Theta} = \infty$. For mol fraction scale the above implies that the fugacity move towards the symmetrical standard state fugacity as its composition approaches purity. The *unsymmetrical standard state* is

denoted by superscript *. The unsymmetrical standard state fugacity, f_i^{*s}, is defined by:

$$\lim_{\substack{x_i \to 0 \\ x_{solv} \to 1}} \frac{\hat{f}_i \, s^{\Theta}}{s_i} = f_i^{*s} \tag{21}$$

$$\lim_{x_{solv} \to 1} \gamma_i^{*s} = 1 \tag{22}$$

The standard state concentration varies with scale. It is 1 molal for molal scale, 1 molar for molar scale etc. f_i^{*m} for example is also known as the unsymmetrical standard state fugacity in a 1 molal solution. The fugacity approaches f_i^{*s} when $s_i \to s_i^{\Theta}$ and $\gamma_i^{*s} = 1$. This is a very hypothetical state since $\gamma_i^{*s} \neq 1$. The activity coefficient is defined as 1 at infinite dilution in *one* solvent, "*solv*", as stated by (22). *Solv* may be an arbitrary solvent, but water is almost always used. If a second solvent is present in the solution, then it is treated as a solute in water. Appendix A.2 shows how to convert fugacities between different types of standard states.
If the mixed-solvent standard state is used, then there is no longer one solvent, but the solvents are treated as separate solvents. This complicates the thermodynamic description and the ion activity coefficient becomes one in the mixture of solvents. This is not used in the combination with unsymmetrical standard state.

2.5   Liquid phase fugacities, γ approach

The fugacity of component *i* in the liquid phase at *(T,P,*$\mathbf{n}$*)*, $\hat{f}_i^L$, where $\mathbf{n}$ and $\mathbf{s}$ signifies a component vector, can be expressed by one of the following relations from (16):

$$\begin{aligned}
\hat{f}_i^L(T,P,\mathbf{n}) &= \gamma_i^{\Theta s}(T,P,\mathbf{s}) s_i f_i^{\Theta s}(T,P,\mathbf{s}) / s_i^{\Theta} \\
&= \gamma_i^{\circ x}(T,P,\mathbf{x}) x_i f_i^{\circ x}(T,P) / x_i^{\circ} \\
&= \gamma_i^{*x}(T,P,\mathbf{x}) x_i f_i^{*x}(T,P) / x_i^{*} \\
&= \gamma_i^{*m}(T,P,\mathbf{m}) b_i f_i^{*m}(T,P) / b_i^{*} \\
&= \gamma_i^{*c}(T,P,\mathbf{c}) c_i f_i^{*c}(T,P) / c_i^{*}
\end{aligned} \tag{23}$$

The calculated value of $\hat{f}_i^L$ is independent of the chosen standard state and concentration scale. Appendix A.2 shows how to convert standard state fugacities between standard states and concentration scales.

2.6   Vapour phase fugacities, ϕ approach

By the ϕ approach indicates that fugacities are modelled using *fugacity coefficients* instead of activities. Instead of applying an activity coefficient and defining many

different standard states, then only one standard state is typically used, the rational symmetrical ideal gas standard state, denoted by superscript $\circ ig$ and y for mol fraction scale. This is normally the only standard state applied for gas phases and it is also known as the ideal gas standard state. This standard state is very different than the liquid phase standard states since it depends on composition.

The fugacity coefficient $\hat{\phi}_i^V (T,P,\mathbf{n})$ defines component *i*'s deviation from the ideal gas law at *(T,P,$\mathbf{n}$)* in the mixture:

$$\hat{f}_i^V (T,P,\mathbf{n}) = \hat{\phi}_i^V (T,P,\mathbf{n}) f_i^{\circ igy} (T,P,\mathbf{n}) \tag{24}$$

$\hat{f}_i^V (T,P,\mathbf{n})$ is the fugacity in the non-ideal gas phase and $f_i^{\circ igy} (T,P,\mathbf{n})$ is the standard state fugacity. The fugacity is essentially modelled like the γ approach. Instead the standard state is a function of composition. $f_i^{\circ igy} (T,P,\mathbf{n})$ as given by:

$$f_i^{\circ igy} (T,P,\mathbf{n}) = y_i P \tag{25}$$

Which inserted in (24) is:

$$\hat{f}_i^V (T,P,\mathbf{n}) = \hat{\phi}_i^V (T,P,\mathbf{n}) y_i P \tag{26}$$

2.7   Liquid phase fugacity, ϕ approach

The ϕ approach for the liquid phase is much like the approach for the gas phase, shown above. The fugacity is given by:

$$\hat{f}_i^L (T,P,\mathbf{n}) = \hat{\phi}_i^L (T,P,\mathbf{n}) f_i^{\circ igx} (T,P,\mathbf{n}) \tag{27}$$

Here the standard state fugacity is modelled as if the liquid is a very non-ideal gas. The liquid phase fugacity coefficient $\hat{\phi}_i^L (T,P,\mathbf{n})$ is defined as the deviation from the ideal gas law. The standard state fugacity is essentially defined equivalent to (25), applying the liquid composition instead of the gas-phase composition:

$$f_i^{\circ igx} (T,P,\mathbf{n}) = x_i P \tag{28}$$

Which inserted in (27) becomes:

$$\hat{f}_i^L (T,P,\mathbf{n}) = \hat{\phi}_i^L (T,P,\mathbf{n}) x_i P \tag{29}$$

and reduces to the pure liquid fugacity, f_i^L, when x_i=1 and $\hat{\phi}_i^L (T,P,\mathbf{n}) = \phi_i^L (T,P)$:

$$f_i^L (T,P) = \phi_i^L (T,P) f_i^{\circ igx} (T,P,\mathbf{n}) , \quad (\text{for } x_i=1) \tag{30}$$

Setting (30) equal to (23), gives the following relation of $f_i^{\circ x}$, since (20) is valid:

$$f_i^{\circ x}(T,P) = \phi_i^L(T,P) \cdot P \tag{31}$$

Combining (23), (29), and (31) gives a relation between the rational symmetrical activity coefficient and the fugacity coefficient:

$$\gamma_i^{\circ x}(T,P,\mathbf{n}) = \hat{\phi}_i^L(T,P,\mathbf{n}) x_i^{\circ} / \phi_i^L(T,P) \tag{32}$$

$\gamma_i^{\circ x}(T,P,\mathbf{n})$ is typically calculated using a Gibbs excess model and $\hat{\phi}_i^L(T,P,\mathbf{n})$ is calculated using an equation of state (EoS). An EoS may therefore be used for calculating the activity through (16). x_i° is the standard state mol fraction which is usually $x_i^{\circ} = 1$.

2.8   The thermodynamic equilibrium criteria

The criterion for equilibrium needs to be defined in order to calculate the equilibrium composition. Imagine a number of containers, each holding a pure chemical. They are mixed in a closed tank of fixed volume. Equilibrium is reached at some point and a number of distinct phases are created, e.g. vapour, liquid, solid or other phases. The temperature and pressure (*T, P*) have reached uniform values in every phase. The general equilibrium criterion is:

$$\mu_i^{\alpha}(T,P,\mathbf{n}) = \mu_i^{\beta}(T,P,\mathbf{n}) = ... = \mu_i^{\pi}(T,P,\mathbf{n}) \tag{33}$$

which states, that the chemical potential of component *i* at *(T,P,*$\mathbf{n}$*)*, $\mu_i^{\pi}(T,P,\mathbf{n})$, is equivalent in all phases from α to π. By inserting (13) in (33) reveals the following relation for a two phase system:

$$\mu_i^{\Theta_1 s_1} + RT\ln\frac{\hat{f}_i^{\alpha}}{\hat{f}_i^{\Theta_1 s_1}} = \mu_i^{\Theta_2 s_2} + RT\ln\frac{\hat{f}_i^{\beta}}{\hat{f}_i^{\Theta_2 s_2}} \tag{34}$$

Inserting (14) in (34) reveals the equilibrium criteria expressed in term of fugacities:

$$\hat{f}_i^{\alpha} = \hat{f}_i^{\beta} \tag{35}$$

which can be proved for an arbitrary number of phases:

$$\hat{f}_i^{\alpha} = \hat{f}_i^{\beta} = ... = \hat{f}_i^{\pi} \tag{36}$$

(33) and (36) are therefore equivalent formulation of the equilibrium criteria.

2.9   Phase equilibrium

Equation (33) or (36) is applied in a speciation routine in order to calculate the equilibrium conditions. The electrolyte system is a system which contains a number

of reactions. The equilibrium condition in a reacting system is given by the following relation obtained from (33):

$$\left(\Delta_k \mu\right)_{T,P} = \left(\Delta_k \overline{G}\right)_{T,P} = 0 \qquad\qquad k = 1...N_{reaction} \qquad\qquad (37)$$

$N_{reaction}$ is the number of reactions. This equilibrium criteria is applicable for all systems including multiple phase systems. $\Delta_k \mu$ is the change in chemical potential of reaction k at constant T and P. Numerous reaction may be defined in the system but rarely all are solved in the same calculation. The reason is that the systems must obey the Gibbs' phase rule, $F=C+2-P$. This indicates that even though 10 solid phases may potentially precipitate, then only the reactions related to the specific salts in interest are included in the calculations. Inserting (15) in (37) gives:

$$\left(\Delta_k \mu\right)_{T,P} = \sum_i \nu_{i,k} \mu_{i,k} = 0 \Leftrightarrow$$
$$\sum_i^{N_{comp}} \nu_{i,k} \left(\left(\mu_{i,p}^{\Theta s}\right)_k + RT \ln\left(a_{i,p}^{\Theta s}\right)_k\right) = 0 \qquad k = 1...N_{reaction} \qquad (38)$$

Subscript p signifies phase number and k is the reaction number. Therefore the reaction may be homogeneous dissociation in the liquid phase or heterogeneous equilibria across phase boundaries in for example SLE and VLE calculations. The above rearranges to:

$$\Delta_{r,k} G^{\Theta} = -RT \ln\left(K_k\right) \qquad\qquad k = 1...N_{reaction} \qquad\qquad (39)$$

$\Delta_{r,k} G^{\Theta}$ is the standard reaction Gibbs energy and K_k is the calculated equilibrium constant of the k'th reaction defined by:

$$\Delta_{r,k} G^{\Theta} = \sum_i^{N_{comp}} \nu_{i,k} \mu_{i,k}^{\Theta s}, \qquad K_k = \prod_i^{N_{comp}} \left(a_{i,p}^{\Theta s}\right)_k^{\nu_{i,k}} \qquad k = 1...N_{reaction} \qquad (40)$$

$\mu_i^{\Theta s}$ is found in open literature as tabulated values of standard Gibbs formation energy or as correlation of the equilibrium constant as function of temperature. A quantity called *solubility index* or *saturation index* is defined by:

$$SI_k = \frac{\displaystyle\prod_i^{N_{comp}} \left(a_{i,p}^{\Theta s}\right)_k^{\nu_{i,k}}}{K_k} \qquad\qquad (41)$$

It is typically used in a speciation routine in order to calculate the equilibrium composition from the number of defined reactions. $a_{i,p}^{\Theta s}$ is obtained from the thermodynamic model and K_k is calculated from tabulated standard state properties through (39). The solubility of a salt is found at $SI_k=1$ which is the criteria for equilibrium saturation. It is determined by varying the liquid composition. Only the reactions for the salts which saturate the solution are included in the equilibrium calculation.

3   Theory of electrolyte mass transport

Some of the theories presented below are known from existing literature, as for example presented by Taylor and Krishna[3]. The theory presented in section 3.4.4 has not previously been presented and should be regarded as extension of the current understanding of mass transport in electrolyte systems.

3.1   The volumetric component mol balance

The non-steady state mol balance across a control volume of section area $A \left[m^2 \right]$, volume $V = A \cdot \Delta z \left[m^3 \right]$ and length $\Delta z \left[m \right]$ of component i is given by equation (42) . The balance is given as the molar flux in, $N_i \big|_z \left[mol/(m^2 s) \right]$, plus production from reaction, $R_i \left[mol/(m^3 s) \right]$, is equal to flux out, $N_i \big|_{z+\Delta z}$, plus accumulation over the time, $\Delta t \left[s \right]$, with concentration, $c_i \left[mol/m^3 \right]$:

$$\left(\Delta t \cdot A \cdot N_i \right)\big|_z + \Delta t \cdot R_i \cdot V = \left(\Delta t \cdot A \cdot N_i \right)\big|_{z+\Delta z} + \left(c_i\big|_{t+\Delta t} - c_i\big|_t \right) V \qquad (42)$$

$N_i\big|_z$ and $N_i\big|_{z+\Delta z}$ are perpendicular to the section area A. Dividing (42) by $A\Delta t\Delta z$ at $\Delta z \to 0$ and $\Delta t \to 0$ rearranges the above to

$$\frac{\partial c_i}{\partial t} = -\frac{\partial N_i}{\partial z} + R_i \qquad (43)$$

which is the component mol balance of the volume shown in figure 3 over time.
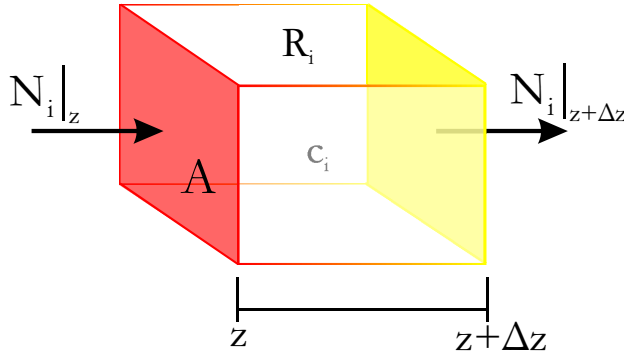
Figure 3: Mol balance of component *i* over time

The mol balance across a differential volume element written equivalent to (43) but for the general case in 3D is given by:

$$\frac{\partial c_i}{\partial t} = -\nabla \cdot \mathbf{N}_i + R_i \qquad (44)$$

Here the differential element $\partial N_i / \partial z$ is substituted by the gradient vector of the molar fluxes $\nabla \cdot \mathbf{N}_i$. The del or Nabla operator, ∇, is the gradient vector

$$\nabla = \begin{bmatrix} \dfrac{\partial}{\partial x} & \dfrac{\partial}{\partial y} & \dfrac{\partial}{\partial z} \end{bmatrix}^T \tag{45}$$

and the molar flux is similarly given by:

$$\mathbf{N}_i = \begin{bmatrix} N_{i,x} & N_{i,y} & N_{i,z} \end{bmatrix}^T \tag{46}$$

Which is a vector of the molar fluxes in the three directions x, y, z. $\nabla \cdot \mathbf{N}_i$ is therefore a scalar given by:

$$\nabla \cdot \mathbf{N}_i = \frac{\partial N_{i,x}}{\partial x} + \frac{\partial N_{i,y}}{\partial y} + \frac{\partial N_{i,z}}{\partial z} \tag{47}$$

Usually $\mathbf{N}_i$ is in it self a function of the del operator and consequently the mass balance (44) results in an equation consisting of the Laplacian operator:

$$\nabla \cdot \nabla f_i = \nabla^2 f_i = \frac{\partial^2 f_{i,x}}{\partial x^2} + \frac{\partial^2 f_{i,y}}{\partial y^2} + \frac{\partial^2 f_{i,z}}{\partial z^2} \tag{48}$$

and the model becomes a parabolic second order partial differential equation (PDE) which describes the un-steady state diffusion problem.
The steady state solution may be found by setting $\partial c_i / \partial t = 0$ and (44) becomes:

$$\nabla \cdot \mathbf{N}_i = R_i \qquad \text{(steady state)} \tag{49}$$

A sufficient amount of boundary conditions or bootstraps are required in order to solve these equations and they shape the final solution of the problem.

3.2   The thermodynamic driving force

The following section goes through defining the driving force for diffusion and lays out the thermodynamic equations related to diffusion.
Imagine a system which contains an amount of stored energy; it may be released as work or heat. The energy is a difference between two states of the system. One state is lower in energy. Take for example a ball on a desk. One scenario is the ball on the desk and a second the ball on the floor. The energy released by the system, on moving the ball from one state to the other, is the stored energy. The difference is also known as the potential energy of the system. The energy is released on applying activation energy, which in our example would be equivalent to rolling the ball over the edge of the desk.
In chemical systems the stored energy is also related to a potential energy, the chemical potential, $\mu_i(n,T,P)$ in $\left[J/mol \sim Nm/mol \right]$. The chemical potential

describes the energy required to move the system from the low energy state to the high energy state.

The potential is the integration over all the forces required. In case of the falling ball it would be the gravity. The forces always point from a high energy level to a low level. The driving force, $\mathbf{d}_i^{driv}$, is therefore the negative of the chemical potential gradient

$$\mathbf{d}_i^{driv} \equiv -\nabla \mu_i \left(T, P, \mathbf{n} \right) \tag{50}$$

The force is given in Newton per mol $\left[N/mol \right]$. Certain authors[3,4] decide to define the driving force as $\mathbf{d}_i^{driv} = -x_i \nabla \mu_i / RT$, this is principally wrong since it has a dimension of $\left[1/m \right]$ and therefore it is not a force.

Contributions to the chemical potential can be temperature, pressure, concentration, or electrical gradients. Other forces could be centrifugal forces, gravity, or related to surface tension. All contributions are contained in the chemical potential, but they are only included if they have a gradient. The temperature gradient is for example zero if the diffusion layer has a uniform temperature.

The electrolytic diffusion process is influenced by the difference in the charge of the components. An ion will influence the diffusion of other ions due to charge interaction. The slower ion drags the faster due to pulling/pushing from the ionic charge difference. For example a big slow diffusing negative ion will drag smaller positive ions and the small positive ion will pull the slow negative ions.

The chemical potential at constant *T*, *P* is given by (15) or in the appendix as (281) to (285). It is valid for electrolytic phase equilibria, but not for diffusion processes. The mean ion charges of a liquid is zero at equilibrium and the ion charges has no influence. Diffusion is not at equilibrium and the distribution of charges becomes important. The resulting chemical potential at constant *T*, *P* is known as the electrochemical potential similar to (15):

$$\mu_i \left(T, P, \mathbf{n} \right) = \mu_i^{\ominus s} \left(T, P \right) + RT \ln \left(a_i^{\ominus s} \left(T, P, \mathbf{n} \right) \right) + z_i F \phi \tag{51}$$

The difference is a contribution from the electrical potential, ϕ. Where z_i is the charge number of the ion and *F* is the Faraday constant, $96485 \, coul/mol$. Any arbitrary standard state can be chosen.

There are only *n*-1 independent driving forces due to the Gibbs-Duhem relation at constant *T*, *P*: $\sum x_i d_i^{chem} = \sum x_i d\mu_i = 0$. Inserting (51) in (50) gives the driving force:

$$\begin{aligned}
-\mathbf{d}_i^{driv} &= \nabla \left(\mu_i^{\ominus s} \left(T, P \right) + RT \ln \left(a_i^{\ominus s} \left(T, P, \mathbf{n} \right) \right) + z_i F \phi \right)_{T,P} \\
&= \nabla \mu_i^{\ominus s} \left(T, P \right)_{T,P} + \nabla RT \ln \left(a_i^{\ominus s} \left(T, P, \mathbf{n} \right) \right)_{T,P} + \left(z_i F \nabla_{T,P} \phi \right)_{T,P}
\end{aligned} \tag{52}$$

The standard state chemical potential does not change with position in the system and the gradient is zero, $\nabla \mu_i^{\ominus s} \left(T, P \right)_{T,P} = 0$. This is only true at constant *T*, *P* since the standard state chemical potential is a function of *T*, *P*. Constant *T*, *P* can be assumed in most applications. When pressure gradients or temperature profiles are observed, then the gradient of the standard state is a function of *T*, *P* and $\nabla \mu_i^{\ominus s} \left(T, P \right)_{T,P} \neq 0$.

Using the rational symmetrical standard state reduces the complexity of the driving force considerably. Therefore $\nabla \mu_i^{\ominus s}\left(T,P\right) = \nabla \mu_i^{\circ x}\left(T,P\right)$ and $a_i^{\ominus s} = a_i^{\circ x}$. If the standard molal unsymmetrical standard was used, it would have posed no problem since:

$$
\begin{aligned}
\nabla \mu_i^{\circ x} &= \nabla\left(\mu_i^{*m} - RT \ln M_s \gamma_i^{\infty x}\right) \\
&= \nabla \mu_i^{*m} - \nabla RT \ln M_s \gamma_i^{\infty x} = 0
\end{aligned}
\tag{53}
$$

because the gradient of μ_i^{*m} and $\gamma_i^{\infty x}$ is zero and they are independent of the position in the system, see equation (331) in the appendix. This indicates that even though the rational symmetrical standard state is chosen, it is equivalent to molal unsymmetrical standard state or any other state as long as the gradient of the conversion factor does not change. The rational symmetrical standard state is therefore used as an example system in order to set up a scheme where any standard state may be used. This gives a general thermodynamic formulation of the driving force and the description becomes independent of standard state properties. This reduces equation (52) to:

$$
-\mathbf{d}_i^{driv} = RT\nabla \ln\left(a_i^{\circ x}\left(T,P,\mathbf{n}\right)\right)_{T,P} + \left(z_i F \nabla \phi\right)_{T,P}
\tag{54}
$$

Equation (54) may be rewritten as the following sum of partial derivatives using the chain rule for multivariate functions:

$$
-\mathbf{d}_i^{driv} = RT\sum_{j=1}^{n}\left(\frac{\partial \ln\left(a_i^{\circ x}\left(T,P,\mathbf{n}\right)\right)}{\partial x_j}\right)_{T,P,x_{j\neq i}} \nabla x_j + \left(z_i F \nabla \phi\right)_{T,P}
\tag{55}
$$

since the derivative of a multivariate function is given by:

$$
\nabla f = \left(\frac{\partial f}{\partial x_1}\right)_{x_{i\neq 1}} \nabla x_1 + \left(\frac{\partial f}{\partial x_2}\right)_{x_{i\neq 2}} \nabla x_2 + ... + \left(\frac{\partial f}{\partial x_n}\right)_{x_{i\neq n}} \nabla x_n \quad (\text{constant } T,P)
\tag{56}
$$

note that the above equation is only valid at constant T, P and the partial derivative of T, P is neglected. The subscript $x_{j\neq i}$ signifies the partial derivative with respect to constant x_j except for $j=i$. The gradients sum to zero:

$$
\sum_{i=1}^{n}\nabla x_i = 0
\tag{57}
$$

this is equivalent to the Gibbs-Duhem relation above and implies again that only n-1 independent driving forces exist. Inserting (16) in (55) gives:

$$-\mathbf{d}_i^{driv} = RT\sum_{j=1}^{n}\left(\frac{\partial \ln\left(\gamma_i^{\circ x}(T,P,\mathbf{n})\,x_i(T,P,\mathbf{n})/x_i^{\circ}\right)}{\partial x_j}\right)_{T,P,x_{j\neq i}} \nabla x_j + z_i F \nabla \phi$$

$$= RT\sum_{j=1}^{n}\left(\frac{\partial \ln\left(x_i(T,P,\mathbf{n})/x_i^{\circ}\right)}{\partial x_j} + \frac{\partial \ln\left(\gamma_i^{\circ x}(T,P,\mathbf{n})\right)}{\partial x_j}\right)_{T,P,x_{j\neq i}} \nabla x_j + z_i F \nabla \phi \tag{58}$$

Which is converted to the following since $\frac{d\ln y}{dx} = \frac{1}{y}\frac{dy}{dx}$ using a relative concentration scale, $x_{i,r} = x_i / x_i^{\circ}$, from (18):

$$-\mathbf{d}_i^{driv} = RT\sum_{j=1}^{n}\left(\frac{1}{x_{i,r}}\frac{\partial x_{i,r}(T,P,\mathbf{n})}{\partial x_j} + \frac{\partial \ln\left(\gamma_i^{\circ x}(T,P,\mathbf{n})\right)}{\partial x_j}\right)_{T,P,x_{j\neq i}} \nabla x_j + z_i F \nabla \phi$$

$$= \frac{RT}{x_{i,r}}\sum_{j=1}^{n}\left(\frac{\partial x_{i,r}(T,P,\mathbf{n})}{\partial x_j} + x_{i,r}\frac{\partial \ln\left(\gamma_i^{\circ x}(T,P,\mathbf{n})\right)}{\partial x_j}\right)_{T,P,x_{j\neq i}} \nabla x_j + z_i F \nabla \phi \tag{59}$$

If rational symmetrical activity coefficient is not applied as the activity coefficient model in (52), then an appropriate conversion can be performed by using (286) from the appendix:

$$\frac{\partial \ln\left(\gamma_i^{\circ x}(T,P,\mathbf{n})\right)}{\partial x_j} = \frac{\partial \ln\left(\gamma_i^{*m}\right)}{\partial x_j} + \frac{\partial \ln\left(\gamma_i^{\infty x}\right)}{\partial x_j} - \frac{\partial \ln(x_s)}{\partial x_j} = \frac{\partial \ln\left(\gamma_i^{*m}\right)}{\partial x_j} \tag{60}$$

It shows that it does not matter which activity coefficient model is used as long as the conversion factor is independent of x_j.

The relative concentration scale, $s_{i,r}$, in the first term of the sum in equation (59), may be a function of T, P, and $\mathbf{n}$. The problem is that some $s_{i,r}$ are dependent on T, P, and n as for example molar scale. It is convenient to chose rational scale since the partial derivative with respect to mol fraction at constant composition is 1 if $i=j$ and 0 if $i\neq j$. The derivative may therefore be substituted by the Kronecker delta function:

$$\left(\frac{\partial s_{i,r}(T,P,\mathbf{n})}{\partial x_j}\right)_{x_{j\neq i}} = \delta_{ij} \tag{61}$$

If any other scale is used then the function becomes complicated. This is one of the primary reasons for applying the rational scale.

The content of the parenthesis in the sum of (59) is defined by:

$$\Gamma_{ij} = \delta_{ij} + x_{i,r}\left(\frac{\partial \ln\left(\gamma_i^{\circ x}(T,P,\mathbf{n})\right)}{\partial x_j}\right)_{x_{j\neq i}} \tag{62}$$

also known as the thermodynamic factor. Examples for a binary mixture are:

$$\Gamma_{11} = 1 + x_{1,r} \frac{\partial \ln\left(\gamma_1^{\circ x}\left(T, P, \mathbf{n}\right)\right)}{\partial x_1} \tag{63}$$

$$\Gamma_{12} = x_{1,r} \frac{\partial \ln\left(\gamma_1^{\circ x}\left(T, P, \mathbf{n}\right)\right)}{\partial x_2} \tag{64}$$

At ideal condition it becomes the unit matrix:

$$\Gamma_{ii} = 1 \ , \quad \Gamma_{ij, i \neq j} = 0 \tag{65}$$

An example of component *i*=1 in an ideal *n* component mixture:

$$\Gamma_{11} = 1 \ , \quad \Gamma_{12} = \Gamma_{13} = ... = \Gamma_{1n} = 0 \tag{66}$$

Inserting (62) in (59) using (61) reduces the driving force to:

$$-\mathbf{d}_i^{driv} = \frac{RT}{x_{i,r}} \sum_{j=1}^{n} \Gamma_{ij} \nabla x_j + z_i F \left(\nabla \phi\right)_{T,P} \tag{67}$$

The driving force for moving an ion, is the sum of the thermodynamic factors times the species gradients. At ideal condition this reduces significantly by using (65) in (67):

$$-\mathbf{d}_i^{driv} = \frac{RT}{x_{i,r}} \nabla x_i + z_i F \nabla \phi \quad \text{(ideal)} \tag{68}$$

The above driving force is essentially a term for transport due to a concentration gradient and a term for the ionic charge effect. Equation (67) is used in the following section to show the relation to diffusion theory.

3.3   The Maxwell-Stefan friction theory

With no further hesitation we present the generalized Maxwell-Stefan equations. For a thorough discussion of the related subject please see Taylor and Krishna[3], Medvedev[4], Newman[5], and Wesselingh and Krishna[6]:

$$\mathbf{d}_i^{friction} = \sum_{j=1}^{n} \frac{RT}{Đ_{ij}} x_j \left(\mathbf{u}_i - \mathbf{u}_j\right) \tag{69}$$

$\mathbf{d}_i^{friction}$ is the friction force which has a dimension of $\left[N/mol\right]$, $\mathbf{u}_i$ is the velocity $\left[m/s\right]$ and $Đ_{ij}$ is the Maxwell-Stefan diffusivity, $\left[m^2/s\right]$. Diffusivity is a concentration dependent diffusion coefficient which is related to the drag between components. For a binary system it becomes equal to the Fickian diffusion coefficient at infinite dilution. $\mathbf{d}_i^{friction}$ originate from the frictional drag of molecules of component *i* moving past or through the remaining components. This is proportional

to the velocity difference, $\mathbf{u}_i - \mathbf{u}_j$, and the drag coefficients, $RT/\mathcal{D}_{ij}$. $\mathcal{D}_{ij}$ is therefore the reverse proportional to the friction between component *i* and *j*. $\mathcal{D}_{ij}$ may also be known as the drag between species. The diffusivities are symmetrical, $\mathcal{D}_{ij} = \mathcal{D}_{ji}$, and $\frac{1}{2}n(n-1)$ diffusivities are required for a *n* component system. For multi component Fick diffusion coefficient are not symmetrical and requires $(n-1)(n-1)$ coefficients for a *n* component system.

It is clear that the $i = j$ contribution to the sum in (69) is zero because the $i = j$ velocities cancel out. Therefore $\mathcal{D}_{ii}$ is not defined for any system. The molar flux, $\mathbf{N}_i$ $\left[mol/(m^2 s) \right]$, is defined by:

$$\mathbf{N}_i \equiv c_i \mathbf{u}_i \tag{70}$$

Where c_i is the molar concentration, $\left[mol/m^3 \right]$. The total concentration is given by:

$$c_t = \sum_{i=1}^{n} c_i \quad , \qquad c_i = x_i c_t \tag{71}$$

Inserting (71) and (70) in (69) gives the friction force as a function of molar flux:

$$\mathbf{d}_i^{friction} = \frac{RT}{x_i c_t} \sum_{j=1}^{n} \frac{x_j \mathbf{N}_i - x_i \mathbf{N}_j}{\mathcal{D}_{ij}} \tag{72}$$

In the treatment of non-ionic systems it is usual to define diffusion fluxes, $\mathbf{J}_i$, with respect to a reference velocity. This way all fluxes are treated relative to that velocity and no absolute values are given. Three types of relative velocity frameworks are normally applied: mass average, molar average and volume average velocity. This implicates that the fluxes are relative to the mean velocity weighted either by mass, molar, or volume. Conversion between the different frameworks can be done with a certain amount of difficulty and it may imply using molar volumes which for most thermodynamic models are inaccurate. $\mathcal{D}_{ij}$ remains independent of the framework.

For diffusion in electrolytes the most commonly used reference velocity is *not* one of the above, but the solvent velocity, $\mathbf{u}_s$. The diffusion flux of component *i* is therefore:

$$\mathbf{J}_i^s = \mathbf{N}_i - c_i \mathbf{u}_s \tag{73}$$

The superscript *s* of the flux signifies solvent reference velocity framework. The diffusive flux of solvent is zero.

$$\mathbf{J}_{i=s}^s = \mathbf{0} \quad \Rightarrow \quad \mathbf{N}_s = c_s \mathbf{u}_s \tag{74}$$

Which is obtained by substituting (70) in (73). Inserting (73) in (72) reveals the generalized Maxwell-Stefan in terms of diffusion flux:

$$\mathbf{d}_i^{friction} = \frac{RT}{x_i c_t} \sum_{j=1}^{n} \frac{x_j \mathbf{J}_i^s - x_i \mathbf{J}_j^s}{\mathcal{D}_{ij}} \tag{75}$$

The above is generalised to:

$$\mathbf{d}_i^{friction} = \frac{RT}{x_i c_t} \sum_{j=1}^{n} B_{ij}^s \mathbf{J}_j^s \tag{76}$$

Where B^s is defined by:

$$B_{ii}^s = \sum_{j=1, i \neq j}^{n} \frac{x_j}{\mathcal{D}_{ij}}$$

$$B_{ij}^s = \frac{-x_i}{\mathcal{D}_{ij}} \quad \text{for } i \neq j \tag{77}$$

Examples of B^s are:

$$B_{11}^s = \frac{x_2}{\mathcal{D}_{12}} + \frac{x_2}{\mathcal{D}_{13}} + ... + \frac{x_n}{\mathcal{D}_{1n}} \tag{78}$$

$$B_{21}^s = \frac{-x_2}{\mathcal{D}_{21}} = \frac{-x_2}{\mathcal{D}_{12}} \tag{79}$$

In vector notation (76) is:

$$\underline{\mathbf{d}}^{friction} = \frac{RT}{c_t} \underline{\underline{X}}^{-1} \underline{\underline{B}} \underline{\mathbf{J}}^s \tag{80}$$

where $\underline{\underline{X}}$ is a diagonal matrix of x_i and $\underline{\underline{X}}^{-1}$ is a diagonal matrix of $1/x_i$. It must be underlined, that there is only n-1 independent $\mathbf{J}_i^s$ and $\mathbf{d}_i^{friction}$ and the last equation is a linear combination of the others. This is identified immediately by equation (74) which states that the relative flux of solvent is zero. Solving (80) for $\underline{\mathbf{J}}^s$ reveals:

$$\underline{\mathbf{J}}^s = \frac{c_t}{RT} \underline{\underline{B}}^{-1} \underline{\underline{X}} \underline{\mathbf{d}}^{friction} \tag{81}$$

The problem of applying the above equations lies in the missing diffusivities between ions, which are rarely known. This is discussed later. The above equations are used in the following sections to derive the theory of diffusion.

3.4   Setting up the diffusion problem

At steady diffusion the driving force is equal to the friction and therefore

$$\mathbf{d}_i^{driv} = \mathbf{d}_i^{friction} \tag{82}$$

Inserting the derived equations from (67) and (76) gives the link between the thermodynamic description and the diffusivities:

$$-\mathbf{d}_i = \frac{RT}{x_i} \sum_{j=1}^{n} \Gamma_{ij} \nabla x_j + z_i F \nabla \phi = -\frac{RT}{x_i c_t} \sum_{j=1}^{n} B_{ij}^s \mathbf{J}_j^s \tag{83}$$

Simplifying (83) may be related to the thermodynamic part, the diffusivities or both. It may neglect some important physical phenomena and the assumption needs to be reconsidered before the final conclusion may be drawn on the model. In the following sections it is shown how (83) can be simplified to some of the popular representations of diffusion descriptions in the literature. Suggestions are given to approach a correct description of the diffusion process but still maintaining accuracy.

Harned and Owen[7] and Robinson and Stokes[8] discuss the theory of electrolytic diffusion. They set up the equations for diffusion in solutions containing one salt. Their equations include all correction to the infinite dilution activity coefficient. This includes thermodynamic factor determined from experimental data. They conclude that there is a discrepancy of a few percent between the calculated and the measured observed diffusion coefficient. Ascribing the effect to some of the same phenomena as the electrical potential, ϕ, which is the pulling and pushing of ions due to charge difference thereby maintaining electro neutrality. The effect is referred to as the *electrophoretic effect* which is partly the concentration dependency of the diffusion coefficients. They also discuss the effect of viscosity. These effects are not shown in the derivation below and are assigned to the concentration dependence of the diffusivities.

3.4.1 Fick diffusion

To prove that Fick's diffusion equation is a subproblem of (83) we need to do an amount of assumptions. For a mixture of non-charged molecules, the potential is zero, $\nabla \phi = 0$. Assume ideal thermodynamic condition. This results in the thermodynamic factors are $\Gamma_{ii} = 1$ and $\Gamma_{ij, i \neq j} = 0$. The composition of the solutes, x_i, are assumed to be close to zero, $x_i \approx 0$. The solvent composition, x_s, is assumed to be close to one, $x_s \approx 1$. $Ð_{is}^{\infty}$ are the diffusivities at infinite dilution in solvent s. This reduces (77) to

$$B_{ii}^s = \frac{1}{Ð_{is}^{\infty}}, \quad B_{ij}^s = 0 \tag{84}$$

Written for a binary system this results in the following relation from (83)

$$-\mathbf{d}_1 = \frac{RT}{x_1}\left(\Gamma_{11}\nabla x_1 + \Gamma_{12}\nabla x_2\right) = -\frac{RT}{x_1 c_t}\left(B_{11}^s \mathbf{J}_1^s + B_{12}^s \mathbf{J}_2^s\right) \tag{85}$$

Only one independent equation may be written for the binary system. Equation (83) reduces to the following relation by applying the above assumptions:

$$\nabla x_i = -\frac{\mathbf{J}_i^s}{c_t \mathcal{D}_{is}^{\infty}} \Leftrightarrow$$

$$\mathbf{J}_i^s = -\mathcal{D}_{is}^{\infty} \nabla c_i \tag{86}$$

Diffusion in one dimension gives Fick's law of diffusion:

$$J_i^s = -\mathcal{D}_{is}^{\infty} \frac{dc_i}{dz} \tag{87}$$

where z is the directional coordinate.

3.4.2   Fick diffusion expressed in terms of activities

Fick's law expressed in terms of activities can not just be derived by substituting concentration in (87) by activities. It can be derived by combining (54) and (76) in (82) which gives the following relation:

$$RT\nabla_{T,P} \ln\left(a_i^{\circ x}(T,P,n)\right) + z_i F \nabla \phi = -\frac{RT}{x_i c_t} \sum_{j=1}^{n} B_{ij}^s \mathbf{J}_j^s \tag{88}$$

Assume that all species are non-charged gives zero gradient of the potential, $\nabla\phi=0$. Since $\frac{d\ln y}{dx} = \frac{1}{y}\frac{dy}{dx}$ it reduces the above equation to:

$$\frac{RT}{a_i^{\circ x}}\nabla a_i^{\circ x} = -\frac{RT}{x_i c_t} \sum_{j=1}^{n} B_{ij}^s \mathbf{J}_j^s \tag{89}$$

Assuming composition of the solutes to be negligible gives a relation similar to (84). This reduces (89) even further to the following:

$$\frac{RT}{a_i^{\circ x}}\nabla a_i^{\circ x} = -\frac{RT}{x_i c_t} \frac{\mathbf{J}_i^s}{\mathcal{D}_{in}^{\infty}} \tag{90}$$

Which rearranges to:

$$\mathbf{J}_i^s = \mathcal{D}_{in}^{\infty} \frac{x_i c_t}{a_i^{\circ x}} \nabla a_i^{\circ x} \tag{91}$$

The molar flux can be calculated by assuming the velocity of the solvent is zero and by inserting (91) in (73):

$$\mathbf{N}_i = \mathcal{D}_{in}^{\infty} \frac{x_i c_t}{a_i^{\circ x}} \nabla a_i^{\circ x} \quad (\mathbf{u}_s = \mathbf{0}) \tag{92}$$

Comparing (86) and (91) shows that the result is different from the above expected result. It is noteworthy that the thermodynamic factors have not been assumed to follow ideality. They are therefore not given by $\Gamma_{ii}=1$ and $\Gamma_{ij,i\neq j}=0$.

3.4.3 The Nernst-Planck equation

The Nernst-Planck equation gives a more correct description of the flux in electrolyte solutions. Still some significant assumptions are introduced which may be regarded as rough approaches in moderately concentrated solutions having an ionic strength above 0.01 *mol/kg H$_2$O*.

Equivalent to the Fick model the thermodynamic factor is assumed ideal, $\Gamma_{ii} = 1$ and $\Gamma_{ij,i\neq j} = 0$. The driving force is then given by:

$$-\mathbf{d}_i^{driv} = \frac{RT}{x_i}\nabla x_i + z_i F\nabla\phi \tag{68}$$

The solvent concentration is assumed to be high compared to all other ions, $x_s = 1$, $x_{i\neq s} \approx 0$. Since the solutes are assumed infinite dilute, the only diffusivity used is the infinite dilute between ion and solvent, $Ð_{is}^{\infty}$. Contributions to the $\underline{\underline{B^s}}$ is given by

$$B_{ii}^s = \frac{x_s}{Ð_{is}^{\infty}} = \frac{1}{Ð_{is}^{\infty}}, \quad B_{ij}^s = 0 \tag{93}$$

Taking (68) and (76) using $\underline{\underline{B^s}}$ from (93) inserted in (82) results in

$$-\mathbf{d}_i = \frac{RT}{x_i}\nabla x_i + z_i F\nabla\phi = -\frac{RT}{x_i c_t Ð_{is}^{\infty}}\mathbf{J}_i^s \tag{94}$$

Rearranging (94) gives the diffusion fluxes, J_i^s

$$\frac{\mathbf{J}_i^s}{c_t} = -Ð_{is}^{\infty}\nabla x_i - Ð_{is}^{\infty}\frac{x_i z_i F}{RT}\nabla\phi \tag{95}$$

The molar fluxes are then given by the following expression by combining (73) and (95) in:

$$\frac{\mathbf{N}_i}{c_t} = -Ð_{is}^{\infty}\nabla x_i - Ð_{is}^{\infty}\frac{x_i z_i F}{RT}\nabla\phi + x_i\mathbf{u}_s \tag{96}$$

Equation (96) is known as the *Nernst-Planck equation*. Usually the potential gradient $\nabla\phi$ is unknown and needs to be either estimated or calculated separately from other relations.

The following derivation considers a procedure which can be performed in order to reach a relation where $\nabla\phi$ is expressed from known variables.

The current carried by the solution is calculated by summing over the fluxes and weighting with respect to ionic charge:

$$\boldsymbol{i} = F \sum_{j=1}^{n} z_j \mathbf{N}_j \tag{97}$$

From (96) and (97) the resulting equation is

$$\boldsymbol{i} = -c_t F \sum_{j=1}^{n} z_j Ð_{js}^{\infty} \nabla x_j - c_t \frac{F^2}{RT} \nabla \phi \sum_{j=1}^{n} Ð_{js}^{\infty} x_j z_j^2 \tag{98}$$

The solvent reference velocity is neglected due to electroneutrality:

$$\sum_{j=1}^{n} c_t z_j x_j u_s = c_t u_s \sum_{j=1}^{n} z_j x_j = 0 \tag{99}$$

To simplify (98) the following three definitions are used, the equivalent conductivity of species i, $\mathcal{K}_i$:

$$\mathcal{K}_i \equiv \frac{F^2}{RT} c_t x_i z_i^2 Ð_{is}^{\infty} \tag{100}$$

The equivalent total conductivity of the solution, $\mathcal{K}_t$:

$$\begin{aligned} \mathcal{K}_t &\equiv \sum_{i=1}^{n} \mathcal{K}_i \\ &= \frac{F^2}{RT} c_t \sum_{i=1}^{n} x_i z_i^2 Ð_{is}^{\infty} \end{aligned} \tag{101}$$

and the transference number of species i which essentially is the current related to species i, t_i:

$$t_i \equiv \frac{\mathcal{K}_i}{\mathcal{K}_t} \tag{102}$$

Applying the above definitions reduces (98) to

$$\boldsymbol{i} = -c_t F \sum_{j=1}^{n} z_j Ð_{js}^{\infty} \nabla x_j - \mathcal{K}_t \nabla \phi \tag{103}$$

which can be rearranged to a relation of the gradient of the electrical potential:

$$\nabla \phi = -\frac{\boldsymbol{i}}{\mathcal{K}_t} - c_t \frac{F}{\mathcal{K}_t} \sum_{j=1}^{n} z_j Ð_{js}^{\infty} \nabla x_j \tag{104}$$

Inserting (104) in (96) result in an equation of the molar flux without the potential gradient:

$$\frac{\mathbf{N}_i}{c_t} = -\DJ_{is}^{\infty}\nabla x_i + x_i \mathbf{u}_s + \DJ_{is}^{\infty}\frac{x_i z_i F}{RT}\left(\frac{\boldsymbol{i}}{\mathcal{K}_t} + \frac{c_t F}{\mathcal{K}_t}\sum_{j=1}^{n} z_j \DJ_{js}^{\infty}\nabla x_j\right) \tag{105}$$

By insertion of (102) reduces the above to

$$\mathbf{N}_i = -c_t \DJ_{is}^{\infty}\nabla x_i + \boldsymbol{i}\,\frac{t_i}{Fz_i} + \frac{c_t t_i}{z_i}\sum_{j=1}^{n} z_j \DJ_{js}^{\infty}\nabla x_j + c_t x_i \mathbf{u}_s \tag{106}$$

For batteries the current is not zero, $\boldsymbol{i} \neq 0$, but in chromatographic processes or ion exchange processes, there is no current flowing through the diffusive layer. For this kind of processes it can be assumed that the current is zero:

$$\boldsymbol{i} = 0 \tag{107}$$

Which simplifies (106) to

$$\mathbf{N}_i = -c_t \DJ_{is}^{\infty}\nabla x_i + \frac{c_t t_i}{z_i}\sum_{j=1}^{n} z_j \DJ_{js}^{\infty}\nabla x_j + c_t x_i \mathbf{u}_s\,, \quad \text{for } \boldsymbol{i} = 0 \tag{108}$$

This is the Nernst-Planck equation assuming that the solution does not transport current over the diffusive layer which avoids the problems in calculating the potential gradient. Comparing equation (108) to the Fickian diffusion model, a model which looks like the Fickian model may be set up:

$$\mathbf{N}_i = -c_t \DJ_{is}^{eff}\nabla x_i + c_t x_i \mathbf{u}_s\,, \quad \text{for } \boldsymbol{i} = 0 \tag{109}$$

where $\DJ_{is}^{eff}$ is the observed effective diffusivity. The coefficient contains a term related to normal transport and a term from migration due to a potential difference. Comparing (108) to (109) it is clear that the effective diffusion is given by

$$\DJ_{is}^{eff} = -\DJ_{is}^{\infty} + \left(\frac{t_i}{z_i}\sum_{j=1}^{n} z_j \DJ_{js}^{\infty}\nabla x_j\right)\frac{1}{n_{dim}}\nabla^{-1}x_i\,, \quad \text{for } \boldsymbol{i} = 0 \tag{110}$$

The effective diffusivity is a function of the infinite dilution diffusivity and a term related to the potential gradient. $\nabla^{-1}x_i$ is a vector of reciprocal gradients and n_{dim} is the number of dimensions in ∇. $\frac{1}{n_{\dim}}\nabla^{-1}x_i$ reduces to one by multiplication of ∇x_i.

3.4.4 Simple Extension of the Nernst-Planck equation

Instead of assuming the liquid to be ideal, we extend the expression to a diffusion scheme, where part of the thermodynamic factor is retained in the equations. The thermodynamic factor between component i and it self, Γ_{ii}, is assumed to follow (62) but other factors are assumed to be ideal $\Gamma_{ij\neq i} = 0$. This scheme is chosen since the driving force for component i then only contains the gradient of component i and not the gradients of other species. It may be illustrated by an example: For the binary system given by (85), $\Gamma_{12}=0$ and $\mathbf{d}_1$ is therefore only related to ∇x_1 and not to ∇x_2.

The infinite dilution diffusivities between a component and the solvent, $Ð_{is}^{\infty}$, are applied since diffusivity rarely deviates at higher concentrations. This is discussed by Wesselingh and Krishna[6] *p.* 131. The $\underline{B}^{s}$ matrix is then given by:

$$B_{ii}^{s} = \frac{x_s}{Ð_{is}^{\infty}}, \qquad B_{ij}^{s} = 0 \tag{111}$$

x_s is the mol fraction of solvent and it is not assumed to be $x_s \approx 1$. However other contributions to the $\underline{B}^{s}$ are neglected. The above assumptions result in the following equation equivalent to the derivation of (94)

$$-\mathbf{d}_i = \frac{RT}{x_i}\Gamma_{ii}\nabla x_i + z_i F\nabla\phi = -\frac{RTx_s}{x_i c_t Ð_{is}^{\infty}}\mathbf{J}_i^s \tag{112}$$

This can be rearranged to the diffusion flux as a function of the thermodynamic factor and the potential gradient.

$$\frac{\mathbf{J}_i^s}{c_t} = -Ð_{is}^{\infty}\frac{1}{x_s}\Gamma_{ii}\nabla x_i - Ð_{is}^{\infty}\frac{x_i z_i F}{x_s RT}\nabla\phi \tag{113}$$

The thermodynamic factor may be calculated by an activity coefficient model. The molar flux is, from (73):

$$\frac{\mathbf{N}_i}{c_t} = -Ð_{is}^{\infty}\frac{1}{x_s}\Gamma_{ii}\nabla x_i - Ð_{is}^{\infty}\frac{x_i z_i F}{x_s RT}\nabla\phi + x_i\mathbf{u}_s \tag{114}$$

The current is now given by the following expression similar to (103) using (97)

$$\boldsymbol{i} = -c_t F\sum_{j=1}^{n} z_j Ð_{js}^{\infty}\frac{1}{x_s}\Gamma_{ii}\nabla x_j - \frac{\mathcal{K}_t}{x_s}\nabla\phi \tag{115}$$

Rearranging to isolate the electrical potential gradient, $\nabla\phi$, and assuming the current to be

$$\boldsymbol{i} = 0 \tag{116}$$

Then equation (117) is obtained similar to (108)

$$\frac{\mathbf{N}_i}{c_t} = -Ð_{is}^{\infty}\frac{1}{x_s}\Gamma_{ii}\nabla x_i + \frac{t_i}{z_i}\sum_{j=1}^{n} z_j Ð_{js}^{\infty}\Gamma_{ii}\nabla x_j + x_i\mathbf{u}_s \ , \quad \text{for } \boldsymbol{i} = 0 \tag{117}$$

where the ion-ion interaction is maintained. Comparing the result to (108) shows that the two equations are more or less the same except the contribution from the thermodynamic factor and the mol fraction of solvent, x_s, is included.

3.4.5 Estimating missing diffusivities

The thermodynamic factors need to be calculated and Maxwell-Stefan diffusivities need to be known in order to solve the full diffusion problem. Then the molar fluxes can be calculated from (83). One bootstrap relation, which simplifies the calculation, is zero solvent velocity. This is valid at low flow conditions. Additional bootstrap relations must be supplied in order to solve the problem since only n-1 independent flux equations may be written.

The thermodynamic factors are obtained from a thermodynamic model. The Maxwell-Stefan diffusivities are most likely not available in the open literature, remembering that $\frac{1}{2}n(n-1)$ diffusivities are needed. Some of the diffusivities are tabulated, e.g. it can be assumed that the infinite dilution diffusivities between solvent and other species are valid in the concentration range of interest, $Ð_{is} \approx Ð_{is}^{\infty}$. $Ð_{is}^{\infty}$ are usually found in data collections. The missing inter-ionic diffusivities may be estimated from $Ð_{is}$ using the correlation from Wesselingh and Krishna[6]:

$$Ð_{ij} \approx \frac{Ð_{is} + Ð_{js}}{2} \frac{i^{0.55}}{\left|z_j z_i\right|^{2.3}}, \quad i = 0.5 \sum_{k=1}^{n} z_k^2 x_k \qquad (118)$$

4 Theory of electrochemical kinetics and corrosion

Corrosion sustained by a current flow is referred to as electrochemical corrosion. This type of corrosion is the basis of many corrosion mechanisms. Crevice corrosion is one of these types. It is caused by galvanic differences between metals or due to formation of concentration cells in a cavity. Corrosion is therefore sustained due to concentration difference between the bottom of the cavity compared to the outer surface. This is similar to pitting or corrosion under insulation (CUI). De-alloying and intergranular corrosion are also caused by a galvanic action where the individual grains or crystals of the alloy are attacked. CO_2 corrosion is also an electrochemical corrosion process.

In this chapter the basic theory of electrochemical kinetics is presented. The current understanding of the theory is extended in the sections below and the theory given in section 4.3.2 to 4.3.4 has not been presented before.

4.1 Electrochemical kinetics

Electrochemical corrosion is described by two or more half cell reaction which exchange electrons through a conducting medium. One half cell is typically the dissolution of metal by oxidation at the anode. The general reaction is written by:

$$M \rightleftharpoons M^{z+} + ze^-$$
(119)

The other half cell is the reduction of a compound in the liquid phase at the cathode. This could be $Y=H^+$ or $Y=HCO_3^-$ or both at the same time.

$$Y^{-m} + ze^- \rightleftharpoons Y^{-(n+z)}$$
(120)

If one of the reactions stops, then the other also stops, since the production and consumption of electrons is no longer sustained as shown by figure 4.
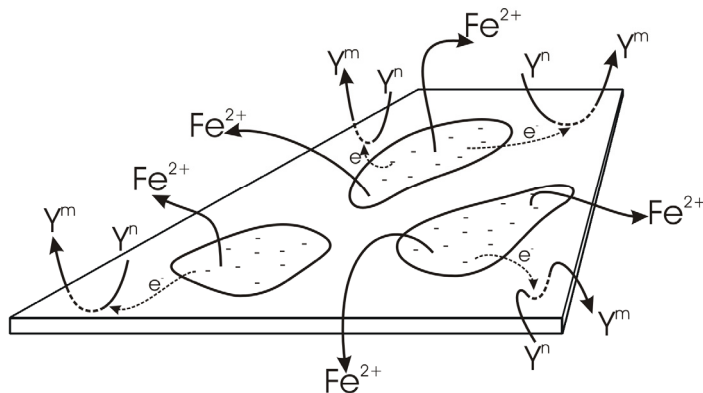

Figure 4: At the anode, metal is dissolved by oxidation of *Fe*; the electrons are transported trough the metal to the cathode area where they go into reduction of other species.

Figure 5 shows the current density in A/m^2 as function of the electrical potential of one half cell reaction, (119). A similar plot could be shown for reaction (120). The figure shows the current produced and consumed by reaction (119). The process always runs forward and backward and it is reversible. The net reaction and current density are dependent on the electrical potential in volts. Figure 5 shows an idealised view of the electrochemical process. In reality at least two half cell reactions would run simultaneously and exchange electrons. Figure 6 shows a more realistic scheme where two half cells react and exchange current. It shows how both cells run forward and backward. The net current is a sum of all anodic and cathodic currents.
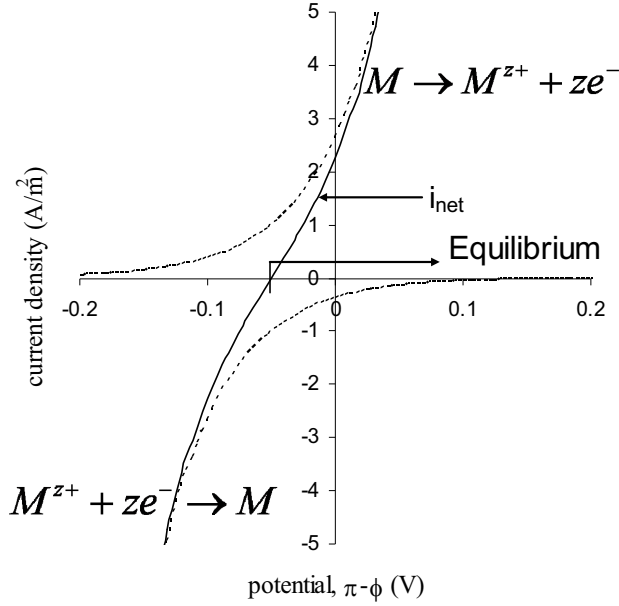

Figure 5: Current density produced and consumed by a half cell reaction.

Within electrochemistry two terms are typically used in order to describe the electrochemical process, these are called "polarization" and "overpotential".
A half cell is said to be polarized if the applied current has changed the potential compared to the half cell equilibrium potential. The overpotential is the voltage by which a half cell has polarized. The overpotential, η, is defined by:

$$\eta \equiv (\pi - \phi) - (\pi - \phi)^{eq} \tag{121}$$

$(\pi\text{-}\phi)$ is the electrical potential difference between the metal and the liquid. Little polarization is seen if a small current is allowed to flow between two half cells. In corrosion there is no control of the current flow and the system is short-circuited. This indicates that the current is allowed to flow freely.
The corrosion process is a multiple step mechanism. M is oxidized to M^+ which involves transport of Y^m to the electrode surface, combination of ions with electrons at the metal surface and diffusion of M^+ away from the surface. Ideally the process

would run instantly, but in reality the oxidation is finite, being limited by the slowest step, also known as the rate determining step (rds).

The total resistance towards current flow may be viewed as a series of equivalent resistances in series, related to the steps in the corrosion process.
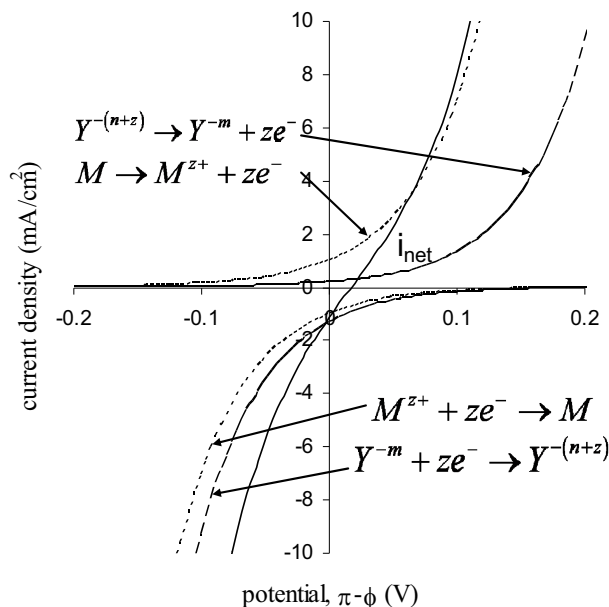

Figure 6: Current density of two half cells.

The overpotential of a half cell reaction is related to these resistances. Four types of mechanisms are typically taken into account:

- Activation polarization
- Concentration polarization
- Reaction polarization
- Resistance polarization (IR drop)

Activation polarization is by far the most important of the four. It is related to the transfer of ions at the metal surface and through the surface during the half cell reaction. The electrons must cross and activation energy barrier in order to proceed.
Concentration polarization is caused by the mass transport of ions to and from the metal surface. If the charge transfer at the electrode is very fast, it may result in a lack of reacting ions at the electrode surface which slows the overall corrosion process. This is often related to slow diffusing compounds retarded by e.g. a film of corrosion product.
Reaction polarization is related to the slow reaction in other parts of the systems not directly related to the surface. This could for example be the dissolution process of $CO_2(g)$ into the liquid phase or other electrolytic speciation reactions in the liquid.
Resistance polarization (IR drop) is observed when measuring current as function of an applied electrical potential and it is related to the resistance of the liquid.

4.2 Activation polarization

Activation polarization was discovered by Julius Tafel in the beginning of the 20th century. He showed experimentally that an applied potential is a logarithmic function the current density. In the following sections a basic set of equations is given with the purpose to show the nomenclature and relations of electrode kinetics.

Consider the electrochemical reaction:

$$\text{Red} \underset{k_b}{\overset{k_f}{\rightleftharpoons}} \text{Ox} + ne^- \tag{122}$$

Red is the reduced species and *Ox* is the oxidised species similar to reaction (119) and (120). k_f and k_b are the forward and backward rate constants, and *n* is the number of electrons produced. The reaction is said to be oxidation and anodic if the net process is forward. Similar the reaction backward is a reduction and cathodic. In principle *Red* and *Ox* are groups of species which are defined by:

$$\text{Red} = \sum_R v_R R, \qquad \text{Ox} = \sum_X v_X X \tag{123}$$

v_i is the stochiometric coefficient of component *i*. *R* and *X* are the reduced and oxidized compounds respectively.

It is assumed in the following derivation that the electron transfer mechanism is a simple one-step reaction. This indicates that the mechanism only contains one elementary reaction. Electrons are often not transferred this way but one by one through numerous elementary reactions. The mechanisms can become complicated for multi electron transfers especially mechanisms which include adsorption phenomena. The theory for this kind of processes may be derived from the equations presented below.

The net current density is the sum of the anodic and cathodic currents:

$$i_{net} = i_a + i_c \tag{124}$$

The anodic current, i_a, is determined by the forward reaction of (122) which is positive, and the cathodic current, i_c, is the backward reaction which is negative. It is important to note that the current density is a function of the electrode areas and they are assumed not to change during the electrochemical process.

The current densities are proportional to the rate of reaction. They are defined by:

$$i_a = nFv_f, \qquad i_c = -nFv_b \tag{125}$$

F is the Faraday's constant and v_f and v_b are the forward and backward rates per area. The rate of reaction is related to the concentrations of the species in reaction (122):

$$v_f = k_f a_{\text{Red}}^*, \qquad v_b = k_b a_{\text{Ox}}^* \tag{126}$$

a are the activities, typically the molar unsymmetrical activities are used. Preferably the rational unsymmetrical should be used. Here the asterisk, *, signifies surface activities. This indicates that the activities are determined at the electrode surface. The bulk concentrations are usually not applicable since the mass transport influences the

liquid composition at the surface. Therefore the surface and bulk concentrations are not the same. k_f and k_b are the forward and backward rate constant and a^*_{Red} and a^*_{Ox} are the activity product of reactants and products, which are consistent with definition (123):

$$a^*_{\text{Red}} = \prod_R \left(a_R^{v_R}\right)^*, \qquad a^*_{\text{Ox}} = \prod_X \left(a_X^{v_X}\right)^* \tag{127}$$

Inserting (125) and (126) in (124) reveals the net current density:

$$i_{net} = nF\left(k_f a^*_{\text{Red}} - k_b a^*_{\text{Ox}}\right) \tag{128}$$

forward and backward rate are equal at equilibrium and the net current density is therefore zero, i_{net}=0. From the theory of Koryta and Dvorak[9] and Rubinstein[10], it is given that the following Arrhenius type equation is valid for the rate constant:

$$k_b = P_b \exp\left(-\frac{\Delta H_b^0 + \alpha n F\left(\pi - \phi\right)}{RT}\right), \; k_f = P_f \exp\left(-\frac{\Delta H_f^0 - \left(1-\alpha\right)nF\left(\pi - \phi\right)}{RT}\right) \tag{129}$$

P is the pre-exponential factor and α is the charge transfer coefficient. The nominator in the exponential terms of (129) is the surface electron transfer activation energy. P and ΔH^0 are independent of the electrode potential. α is 0<α<1 and typically α=0.5. This is only true for reactions represented by (122) because only one elementary reaction takes place.

In order to derive a rate constant which is independent of ΔH^0 and liquid composition, it is necessary to introduce the standard state potential, $\left(\pi - \phi\right)^\circ$. In the standard state the potential is equal to the standard state potential, $\left(\pi - \phi\right) = \left(\pi - \phi\right)^\circ$. In this state the activities are one, $a^*_{\text{Red}} = a^*_{\text{Ox}} = 1$, as indicated by (16). At equilibrium the current is zero, i_{net}=0, and therefore (128) becomes $k_f a^*_{\text{Red}} = k_b a^*_{\text{Ox}}$ which gives $k_f = k_b$. In combination with (129) this gives:

$$
\begin{aligned}
k^\circ &= k_f = k_b \\
&= P_b \exp\left(-\frac{\Delta H_b^0 + \alpha n F\left(\pi - \phi\right)^\circ}{RT}\right) \\
&= P_f \exp\left(-\frac{\Delta H_f^0 - \left(1-\alpha\right)nF\left(\pi - \phi\right)^\circ}{RT}\right)
\end{aligned}
\tag{130}
$$

k° is the rate constant at equilibrium at the standard state. One could choose another state as standard state, e.g. the equilibrium state. Then the potential would be equal to $\left(\pi - \phi\right) = \left(\pi - \phi\right)^{eq}$ and i_{net}=0. If this potential was used, then k becomes concentration dependent, since $\left(\pi - \phi\right)^{eq}$ is concentration dependent through the Nernst equation. It is therefore important that literature values of k are used with care, in order to

determine which standard state was used. It is of cause also important to recognise for which systems it can be applied because some rate constants are obviously concentration dependent. Dividing (129) by (130) reveals the following relations:

$$k_b = k^\circ \exp\left(\frac{-\alpha nF\left((\pi-\phi)-(\pi-\phi)^\circ\right)}{RT}\right), \; k_f = k^\circ \exp\left(\frac{(1-\alpha)nF\left((\pi-\phi)-(\pi-\phi)^\circ\right)}{RT}\right) \quad (131)$$

By defining $\Delta\pi^\circ \equiv (\pi-\phi)-(\pi-\phi)^\circ$ and inserting (131) in (128) gives:

$$i_{net} = nFk^\circ\left(\exp\left(\frac{(1-\alpha)nF\Delta\pi^\circ}{RT}\right)a_{Red}^* - \exp\left(\frac{-\alpha nF\Delta\pi^\circ}{RT}\right)a_{Ox}^*\right) \quad (132)$$

The activities of the compounds at the surface, a^*, can not be measured and are typically not equal to the bulk activities. Instead we may rewrite (132) as a function of the equilibrium potential. This potential is important in relation to corrosion. The Nernst equation written for reaction (122) is a function of the standard state potential and the surface activities:

$$(\pi-\phi) = (\pi-\phi)^\circ + \frac{RT}{nF}\ln\frac{a_{Ox}^*}{a_{Red}^*} \quad (133)$$

Liquid phase composition will distribute evenly up to the electrode surface at equilibrium. The Nernst equation (133) at equilibrium is therefore a function of the bulk concentration since the activities in the bulk and at the surface are identical. The equilibrium potential, $(\pi-\phi)^{eq}$, is therefore calculated by:

$$(\pi-\phi)^{eq} = (\pi-\phi)^\circ + \frac{RT}{nF}\ln\frac{a_{Ox}}{a_{Red}} \quad (134)$$

Substitution of $(\pi-\phi)^\circ$ in (132) by (134) reveals:

$$i_{net} = nFk^\circ \exp\left(\frac{(1-\alpha)nF\left((\pi-\phi)-(\pi-\phi)^{eq}\right)}{RT}\right)\left(\frac{a_{Ox}}{a_{Red}}\right)^{1-\alpha}a_{Red}^*$$

$$-nFk^\circ \exp\left(\frac{-\alpha nF\left((\pi-\phi)-(\pi-\phi)^{eq}\right)}{RT}\right)\left(\frac{a_{Ox}}{a_{Red}}\right)^{-\alpha}a_{Ox}^* \quad (135)$$

k° is still not a function of the liquid concentration. The net current density has become a function of both surface and bulk activities. Equation (135) reduces to the following equation by insertion of (121)

$$i_{net} = i_0 \left(\frac{a_{Red}^*}{a_{Red}} \exp\left(\frac{(1-\alpha)nF\eta}{RT} \right) - \frac{a_{Ox}^*}{a_{Red}} \exp\left(\frac{-\alpha nF\eta}{RT} \right) \right) \qquad (136)$$

Where i_0 is the exchange current density defined by:

$$i_0 \equiv nFk^{\circ} \left(a_{Ox} \right)^{1-\alpha} \left(a_{Red} \right)^{\alpha} \qquad (137)$$

i_0 is the current density at equilibrium where the backward and forward reaction rate of (122) are equal.

A high i_0 correspond to a case with no activation control. This is equivalent to a complete reversible behaviour where equilibrium is obtained instantly. It corresponds physically to a surface where the activation energy to transport electrons is low and the electron transport is high. This is also known as a Nernstian behaviour.

If i_0 is low then electron transport is low and the reaction runs slowly.

One way to determine the charge transfer coefficient, α, is to plot i_0 as a function of a_{Ox} and a_{Red} and α is determined through (137).

By assuming that bulk activities and surface activities are equal then $a^*=a$. This reduces equation (136) to the well known *Volmer-Butler equation*:

$$i_{net} = i_0 \left(\exp\left(\frac{(1-\alpha)nF\eta}{RT} \right) - \exp\left(\frac{-\alpha nF\eta}{RT} \right) \right) \qquad (138)$$

This equation gives an idealised representation of a system. In this equation it is assumed that the electrode does not have a diffusion film up to the surface. The Volmer-Butler equation is only valid at constant activity, since η and i_0 are concentration dependent through equations (134) and (137) respectively. The anodic, i_a, and cathodic, i_c, current densities listed in equation (124) are given by the following relation, obtained from (138):

$$i_a = i_0 \exp\left(\frac{(1-\alpha)nF\eta}{RT} \right), \quad i_c = -i_0 \exp\left(\frac{-\alpha nF\eta}{RT} \right) \qquad (139)$$

the two currents are impossible to measure independently even though they are given explicitly by (139). Plots of equations (138) and (139) are shown in figures 7 and 8. It is seen how the net current density is the sum of the anodic and cathodic current densities. At equilibrium $(\pi - \phi) = (\pi - \phi)^{eq}$ and $i_{net}=0$, but i_a and i_c are not zero. The difference between i_a and i_c is the exchange current, i_0. Figure 8 shows a logarithmic plot of the numerical current in figure 7. The dotted lines are the anodic and cathodic currents in (139). The cathodic current approaches zero, $i_c \rightarrow 0$, at high overpotential where $\eta >> -0.05$ and i_{net} moves asymptotically towards i_c. Similarly for low overpotential, $\eta << -0.05$, $i_{net} \rightarrow i_a$.

i_a and i_c meet in the encircled point which is $((\pi-\phi)^{eq}, i_0)$. i_0 is typically determined by intersection of the asymptotical values of i_{net} at high and low η in figure 8.
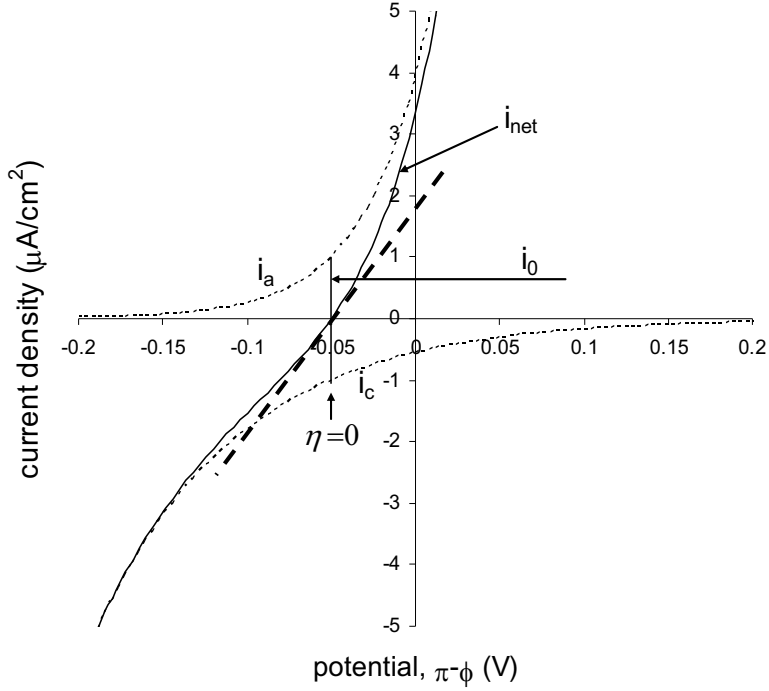
Figure 7: The net current density, i_{net}, is a sum of the anode and cathode current densities, i_a and i_c. Plotted for $i_0=1\mu A/cm^2$, $\alpha=0.3$. Note how $\eta=0$ at $i_{net}=0\mu A/cm^2$ where $(\pi-\phi)^{eq}=-0.05V$. The thick dashed line shows the slope of i_{net} at $(\pi-\phi)\rightarrow(\pi-\phi)^{eq}$ also known as the polarization resistance, R_p.
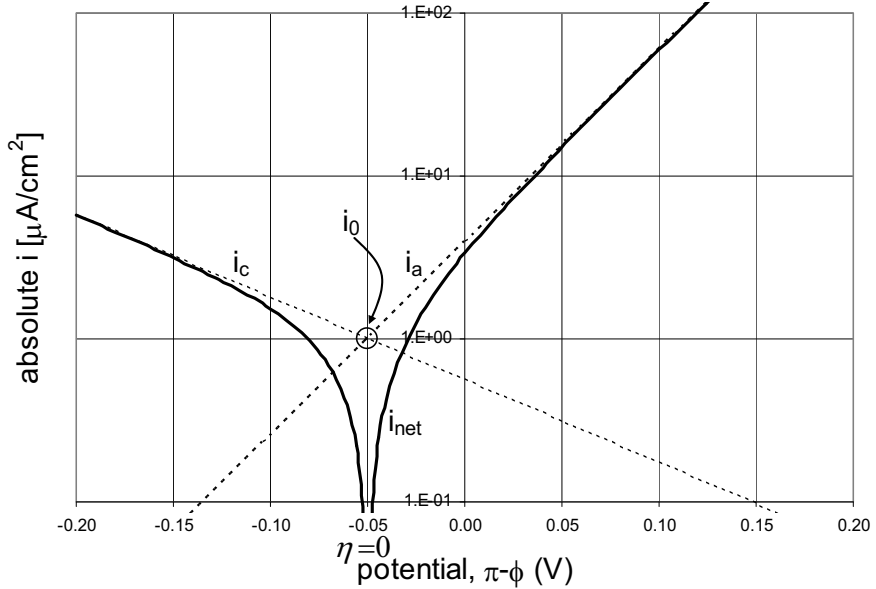

Figure 8: Showing the same as figure 7 just represented in a numerical log plot of the current density.

4.2.1   General activation controlled kinetics

In the above equations it was assumed, that one elementary reaction took place. It was also assumed that it transferred all the electrons in one step.

In reality electrons are transferred in several steps. One of the steps is the rate determining step and it has a much lower i_0 value than all the other reactions. It is therefore the bottleneck of electron transfer.

An empirical equation similar to (136) and (138), which is applicable to real system, contains an anodic and a cathodic current density. The *rds* of the two are not the same and the charge transfer coefficient, α, of the anode and cathode are therefore not the same. Then α and $(1-\alpha)$ in equation (136) or (138) becomes decoupled and may instead be represented by two separate empirical variables, α_c and α_a, for the cathode and anode. A general empirical Volmer-Butler equation is then

$$i_{net} = i_0 \left(\exp\left(\frac{\alpha_a nF\eta}{RT} \right) - \exp\left(\frac{-\alpha_c nF\eta}{RT} \right) \right) \tag{140}$$

The α's are no longer bound the same way as in (136) and (138). The α's may become higher then one but not less than zero. The new charge transfer coefficients are found experimentally from voltamograms where a potential is applied while the current density is measured. A more general equation can be given, if information are known of the *rds* or the number of electrons transferred, see Rubinstein[10].

A general set of equation for activation controlled reactions may be written. If all reactions are similar to (122), then the total transferred current is the sum of all currents transferred from the kth reaction:

$$i_{net} = \sum_k i_{net,k} \tag{141}$$

The general Volmer-Butler description follows by combining (138) and (141):

$$i_{net} = \sum_k i_{0,k} \left(\exp\left(\frac{(1-\alpha_k)n_k F\eta_k}{RT} \right) - \exp\left(\frac{-\alpha_k n_k F\eta_k}{RT} \right) \right) \tag{142}$$

There is a new exchange current density, $i_{0,k}$, charge transfer coefficient, α_k, electron number, n_k, and overpotential, η_k, for every k redox reaction. η_k is defined relative to the equilibrium potential of the k'th reaction by:

$$\eta_k \equiv (\pi - \phi) - (\pi - \phi)^{eq,k} \tag{143}$$

4.2.2   The Tafel law

The study by Tafel[11] revealed experimentally that a measured current density is an exponential function of the applied overpotential as shown by figure 8. It was shown that for potentials far from equilibrium, that is $\eta \gg 0$ or $\eta \ll 0$, follow a relation of the form:

$$\eta = a + \beta \log i \tag{144}$$

Where a and β are regressed parameters. This relation is equivalent to the following equation if $a=-\beta\log(i_0)$:

$$\eta = \beta \log\left(\frac{i}{i_0}\right) \tag{145}$$

It is evident that equations (138) and (139) reveals the same result at $\eta>>0$ and $\eta<<0$. Because equation $(138)\rightarrow i_0 10^{(\eta/\beta_a)}$ for $\eta\rightarrow\infty$ and equation $(138)\rightarrow -i_0 10^{(-\eta/\beta_c)}$ for $\eta\rightarrow-\infty$. Where the anodic and cathodic Tafel constants, β_a and β_c, are defined by:

$$\beta_a = \frac{\ln(10)RT}{nF(1-\alpha)}, \qquad \beta_c = \frac{\ln(10)RT}{nF\alpha} \tag{146}$$

Figure 8 shows the logarithmic plot of the current density of figure 7. This type of plot is known as a Tafel plot. The slope of the asymptotical values at $\eta>>(\pi-\phi)^{eq}$ and $\eta<<(\pi-\phi)^{eq}$ are β_a and β_c. The two constant are usually determined experimentally from a plot similar to figure 8 and then evaluate together with (146) in order to determine what $n\cdot\alpha$ is.

4.2.3 Stern and Geary's theory

The basis of modern electrochemical corrosion theory was presented by Stern and Geary[12] (SG) and discussed in detail by Stern[13,14]. They assumed that two redox reactions of (122) contribute to the net current density. It was additionally assumed that the anode is only anodic and the cathode is only cathodic. This implies that the anodic reaction only runs forward and the cathode reaction only runs backward. This assumption is valid far from the equilibrium potential of the two reactions. The equations are derived from (142) for a system of two redox reactions:

$$i_{net} = \underbrace{i_{02}\exp\left(\frac{(1-\alpha_2)n_2F\eta_2}{RT}\right)}_{i_{net,2}} \underbrace{-i_{01}\exp\left(\frac{-\alpha_1 n_1 F\eta_1}{RT}\right)}_{i_{net,1}} \tag{147}$$

The net current is a sum of the two redox reactions and subscript 1 identifies the first redox and subscript 2 the second. It should be noted that reaction 1 is only cathodic and reaction 2 is only anodic. The anodic part of reaction 1 and the cathodic part of reaction 2 have been neglected. Therefore two different exchange current densities are obtained, i_{01} and i_{02}. But also two different α's, η's and n's since they are related to each their redox reaction. The equilibrium potential of the two reactions are not the same and therefore $\eta_1\neq\eta_2$ since $(\pi-\phi)^{eq,1}\neq(\pi-\phi)^{eq,2}$.

When the corrosion process runs freely, then the potential is equal to the corrosion potential $(\pi-\phi)=(\pi-\phi)^{corr}$. The net current density is zero, $i_{net}=0$, since the cathode consumes the exact same amount of electron produced by the anode. This is of cause only true when electrons are not supplied from the outside. During corrosion, equation (147) reduces to $i_{corr}=i_{net,1}=-i_{net,2}$ since $i_{net}=0$. i_{corr} is similar to the exchange current density, i_0. i_{corr} is used in the corroding system of multiple redox reactions. i_0 is related

to a single redox reaction. i_{corr} is therefore the current which flows during corrosion. It is determined from (147) and $i_{net}=0$ by

$$i_{net} = i_{net,2} + i_{net,1} = 0 \text{ at } (\pi - \phi) = (\pi - \phi)^{corr} \Rightarrow$$

$$i_{corr} = i_{02} \exp \left(\frac{(1-\alpha_2) n_2 F \left((\pi - \phi)^{corr} - (\pi - \phi)^{eq,2} \right)}{RT} \right) \tag{148}$$

$$= i_{01} \exp \left(\frac{-\alpha_1 n_1 F \left((\pi - \phi)^{corr} - (\pi - \phi)^{eq,1} \right)}{RT} \right)$$

On substituting i_{01} and i_{02} from (148) in (147) results in the net current as function of i_{corr}:

$$i_{net} = i_{corr} \left(\exp \left(\frac{(1-\alpha_2) n_2 F \left((\pi - \phi) - (\pi - \phi)^{corr} \right)}{RT} \right) - \exp \left(\frac{-\alpha_1 n_1 F \left((\pi - \phi) - (\pi - \phi)^{corr} \right)}{RT} \right) \right)$$

$$= i_{corr} \left(\exp \left(\frac{(1-\alpha_2) n_2 F \eta^{corr}}{RT} \right) - \exp \left(\frac{-\alpha_1 n_1 F \eta^{corr}}{RT} \right) \right) \tag{149}$$

Where the corrosion overpotential, η^{corr}, is defined by:

$$\eta^{corr} = (\pi - \phi) - (\pi - \phi)^{corr} \tag{150}$$

By rearranging (149) as a function of the 10-base logarithm and using the Tafel constant from (146), gives the following expression of the net current density:

$$i_{net} = i_{corr} \left(10^{\eta^{corr}/\beta_{a2}} - 10^{-\eta^{corr}/\beta_{c1}} \right) \tag{151}$$

β_{a2} and β_{c1} are not identical since $\alpha_1 \neq \alpha_2$ and $n_1 \neq n_2$. By expanding the above logarithmic terms in (151) by a first order Taylor series results in the following relation of the net current density:

$$i_{net} = i_{corr} \ln(10) \eta^{corr} \left(\frac{1}{\beta_{a2}} + \frac{1}{\beta_{c1}} \right)$$

$$= i_{corr} \ln(10) \eta^{corr} \left(\frac{\beta_{a2} + \beta_{c1}}{\beta_{a2} \beta_{c1}} \right) \tag{152}$$

This equation is only valid at low overpotentials due to the Taylor expansion. The corrosion current density, i_{corr}, is calculated by rearrangement of the above:

$$i_{corr} = \frac{i_{net}}{\ln(10)\eta^{corr}} \left(\frac{\beta_{a2}\beta_{c1}}{\beta_{a2} + \beta_{c1}} \right)$$

$$= \frac{1}{\ln(10)R_p} \left(\frac{\beta_{a2}\beta_{c1}}{\beta_{a2} + \beta_{c1}} \right) \tag{153}$$

which is known as the original *Stern and Geary equation*. The polarization resistance, R_p, follows Ohm's law at low polarization and it is defined by:

$$\frac{1}{R_P} = \frac{i_{net}}{\eta^{corr}} \tag{154}$$

η^{corr} is typically applied in a broad interval while i_{net} is measured. This is done in order to determine the β values through a Tafel plot as mentioned previously. R_P is determined online by polarizing the corrosion cell both anodic and cathodic. The slope of a (η^{corr}, i_{net}) plot reveals R_P. This is shown as an example in figure 7 as the thick dashed line. Thereby i_{corr} may be determined through equation (154) and it can be converted directly to corrosion rate in *mm/year* which is illustrated below.
The SG equation is only valid if activation polarization is the only corrosion mechanism. It is also assumed the net current may be described by (147). Therefore it is assumed that the cathodic reaction of the anode and the anodic reaction of the cathode do not contribute significantly to i_{net}. A consequence is that the theory is only valid if the corrosion potential is not close to the two redox equilibrium potentials. If this is not the case, then the two ignored reactions become significant and the theory fails.

4.2.4   Corrosion rate (mm/y) from current measurements

It is possible to derive an equation which may be used for converting a measured corrosion current density to a corrosion rate in *mm/year*. Assume iron dissolution is the only anodic reaction which is given by:

$$Fe(s) \rightarrow Fe^{2+}(aq) + 2e^- \tag{155}$$

The number of moles iron which dissolve, n_M, may be determined by using Faraday's law written for reaction (155):

$$n_M = \frac{\nu_M Q}{zF} \tag{156}$$

M signifies an arbitrary metal. Q is the quantity of electrons produced, $z=2$ is the number of electron per reaction, $\nu_M=1$ is the stoichiometric coefficient of iron, and F is the Faraday constant. The mass of metal dissolved, m_M, is calculated by a stoichiometric relation in combination with (156):

$$m_M = M_M \cdot n_M \Rightarrow m_M = \frac{\nu_M I t}{zF} M_M \tag{157}$$

because $Q = I \cdot t$ where t is the time in seconds and I the current in amperes. M_M is the molecular weight of metal (*kg/mol*). The corrosion rate of metal M in *m/s*, CR_M, is calculated by:

$$CR_M = \frac{m_M}{At\rho_M} \tag{158}$$

Which states that the mass dissolved, m_M, in *kg* divided by the area from which it is dissolved, A; in m^2 over the time, t, together with the metal density, ρ_M, in kg/m^3, gives the corrosion rate in *m/s*. Equation (157) relates the dissolved mass to the current which inserted in (158) gives:

$$CR_M = \frac{m_M}{At\rho_M} = \frac{\nu_M I M_M}{A\rho_M nF} = \frac{\nu_M i M_M}{\rho_M nF} \tag{159}$$

Where $i = I/A$ is the current density in A/m^2. Equation (159) relates the measured or calculated corrosion current, i, to the corrosion rate in *m/s*. The corrosion rate is then calculated using the SG equation by insertion of (153) in (159). i_{corr} could also be determined by a direct experimental method in order to calculate what the corrosion rate is in *mm/y*, by using (159). This is of cause under the assumption that corrosion is uniform. The pre-exponential factor in (159), $\nu_M M_M / (\rho_M nF)$, of iron is 1.16 *mm/year·m²/A*. The corrosion rate in *mm/year* is therefore 1.16 times greater than the current density measured in A/m^2 or $\mu A/mm^2$.

It must be noted that equation (159) can be applied for calculation of corrosion rate in a system where several metals dissolve simultaneously, for example a system where two different metals dissolve simultaneously. This is done by separating the current related to the dissolution of the specific metal. This may be difficult.

4.2.5 Extension of Stern and Geary theory for activation control

The SG theory can be extended to include a more general activation controlled processed. In order to do this it must be understood how the SG theory is used in practise. The principles of the theory is that the potential, *(π-φ)*, is varied around the corrosion potential, *(π-φ)^corr*, in order to determined the slope of a (η^{corr}, i_{net}) plot so i_{corr} can be determined numerically. The corrosion rate may then be determined by using i_{corr} in equation (159). The slope of a (i_{net}, η^{corr}) plot is called the polarization resistance, R_p. The reciprocal of R_p is therefore given by:

$$\frac{1}{R_P} = \left(\frac{di_{net}}{d(\pi - \phi)} \right)_{(\pi-\phi)=(\pi-\phi)^{corr}} \tag{160}$$

By insertion of the net current defined by (141) results in the general equation of the polarization resistance:

$$\frac{1}{R_p} = \left(\frac{d}{d(\pi-\phi)} \left(\sum_{k}^{k} i_{net,k} \right) \right)_{(\pi-\phi)=(\pi-\phi)^{corr}} = \sum_{k}^{k} \left(\frac{di_{net,k}}{d(\pi-\phi)} \right)_{(\pi-\phi)=(\pi-\phi)^{corr}} \tag{161}$$

It can be shown that the SG theory can be extended to a more general scheme by using the following net current density instead of (147).

$$i_{net} = i_{01}\left(\exp\left(\frac{(1-\alpha_1)n_1F\eta_1}{RT} \right) - \exp\left(\frac{-\alpha_1 n_1 F \eta_1}{RT} \right) \right)$$
$$+ i_{02}\left(\exp\left(\frac{(1-\alpha_2)n_2F\eta_2}{RT} \right) - \exp\left(\frac{-\alpha_2 n_2 F \eta_2}{RT} \right) \right) \tag{162}$$

This equation contains both the forward and the backward reactions of two redox reactions. One reaction will primarily run forward and the other will mostly run backward. The effect of the opposite reactions can be introduced in the SG theory in order to present a more exact version of the theory. Appendix B.2 shows that the resulting polarization resistance can be expressed by:

$$\frac{1}{R_p} = \left(\frac{di_{net}}{d(\pi - \phi)} \right)_{(\pi-\phi)=(\pi-\phi)^{corr}}$$
$$= i_{corr}\left(\frac{\ln(10)}{\beta_{a1}} + \frac{n_1 F}{RT}\left(\exp\left(\frac{n_1 F \eta_1^{(\pi-\phi)^{corr}}}{RT} \right) - 1 \right)^{-1} \right. \tag{163}$$
$$\left. + \frac{\ln(10)}{\beta_{c2}} + \frac{n_2 F}{RT}\left(\exp\left(\frac{-n_2 F \eta_2^{(\pi-\phi)^{corr}}}{RT} \right) - 1 \right)^{-1} \right)$$

Where β_{a1} and β_{c2} are defined by (146) for the two reactions and i_{corr} is given in the appendix as equation (333). The overpotential at the corrosion potential, $\eta_k^{(\pi-\phi)^{corr}}$, is defined by:

$$\eta_k^{(\pi-\phi)^{corr}} \equiv (\pi - \phi)^{corr} - (\pi - \phi)^{eq,k} \tag{164}$$

It can be seen by comparing (152) and (163) that equation (163) reduces to (152) when $\eta_1^{(\pi-\phi)^{corr}} \to \infty$ and $\eta_2^{(\pi-\phi)^{corr}} \to -\infty$. This is the case when $(\pi-\phi)^{eq,1}$ and $(\pi-\phi)^{eq,2}$ are far apart and $(\pi-\phi)^{corr}$ is far from both equilibrium potentials. This is expected. If $(\pi-\phi)^{corr}$ is close to the equilibrium potentials, then the back- and forward reactions become important in (148). These were neglected during the derivation of (152).

One of the difficult tasks of using equation (163) is to determine $\eta_k^{(\pi-\phi)^{corr}}$. It requires the knowledge of the equilibrium potentials, which can be determined through the Nernst equation, (134). This can be problematic since it requires the liquid phase activities. It is therefore necessary to analyse the liquid phase composition in order to use (163). Indeed equation (163) is an improvement of the SG theory, but the practical application can be challenging compared to (152).
The problems can be justified, if the corrosion potential approaches one of the equilibrium potentials.

4.3   Concentration & activation polarization

The derivation of the SG theory, (152), required that the Volmer-Butler kinetics, (138), was assumed to be valid. Sometimes this is acceptable, but there will be cases where surface activities, a^*, are not equal to the bulk activities. This is the case when films cover the electrode surface. These films may either be porous corrosion product or a liquid diffusion films. Equation (136) gives the exact electrode kinetic of a redox reaction, and the surface activities are not known.

Transport of ions through the solution is governed by three mechanisms: Diffusion due to gradients in the chemical potential, μ_i, or migration due to an externally applied potential or from attraction due to charged species. Assume migration is negligible. This will be true at low potentials or high concentration of a supporting electrolyte. Also assume component fluxes in mol/m^2, j_k, obeys Fick's law. Fick's law written as function of activities are given by (92) which rewrites to:

$$j_k = -D_k \frac{x_k c_t}{a_k} \frac{da_k}{dz} \tag{165}$$

Where D_k is the diffusivity at infinite dilution and a_k is the rational symmetrical activity of component k. x_k is the mol fraction, c_t is the total concentration in mol/m^3 and z is the directional coordinate. The flux is related to the net current density by:

$$i_{net} = \frac{nF}{v_X} j_X, \qquad i_{net} = -\frac{nF}{v_R} j_R \tag{166}$$

It states that the current density is proportional to the number of electrons transferred. v_k is the stoichiometric coefficient. The subscript R refers to the reduced compound and X refers to the oxidised, defined by equation (123). Assuming a linear concentration profile in the diffusive layer up to the electrode gives the following from equation (165):

$$j_k = -D_k \frac{x_k c_t}{a_k} \frac{a_k - a_k^*}{\delta} = D_k \frac{x_k c_t}{a_k} \frac{a_k^* - a_k}{\delta} \tag{167}$$

δ is the diffusion layer thickness and it is assumed constant. This constraint may be applied experimentally by using a rotating disk electrode (RDE) setup[5,15]. δ has a typical magnitude of 0.001cm to 0.05cm. (166) and (167) are combined in order to derive an expression for the surface activities:

$$a_X^* = a_X + a_X \frac{i_{net} v_X \delta}{nFD_X x_X c_t}, \qquad a_R^* = a_R - a_R \frac{i_{net} v_R \delta}{nFD_R x_R c_t} \tag{168}$$

The maximum current density is reached when the difference between activities are maximum. This is obtained when $a_k^* = 0$. The phenomenon is called the limiting current density.

The flux of compounds is at its maximum when this current is reached, since the bottleneck is no longer the transfer of electrons through the surface but the supply of ions to the surface. Even though the current transfer could run faster it is limited by

the diffusion process. The maximum current, limited by diffusion, is obtained by setting $a_k^* = 0$ in (168) which reveals the limiting current density, i^d:

$$i_X^d = -\frac{nFD_X}{\nu_X \delta} x_X c_t, \qquad i_R^d = \frac{nFD_R}{\nu_R \delta} x_R c_t \qquad (169)$$

The limiting current density of X is negative whereas the limiting current density of R is positive. Back substituting (168) in (169) gives the following expression of the surface activities as function of the net and limiting current densities:

$$a_X^* = a_X \left(1 - \frac{i_{net}}{i_X^d} \right), \qquad a_R^* = a_R \left(1 - \frac{i_{net}}{i_R^d} \right) \qquad (170)$$

The general equation which contains the terms for both activation and diffusion control kinetics are derived by inserting (170) into (136) using (127):

$$i_{net} = i_o \left(\prod_X \left(1 - \frac{i_{net}}{i_X^d} \right)^{\nu_X} \exp\left(\frac{(1-\alpha)nF\eta}{RT} \right) - \prod_R \left(1 - \frac{i_{net}}{i_R^d} \right)^{\nu_R} \exp\left(\frac{-\alpha nF\eta}{RT} \right) \right) \qquad (171)$$

The function gives the net current density as function of the overpotential and limiting current densities. The above equation is not an explicit function of i_{net} because the multiplication symbol and the stoichiometric coefficients, ν_i, prevents the isolation of i_{net} at the left hand side of the equation. It is apparent that if $i_R^d \gg i_{net}$ and $i_X^d \ll i_{net}$, then equation (171) reduces to a purely kinetic controlled relation, the Volmer-Butler equation, (138).

Equation (171) can be rearranged in order to express i_{net} explicitly. This is done by including a suitable number of assumptions. Assume that only one reduced compound, R, and one oxidised component, X, contribute to the limiting current. This is usually an acceptable assumption since one compound is typically the limiting, and not a collection of compounds. This removes the multiplication symbols in (171). Assume also that the stoichiometric coefficients of reaction (122) are one, $\nu_R = \nu_X = 1$. Under these assumptions and isolating the net current from (171) gives

$$i_{net} = \frac{i_0 \left(\exp\left(\frac{(1-\alpha)nF\eta}{RT} \right) - \exp\left(\frac{-\alpha nF\eta}{RT} \right) \right)}{1 + i_0 \left(\frac{1}{i_R^d} \exp\left(\frac{(1-\alpha)nF\eta}{RT} \right) - \frac{1}{i_X^d} \exp\left(\frac{-\alpha nF\eta}{RT} \right) \right)} \qquad (172)$$

The derivation if found in appendix B.1. The above equation incorporates both the kinetics from resistance to current transfer, but also the limiting current due to diffusion control. It is similar to the Volmer-Butler equation, (138), except that it includes a denominator term which corrects for limiting currents. The anodic and cathodic current densities are calculated equivalent to (139) by the following two equations:

$$i_a = \frac{i_0 \exp\left(\frac{(1-\alpha)nF\eta}{RT}\right)}{1 + i_0\left(\frac{1}{i_R^d}\exp\left(\frac{(1-\alpha)nF\eta}{RT}\right) - \frac{1}{i_X^d}\exp\left(\frac{-\alpha nF\eta}{RT}\right)\right)} \tag{173}$$

$$i_c = \frac{-i_0 \exp\left(\frac{-\alpha nF\eta}{RT}\right)}{1 + i_0\left(\frac{1}{i_R^d}\exp\left(\frac{(1-\alpha)nF\eta}{RT}\right) - \frac{1}{i_X^d}\exp\left(\frac{-\alpha nF\eta}{RT}\right)\right)} \tag{174}$$

Figures 9 and 10 shows a plot of (172) to (174). The figures are plotted at the same conditions as figures 7 and 8. Even though, figures 7 and 9 should be comparable, but they are significantly different. This is also the case for figure 8 and 10. The reason is that, in this example, i_{net} no longer follow the dotted asymptotes though i_0 instead it goes asymptotically towards $i_R^d = 5\mu A/cm^2$ and $i_X^d = -4\mu A/cm^2$. Figure 10 also shows that i_a and i_c are no longer crossing at i_0 where $\eta=0$ or $(\pi\text{-}\phi)^{eq}=$-0.05V since the i^d's are close to i_0 and therefore affects i_a and i_c. The thick dotted lines in figure 9 shows the slope of i_{net} at $\eta=0$. The dashed lines are the previous slope obtained in figure 7 and the small-dotted line is the new slope which has been influenced by limiting currents. This indicates that the SG theory can be improved in order to take care of limiting currents.
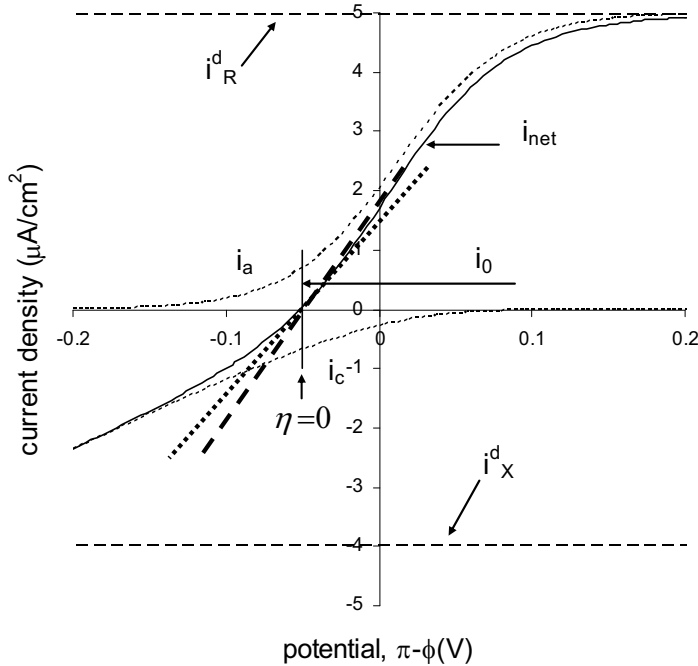
Figure 9: Parameters are the same as figure 7, except that $i_R^d = 5\mu A/cm^2$ and $i_X^d = -4\mu A/cm^2$. The dashed line is the old line of figure 7, the small-dotted line obtained by the influence of i^d.
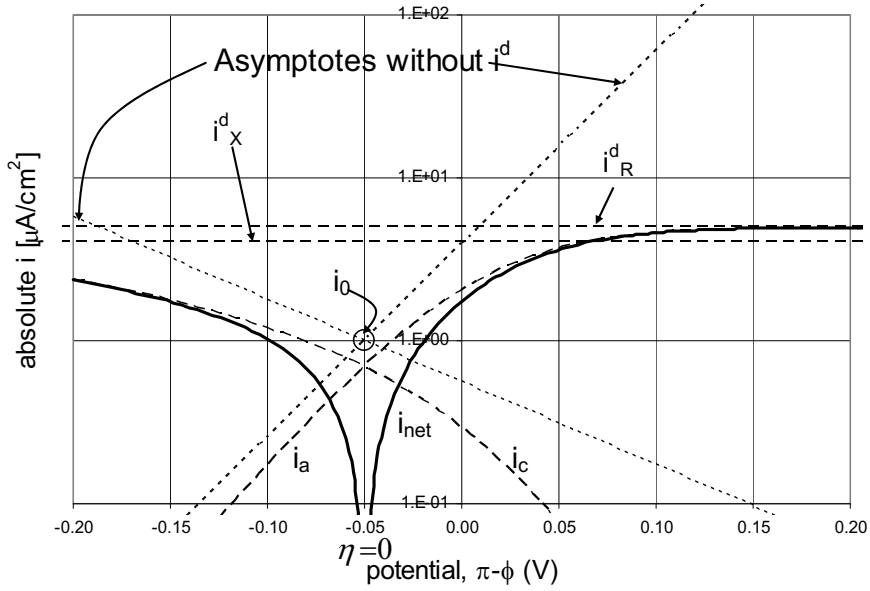
Figure 10: Obtained by the same parameters as figure 9. It shows the effect of limiting currents which was not shown in figure 8.

4.3.1   General activation and concentration polarization

It was previously shown by (142), that a general equation may be written for i_{net} which is activation controlled. A general equation which is valid for both activation and concentration controlled kinetics can be derived by combining (141) and (172). The result for a k number of redox reactions is:

$$i_{net} = \sum_k \left(\frac{\exp\left(\dfrac{(1-\alpha_k)n_k F \eta_k}{RT}\right) - \exp\left(\dfrac{-\alpha_k n_k F \eta_k}{RT}\right)}{1/i_{0k} + \dfrac{1}{i_{Rk}^d}\exp\left(\dfrac{(1-\alpha_k)n_k F \eta_k}{RT}\right) - \dfrac{1}{i_{Xk}^d}\exp\left(\dfrac{-\alpha_k n_k F \eta_k}{RT}\right)} \right) \tag{175}$$

There is a variable collection (η, α, i_0 and i^{d}'s) for every k redox reaction. The anodic and cathodic currents of the kth redox is given by an expression similar to (173) and (174).

4.3.2   Stern and Geary theory with concentration polarization

It is possible to include both activation and concentration controlled kinetics in the SG theory. It requires that i_{net} is no longer given by (147) or (162), instead it is assumed, that two redox reactions are given by the following two reactions derived from (171):

$$i_{net,1} = -i_{01}\left(\left(1 - \frac{i_{net,1}}{i_1^d}\right)\exp\left(\frac{-\alpha_1 n_1 F \eta_1}{RT}\right)\right) \tag{176}$$

$$i_{net,2} = i_{02}\left(\left(1 - \frac{i_{net,2}}{i_2^d}\right)\exp\left(\frac{(1-\alpha_2)n_2 F \eta_2}{RT}\right)\right) \tag{177}$$

It is assumed that one redox reaction will only react forward and the other will only react backward. The two redox reactions are similar to (147), except that the limiting current densities have been included. The total net current density is calculated by:

$$i_{net} = i_{net,1} + i_{net,2} \tag{178}$$

Appendix B.3 shows that the polarisation resistance at $(\pi - \phi) = (\pi - \phi)^{corr}$ can be expressed by the following equation as a function of the limiting current densities:

$$\left(\frac{di_{net}}{d(\pi - \phi)}\right)_{(\pi-\phi)=(\pi-\phi)^{corr}} = i_{corr}\left(\frac{\alpha_1 n_1 F}{RT}\left(1 - \frac{i_{corr}}{i_1^d}\right) + \frac{(1-\alpha_2)n_2 F}{RT}\left(1 - \frac{i_{corr}}{i_2^d}\right)\right) \tag{179}$$

i_{corr} is given in the appendix as equation (344). The above equation is applicable to kinetics which has both activation and concentration controlled kinetics. i_1^d is the cathodic limiting current which is negative and i_2^d is the anodic limiting current which is positive. If there are negligible limiting current densities, $i_1^d \ll i_{corr}$ and $i_2^d \gg i_{corr}$, then the above equation reduces to the original SG equation, (152). It is important to point out, that the above equation is 2nd order with respect to i_{corr}, and has two solutions. This can be seen by writing the above equation as:

$$0 = i_{corr}^2\left(-\frac{(1-\alpha_2)n_2 F}{RT}\frac{1}{i_2^d} - \frac{\alpha_1 n_1 F}{RT}\frac{1}{i_1^d}\right) + i_{corr}\left(\frac{\alpha_1 n_1 F}{RT} + \frac{(1-\alpha_2)n_2 F}{RT}\right) - \left(\frac{di_{net}}{d(\pi - \phi)}\right)_{(\pi-\phi)=(\pi-\phi)^{corr}}$$

4.3.3 A general Stern and Geary theory

It is necessary to neglect the major assumptions, which were introduced in the SG theory, in order to set up a general equation of the SG theory. Let the system consist of k number of redox reactions and let these include limiting currents of anodic and cathodic reactions. The net current is given by the general relation, (175). The corrosion exchange current, i_{corr}, is the current flowing while corrosion runs freely. It is difficult to define in a general scheme. The reason is that there are several anodic and cathodic reactions running at the same time. At $(\pi-\phi)=(\pi-\phi)^{corr}$ they all contribute to i_{net}.

The corrosion rate is no longer related to i_{corr}, at $(\pi-\phi)=(\pi-\phi)^{corr}$, as previously, but by the sum of current densities which are related to the dissolution of the metal in focus. This can be explained by visualizing corroding iron which dissolves by an anodic process. If another anodic process is running in parallel, then only the current

transported by the iron redox reaction would be the actual corrosion current density. It is therefore necessary to redefine what corrosion current is. It is possible to present some of the theory. Solution of the problem would require more advanced computer power, and the solution can not be given explicitly.

In the following derivations we seek an equation which can be used for calculating the net current density. This is done in order to calculate the polarization resistance, R_P, at the corrosion potential, $(\pi\text{-}\phi)=(\pi\text{-}\phi)^{corr}$. The theory can be set up differently, but this approach is used, with the purpose of comparing the theory to the previously derived SG equations.

Assume $i_{net,k}$ are defined by (172) for the k'th reaction and the net current density is calculated by (175). Differentiating (175) with respect to the potential reveals, R_P, as defined by (161). The derivative of the k'th redox is given by the following relation as shown in appendix B.4:

$$\frac{di_{net,k}}{d\left(\pi-\phi\right)}=\frac{\frac{n_k F}{RT}\left(\left(1-\alpha_k\right)\left(1-\frac{i_{net,k}}{i_{Rk}^d}\right)\exp\left(\frac{\left(1-\alpha_k\right)n_k F\eta_k}{RT}\right)-\alpha_k\left(1-\frac{i_{net,k}}{i_{Xk}^d}\right)\exp\left(\frac{-\alpha_k n_k F\eta_k}{RT}\right)\right)}{\frac{1}{i_{0k}}+\frac{1}{i_{Rk}^d}\exp\left(\frac{\left(1-\alpha_k\right)n_k F\eta_k}{RT}\right)-\frac{1}{i_{Xk}^d}\exp\left(\frac{-\alpha_k n_k F\eta_k}{RT}\right)} \quad (180)$$

This equation is not simple compared to the original SG theory, (154). On the contrary this equation includes concentration and activation polarization of all redox reactions and the SG equations represented by (154), (163) and (179) can be derived from (180).

4.3.4 Comparison of Stern and Geary equations

Four different versions of the SG theory have been presented in the above sections: The original SG theory, (154), the theory for advanced activation controlled kinetics, (163), the original theory extended to concentration controlled kinetics, (179), and finally a general formulation, (180).

The original SG theory includes the important activation controlled kinetics. The extension given by (163), is beneficial for mechanism where the corrosion potential is close to any of the equilibrium potentials. The drawback is that activities in the liquid phase must be known.

The SG theory extended to concentration controlled kinetics, (179), is applicable to diffusion controlled mechanisms. The activities of species have to be measured in order to calculate the limiting currents. This may be avoided if limiting currents are determined from measurements. The drawback is similar to the original SG theory. The corrosion potential may not be too close to the equilibrium potentials.

The general SG theory given by (180) is of cause generally applicable, but much information is needed in order to apply it.

Here two redox systems are used as a case study. They include limiting current densities. This is with the intention to compare the various SG equations. Figure 11 shows the two redox reactions and the parameters used. The dotted lines are the asymptotes of the anodic and cathodic reactions for pure activation polarization which are used by the original SG theory. The circles indicate the exchange current densities. The original SG theory predicts a corrosion exchange current density, indicated by $i_{Stern\text{-}Geary}$, which is much higher than the real i_{corr}. This is due to the

limiting current densities which are close i_{corr}. This is also the reason why the corrosion potential, $(\pi\text{-}\phi)^{corr}$, is not predicted very well.
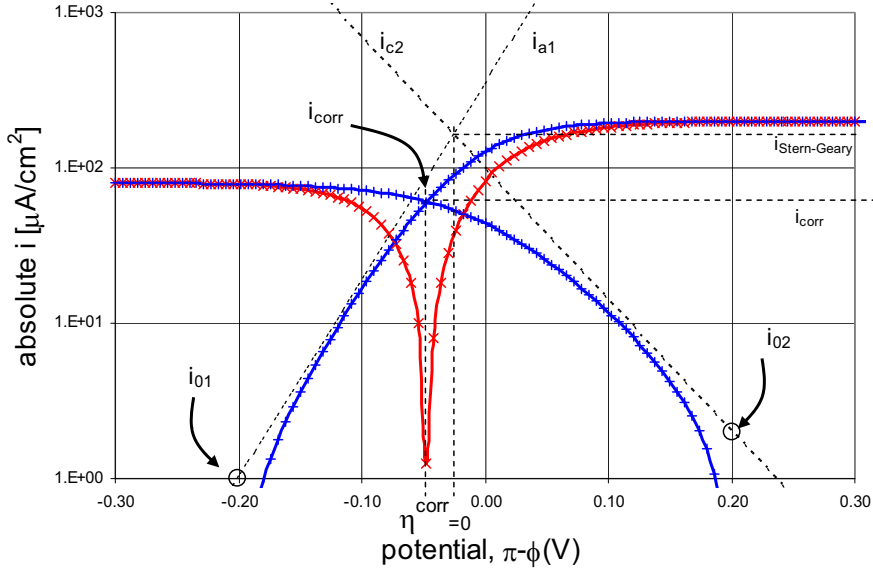

Figure 11: Shows a plot of the net anodic and cathodic currents densities (blue) and the net current density (red). Equilibrium potential are ±0.2, anodic and cathodic limiting currents are $-80\mu A/cm^2$ and $200\mu A/cm^2$. Exchange currents are $1\mu A/cm^2$ and $2\mu A/cm^2$, α's are 0.25 and 0.5.

Table 3 shows the polarization resistance, R_p, calculated by the various SG methods (154), (163), (179), and (180) defined (161). An additional method has been used, where R_p is determined numerically by the slope of (i_{net}, η^{corr}) at $(\pi\text{-}\phi)=(\pi\text{-}\phi)^{corr}$. It is obvious from the table, that the original SG theory, (154), performs not as good in a system with limiting currents, (179) and (180). Equation (163) suffers the same problems. R_p is under predicted an order of magnitude and therefore the corrosion rate is over predicted by a factor two. The exact solution, (180), and the slope of the graph give identical results.

Table 3: Comparison of the Stern and Geary equations applied for the case presented in figure 11.

	Exact (180)	Graph slope	SG, Eq. (154)	Eq. (163)	Eq. (179)
$R_P(Vcm^2/\mu A)$	0.0006579	0.0006579	0.000340080	0.00034081	0.0006581

$i_{Corr}=60.4095\mu A/cm^2$, $(\pi-\phi)_{corr} = -0.04727V$

These methods give almost the same results with minor variation. The original SG theory is a conservative method since it will always tend to over-predict the corrosion exchange current density and therefore over predict the corrosion rate. This may be explained by the limiting currents which will tend to lower the corrosion exchange current density compared to the purely activation controlled kinetics. From these result it is clear that the original SG theory actually perform quite well compared to the more exact methods. The theory becomes complicated when concentration polarization is included in the equation scheme. It is a matter of weighing the benefit from the more exact corrosion measurements using the advanced theory compared to a less accurate result with the original SG theory. There is no reason why not to apply

the advanced theory since the advanced theory is consistent with the original SG theory by setting the limiting current densities to infinite values. The result of the advanced theory is that corrosion measurements can easily be improved if the limiting current densities are known.

4.4   Reaction polarization and IR drop

Reaction polarization is due to slow reaction in the aqueous phase. It can become the limiting variable in the electrode kinetics. The reaction is not related to the kinetics at the metal surface and it is independent of the electrode. It can be related to the limiting current density since it may influence the concentration of species in the bulk. For example CO_2 dissolution is slow, but the electrode reaction is fast as discussed by Nesic *et al.*[16] and Nesic and Postlewaite[17,18]. The used mechanism is:

$$CO_2(g) \rightleftharpoons CO_2(aq) \qquad\qquad (slow) \qquad\qquad (181)$$

$$CO_2(aq) + e^- \rightarrow \tfrac{1}{2} H_2(g) + HCO_3^-(aq) \qquad (fast) \qquad\qquad (182)$$
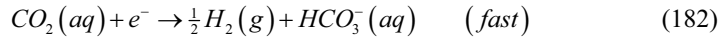
a limiting current may be observed, due to the slow production of $CO_2(aq)$. The physical phenomena would enter into equation (172), but the derivation is not given here. Nesic *et al.*[16] and Nesic and Postlewaite[17,18] uses a slightly different representation of the compounds shown in reaction (181) and (182). The corrosion literature often uses H_2CO_3 in the speciation scheme. This includes $CO_2(g)$ dissolution to $CO_2(aq)$, which hydrates to H_2CO_3 and dissociates to HCO_3^- and CO_3^{2-}. In this speciation scheme $CO_2(aq)$ and H_2CO_3 are separate compounds which are present simultaneously. This contradicts basic thermodynamic properties given by NIST[19] and CODATA[20]. NIST presents properties of H_2CO_3, but they are identical to $H_2O(l) + CO_2(aq)$. This indicate that either $H_2O(l) + CO_2(aq)$ is used or H_2CO_3, not all three compounds at the same time. This is supported by CODATA which does not include H_2CO_3. The problem has not been addressed here, but needs to be solved in the future. IR-drop is due to the resistance in the liquid phase. The potential drops and the transported current is lower. This enters as a linear term in the net current density. IR drop is not included in the derived equations above.

5   CO₂ corrosion

The amount of literature related to *CO₂* corrosion is extreme. A number of review papers which gives an overview of the subject have been published. A brief historical overview was given by Crolet[21,22]. Schmitt[23] gave one of the first overviews of *CO₂* corrosion literature in the beginning of the 1980s. He stated that *CO₂* exhibited higher corrosion rate compared to *HCl* at the same *pH*. This is one of the reasons why *CO₂* corrosion receives so much attention. Modelling is not possible using standard acid corrosion models.

A number of books were published [24,25,26], they summarized the latest development during the beginning of the 1980's. The focus on *CO₂* corrosion in the oil and gas industry has increased exponentially since then. One of the main areas is cost. This was discussed by Kermani and Harrop[27]. During the 1990's some of the more advanced *CO₂* corrosion models were developed using computers. Dawson *et al.*[28,29] summarized many of these models and Nesic[30] gave a detailed overview of the mathematical models which are the basis of most models today, ten years later.

The most comprehensive reviews of *CO₂* corrosion was presented by Kermani and Morshed[31]. It gives a general overview and insight of the *CO₂* corrosion literature and key corrosion parameters. Recently Schmitt and Hörstmeier[32] presented an overview of many of the discussed subjects within *CO₂* corrosion.
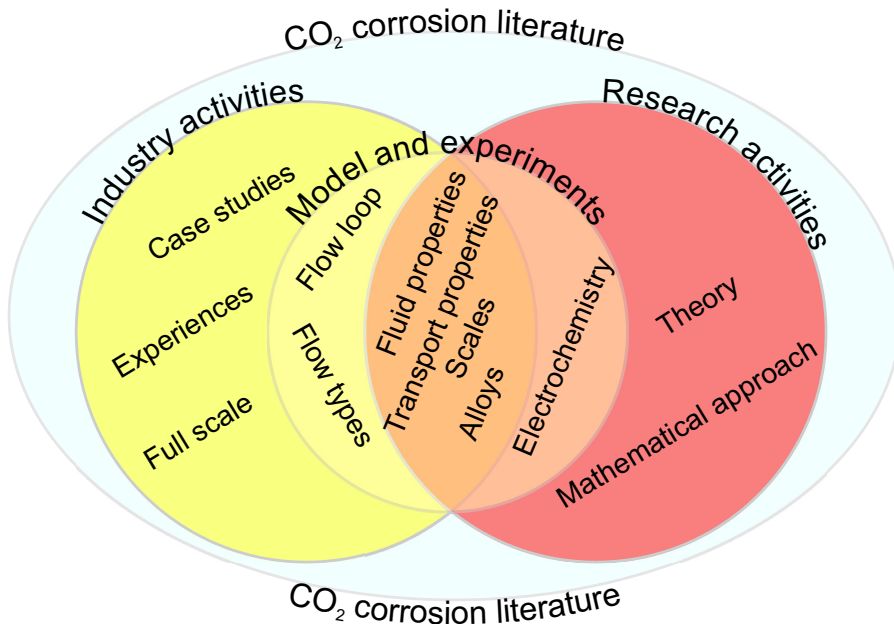
Figure 12: Overview of the topics discussed in the *CO₂* corrosion literature.

Figure 12 gives an overview of the topics discussed within the *CO₂* corrosion literature. The industry and universities are the two parties which have different approaches to corrosion. Industry related literature concerns mainly production facilities issues. Field cases are often discussed in order to give a direct application of the obtained solutions. Research institutions on the other hand often explore the

theoretical or experimental details. This is often related to electrochemical kinetics of CO_2 corrosion. The industry and research meet in the middle. The common focus areas are corrosion rate measurements, modelling and work related to improving the understanding of the CO_2 corrosion mechanism. Corrosion rate is a function of many variables and the topics discussed over the years are

- ▫ Corrosion rate measurements/models
    - o General CO_2 corrosion mechanism
        - ▪ Alloys/steel types
    - o Effect of Fluid properties
        - ▪ Temperature, pressure, composition
        - ▪ *pH*, ionic strength
        - ▪ Additional components (H_2S, acetic acid, O_2)
        - ▪ Inhibitors
        - ▪ Transport properties
    - o Corrosion scales
        - ▪ Equilibrium/solubility
        - ▪ Kinetics
    - o Mass transport/flow
    - o "Top of the line" corrosion
    - o Effect of liquid wetting

The variables are investigated both experimentally and by models. The experimental work is used in order to get a first hand impression and validation of theories and the modelling is performed to get a general understanding of the corrosion mechanisms. The CO_2 corrosion mechanism is an electrochemical process and the corrosion exchange current is a function of the liquid phase surrounding the alloy. The kinetic parameters are affected by the composition of the alloy.
Temperature and pressure are two of the main variables, especially the partial pressure of CO_2. *pH* and ionic strength are also important and plays a key role in the corrosion mechanism. Other species like H_2S, oxygen, or acetic acid, contribute similar to CO_2 in the corrosion process. An overview of literature related to acetic acid was presented by Dougherty[33]. The CO_2 corrosion models are currently being extended in the open literature, in order to take care of the above phenomena.
Corrosion scales has been known for a long time to play an important role in the protection of the steel surfaces. The scales form a diffusion boundary which prevents the corrosive species from diffusing to the surface and corroding it. The solubility of the scales is closely related to the *pH* and recently the focus has been the solubility and kinetics of scale precipitation. Iron carbonate, $FeCO_3$, is typically formed as a corrosion product. The transport properties of ions and the diffusive film layer thicknesses has also become a focus area.
CO_2 corrosion is normally observed in the liquid phase at the bottom of the pipeline. Sometimes it corrodes under the "roof" of the pipeline. This is also known as top-of-line-corrosion (TLC), TOL corrosion, or TOP corrosion. TLC is CO_2 corrosion, but it is often related to the corrosion by acetic acid. It is connected to the condensation rate of water and the physical transport of iron off the surface as shown by figure 13. The increased dissolution is due to the acidification by acetic acid and the following dissolution of $FeCO_3$ as indicated by figure 2. The problem is a great concern to the oil and gas industry since the rate of corrosion is higher in the top than in the bottom. Corrosion inhibitors are usually injected in the pipelines. TLC is difficult to inhibit

because the liquid ends up in the bottom of the pipes. Therefore inhibitors will never reach the top of the line.
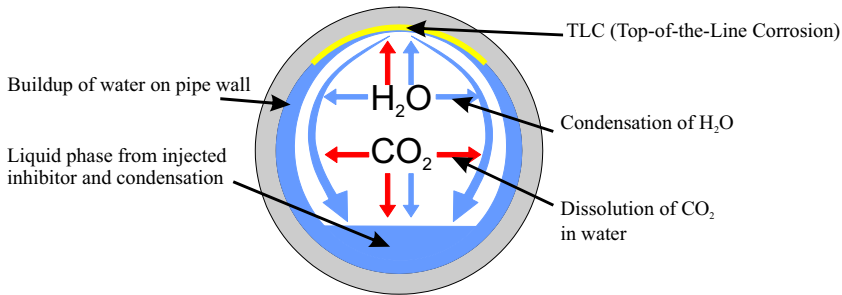

Figure 13: Cross section of pipeline showing the condensation of water which influences the corrosion process under the pipeline "roof".

Volatile corrosion inhibitors (VCI) are sometimes used to prevent TLC. VCI's condense in the top of the pipeline and protect against corrosion. VCI's are not preferred due to the volatility and hazardous properties. Pipelines may also be inspected regularly in order to inhibit TLC. This is done using special pigs which wet the top using inhibitors from the bottom liquid phase.
The mechanism of *CO$_2$* corrosion in wet gas pipelines is generally the same in oil pipelines. Therefore one of the new focus areas in corrosion literature has become wetting of the surfaces since corrosion is only observed in water wet pipelines.

5.1 CO$_2$ corrosion types

CO$_2$ corrosion may cause four types of corrosion:
- Pitting corrosion
- Mesa attack
- Flow induced corrosion
- General uniform corrosion

Pitting or localized corrosion is a stochastic process which is difficult to predict. It is observed as small areas of surface which are attacked heavily. Deep cavities are formed and the corrosion rate is very high. The rate if often mm per year and failures are most often related to pitting. Pitting is often observed at low fluid velocities. An explanation is that pitting may be caused by a local electrochemical concentration cell between the pit cavity and the pipe surface.
Pitting has been known since the beginning of *CO$_2$* corrosion research as discussed by Baylis[34,35]. It was discussed by Xia *et al.*[36] in relation to film formation and recently by Sun *et al.*[37,38,39] and Kvarekvål[40]. The stochastic phenomena was modelled by Xiao and Nesic[41,42]. The oil and gas industry often use the empirical ASME B31G method[43] to evaluate the remaining lifetime of pipelines attacked by pitting.
Mesa attack is also a stochastic pitting process. It is similar to normal pitting but the mechanism is only observed at high flow rates. Figure 14 shows the mechanism of mesa attack. It is caused by the dissolution of iron under the corrosion film. At a certain point the film breaks and it is removed by the high flow rate. The dissolution and removing of more film is a continuous process where more iron dissolves and

film breaks off. Corrosion rate is very high and equivalent to normal pitting. Mesa attack has been known since the first corrosion model was published[44]. The phenomenon was discussed by Dunlop *et al.*[45] and Videm and Dugstad[46]. It was not until the late 1990's that Nyborg[47,48,49] discovered the mechanism sketched in figure 14, using a video camera. A model which describes how to avoid mesa attack, is available[50]. No models can predict mesa attack.
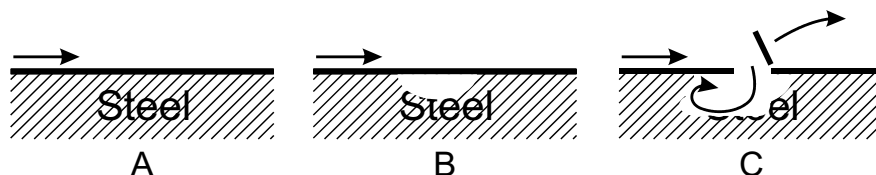

Figure 14: Illustrates mesa attack. A: High flow rate. B: Iron dissolves under corrosion product. C: Corrosion product breaks off and more iron dissolves. Corrosion product breaks off continuously.

Flow induced corrosion typically contribute to mesa attack at high flow rates by eating away the corrosion scales due to liquid vortices. A theoretical model was discussed[51].

General or uniform corrosion is defined by the dissolution of the corroding surface which dissolves evenly. General corrosion is by far the most widely researched form of corrosion in the literature. There are models to calculate electrochemical kinetics, fluid properties, transport properties and a vast number of models to predict corrosion rate. Three types of rate models are found in the literature:

- Empirical or purely correlative models
- Semi-empirical models
- Mechanistic models

The number of models has grown considerably during the last two decades. The performance, review, and comparison of the models have been published in a number of studies. Kermani and Smith[52] compared some of the semi-empirical models for the European Federation of Corrosion. Similarly Nordsveen *et al.*[53], Srinivasan[54], and Wang *et al.*[55] gave brief overviews of the available software in the industry. Recently Nesic *et al.*[30], Woollam and Hernandez[56], and Nyborg[57,58,59] evaluated and described the majority of empirical, semi-empirical, and mechanistic models. The history and mathematical schemes were discussed. This was summarised by Kapusta *et al.*[60].

5.2 Empirical or purely correlative models

Empirical models are correlation of measured corrosion rate in *mm/year* to a number of input variables. The models have empirical parameters which are regressed to corrosion rate data. The principles of the model have no physical meaning. These models have won some acceptance in the industry since it is unimportant to the companies how the predicted corrosion rate is obtained or at least unimportant which scientific framework was used. Some models are purely data driven, where corrosion rate is predicted by interpolating between previously observed cases to new unknown cases[61]. Other models are fitted to databases using linear correlation[62,63,64,65] or non-linear correlations[66]. Some of the models are known by name e.g. the COPRA[67,68] and SWEETCOR[69] correlations. Neural network models have become popular for

correlating corrosion rate. Cottis *et al.*[70] and Sinha and Pandey[71] presented some of the network theory. The principle of a model which is continuously being developed was presented by Nesic *et al.*[72,73,74,75]. The drawback of these models is that they all rely on huge databases, extrapolate very poorly, and can not be used for systems which where not used in the parameter fitting process. The models require much new data in order to extend the applicability to other systems. These models have not been a focus of this study.

5.3 Semi-empirical models

These models are similar to the empirical models since they are fitted to corrosion rate data. The semi-empirical models are set up to resemble some of the physical principles of the real system and are not pure correlation. The unknown parameters in the model are fitted in order to reproduce measured experimental corrosion rate data. Semi-empirical models are some of the most frequently applied models. There are two reasons for this. First of all they have been available for a long time and are evaluated. They are simple and therefore easy to implement and use. They have been fitted to measured corrosion rate data.

The drawback is the same as empirical models. The fitted parameters do not give information of the mechanism of the system, they extrapolate poorly and it requires much new data in order to extend the usage to other systems.

The amount of semi-empirical models is great and covers a subject in it self. Here the significant works within the area are given. De Waard and Milliams presented the first model in 1975[76,77,44], it has since then become very popular. The model was based on a simple electrochemical model which depended on *pH* and temperature. From this model the corrosion rate was related to an exponential function of *pH*. A simple correlation of *pH* with partial pressure of *CO₂* was given. The two combined equations were given and the corrosion could be calculated by:

$$\log\left(CR\left(mm\,/\,year\right)\right)=7.96-\frac{2.32\cdot10^3}{t/°C+273}-5.55\cdot10^{-3}\,t/°C+0.67\log\left(p_{CO_2}/bar\right) \quad (183)$$

Where *CR* is the corrosion rate in *mm/year*. The model was fitted to corrosion rate measured for grit blasted carbon steel. Protective layers of *FeCO₃* were not formed. Some of the first experimental relations were presented by Townshend *et al.*[78]. The success of the model lays in the simplicity, the experimental basis and the nomogram/nomograph presented in the papers. A nomogram is a simple figure which gives the user an easy tool to directly evaluate a complicated relation, using a ruler. The model was updated approximately ten years later[79]. The empirical extension could take care of protective *FeCO₃* scales and triethylene glycol or methanol. The implementation was made as correction factors to equation (183). Which indicates that corrosion rate was calculated using (183) and then a correction factor was multiplied to obtain the final corrosion rate. It was discussed how to differentiate between corrosion rates in the top and bottom of the pipeline. In the spirit of the previous publication the model was again extended[80,81] by empirical correction factors. The scale related corrosion was improved and therefore the overall temperature dependence was improved. A more accurate *pH* correlation was introduced and the model could now also take care of condensation rate,

hydrocarbons and effect of *MEG* and diethylene glycol (*DEG*). The inclusion of inhibitor efficiency was discussed.

The whole principles of the model was revised in 1993[82,83]. This was done since the old models could not take flow velocity into account. The new model was a film resistance model. Two contributions were considered, diffusion resistance and reaction resistance. Parameters in the model were fitted to experimental corrosion rate data. The new model was further improved[84] in 1995 to take care of steel composition and steel types. A correction factors for *FeCO₃* were again introduced and improved. Recently a correction factor for oil wetting were fitted to experimental data[85,86,87] and addition of acetic acid has been discussed[88]. The model has been used as a sub-model for evaluation of TLC as discussed by Vitse *et al.*[89] and as a sub-model in multi flow simulators[53,90,91]. Models which are similar to the pre-1993 model of de Waard were presented by Dugstad *et al.*[92] and Mishra *et al.*[93].

Another type of model was presented by Efird[94] and followed up by Jepson and co-workers[95,96,97,98]. The model relates the corrosion rate to the shear stress, τ_w, by the following relation:

$$CR = a \cdot \tau_w^b \tag{184}$$

Where *a* and *b* are variables which depend on the system.

Many models are denoted by name since they have been developed as computer programs. Some authors give all or close to all model details. Other authors avoid giving enough information and the model can be difficult to reproduce. The oil and gas companies typically have each their *CO₂* corrosion model implementation.

The NORSOK M-506 model[50,99,100,101,102] was developed by the Norwegian institute of standards together with Statoil, Hydro, and IFE. It is the only documented and publicly available program. Several other programs are used in the literature. They are not described in detail and are only available to the companies. A lot of the models are de Waard type, which indicates they have close resemblance to the models of de Waard, e.g. HYDROCOR developed by Shell[60,103,104], LIPUCOR developed by Total[105,106], Cassandra developed by BP[107,108], CORPOS a position dependent model developed by CorrOcean[109,110], and PREDICT developed by Intercor[111,112,113,114,115,116]. Other types of programs where the principles are not revealed but the models are fitted to experimental corrosion rate data are given by USL/ULL(University of Louisiana at Lafayette)[117,118,119,120] developed for an industrial consortium and CORMED developed by Elf[121,122,123,124,125,126,127,128]. There are other semi-empirical models available, but the above have received some attention. These models have not been the focus of this study since they do not identify the corrosion mechanism but merely correlates corrosion rate measurements.

5.4   Mechanistic models

Mechanistic models are chemically mechanistic in the sense that they rely only on chemical relations and the model has not been fitted to experimental corrosion rate measurements.
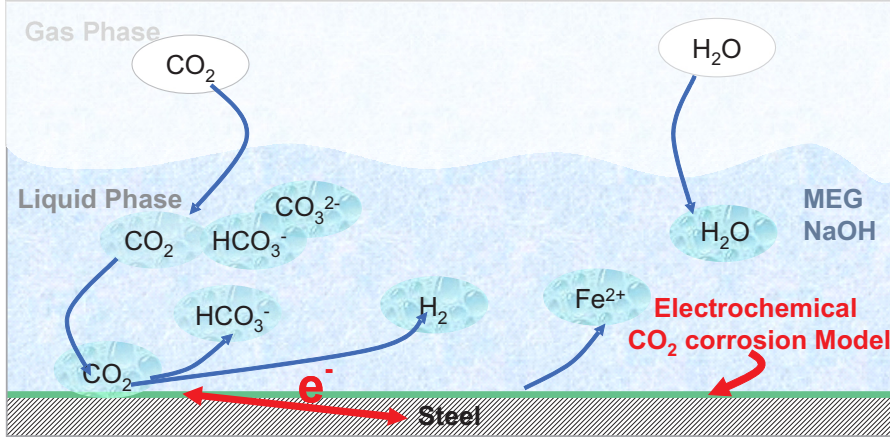
Figure 15: The *CO₂* corrosion mechanism. *CO₂* dissolves in the condensed aqueous liquid phase diffuses to the surface and dissolves iron by an electrochemical mechanism.

Figure 15 shows the principles of all available mechanistic models. The liquid phase consists of water and additives. $CO_2(g)$ dissolves in the liquid phase, it hydrates, dissociates to HCO_3^- and CO_3^{2-} and makes the liquid acidic. $CO_2(aq)$ diffuses to the pipe surface and reacts cathodically at the surface by using electrons and producing HCO_3^- and $H_2(aq)$:

$$CO_2(aq) + H_2O(l) + e^- \rightleftarrows \tfrac{1}{2} H_2(aq) + HCO_3^- \qquad (185)$$

$$H^+ + e^- \rightleftarrows \tfrac{1}{2} H_2(aq) \qquad (186)$$
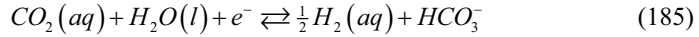
In corrosion literature $CO_2(aq)$ is often substituted by $H_2CO_3(aq)$. There are slight inconsistencies between thermodynamic modelling and corrosion literature. This is pointed out in section 4.4. The above reactions proceed only if the electrons are supplied by other reactions. The anodic process supplies the electrons by dissolution of iron:

$$Fe(s) \rightleftarrows Fe^{2+} + 2e^- \qquad (187)$$

The produced species diffuses away from the surface. If the conditions are right, $FeCO_3(s)$ precipitate on the pipe wall and forms a corrosion protective carbonate layer. Figure 16 shows how $FeCO_3$ becomes a diffusion barrier and the reaction rate is lowered due to lack of $CO_2(aq)$ and similarly the electron transfer is smaller and less iron dissolves.
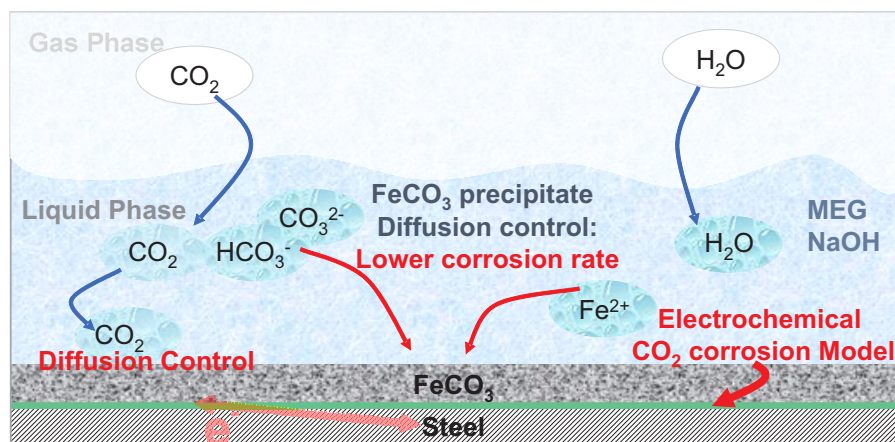
Figure 16: The *CO₂* corrosion mechanism. If *pH* is high enough and if the temperature and liquid composition is correct, then *FeCO₃* precipitate and forms a diffusion controlled mechanism which inhibits the electrochemical corrosion process.

The core of all mechanistic corrosion models is the electrochemical kinetic model. There are different variations of the mechanism and the above represented by (185) to (187) is one of the suggested reaction mechanisms. The mathematical formulation of the mechanism is commonly given by an equation similar to (142) or (175).

Not all models include *FeCO₃* scales. This was the case for the model by Turgoose *et al.*[129] from 1990. It is one of the first mechanistic *CO₂* corrosion models. The authors showed the principles of solving an electrochemical model coupled to a diffusion model. This was done in order to account for the Nernst diffusion layer, since the concentration at the surface and in the bulk is not the same, as indicated by equation (136). Much of the principles resembles the crevice corrosion model by Watson and Postlethwaithe[130] of the same year.

The Turgoose *et al.*[129] model was a simulation of a rotating disk electrode. The electrochemical model were therefore not given by a standard Volmer-Butler mechanism similar to (136). Instead the current density was calculated by a hydrodynamic equation which related the current density and Nernst diffusion layer thickness to the diffusion coefficients and the rotation frequency.

Ficks law was assumed to be valid and the solution of the mathematical problem was treated as a hyperbolic PDE (partial differential equation), where the diffusion model was discretized in the diffusive layer in order to solve the system numerically. The electrochemical model and the bulk composition were boundary conditions as shown in figure 17.
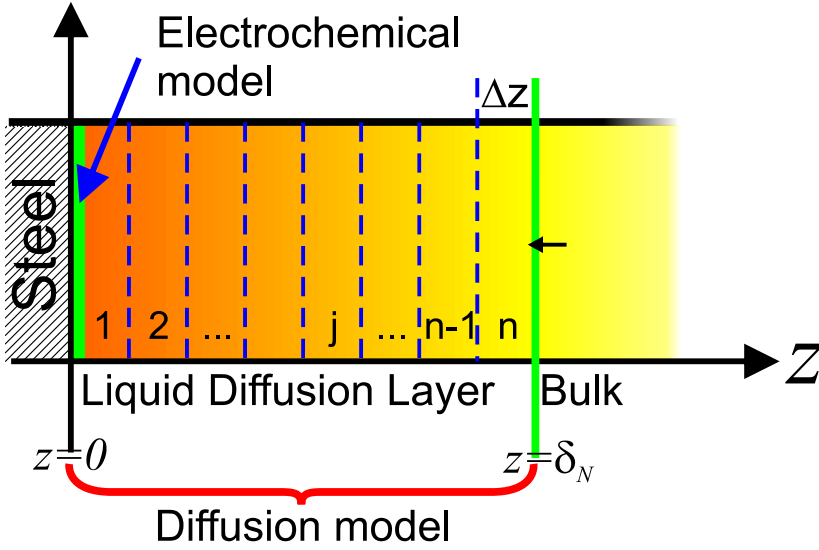
Figure 17: Principles of a discetized *CO₂* corrosion model. Green lines are boundaries. Blue lines are discretization. Compartment numbered *j*, thickness *Δx*, and total thickness *δ_N*.

Turgoose *et al.*[129] set up a mol balance for every discretized compartment, *j*, by use of equation (43) written for compound *i* for a system where R_i=0, using (73) and (87) and assumed a stagnant solvent, u_s=0:

$$\left(\frac{dc_i}{dt}\right)_j = Đ_i^\infty \left(\frac{d^2 c_i}{dz^2}\right)_j \tag{188}$$

This gives a set of *n* coupled PDE's which can be solved numerically on a computer. The right hand side of (188) was calculated by the following second order Taylor approximation.

$$\left(\frac{\partial^2 c_i}{\partial z^2}\right)_j = \frac{c_{j-1} - 2c_j + c_{j+1}}{(\Delta z)^2} \tag{189}$$

Combining (188) and (189) results in an equation which converts equation (188) to a set of *n* coupled ODE's (ordinary differential equations). It rearrange to:

$$(dc_i)_j = \frac{Đ_i^\infty dt}{(\Delta z)^2}\left(c_{j-1} - 2c_j + c_{j+1}\right) \tag{190}$$

The equation system was solved by using $Đ_i^\infty dt / (\Delta z)^2$ =0.45 for H^+, which had the highest $Đ_i^\infty$. The concentration at the next time step was calculated assuming $dc_i \approx \Delta c_i$ and therefore $(c_i)_{k+1} = (c_i)_k + (\Delta c_i)_k$ for time step *k*+1.

The initial composition at t=0 was assumed to be the equilibrium concentration at the given *CO₂* pressure. *Boundary conditions* at the Nernst diffusion layer, z=δ_N, was

assumed to be constant for $t\geq0$ and equal to the bulk concentration. Boundary condition at $z=0$ for $t\geq0$ follows Faraday's law. This indicates that the species converted at the surface, produces or consumes current. The flux is related to the current density by Faraday's law:

$$N_i = \pm \frac{\nu_i}{n_i F} i_i \qquad \text{(for z=0)} \qquad (191)$$

Where n and ν are the stochiometric coefficients of the electron and the reacting species. The flux of non-reacting compounds are zero. Some of the fluxes are for example given by:

$$N_{Fe^{2+}} = -\frac{i_{Fe^{2+}}}{2F} \qquad \text{(for z=0)} \qquad (192)$$

$$N_{H^+} = +\frac{i_{H^+}}{F} \qquad \text{(for z=0)} \qquad (193)$$

$$N_{H_2O} = 0 \qquad \text{(for z=0)} \qquad (194)$$

The flux of iron has a negative sign since Fe^{2+} is produced at the surface. This is opposite for H^+ as shown by (186) and (187). The flux of water is zero since it does not react on the surface. The model was used for evaluating the concentration profiles up to the surface and was not used for prediction corrosion rate.

Crolet *et al.*[131,132,133] presented a qualitative model which used some of the principles similar to Turgoose *et al.*[129].

Nesic[134,135] gave a more physically correct model which included the carbonate equilibria in the liquid phase. The boundary conditions at the Nernst diffusion layer, $z=\delta_N$, was similar to Turgoose *et al.*[129]. The boundary conditions at $z=0$ for $t\geq0$ was set up to be a diffusion controlled scheme. Nesic made it clear that the model could not predict corrosion rate but the model could, similar to Turgoose *et al.*[129], predict the concentration profiles in the diffusion layer. The model showed that *pH* increased towards the surface by a value of 1.5. This effect was also shown by Turgoose *et al.*[129]. They showed the increase was less than 0.01.

Pots[136] presented the first mechanistic model in 1995 which could predict corrosion rate. The boundary conditions were equivalent to Turgoose *et al.*[129] except that the kinetic model at the surface was calculated by a Volmer-Butler model similar to (138). The exchange current density, i_0, was a function of the surface concentrations. These were calculated from the diffusion model. The flux of species was assumed to follow the more detailed Nernst-Planck equation, (96), instead of Fick's law. The potential gradient, $\nabla\phi$, was evaluated as part of the model. The results showed that the model could predict both activation and diffusion controlled corrosion schemes.

Dayalan *et al.*[137] used a different approach. They modelled the mass transport in the Nernst diffusion layer using the Chilton-Coulburn correlation. The boundary conditions were similar to Pots[136] and they also applied a Volmer-Butler model for the surface kinetics. The model was solved as a non-linear problem of fifteen variables and fifteen unknowns. Six surface concentrations, four current densities, four equilibrium potentials and the corrosion potential.

Sundaram *et al.*[138] made an elaborate mathematical description of the corrosion phenomena in 1996. Figure 18 shows the model principles.
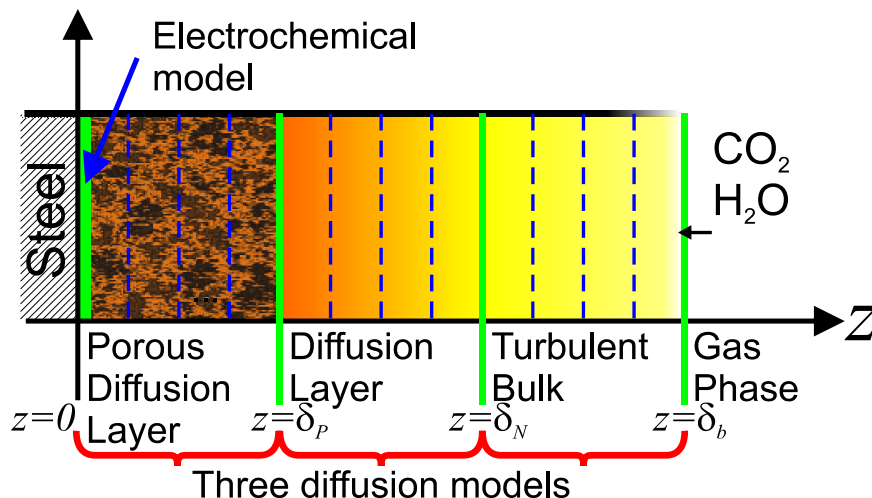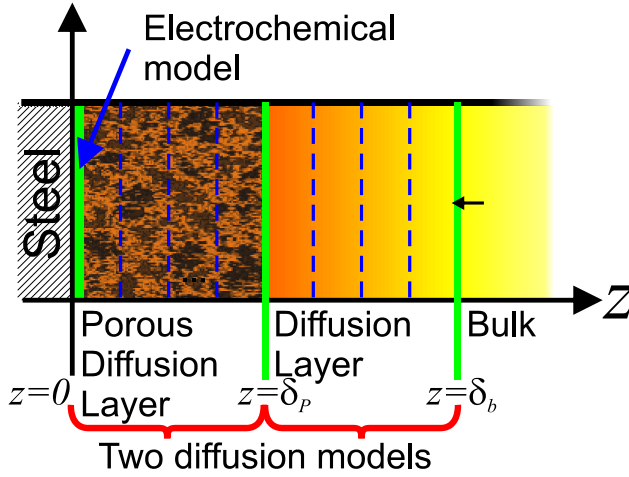

Figure 18: Principles of Sundaram *et al.*'s[138] *CO₂* corrosion model which includes three diffusion models. The distances to the interfaces are δ_P, δ_N, and δ_b from the surface.

The core of the corrosion model was still the electrochemical kinetic model at the surface. The diffusion model was extended compared to previous models. It contained three compartments instead of one as the Turgoose *et al.*[129] and Pots[136] models in figure 17. The turbulent layer was described by a mass transfer correlation in order to take care of two-phase flow. Activity coefficients were mentioned in order to perform an exact calculation of the phase composition. The diffusion layer was set up similar to Pots[136], with a Nernst-Planck description of the flux. The porous layer was assumed to follow a Fick's law diffusion and it was assumed diffusion controlled. This indicate that the surface concentration of species were assumed low compared to the interface concentrations at $z=\delta_P$. The mass balance was similar to (43) solved in steady state, $dc_i/dt = 0$, and $R_i \neq 0$. Parameters used in the model were not given and the model is not easy to reproduce. The model was further described and simplified during 2000 by High *et al.*[139].

A model similar to Nesic[134,135] was discussed by Kvarekvål[140] in 1997. The model could only reproduce diffusion controlled corrosion mechanisms. It was extended in order to account for slow reactions in the liquid phase by deriving a term for R_i as given in equation (43). The liquid film thickness was calculated by using a correlation of wall shear stress. The model showed that the carbonate concentration was distinctively higher at the surface compared to the bulk concentration. This could indicate formation of a protective porous *FeCO₃* layer which was not included in the model.

Zhang *et al.*[141] and Rajappa *et al.*[142] discussed a mass transport equation similar to Dayalan *et al.*[137]. They tested different correlation, one being the Chilton-Coulburn model. Activity coefficients were included for the bulk composition calculations similar to Sundaram *et al.*[138]. Many of the electrochemical rate constants were not given. The same year Dayalan *et al.*[143] extended their model to include a porous diffusion layer and the set up is sketched in figure 19.

Figure 19: Principles of Dayalan *et al.*'s[143] CO_2 corrosion model which includes two diffusion models. The distances to the interfaces are δ_P and δ_N from the surface.

The mass transport was modelled using transport correlations and the transport in the porous layer was modelled by scaling the diffusion coefficients and the effective diffusivity, $\DJ_{eff}$. This was done by assuming the diffusion coefficients in the porous media were related to the free diffusivity, $\DJ$, by:

$$\DJ_{eff} = \frac{\DJ}{\tau} \tag{195}$$

where τ is the tortuosity. The equation is erroneous and should instead be given by:

$$\DJ_{eff} = \frac{\DJ \phi}{\tau^2} \tag{196}$$

as discussed in appendix C.1, where ϕ is the porosity. The work was continued by Wang *et al.*[55] in order to test new mass transport correlations for slug flow. The model was simplified and the porous layer and activity coefficients were neglected. Later Anderko *et al.*[144,145,146,147,148,149] (OLI) gave an electrochemical model coupled to an activity coefficient model. The majority of surface activities were assumed to be equal to the bulk activities. Some compounds were diffusion controlled by applying a mass transport correlation equivalent to Dayalan *et al.*[137].

A discretized two-dimensional PDE model was discussed by Wang and Postlethwaite[150,151,152]. The model did not include a porous corrosion product film as illustrated in figure 18 and 19. Sridhar *et al.*[90] presented also a 2D model during 2000 similar to Wang and Postlethwaite[150,151,152]. The model was not intended for CO_2 corrosion prediction. Instead a general equation scheme for mechanistic corrosion models was presented and results applied for crevice corrosion was given. Few results of CO_2 effect were shown.

Recently Nesic *et al.*[153,154,155] demonstrated an advanced mechanistic model known as the KSC model. The setup was comparable to the work by Sundaram *et al.*[138] and Pots[136]. Figure 20 shows a sketch of their discretized diffusion model.
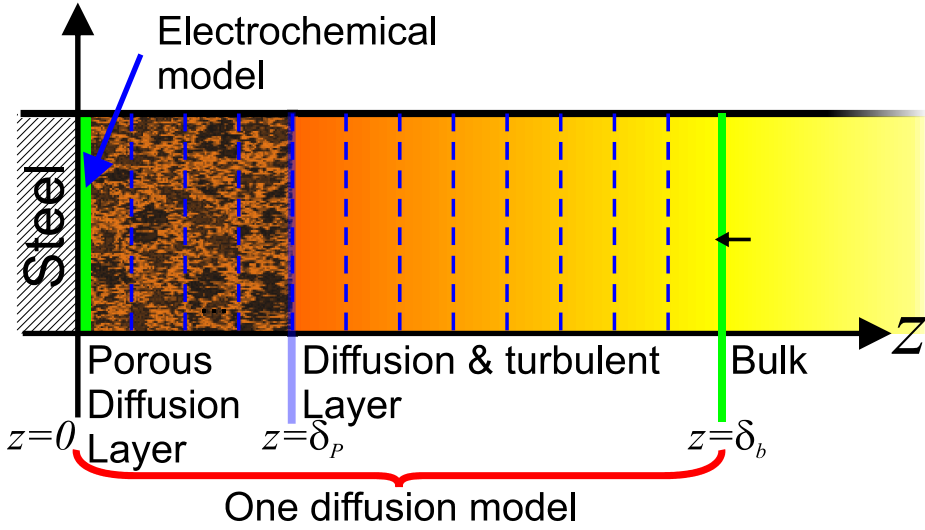
Figure 20: Principles of Nesic *et al.*'s[154,156,155] *CO₂* corrosion model which includes one diffusion model. The distances to the interfaces are δ_P and δ_b from the surface. The diffusion coefficients are position dependent. δ_P signifies a change in porosity and not a boundary.

The model was solved by applying a Nernst-Planck description of the flux in the whole diffusive layer, from the surface to the bulk. The used mass balance was similar to (43) except that porosity was empirically included by:

$$\frac{d(\varepsilon c_i)}{dt} = -\frac{d\left(\varepsilon^{\frac{3}{2}} N_i\right)}{dz} + \varepsilon \cdot R_i \tag{197}$$

Where ε was the porosity. The initial condition was set equal to the equilibrium bulk composition. The boundary condition was a kinetic electrochemical surface model and a constant bulk composition The electrochemical model was linked to the diffusion model by use of (191). A position dependent porosity and a position dependent diffusion coefficient were used in order to account for the porous layer and the turbulence. ε and $Đ_i^\infty$ were therefore functions of z. It was assumed, in their test cases, that the porosity was $\varepsilon=0.1$ from $z=0$ to $z=\delta_P=10\mu m$. The remaining "free" diffusion from δ_P to δ_b was modelled using $\varepsilon=0.6$. An effective diffusion coefficient, $Đ_{eff,i}^\infty$, was used in the Nernst-Planck equation in order to account for turbulence. The diffusion coefficient contained a term from free diffusion, $Đ_i^\infty$, and a contribution from turbulence, $Đ_{i,t}^\infty$:

$$Đ_{eff}^\infty = Đ_i^\infty + Đ_{i,t}^\infty \tag{198}$$

$Đ_{i,t}^\infty$ was zero at $z \leq \delta_P$ and increased towards $z=\delta_b$. They concluded that the porosity has a greater influence on the model result compared to the film layer thickness. The ε and δ_P were considered input parameters and δ_b was calculated using correlation of

the Reynolds number. The model was apparently simplified by Nesic *et al.*[156,157,158] in order to calculate ε and δ_P. A Fick term was used instead of the Nernst-Planck formalism. Nesic *et al.*[159] also linked it to the stochastic model of Xiao and Nesic[41,42] for estimation of pitting and it was linked to a two-phase flow model[160,161,162] for evaluation of wetting.

A model scheme for crevice corrosion was presented by Heppner[163]. They did not focus on *CO₂* corrosion. Instead they presented an elaborate description of the mechanistic equations which included a Pitzer model for bulk calculation and an ideal Nernst-Planck diffusion model. The diffusion model was not linked to an activity coefficient model. A new model was given by Song *et al.*[164,165,167] during 2004. It followed the principles of Pots[136] using Fick's law instead of the Nernst-Planck equation. The model did not include a porous diffusion layer.

It seems the most recent development will be a publicly available mechanistic corrosion model made by Nesic and co-workers[166]. One of the benefits will be a feature to plug-in 3rd party modules and thereby create a framework for further corrosion model development. The model will be called FREECORP and will be available during NACExpo 2008, but no results have been presented yet.

The focus of this study is the mechanistic corrosion models. It is clear from the above list of empirical, semi-empirical, and mechanistic models, that a great amount of work has already been performed for constructing a general *CO₂* corrosion model. The above discussion shows the principles and assumptions for creating a mechanistic corrosion model. Several crude assumptions are still used in the corrosion models; these are discussed and evaluated in the following sections.

5.5   Electrochemical models

The core of all mechanistic *CO₂* corrosion models is an electrochemical kinetic model. Two types of models are usually used either the Levich[168] model used by Turgoose *et al.*[129] or a kinetic model similar to the Vomer-Butler description (142). The Levich model is a hydrodynamic model used for RDE setups. The mechanism is always diffusion controlled and the Nernst diffusion layer thickness is well defined due to the rotation of the electrode. The Volmer-Butler model is normally used since it is independent of the hydrodynamics and may be used for modelling activation controlled mechanisms.

The steel composition is reflected in the kinetic model and the kinetic parameters are directly related to the composition of the alloy as discussed by Lopez *et al.*[169]. The mechanism used by most authors is represented by the steel dissolution (187) as the anodic process. The cathodic reaction e.g. (186) is typically also observed in acid corrosion. The reaction mechanism is not the same in all acids. *CO₂* reacts differently compared to *HCl* as pointed out by Smitt[23]. *CO₂* corrosion is a combined mechanism of (185) and (186). Therefore *CO₂* corrosion is faster compared to normal acidic corrosion. The reason is that more current flows and the dissolution process is faster.

The reaction mechanism of *CO₂* corrosion has been discussed by many authors. An overview of the most important works was recently given by Dugstad[170] and was briefly given Ogundele and White[171], Dawson[28], and Nesic *et al.*[30].

Authors of electrochemical *CO₂* corrosion literature have dealt with three aspects of the electrochemical mechanism: The cathodic process, the anodic process of iron dissolution, or both.

The cathodic process is typically a reduction of *H⁺* to *H₂*. The total reaction contains several elementary reactions and the total process is given by (186). Stern[172] was one

of the first authors who discussed the cathodic process principles. Later Smith and Rothmann[173,174,175] argued that the hydration of CO_2 and direct reduction on the surface, contributed to the current transport as described by (185). This was also discussed by Wieckowski *et al.*[176,177], Schmitt[23], Eriksrud and Søntvedt[204], and Gray *et al.*[179]. Hurlen *et al.*[180,181] suggested that direct reduction of HCO_3^- could have an influence on the CO_2 corrosion mechanism which was supported by Ogundele and White[171] and Gray *et al.*[182]. Nesic *et al.*[183,184] presented the recently accepted mechanism which was given by the two overall reaction represented by (185) and (186).

The anodic process was discussed by Bockris *et al.*[185,186] who gave one of the first well described anodic mechanism of iron dissolution and Drazic[187] summarised the older significant works on the subject.

The mechanism by Bockris *et al.*[185,186] was later used in many studies e.g. Gray *et al.*[179,182]. Smith and Rothmann[188] stated that the total anodic reaction was given by (187). Davies and Burstein[189] also discussed the dissolution process. Nesic *et al.*[190,30] recently spread some doubts to the accuracy of the work of Bockris *et al.*[185,186] at *pH*>4. Nesic *et al.*[190] stated that the previous anodic mechanism of iron dissolution was erroneous and that the reactions were very dependent of *pH*. It was stated that the mechanism changed completely between *pH*<4 and 4<*pH*<5 and again at *pH*>6.

Both cathodic and anodic currents were modelled by Rogers and Rowe[191]. The result should be seen as a first attempt to estimate the electrochemical process. A complete mechanism of anodic and cathodic current was presented by Nesic *et al.*[154,155]. Recently Anderko *et al.*[144,145,146,147,148,149] presented an extended electrochemical model based of activities as given by (142) coupled to a Pitzer model. Unfortunately, no parameters were published and the model can not be reproduced.

The number of works related to the electrochemical investigation of CO_2 corrosion is not elaborate. Many of the above studies give qualitative descriptions of the process and there is still a need for a complete Volmer-Butler model which is valid in the whole temperature, pressure, composition, and *pH* range. It is noteworthy that even though an electrochemical model is the core of all mechanistic CO_2 corrosion models, then no one has published a precise description of the electrochemistry. Nesic *et al.*[154,155] give to date the most complete electrochemical model even though it can be improved.

5.6 Improving CO₂ corrosion models

5.6.1 Assumptions of mechanistic models

The above sections confirm that there is a noticeable amount of predictive CO_2 corrosion models. The focus of this study is to improve the mechanistic models instead of repeating the already known phenomena. The existing models apply a number of assumptions. Two important phenomena are discussed in this study: The non-ideality of the liquid phase and the properties of the porous $FeCO_3$ corrosion products which have not been thoroughly discussed before.

5.6.2 Thermodynamics of the fluid phases in CO₂ corrosion

Table 2 shows a typical fluid composition in a wet gas pipeline. The ionic strength (*I*) is very high, it is approximately 3 to 10 *mol/kg H₂O* at the inlet and 0.1 *mol/kg H₂O* at

the outlet due to dilution by the condensed water. This indicates that the solutions behave thermodynamically non-ideally. The well known Debye-Hückel limiting law activity coefficient model is valid at $I \leq 0.01$ *mol/kg H_2O* and the extended Debye-Hückel law is valid at $I \leq 0.1$ *mol/kg H_2O*. The working window can be extended slightly by using the Davies rule[192,193] which is valid at $I \leq 0.3$ *mol/kg H_2O*. An advanced activity coefficient model is required in order to model the solutions relevant for the work in this study. The Pitzer[194,195] equation is typically valid up to $I=6$ *mol/kg H_2O*. None of these models can be used for multi-solvent systems.

It is assumed, in the majority of the above mentioned mechanistic *CO₂* corrosion models, that the electrolytic solutions behave ideal. It is therefore assumed that $I < 0.001$ *mol/kg H_2O*. It is noteworthy that an activity coefficient model was not applied, since the condition in a wet gas pipelines are up to $I=10$ *mol/kg H_2O*. It is not only the bulk calculation which can be improved. The diffusion calculation was shown by Newman[5] and Wesselingh and Krishna[6] to deviate from Ficks law at $I>1$ *mol/kg H_2O*, and the electrochemical surface reactions are in principle not functions of the surface concentrations, but functions of the activities as shown by (136).

Few of the mechanistic *CO₂* corrosion models have an integrated activity coefficient model. This was done in order to account for the non-ideality of either the bulk phase or the electrochemical surface calculations. None of the corrosion models were improved by an activity coefficient in the diffusion calculation, and none were improved in both electrochemical and bulk calculations. An activity coefficient model should be implemented in order to account for non-ideality of the bulk calculation, the diffusion calculation, and the surface kinetic models.

The authors who discussed activity coefficients in mechanistic *CO₂* corrosion models were Sundaram *et al.*[138] who used a Davies approximation and a Henry's law. This was done in order to account for non-ideality of the bulk. They assumed ideality in electrochemical and diffusion calculations. Zhang *et al.*[141] and Rajappa *et al.*[142] similarly used a Davies rule for their bulk calculations and assumed ideality in the remaining parts of the model. A Pitzer model was applied in the electrochemical surface model by Anderko *et al.*[144,145,146,147,148,149]. The model parameters are unfortunately not available. None of the activity coefficient models gave a satisfactory description of the bulk and surface calculation since they can not be applied to high ionic strengths and mixed solvents.

An advanced thermodynamic model has still not been incorporated in a mechanistic *CO₂* corrosion model. A mechanistic *CO₂* corrosion model would include a full bulk calculation by applying (41) in a speciation routine. It would include the diffusion scheme as presented in equation (83), or one of the simplification by (92) or (117), and a kinetic model as given by (136). All equation should be expressed in terms of activities.

The equation scheme for doing a more correct bulk calculation, diffusion calculation, and kinetic surface reaction model is presented in this study. The extended UNIQUAC model given by Thomsen *et al.*[196,197,198] has shown to be able to predict activities of multi-solvent electrolyte systems up high ionic strengths. The model will be used for showing how the bulk, diffusion, and surface kinetics calculations can be improved. Results of the thermodynamic modelling are shown in chapter 7 and 9.

5.6.3 Properties of FeCO₃

It has been confirmed within the *CO₂* corrosion literature, that *FeCO₃* plays a central role in the modelling of *CO₂* corrosion. *FeCO₃* is also known as siderite and chalybite.

FeCO₃ was discovered as a corrosion product very early by Baylis[34,35] during the 1920's. The precipitated corrosion film of *FeCO₃* forms a layer of impermeable corrosion product which retards the corrosion process and lowers the corrosion rate by diffusion control. Few authors continued the research immediately after Baylis. Kooijmans[199] confirmed that *FeCO₃* formed in 1938. Later Riesenfeld and Blohm[200] discovered that acid gas scrubbers corroded and *FeCO₃* precipitated due to a specific temperature and saturation cycle. Hackerman and Glenn[201] and Sowards and Hackerman[202] confirmed by X-ray diffraction that *FeCO₃* indeed precipitated and formed a protective corrosion film. It was not until the late 1970's *FeCO₃* again received attention. De Waard and Milliams[76] published their well known semi-empirical corrosion model. They were aware that *FeCO₃* could form, but it was not observed in their studies.

A number of studies are available which discuss the thermodynamics of *FeCO₃*. There is some confusion to which properties are reliable.

An objective of this study has been to collect standard thermodynamic properties of *FeCO₃* to compare and discuss the most reliable values. This was done since *FeCO₃* receives increasing attention in the oil and gas industry.

The amount of literature focused on *FeCO₃* in relation to corrosion has grown considerably since the beginning of the 1980's. Sontheimer *et al.*[203] discussed protective *FeCO₃* corrosion scales and Schmitt[23], Eriksrud and Søntvedt[178], and Dunlop *et al.*[45] determined that *FeCO₃* is a significant factor in the oil and gas production for corrosion protection. At the same time Wieckowski *et al.*[176] used an electrochemical approach to show that *FeCO₃* change the surface properties of corroding iron.

One method is typically applied for preventing corrosion of mild carbon steel. The method is called *pH*-stabilization. In this method *FeCO₃* is precipitated to form a protective *FeCO₃* corrosion film. This is done by increasing the *pH* using *NaOH*, *NaHCO₃*, or a similar base since the solubility of *FeCO₃* is closely related to the *pH* of a solution as shown by figure 2. The method has been known since the beginning of the 20th century as discussed by Whitman *et al.*[205], Leybold[206,207], and Baylis[34,35]. The use of *pH*-stabilization for industrial purposes has a long history. Crolet and Samaran[208] mentioned some of the first cases but Dunlop *et al.*[45] published one of the first newer discussions of the subject. *pH*-stabilization continues to be one of the focus areas of the literature. Recent work was given by Haarberg *et al.*[209], Olsen *et al.*[210], and Dugstad and Seiersten[211] who described a corrosion control system running continually in order to precipitate *FeCO₃* to protect against corrosion.

The discussion of *FeCO₃* properties is given in chapter 8.

6   Literature cited

[1]   CorrosionCost.com: http://www.corrosioncost.com/infrastructure/gasliquid/index.htm, http://www.corrosioncost.com/utilities/gas/index.htm and http://www.corrosioncost.com/prodmanu/oilgas/index.htm, July 2007.

[2]   Wang, P. M.; Anderko, A,; Young, R. D. A speciation-based model for mixed-solvent electrolyte systems. Fluid Phase Equilibria 203(1-2), 141-176, 2002.

[3]   Taylor R.; Krishna R. Multicomponent Mass Transfer. John Wiley & sons, 1993.

[4]   Medvedev, Oleg. Diffusion Coefficient in Multicomponent Mixtures. PhD. Thesis, IVC-SEP, Technical University of Denmark, 2005.

[5]   Newman, John. Electrochemical systems. John Wiley & Sons, 2004.

[6]   Wesselingh, J. A.; Krishna, R. Mass transfer in Multicomponent Mixtures. Delft University Press, first edition, 2000.

[7]   Harned, H. S.; Owen, B. B. The physical chemistry of electrolytic solutions. Reinhold Publishing Corporation, New York, third edition, 1964.

[8]   Robinson, R. A.; Stokes, R. H. Electrolyte solutions. Butteroworths Publications, London, second edition, revised, 1965.

[9]   Koryta, J.; Dvorak, J. Principles of Electrochemistry. John Wiley & Sons, 1987.

[10]   Rubinstein, Israel. Physical Electrochemistry – principles, methods, and applications. Marcel Dekker, 1995.

[11]   Tafel, J.; Emmert, E. The cause of the spontaneous depression of cathode potential during the electrolysis of dilute sulphuric acid. Zeitschrift fuer Physikalische Chemie, Stoechiometrie und Verwandtschaftslehre 52, 349-73, 1905.

[12]   Stern, M.; Geary, A. L. Electrochemical Polarization I. A Theoretical Analysis of the Shape of Polarization Curves. Journal of the Electrochemical Society 104(1), 56, 1957.

[13]   Stern, M. Electrochemical Polarization .2. Ferrous-Ferric Electrode Kinetics on Stainless Steel. Journal of the Electrochemical Society 104(9), 559-563, 1957.

[14]   Stern, M. Electrochemical Polarization .3. Further Aspects of the Shape of Polarization Curves. Journal of the Electrochemical Society 104(11), 645-650, 1957.

[15]   Levich, V. Physical Hydrodynamics. Prentic-Hall, New York and London, 1962.

[16]   Nesic, S.; Pots, B. F. M.; Postlethwaite, J.; Thevenot, N. Superposition of Diffusion and Chemical Reaction Controlled Limiting Currents - Application to CO_2 Corrosion. JCSE 1, paper 3, 1995.

[17]   Nesic, S.; Postlethwaite, J. A predictive model of CO_2 corrosion. NACE Canadian Region Western Conference, p. 397-417, Calgary, 1994.

[18]   Nesic, S.; Postlethwaite, J. Modelling of CO_2 corrosion mechanisms. In: Trethewey, K. R.; Roberge, P. R. Modelling Aqueous Corrosion. NATO ASI series, Kluwer Academic Publishers, p. 317, 1994.

[19]   D. D. Wagman, W. H. Evans, V. B. Parker, R. H. Schumm, I. Halow and S. M. Bailey. NIST Chemical Thermodynamics Database Version 1.1. J. Phys. Chem. Ref. Data, 1982, 11 Supplement No. 2.

[20]   J. D. Cox, D. D. Wagman and V. A. Medvedev. CODATA Key values for thermodynamics. Hemisphere Publishing Corp., New York, 1989.

[21]   Crolet, J.-L. Which CO_2 Corrosion, Hence Which Prediction? Progress in the Understanding and Prevention of Corrosion, Vol. 1, p. 473-497, London, UK, The Institute of Materials, 1993.

[22]   Crolet, J.-L. Which CO_2 Corrosion, Hence Which Prediction? European Federation of
         Corrosion (EFC) 13, p. 1, 1994.

[23]   Schmitt, G. Fundamental Aspects of CO_2 Corrosion. CORROSION/83 paper no. 43, NACE,
         1983.

[24]   Newton, L. E; Hausler, R. H. CO_2 corrosion in oil and gas production - selected papers,
         abstracts, and references. NACE, 1984.

[25]   Hausler, R. H.; Godard, H. P. Advances in CO_2 Corrosion. NACE, vol. 1, 1984

[26]   Burke, P. A.; Asphahani, A. I.; Wright, B. S. Advances in CO_2 corrosion. vol. 2, NACE, 1985.

[27]   Kermani, M. B.; Harrop, D. The impact of corrosion on the oil and gas industry. SPE
         Production & Facilities 11(3), 186-190, 1996.

[28]   Dawson, J. L.; Shih, C. C.; Bartlett P. K. N. Models and prediction of CO_2 corrosion Erosion-
         corrosion under flowing conditions. European Federation of Corrosion (EFC) 13, paper no. 8,
         151, 1994.

[29]   Dawson, J. L.; Shih, C. C.; Bartlett, P. K. N. Models and prediction of CO_2 corrosion Erosion-
         corrosion under flowing conditions. Progress in the Understanding and Prevention of
         Corrosion 1, p. 513, 1993.

[30]   Nesic, S.; Postlewaite, J.; Vrhovac, M. CO_2 Corrosion of carbon steel - from mechanistic to
         empirical modelling. J. Corrosion Reviews 15, 211, 1997.

[31]   Kermani, M. B.; Morshed, A. Carbon dioxide corrosion in oil and gas production - A
         compendium. Corrosion 59(8), 659-683, 2003.

[32]   Guenter, Schmitt; Michaela, Hörstemeier. FUNDAMENTAL ASPECTS OF CO_2 METAL
         LOSS CORROSION – PART II: INFLUENCE OF DIFFERENT PARAMETERS ON CO_2
         CORROSION MECHANISMS. CORROSION/06 paper no. 112, NACE, 2006.

[33]   Dougherty, James A. A Review of the Effect of Organic Acids on CO_2 Corrosion.
         CORROSION/04 paper no. 376, NACE, 2004.

[34]   Baylis, John R. Factors other than dissolved oxygen influencing the corrosion of iron pipes.
         Journal of Industrial and Engineering Chemistry 18(4), 370-80, 1926.

[35]   Baylis, John R. How to avoid loss by pipe corrosion. Water Works Engineering 83, 13-4 31-2
         35-6, 1930.

[36]   Xia, Z.; Chou, K. C.; Szklarska-Smialowska, Z. Pitting corrosion of carbon steel in carbon
         dioxide-containing sodium chloride brine. Corrosion 45(8), 636-42, 1989.

[37]   Yuhua, Sun; Nesic, Srdjan. A Parametric Study and Modeling on Localized CO_2 Corrosion in
         Horizontal Wet Gas Flow. CORROSION/04 paper no. 380, NACE, 2004.

[38]   Sun, Yuhua. Localized CO_2 Corrosion in Horizontal Wet Gas Flow. PhD Thesis, Ohio
         University, Chemical Engineering, 2003.

[39]   Sun, Yuhua; George, Keith; Nesic, Srdjan. The Effect of Cl^- and Acetic Acid on Localized
         CO_2 Corrosion in Wet Gas Flow. CORROSION/03, paper no. 327, NACE, 2003.

[40]   Kvarekval, Jon. Morphology of localised corrosion attacks in sour environments.
         CORROSION/07 paper no. 659, NACE, 2007.

[41]   Xiao, Ying; Nesic, Srdjan. A Stochastic Prediction Model of Localized CO_2 Corrosion.
         CORROSION/05 paper no. 57, NACE, 2005.

[42]   Xiao, Ying. A Two-Dimensional Stochastic Model for Prediction of Localized Corrosion.
         Master of Science thesis, Ohio University, Chemical Engineering, 2004.

[43]   Feigel, R. E.; Hayden, L. E.; Gomez, G. J. Manual for Determining the Remaining Strength of
         Corroded Pipe - A supplement for the ASME B31 pressure piping. ASME B31G, 1991.

[44]   de Waard, C.; Milliams, D.E. Prediction of Carbonic Acid Corrosion in Natural Gas Pipelines.
         Ind. finishing and surface coatings 28(340), 24, 1976.

[45]   Dunlop, A. K.; Hassell, H.L; Rhodes, P. R. Fundamental considerations in sweet gas well corrosion. CORROSION/83 paper No. 46, NACE, 1983.

[46]   Videm, K.; Dugstad, A. Effect of Flow Rate, pH, Fe^{2+} Concentration, and Steel Quality on the CO_2 Corrosion of Carbon Steels. CORROSION/87 paper no. 42, NACE, 1987.

[47]   Nyborg, Rolf. INITIATION AND GROWTH OF MESA CORROSION ATTACK DURING CO_2 CORROSION OF CARBON STEEL. CORROSION/98 Paper no. 48, NACE, 1998.

[48]   Nyborg, Rolf; Dugstad, Ame. MESA CORROSION ATTACK IN CARBON STEEL AND 0.5 % CHROMIUM STEEL. CORROSION/98 paper no. 29, NACE, 1998.

[49]   Nyborg, Rolf; Dugstad, Arne. Understanding and Prediction of Mesa Corrosion Attack. CORROSION/03 paper no. 642, NACE, 2003.

[50]   Halvorsen, A. M. K.; Søndtvedt, T. CO_2 Corrosion Model for Carbon Steel Including a Wall Shear Stress Model for Multiphase Flow and Limits for Production Rate to Avoid Mesa Attack. CORROSION/99 paper no. 42, NACE, 1999.

[51]   Schmitt, G.; Bosch, C.; Mueller, M.; Siegmund, G. A PROBABILISTIC MODEL FOR FLOW INDUCED LOCALIZED CORROSION. CORROSION/00 paper no. 49, NACE, 2000.

[52]   Kermani, M. B.; Smith, L. M. CO_2 corrosion control in oil and gas production - design considerations. European Federation of Corrosion (EFC) 23, 1997.

[53]   Nordsveen, M.; Nyborg, R.; Hovden, L. Implementation of CO_2 Corrosion Models in the OLGA Three-Phase Flow Code. Multiphase '99 (Cranfield, UK: BHR Group), 279-292, 1999.

[54]   Srinivasan, Sridhar. REVIEW OF COMPUTER APPLICATIONS IN CORROSION SCIENCE AND ENGINEERING. CORROSION/00 paper no. 473, NACE, 2000.

[55]   Wang, Hongwei; Cai, Ji-Yong; Jepson, William Paul. CO_2 CORROSION MECHANISTIC MODELING AND PREDICTION IN HORIZONTAL SLUG FLOW. CORROSION/02 paper no. 238, NACE, 2002.

[56]   Woollam, R.C.; Hernandez, S.E. Assessment and Comparison of CO2 Corrosion Prediction Models. SPE International Oilfield Corrosion Symposium, paper 100673-MS, 2006.

[57]   Nyborg, Rolf. Overview of CO_2 Corrosion Models for Wells and Pipelines. CORROSION/02 paper no. 233, NACE, 2002.

[58]   Nyborg, Rolf; Dugstad, Arne. Flow assurance of wet gas pipelines from a corrosion viewpoint. Proceedings of the International Conference on Offshore Mechanics and Arctic Engineering - OMAE 4, 125-132, 2002.

[59]   Nyborg, Rolf. Field Data Collection, Evaluation and Use for Corrosivity Prediction and Validation of Models. CORROSION/06, paper no. 118, NACE, 2006.

[60]   Kapusta, Sergio D.; Pots, Bernardus F.M.; Rippon, Ian J. The Application of Corrosion Prediction Models to the Design and Operation of Pipelines. CORROSION/04 paper no. 633, NACE, 2004.

[61]   Khajotia, Burzin; Sormaz, Dusan; Nesic, Srdjan. Case-based reasoning model CO_2 corrosion based on field data. CORROSION/07, paper no. 553, NACE, 2007.

[62]   Adams, C. D.; Garber, J. D.; Walter, F. H.; Singh, C. Verification of computer modelled tubing life predictions by field data. CORROSION/93 paper no. 82, NACE, 1993.

[63]   Garber, J. D.; Walters, F. H.; Alapati, R. R.; Adams, C. D. Downhole parameters to predict tubing life and mist flow in gas condensate wells. CORROSION/94 paper no. 25, NACE, 1994.

[64]   Walters, Frederick H. Uphole parameters indicate corrosion in gas-condensate wells. Oil and Gas Journal 92(3), 59-60, 1994.

[65]   Lyle, F.F.; Schutt, H.U. CO_2/H_2S corrosion under wet gas pipeline conditions in the presence of bicarbonate, chloride and oxygen. CORROSION/98 paper no. 11, NACE, 1998.

[66]   van Bodegom, L.; Gelder, K. V.; Paksa, M. K. F.; Raam, L. V. Effect of Glycol and Methanol on CO_2 Corrosion of Carbon Steel. CORROSION/87 paper no. 55, NACE, 1987.

[67]   Gatzke, L.K.; Hausler, R. H. The COPRA correlation. A Quantitative assessment of deep, hot gas well and its control. CORROSION/83 Paper no. 48, NACE, 1983.

[68]   Hausler, R. H.; Garber, J. D. The Copra correlation revisited. CORROSION/90 paper no. 45, NACE, 1990.

[69]   John, R. C.; Jordan, K. G.; Kapusta, S. D.; Young, A. L.; Thompson, W. T. SweetCor: An Information System for the Analysis of Corrosion of Steels by Water and Carbon Dioxide. CORROSION/98 paper no. 20, NACE, 1998.

[70]   Cottis, R. A.; Oing, Li; Owen, G.; Gartland, S. J.; Helliwell, I. A.; Turega, M. Neural network methods for corrosion data reduction. Materials and Design 20(4), 169-178, 1999.

[71]   Sinha, S. K.; Pandey M. D. Probabilistic neural network for reliability assessment of oil and gas pipelines. Comput.-Aided Civ. Inf. Eng. 17(5), 320-329, 2002.

[72]   Nesic, Srdjan; Vrhovac, Miran. A Neural Network Model for CO_2 Corrosion of Carbon Steel. JCSE 1, paper 6, 1999.

[73]   Nesic, S.; Nordsveen, M.; Maxwell, N.; Vrhovac, M. Probabilistic modelling of CO_2 corrosion laboratory data using neural networks. Corrosion Science 43(7), 1373-1392, 2001.

[74]   Hernández, S.; Nesic, S.; Weckman, G.; Ghai, V. Use of Artificial Neural Networks for Predicting Crude Oil Effect on CO_2 Corrosion of Carbon Steels. CORROSION/05 paper no. 554, NACE, 2005.

[75]   Hernandez, S.; Nesic, S.; Weckman, G.; Ghai, V. Use of artificial neural networks for predicting crude oil effect on carbon dioxide corrosion of carbon steels. Corrosion 62(6), 467-482, 2006.

[76]   de Waard, C.; Milliams, D. E. Prediction of Carbonic Acid Corrosion in Natural Gas Pipelines. First international conference on the internal and external protection of pipes, paper no. F1, 1-8, X85-X87, 1975.

[77]   de Waard, C.; Milliams, D. E. Carbonic-Acid Corrosion of Steel. Corrosion 31(5), 177-181, 1975.

[78]   Townshend, P. E.; Colegate, G. T.; van Waart, T. L. Carbon dioxide corrosion at low partial pressure in major submarine pipelines. SPE European spring meeting, paper no. 741, 1972.

[79]   Simon Thomas, M. J. J.; de Waard, C.; Smith, L.M. Controlling factors in the rate of CO_2 corrosion. UK corrosion '87, 147, Brighton, 1987.

[80]   de Waard, C.; Lotz, U.; Milliams, D.E. Predictive model for CO_2 corrosion engineering in wet natural gas pipelines. Corrosion 47(12), 976-985, 1991.

[81]   de Waard, C.; Lotz, U.; Milliams, D. E. Predictive Model for CO_2 Corrosion Engineering. CORROSION/91 paper no. 577, NACE, 1991.

[82]   de Waard, C.; Lotz, U. Prediction of CO_2 Corrosion of Carbon Steel. CORROSION/93 paper No. 69, NACE, 1993.

[83]   de Waard, C.; Lotz, U. Prediction of CO_2 corrosion of Carbon Steel. European Federation of Corrosion (EFC) 13, 30-49, 1994.

[84]   de Waard, C.; Lotz, U.; Dugstad, A. Influence of Liquid Flow Velocity on CO_2 Corrosion, A Semi-Empirical Model. CORROSION/95 paper No. 128, NACE, 1995.

[85]   de Waard, C.; Smith, L.; Craig, B. D. The influence of crude oil on well tubing corrosion rates. EUROCORR 2001 paper no. 174, Riva del Garda, Italy, 2001.

[86]   de Waard, C.; Smith, L.: Bartlett, P.; Cunningham, H. Modelling Corrosion Rates in Oil Production Tubing. EUROCORR 2001 paper No. 254, Riva del Garda, Italy, 2001.

[87]   de Waard, C.; Smith, L. M.; Craig, B. D. THE INFLUENCE OF CRUDE OILS ON WELL TUBING CORROSION RATES. CORROSION/03 paper no. 629, NACE, 2003.

[88]   Smith, Liane; de Waard, Kees. Corrosion Prediction and Materials Selection for Oil and Gas Producing Environments. CORROSION/05 paper no. 648, NACE, 2005.

[89]   Vitse, F.; Alam, K.; GunalTun, Y.; de Torreben, D. Larrey; Duchet-Suchaux, P. Semi-Empirical model for prediction of the Top-of-the-line Corrosion Risk. CORROSSION/02 paper no. 245, NACE, 2002.

[90]   Sridhar, N.; Dunn, D.S.; Seth, M. APPLICATION OF A GENERAL REACTIVE TRANSPORT MODEL TO PREDICT ENVIRONMENT UNDER DISBONDED COATINGS. CORROSION/00 paper no. 366, NACE, 2000.

[91]   Nyborg, Rolf; Andersson, Peter; Nordsveen, Magnus. Implementation of CO_2 Corrosion Models in a Three-Phase Fluid Flow Model. CORROSION/00 paper no. 48, NACE, 2000.

[92]   Dugstad, Arne; Lunde, Liv; Videm, Ketil. Parametric Study of CO_2 Corrosion of Carbon Steel. CORROSION/94 paper No. 14, NACE, 1994.

[93]   Mishra, B.; Al-Hassan, S.; Olson, D. L.; Salama, M. M. Development of a predictive model for activation-controlled corrosion of steel in solutions containing carbon dioxide. Corrosion 53(11), 852-859, 1997.

[94]   Efird, K. D.; Wright, E. J.; Boros, J. A.; Hailey, T. G. Experimental Correlation of Steel Corrosion in Pipe Flow with Jet Impingement and Rotating Cylinder Laboratory Tests. Corrosion 49(12), 992, 1993.

[95]   Kanwar, D.; Jepson, W. P. A model to predict sweet corrosion of multiphase flow in horizontal pipelines. CORROSION/94 paper no. 24, NACE, 1994.

[96]   Jepson, W. P.; Bhongale, S.; Gopal, M. PREDICTIVE MODEL FOR SWEET CORROSION IN HORIZONTAL MULTIPHASE SLUG FLOW. CORROSION/96 paper no. 19, NACE, 1996.

[97]   Jepson, W. P.; Kang, C.; Gopal, M.; Stitzel, S. Model for Sweet Corrosion in Horizontal Multiphase Slug Flow. CORROSION/97 paper no. 11, NACE, 1997.

[98]   Jepson, W. P.; Stitzel, S.; Kang, C.; Gopal, M. MODEL FOR SWEET CORROSION IN HORIZONTAL MULTIPHASE SLUG FLOW. CORROSION/97 paper no. 602, NACE, 1997.

[99]   http://www.standard.no/imaker.exe?id=1369. NORSOK M-506 CO_2 Corrosion Rate Calculation Model (reversion 1, june 1998). Standardiseringen i Norge, 2007.

[100]   http://www.standard.no/imaker.exe?id=10405. NORSOK M-506 CO_2 Corrosion Rate Calculation Model (reversion 2, june 2005). Standardiseringen i Norge, 2007.

[101]   Olsen, Stein. CO2 Corrosion Prediction by use of the NORSOK M-506 Model – Guidelines and Limitations. CORROSION/03 paper no. 623, NACE, 2003.

[102]   Olsen, Stein; Halvorsen, Anne Marie; Lunde, Per G. CO_2 Corrosion Prediction Model - Basic Principles. CORROSION/05 paper no. 551, NACE, 2005.

[103]   Pots, B.F.M.; Hendriksen, E. L. J. A. CO_2 CORROSION UNDER SCALING CONDITIONS - THE SPECIAL CASE OF TOP-OF-LINE CORROSION IN WET GAS PIPELINES. CORROSION/00 paper no. 31, NACE, 2000.

[104]   Pots, Bert.F.M.; John, Randy C.; Rippon, Ian J.; Simon-Thomas, Maarten J. J.; Kapusta, Sergio D.; Girgis, Magdy M.; Whitham, Tim. IMPROVEMENTS ON DE WAARD-MILLIAMS CORROSION PREDICTION AND APPLICATIONS TO CORROSION MANAGEMENT. CORROSION/02 paper no. 235, NACE, 2002.

[105]   Gunaltun, Y.M. Combining research and field data for corrosion rate prediction. CORROSION/96 paper no. 27, NACE, 1996.

[106]   Gunaltun, Y. M.; Larray, D. CORRELATION OF CASES OF TOP OF LINE CORROSION WITH CALCULATED WATER CONDENSATION RATES. CORROSION/00, paper no. 71, NACE, 2000.

[107] Paisley, Dominic; Barrett, Nathan; Wilson, Owen. PIPELINE FAILURE: THE ROLES PLAYED BY CORROSION, FLOW AND METALLURGY. CORROSION/99 paper no. 18, NACE, 1999.

[108] Hedges, Bill; McVeigh, Lorraine. THE ROLE OF ACETATE IN CO_2 CORROSION: THE DOUBLE WHAMMY. CORROSION/99 paper no. 21, NACE, 1999.

[109] Gartland, Per Olav. CHOOSING THE RIGHT POSITIONS FOR CORROSION MONITORING ON OIL AND GAS PIPELINES. CORROSION/98 paper no. 83, NACE, 1998.

[110] Gartland, Per Olav; Salomonsen, Jan Erik. A PIPELINE INTEGRITY MANAGEMENT STRATEGY BASED ON MULTIPHASE FLUID FLOW AND CORROSION MODELLING. CORROSION/99 paper no. 622, NACE, 1999.

[111] Srinivasan, Sridhar; Kane, Russell D. PREDICTION OF CORROSIVITY OF CO_2/H_2S PRODUCTION ENVIRONMENTS. CORROSION/96 paper no. 11, NACE, 1996.

[112] Jangama, V. R.; Srinivasan, S. A Computer Model for Prediction of Corrosion of Carbon Steels. Corrosion/97 paper No. 318, NACE, 1997.

[113] Srinivasan, Sridhar; Tebbal, Saadedine. CRITICAL FACTORS IN PREDICTING CO_2/H_2S CORROSION IN MULTIPHASE SYSTEMS. CORROSION/98 paper no. 38, NACE, 1998.

[114] Srinvasan, Sridhar; Kane, Russell D. Corrosion prediction models need to include field, lab data - Using software system with full range of key parametric effects, a model can accurately predict corrosion rates in carbon steel. Pipe Line and Gas Industry 82(6), 39-48, 1999.

[115] Sangita, Kiran A.; Srinivasan, Sridhar. An Analytical Model to Experimentally Emulate Flow Effects in Multiphase CO_2/H_2S Systems. CORROSION/00 paper no. 58, NACE, 2000.

[116] Srinivasan, Sridhar; Kane, Russell D. CRITICAL ISSUES IN THE APPLICATION AND EVALUATION OF A CORROSION PREDICTION MODEL FOR OIL AND GAS SYSTEMS. CORROSION/03 paper no. 640, NACE, 2003.

[117] Garber, James D.; Perkins, Richard S.; Jangama, Vamshidhar R.; Alapati, Rama R. CALCULATION OF DOWNHOLE pH AND DELTA pH IN THE PRESENCE OF CO_2 AND ORGANIC ACIDS. CORROSION/96 paper no. 176., NACE, 1996.

[118] Fang, C. S.; Garber, J. D.; Perkins, R. S.; Reinhardt, J. R. Computer model of a gas condensate well containing CO_2 - phase II. CORROSION/89 paper no. 465, NACE, 1989.

[119] Farshad, F. F.; Garber, J. D.; Polaki, Venugopal. Comprehensive model for predicting corrosion rates in gas wells containing CO_2. SPE Production & Facilities 15(3), 183-190, 2000.

[120] Garber, James D.; Farshad, Fred; Reinhardt, James R.; Chen, Wei; Tadepally, Vamsee Priya; Winters, Robert. INTERNAL CORROSION RATE PREDICTION IN PIPELINES AND FLOWLINES USING A COMPUTER MODEL. CORROSION/04 paper no. 155, NACE, 2004.

[121] Crolet, J. L.; Bonis, M. R. A tentative method for predicting the corrosivity of wells in new CO_2 fields. In: Burke, P. A.; Asphahani, A. I.; Wright, B. S. Advances in CO_2 corrosion vol. 2, 23, 1985.

[122] Crolet, J. L.; Bonis, M. R. A tentative method for predicting the corrosivity of wells in new CO_2 fields. CORROSION/85 paper no. 27, NACE, 1985.

[123] Crolet, J. L.; Bonis, M. R. A tentative method for predicting the corrosivity of wells in new CO_2 fields. Materials performance 25(3), 41, 1986.

[124] Crolet, J.L.; Bonis, M. R. An optimized procedure for corrosion testing under CO_2 and H_2S gas pressure. Memoires et Etudes Scientifiques de la Revue de Metallurgie 85(7-8), 375-386, 1988.

[125] Crolet, J. L.; Bonis, M. R. An Optimized Procedure for Corrosion Testing Under CO_2 and H_2S Gas Pressure. CORROSION/89 paper no. 17, NACE, 1989.

[126] Bonis, M. R.; Crolet, J. L. Basics of the Prediction of the Risks of CO_2 Corrosion in Oil and Gas Wells. CORROSION/89 paper no. 466, NACE, 1989.

[127] Crolet, Jean-Louis; Bonis, Michel R. An Optimized procedure for corrosion testing under CO_2 and H_2S gas pressure. Materials Performance 29(7), 81-86, 1990.

[128] Crolet, Jean-Louis; Bonis, M. R. Prediction of the risks of CO_2 corrosion in oil and gas wells. SPE Production Engineering 6(4), 449-453, 1991.

[129] Turgoose, S.; Cottis, R. A.; Lawson, K. Modelling of Electrode Processes and Surface Chemistry in Carbon Dioxide Containing Solutions. ASTM Symposium on computer modelling of corrosion, STP 1154, San Antonio, Texas, 1990.

[130] Watson, M. K.; Postlethwaite, J. Numerical simulation of crevice corrosion of stainless steels and nickel alloys in chloride solutions. Corrosion 46, 522, 1990.

[131] Crolet, J. L. Mechanisms of Uniform Corrosion Under Corrosion Deposits. Journal of Materials Science 28(10), 2589-2606, 1993.

[132] Crolet, J.L. The electrochemistry of corrosion beneath corrosion deposits. Journal of Materials Science 28(10), 2577-2588, 1993.

[133] Crolet, J. L.; Thevenot, N.; Nesic, S. Role of conductive corrosion products in the protectiveness of corrosion layers. Corrosion 54, 194–203, 1998.

[134] Nesic, S. Prediction of Transport Processes in CO_2 Corrosion. European Federation of Corrosion (EFC) 13 paper 6, 120, 1994.

[135] Nesic, S. Prediction of Transport Processes in CO_2 Corrosion. Progress in the understanding and prevention of corrosion 1, Institute of metals, London, 539, 1993.

[136] Pots, B. F. M. Mechanistic Models for the Prediction of CO_2 Corrosion Rates Under Multi-Phase Flow Conditions. CORROSION/95 paper no. 137, NACE, 1995.

[137] Dayalan, E.; Vani, G.; Shadley, J. R.; Shirazi, S. A.; Rybicki, E. F. MODELING CO_2 CORROSION OF CARBON STEELS IN PIPE FLOW. CORROSION/95 paper no. 118, NACE, 1995.

[138] Sundaram, M.; Raman, V.; High, M. S.; Tree, D. A.; Wagner, J. Deterministic Modeling of Corrosion in Downhole Environments. CORROSION/96 paper no. 30, NACE, 1996.

[139] High, M. S.; Wagner, J.; Natarajan, S. Mechanistic Modelling of Mass Transfer in the Laminar Sublayer in Downhole Systems. CORROSION/00 paper no. 62, NACE, 2000.

[140] Kvarekvål, Jon. A KINETIC MODEL FOR CALCULATING CONCENTRATION PROFILES AND FLUXES OF CO_2-RELATED SPECIES ACROSS THE NERNST DIFFUSION LAYER. CORROSION/97 paper no. 5, NACE, 1997.

[141] Zhang, R.; Gopal, M.; Jepson, W. P. DEVELOPMENT OF A MECHANISTIC MODEL FOR PREDICTING CORROSION RATE IN MULTIPHASE OIL/WATER/GAS FLOWS. CORROSION/97 paper no. 601, NACE, 1997.

[142] Rajappa, S.; Zhang, R.; Gopal, M. MODELING THE DIFFUSION EFFECTS THROUGH THE IRON CARBONATE LAYER IN THE CARBON DIOXIDE CORROSION OF CARBON STEEL. CORROSION/98 paper no. 26, NACE, 1998.

[143] Dayalan, E.; de Moraes, F. D.; Shirazi, S. A.; Rybicki, E. F. CO_2 CORROSION PREDICTION IN PIPE FLOW UNDER FECO3 SCALE-FORMING CONDITIONS. CORROSION/98 paper no. 51, NACE, 1998.

[144] Anderko, Andrzej; Young, Robert D. SIMULATION OF CO_2/H_2S CORROSION USING THERMODYNAMIC AND ELECTROCHEMICAL MODELS. CORROSION/99 paper no. 31, NACE, 1999.

[145] Anderko, Andrzej; McKenzie, Patrice ; Young, Robert D. COMPUTATION OF RATES OF GENERAL CORROSION USING ELECTROCHEMICAL AND THERMODYNAMIC MODELS. CORROSION/00 paper no. 479, NACE, 2000.

[146] Anderko, A. Simulation of FeCO3/FeS Scale Formation Using Thermodynamic and Electrochemical Models. CORROSION/2000 paper no. 102, NACE, 2000.

[147] Anderko, A.; McKenzie, P.; Young, R. D. Computation of rates of general corrosion using electrochemical and thermodynamic models. Corrosion 57(3), 202-213, 2001.

[148]   Anderko, Andrzej; Sridhar, Narasi. CORROSION SIMULATION FOR THE PROCESS INDUSTRY. CORROSION/01 paper no. 348, NACE, 2001.

[149]   Anderko, Andrzej; Young, Robert D. A MODEL FOR CALCULATING RATES OF GENERAL CORROSION OF CARBON STEEL AND 13% Cr STAINLESS STEEL IN CO_2/H_2S ENVIRONMENTS. CORROSION/01 paper no. 86, NACE, 2001.

[150]   Postlethwaite, J.; Wang, F. Modelling mass transport in aqueous CO_2 corrosion in turbulent pipe flow. Materials Science forum 289-292(ELECTROCHEMICAL METHODS IN CORROSION RESEARCH VI - part 2), 771-788, 1998.

[151]   Wang, Fangyou. Modelling of Aqueous Carbon Dioxide Corrosion in Turbulent Pipe Flow. PhD Theses, University of Saskatchewan, Chemical Engineering, Canada, 1999.

[152]   Wang, F.; Postlethwaite, J. MODELLING OF AQUEOUS CO_2 CORROSION OF IRON IN TURBULENT PIPE FLOW. CORROSION/01 paper no. 41, NACE, 2001.

[153]   Nesic, Srdjan; Nordsveen, Magnus; Nyborg, Rolf; Stangeland, Aage. A Mechanistic Model for CO_2 Corrosion with Protective Iron Carbonate Films. CORROSION/01 paper No. 40, NACE, 2001.

[154]   Nesic, S.; Nordsveen, M.; Nyborg, R.; Stangeland, A. A diffusion-based model for uniform corrosion. Diffusions In Materials, DIMAT2000 194-199(PTS 1 & 2 Defect And Diffusion Forum), 1661-1674, 2001.

[155]   Nordsveen, M.; Nesic, S.; Nyborg, R.; Stangeland, A. A Mechanistic Model for Carbon Dioxide Corrosion of Mild Steel in the Presence of Protective Iron Carbonate Films - Part 1: Theory and Verification. Corrosion 59(5), 443-456, 2003.

[156]   Nesic, Srdjan; Lee, Kun-Lin John; Ruzic, Vukan. A MECHANISTIC MODEL OF IRON CARBONATE FILM GROWTH AND THE EFFECT ON CO_2 CORROSION OF MILD STEEL. CORROSION/02 paper no. 237, NACE, 2002.

[157]   Nesic, S.; Nordsveen, M.; Nyborg, R.; Stangeland, A. A Mechanistic Model for Carbon Dioxide Corrosion of Mild Steel in the Presence of Protective Iron Carbonate Films - Part 2: A Numerical Experiment. Corrosion 59(6), 489-497, 2003.

[158]   Nesic, S; Lee, K. L. J. A Mechanistic Model for Carbon Dioxide Corrosion of Mild Steel in the Presence of Protective Iron Carbonate Films - Part 3: Film Growth Model. Corrosion 59(7), 616-628, 2003.

[159]   Nesic, Srdjan; Xiao, Ying; Pots, Bernardus F. M. A Quasi 2-D Localized Corrosion Model. CORROSION/04 paper no. 628, NACE, 2004.

[160]   Nesic, Srdjan; Wang, Shihuai; Xiao, Jiyong Ying. Integrated CO_2 Corrosion - Multiphase flow model, SPE paper 87555, Aberdeen, 2004.

[161]   Nesic, Srdjan; Cai, JiYong; Wang, Shihuai; Xiao, Ying. Integrated CO_2 Corrosion - Multiphase Flow Model. CORROSION/04 paper no. 626, NACE, 2004.

[162]   Nešic, Srdjan; Cai, Jiyong; Lee, Kun-Lin John. A MULTIPHASE FLOW AND INTERNAL CORROSION PREDICTION MODEL FOR MILD STEEL PIPELINES. CORROSION/05 paper no. 556, NACE, 2005.

[163]   Heppner, K. L.; Evitts, R. W.; Postlethwaite, J. Determining The Crevice Corrosion Incubation Period of Passive Metals for Systems With Moderately High Electrolyte Concentrations – Application of Pitzer's Ionic Interaction Model. CORROSION/03 paper no. 691, NACE, 2003.

[164]   Song, F. M.; Kirk, D. W.; Graydon, J. W.; Cormack, D. E. PREDICTION FOR CO_2 CORROSION OF ACTIVE STEEL UNDER A PRECIPITATE. CORROSION/04 paper no. 382, NACE, 2004.

[165]   Song, F. M.; Kirk, D. W.; Cormack, D. E. A Comprehensive Model for Predicting CO_2 Corrosion in Oil and Gas Systems. CORROSION/05 paper no. 180, NACE, 2005.

[166]   Nesic, Srdjan; Seagraves, Sam; Zhang1, Ziru; Li, Hui; Sormaz, Dusan. FREECORP OS: A Free Open Source Model for Internal Corrosion of Mild Steel Oil and Gas Pipelines. CORROSION/08, paper nr. not available yet, NACE, 2008.

[167] Song, F. M.; Kirk, D. W.; Graydon, J. W.; Cormack, D. E. Predicting carbon dioxide corrosion of bare steel under an aqueous boundary layer. Corrosion 60(8), 736-748, 2004.

[168] Levich, V. G. Physicochemical Hydrodynamics. Prentice-Hall, Englewood Cliffs, New Jersey, 1962.

[169] Lopez, D. A.; Perez, T.; Simison, S. N. The influence of microstructure and chemical composition of carbon and low alloy steels in CO_2 corrosion. A state-of-the-art appraisal. Materials and design 24, 561-575, 2003.

[170] Dugstad, Arne. Fundamental Aspects of CO_2 Metal Loss Corrosion Part 1: Mechanism. CORROSION/06 paper no. 111, NACE, 2006.

[171] Ogundele, G. I.; White, W. E. Some Observations on Corrosion of Carbon-Steel in Aqueous Environments Containing Carbon-Dioxide. Corrosion 42(2), 71-78, 1986.

[172] M. Stern. The Electrochemical Behavior, including hydrogen overvoltage, of iron in acid environments. J. Electrochemical Soc. 102, 609, 1955.

[173] Schmitt, G.; Rothmann, B. Untersuchungen zum Korrosionsmechanismus von unlegiertem Stahl in sauerstofffreien Kohlensäurelösungen. I - Kinetik der Wasserstoffabscheidung. Werkstoffe und Korrosion 28, 816, 1977.

[174] Schmitt, G.; Rothmann, B. Zum Korrosionsverhalten von unlegierten und niedriglegierten Stählen in Kohlensäurelösungen. Werkstoffe und Korrosion 29, 237, 1978.

[175] Schmitt, G.; Rothmann, B. Studies on the corrosion mechanism of unalloyed steel etc. - I kinetics of the liberation of hydrogen. Advances in CO_2 corrosion vol. 1, 72, 1984.

[176] Wieckowski, A.; Ghali, E.; Szklarczyk, M.; Sobokowski, J. The behaviour of iron electrode in CO_2 saturated neutral electrolyte—I. Electrochemical study. Electrochimica Acta 28(11), 1619, 1983.

[177] Wieckowski, A.; Ghali, E.; Szklarczyk, M.; Sobokowski, J. The behaviour of iron electrode in CO_2 saturated neutral electrolyte—II. Radiotracer study and corrosion considerations. Electrochimica Acta 28(11), 1627, 1983.

[178] Eriksrud, E.; Søntvedt, T. Effect of Flow on CO_2 Corrosion Rates in Real and Synthetic Formation Waters. CORROSION/83 paper no. 44, NACE, 1984.

[179] Gray, L. G. S.; Anderson, B. G.; Danysh, M. J.; Tremaine, P. R. Mechanisms of Carbon Steel Corrosion in Brines Containing Dissolved Carbon Dioxide. CORROSION/89 paper no. 464, NACE, 1989.

[180] Hurlen, T.; Gunvaldsen, S.; Tunold, R.; Blaker, F.; Lunde, P. G. Effects of carbon dioxide on reactions at iron electrodes in aqueous salt solutions. Journal of Electroanalytical Chemistry and Interfacial Electrochemistry 180(1-2), 511-26, 1984.

[181] Hurlen, T.; Gunvaldsen, S. Effects of buffers on hydrogen evolution at iron electrodes. Electrochem. Acta 29, 1163, 1984.

[182] Gray, L. G. S.; Anderson, B. G.; Danysh, M. J.; Tremaine, P. R. Effect of pH and Temperature on the Mechanism of Carbon Steel Corrosion by Aqueous Carbon Dioxide. CORROSION/90 paper no. 40, NACE, 1990.

[183] Nesic, S.; Postlethwaite, J.; Olsen, S. An Electrochemical Model for Prediction of CO_2 Corrosion. CORROSION/95 paper no. 131, NACE, 1995.

[184] Nesic, S; Postlethwaite, J; Olsen, S. An Electrochemical Model for Prediction of Corrosion of Mild Steel in Aqueous Carbon Dioxide Solutions. Corrosion 52(4), 280-294, 1996.

[185] Bockris, J. O'M.; Drazic, D.; Despic, A. R. The electrode kinetics of the deposition and dissolution of iron. Electrochimica Acta 4(2-4), 325-361, 1961.

[186] Bockris, J. O'M.; Reddy, A. K. N. Modern Electrochemistry volume 1 and 2, Plenum Press, New York, 1970.

[187] Drazic, D.M. Iron and its Electrochemistry in an Active State. In: Conway, B.E.; Bockris, J. O'M; White, R. E. Modern Aspects of Electrochemistry, vol. 19, Plenum Press, New York, 69, 1989.

[188] Schmitt, G.; Rothmann, B. Untersuchungen zum Korrosionsmechanismus von unlegiertem Stahl in sauerstofffreien Kohlensäurelösungen. II - Kinetik der Eisenauflösung. Werkstoffe und Korrosion 29, 98, 1978.

[189] Davies, D. H.; Burstein, G. T. The Effects of Bicarbonate on the Corrosion and Passivation of Iron. Corrosion 36(8), 416-422, 1980.

[190] Nesic, S.; Thevenot, N.; Crolet, J.L.; Drazic, D. Electrochemical Properties of Iron Dissolution in the Presence of CO_2 — Basics Revisited. CORROSION/96 paper no. 3, NACE, 1996.

[191] Rogers, W. F.; Rowe, J. A. Corrosion effects of hydrogen sulphide and carbon dioxide in oil production. Proc. 4th World Petroleum Congress, paper 3, 479-99, 1955.

[192] Davies, C. W. The extent of dissociation of salts in water. VIII. An equation for the mean ionic activity coefficient of an electrolyte in water, and a revision of the dissociation constants of some sulfates. Journal of the Chemical Society 2, 2093-8, 1938.

[193] Davies, C. W. Ion Association. Butterworths, London, 1962.

[194] Zemaitis, F. D., Jr.; Clark, D. M.; Rafal, M.; Scrivner, N. C. Handbook of Aqueous Electrolyte Thermodynamics. Theory & Application. DIPPR, AIChE: New York, 1986.

[195] Pitzer, K. S. Activity coefficients in electrolyte solutions. CRC Press, 2nd ed., 1991.

[196] Thomsen, K. Aqueous Electrolytes, model parameters and process simulation. Ph.D. Thesis, IVC-SEP, Technical University of Denmark, 1997.

[197] Iliuta, M.; Thomsen, K.; Rasmussen, P. Extended UNIQUAC model for correlation and prediction of vapor-liquid-solid equilibria in aqueous salt systems containing non-electrolytes. Part A. Methanol-water-salt systems. Chemical Engineering Science 55, 2673-2686, 2000.

[198] Thomsen, K.; Rasmussen, P.; Gani, R. Correlation and prediction of thermal properties and phase behaviour for a class of electrolyte systems. J. Chem. Eng. Science 51, 3675-83, 1996.

[199] Kooijmans, Johannes. Corrosion and protective coating formation in water mains. GWF, das Gas- und Wasserfach 81, 611-15 628-33, 1938.

[200] Riesenfeld, F. C.; Blohm, C. L. Corrosion problems in gas-purification units employing MEA (monoethanolamine) solutions. Petroleum Refiner 29(4), 141, 1950.

[201] Hackerman, N.; Glenn Jr., E. E. Corrosion of steel by air-free, dilute, weak acids. Journal of the Electrochemical Society 100, 339-44, 1953.

[202] Sowards, D. M.; Hackerman, N. Kinetics of surface reactions of metals. I. Iron. Journal of the Electrochemical Society 102, 297-303, 1955.

[203] Sontheimer, H.; Kölle, W.; Snoeyink, V. The siderite model of the formation of corrosion resistant scales. American Water Works Association 73, 572-579, 1981.

[204] Eriksrud, E.; Søntvedt, T. Effect of Flow on CO_2 Corrosion Rates in Real and Synthetic Formation Waters. CORROSION/83 paper no. 44, NACE, 1984.

[205] Whitman, G. W.; Russell, R. P.; Altieri, V. J. Effect of Hydrogen-Ion Concentration on the Submerged Corrosion of Steel. Industrial & Engineering Chemistry 17(7), 665, 1924.

[206] Leybold, W. The solution of iron by carbonic acid. Angewandte Chemie 37, 190-1, 1924.

[207] Leybold, W. Protection of wet gas meters against corrosion. GWF, das Gas- und Wasserfach 70, 294-5, 1927.

[208] Crolet, J. L.; Samaran, J. P. The use of the anti-hydrate treatment for the prevention of CO_2 corrosion in long crude gas pipelines. CORROSION/93 paper No. 102, NACE, 1993.

[209] Haarberg, T.; Jakobsen, J. E.; Oestvold, T. The effect of ferrous iron on mineral scaling during oil recovery. Acta Chemica Scandinavica 44(9), 907-15, 1990.

[210] Olsen, S.; Lunde, O.; Dugstad, A. Stabilizing pH in Troll pipelines solves glycol-regen problems. Oil & Gas Journal 97, 59-62, 1999.

[211] Dugstad, A.; Seiersten, M. pH-stabilisation, a Reliable Method for Corrosion Control of Wet Gas Pipelines. SPE paper 87560, Aberdeen, 2004.

7 Thermodynamic model and experiments in the mixed solvent electrolyte system CO₂-Na₂CO₃-NaHCO₃-MEG-H₂O

Experimental work and modelling has been studied for the *CO₂-NaHCO₃-Na₂CO₃-Monoethyle glycol(MEG)-water* system. Measurements were conducted at 2 to 60 °C at atmospheric conditions. 212 new solid-liquid equilibrium (SLE) experimental data points are presented here. The extended UNIQUAC model was used for correlating SLE, vapour-liquid equilibrium (VLE), excess enthalpy, and excess heat capacity based on 751 experimental data points. The determined parameters are valid between -50 and 90 °C. A method based on the principles of Schreinemakers *et al.*[1,2] is developed for interpreting the measured data. A simple density model of *NaHCO₃-Na₂CO₃-NaCl-MEG-water* is given.

The aim of this study is to investigate *CO₂* corrosion through experimental work and modelling. The experimental work is focused on the *CO₂-NaOH-MEG-H₂O* system found in wet gas pipelines. The system is a sub-system of *CO₂-Na₂O-H₂O-MEG* as shown by the grey line in figure 21. Similarly *Na₂CO₃-NaHCO₃-MEG-H₂O* is also a sub-system of *CO₂-Na₂O-MEG-H₂O* shown by the black line in figure 21. Therefore solubility measurements may by conducted for the *Na₂CO₃-NaHCO₃-MEG-H₂O* system in order to model the *CO₂-NaOH-MEG-H₂O* system.
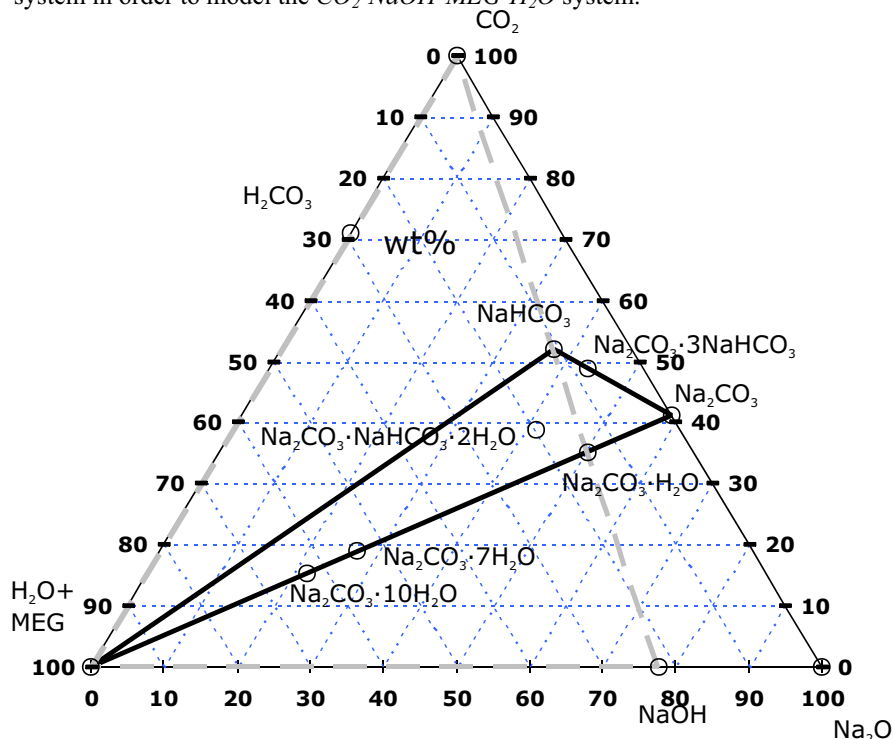
Figure 21: An overview of the components in the *CO₂-Na₂O-H₂O* system. Black line is the ternary *Na₂CO₃-NaHCO₃-H₂O* system and the grey dotted line is the *CO₂-NaOH-H₂O system.*

An activity coefficient model based on the Pitzer methodology was previously developed by Kaasa[3] for the aqueous $NaHCO_3$-Na_2CO_3-MEG-H_2O system. Sandengen[4] recently extended the model to glycol solutions of Na_2CO_3-$NaHCO_3$-MEG-H_2O.

Only a few experimental studies of the Na_2CO_3-$NaHCO_3$-MEG-H_2O system have been published. This includes Oosterhof *et al.*[5] who published solubility of Na_2CO_3 in MEG-H_2O at relatively high temperature. Gärtner *et al.*[6] continued their work with *MEG* concentrations larger than 50 *w % MEG*. The work by Gärtner *et al.*[6] was mainly focused on solubility in the quaternary Na_2CO_3-$NaHCO_3$-MEG-H_2O system. Only few of these data concerned solubility in the ternary $NaHCO_3$-MEG-H_2O system. Sandengen[4] recently published solubility measurements of $NaHCO_3$ in *MEG*-H_2O at low temperature and high *MEG* concentration. Their main objective was scale prediction and not corrosion modelling.

The Na_2CO_3-$NaHCO_3$-MEG-H_2O system is modelled here, in order to describe the activity coefficient through correlation of the experimental VLE, SLE and excess enthalpy data using the extended UNIQUAC thermodynamic model for electrolytes and non-electrolytes. It has previously been shown by Thomsen and co-workers[7,8,9] that the model may be applied for mixed solvent electrolyte systems. Here the model, method, and theory are used unchanged compared to previous works. A brief overview of the thermodynamic model is given in appendix D.2 and D.3. The model allows for estimation of *pH*, activity coefficients, and CO_2 solubility in the liquid phase which is important for corrosion estimation.

Two modelling approaches are used. One parameter set *A* is estimated based on previously published parameters. In another parameter set *B,* new parameters for the Na_2CO_3-$NaHCO_3$-H_2O sub-system is estimated using experimental values extracted from the IVC-SEP electrolyte database[10].

7.1   Thermodynamic modelling details

The extended UNIQUAC model is an activity coefficient model. It consists of the original UNIQUAC model plus a Debye-Hückel long-range term. The gas phase fugacities are calculated using the Soave-Redlich-Kwong (SRK) equation of state employing a quadratic mixing rule for the "a" parameter and a linear mixing rule for the "b" parameter. The used critical properties and the acentric factor, ω, is given in table 4 The gas phases in this study is close to ideal and the accuracy of the properties are not significant. No equation of state interaction parameters were used.

Table 4: Gas-phase properties used in the SRK equation.

	T_c (K)	P_c (Bar)	ω
H_2O	637.096	220.64	0.344
CO_2	304.2	72.83	0.225

Generally the extended UNIQUAC parameter set is consistent and it allows for simultaneous calculation of SLE, VLE, Liquid-Liquid equilibrium (LLE), excess enthalpy, excess heat capacity, heat of solution, heat of dilution, activity, and osmotic coefficient with the same set of parameters. The extended UNIQUAC model reduces to the original UNIQUAC model if no ions are present and the model may also be used for calculation of properties in the non-electrolyte system *MEG-H_2O*.

A Gibbs energy minimization routine supports the calculation of the properties of the electrolytic fluid phase. This is done in order to perform speciation equilibrium calculations and phase equilibrium calculations. The method of calculating the SLE, VLE, excess enthalpy, heat of solution and excess heat capacity was briefly mentioned by Iliuta *et al.*[9] and in detail by Thomsen[7].

The following equilibria are considered in this work:

Speciation equilibria:

$$H_2O(l) \rightleftharpoons H^+ + OH^- \tag{199}$$

$$CO_2(aq) + H_2O(l) \rightleftharpoons H^+ + HCO_3^- \tag{200}$$

$$HCO_3^- \rightleftharpoons H^+ + CO_3^{2-} \tag{201}$$

Vapour-Liquid Equilibria (VLE):

$$H_2O(g) \rightleftharpoons H_2O(l) \tag{202}$$

$$CO_2(g) \rightleftharpoons CO_2(aq) \tag{203}$$

Solid-Liquid Equilibria (SLE):

$$H_2O(s) \rightleftharpoons H_2O(l) \tag{204}$$

$$MEG(s) \rightleftharpoons MEG(aq) \tag{205}$$

$$MEG \cdot H_2O(s) \rightleftharpoons MEG(aq) + H_2O(l) \tag{206}$$

$$NaHCO_3(s) \rightleftharpoons Na^+ + HCO_3^- \tag{207}$$

$$Na_2CO_3(s) \rightleftharpoons 2Na^+ + CO_3^{2-} \tag{208}$$

$$Na_2CO_3 \cdot H_2O(s) \rightleftharpoons 2Na^+ + CO_3^{2-} + H_2O \tag{209}$$

$$Na_2CO_3 \cdot 7H_2O(s) \rightleftharpoons 2Na^+ + CO_3^{2-} + 7H_2O \tag{210}$$

$$Na_2CO_3 \cdot 10H_2O(s) \rightleftharpoons 2Na^+ + CO_3^{2-} + 10H_2O \tag{211}$$

$$Na_2CO_3 \cdot NaHCO_3 \cdot 2H_2O(s) \rightleftharpoons 3Na^+ + CO_3^{2-} + HCO_3^- + 2H_2O \tag{212}$$

$$Na_2CO_3 \cdot 3NaHCO_3(s) \rightleftharpoons 5Na^+ + CO_3^{2-} + 3HCO_3^- \tag{213}$$
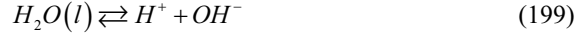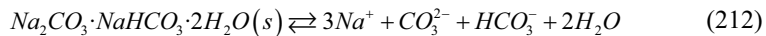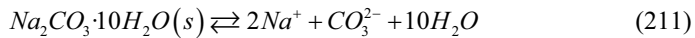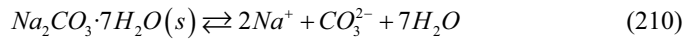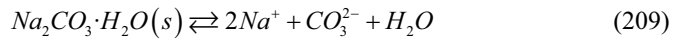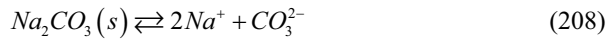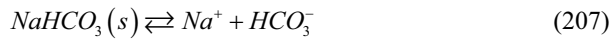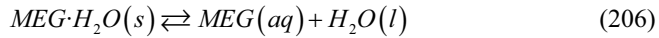
The equilibria (202) and (203) are used in the VLE calculations. It is assumed that *MEG* is not present in the gas phase since we restrict VLE data to 90 °*C*. Glycol contributes 1.5 % to the total pressure at 90 °C and less than 1 % at most temperatures[11]. The equilibria (199), (200), and (201) describe the speciation. Reaction (201) results in an increased challenge in the experimental work and modelling, since it shows how carbonate and bicarbonate salts may convert to the other. The equilibria (204) through (213) shows the formation of possible solid phases. Four hydrates may form in addition to the two double salts, trona (*$Na_2CO_3 \cdot NaHCO_3 \cdot 2H_2O$*) and wegscheiderite *($Na_2CO_3 \cdot 3NaHCO_3$)*. The molal equilibrium constants, $K_{T,P_o,k}$, of reactions k at temperature T and pressure P_o is calculated from the standard state properties and the thermodynamic relations:

$$\frac{d\ln K_{T,P_o,k}}{dT} = \frac{\Delta_k H^o_{T,P_o}}{RT^2}, \qquad \frac{d\Delta_k H^o_{T,P_o}}{dT} = \Delta_k C^o_p\left(T,P_o\right) \qquad (214)$$

Δ_k signifies the change in enthalpy(H) or heat capacity(C_p) of reaction (202) to (213). Superscript ^{o} indicates standard state values. NIST[12] standard state properties were used at reference conditions T_o=298.15 K and P_o=1 bar. The correlation of the heat capacity is given by the following equation, defined by Thomsen[7]:

$$C^o_{p,i} = a_i + b_i T + \frac{c_i}{T - T_\Theta} \qquad (215)$$

By integrating equation (214) using (215) results in the following temperature function of the equilibrium constants expressed in terms of the standard state thermodynamic properties, Gibbs energy (*G*) and enthalpy:

$$R\ln K_{T,P_o,k} = -\Delta_k G^o_{T_o,P_o}\Big/T_o + \Delta_k H^o_{T_o,P_o}\left(\frac{1}{T_o} - \frac{1}{T}\right) + \Delta a\left(\ln\frac{T}{T_o} + \frac{T_o}{T} - 1\right)$$
$$+ 0.5\Delta b\left(\frac{(T-T_o)^2}{T}\right) + \frac{\Delta c}{T_\Theta}\left(\frac{T-T_\Theta}{T}\ln\frac{T-T_\Theta}{T_o-T_\Theta} + \ln\frac{T_o}{T}\right) \qquad (216)$$

where T_Θ=200K and Δa, Δb and Δc are calculated using the stoichiometric coefficients of component i in reaction k, v_{ik}, by $\Delta u = \sum_{i=1}^{N} v_{ik} u_i$, $u = a,b,c$.

Coefficient b_i and c_i are assumed to be zero for all solid and gaseous species. Lists of used *a*, *b* and *c*'s are found in the tables page 116 and 117. A constant heat capacity is therefore used for these species. Heat capacities used in set *A* were either those from NIST[12] or were determined in a previous study by Thomsen *et al.* [7,8,13]. The heat capacities for solids were updated in parameter set *B* by using a modified Kopps rule[14] for the values that were not listed in NIST[12].

7.2   Experimental methods and apparatus

7.2.1   Chemicals

The purity of the chemicals is listed in table 5. The solid chemicals were additionally analysed by powder X-ray diffraction and titration and showed no impurities. The used demineralised water was produced onsite and had a conductivity of less than 0.2 μS.

Table 5: Purity of the used chemicals.

Chemical	CAS	Purity	Supplier
MEG	107-21-1	Puriss p.a. ACS >99.5 %	Riedel-deHaën
NaHCO₃	144-55-8	Puriss p.a. ACS >99.7 % Puriss >99.5 %	Fluka ACROS
Anhydrous *Na₂CO₃*	487-19-8	Puriss p.a. ACS >99.8 % dried at 300 °C	Riedel-deHaën
HCl	7647-01-00	36 %-38 %	J. T. Baker
Water	7732-18-5	Demineralised, < 0.2 μS	Technical University of Denmark

7.2.2   Experimental setup

The experimental setup consisted of two units, an equilibrium unit and an analysis unit. The equilibrium unit consisted of seven cells connected in parallel to a Julabo F25 heating/cooling circulation bath which controlled temperature within ±0.01K.
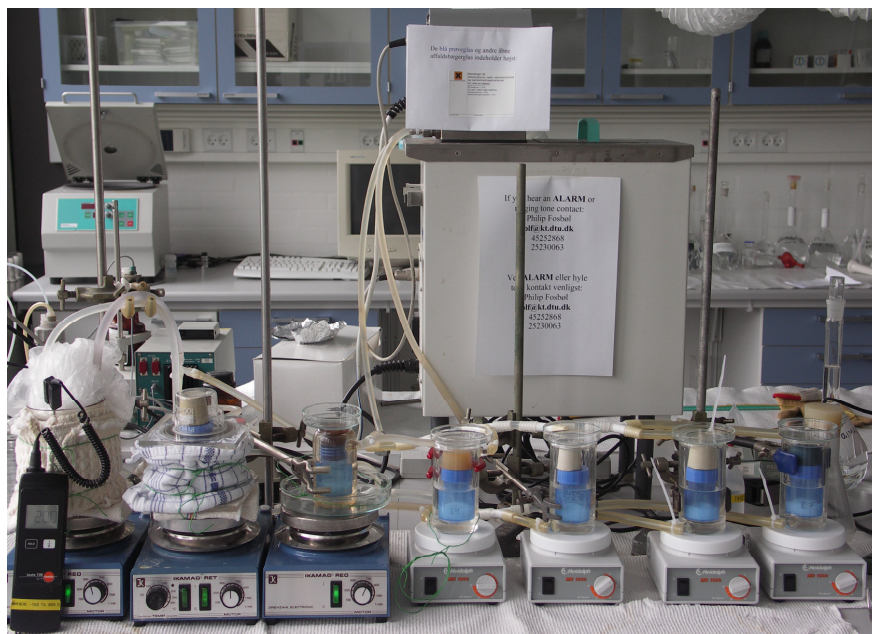
Figure 22: The seven equilibrium cells connected in parallel to the heating/cooling unit.

Figure 22 shows the equilibrium cells. The first three on the left consisted of equipment assembled from spare parts in the laboratories. The last four on the right was custom made for this setup. Each cell consisted of a glass lid and a heat jacket surrounding an equilibrium chamber. A cell is sketched in figure 23. The equilibrium chamber was a closed 50 mL poly ethylene container with screw cap and a magnetic stirrer. A dead weight was placed on top of the containers to keep them submerged. Water was used for transferring heat from the heat jacket to the equilibrium chamber.
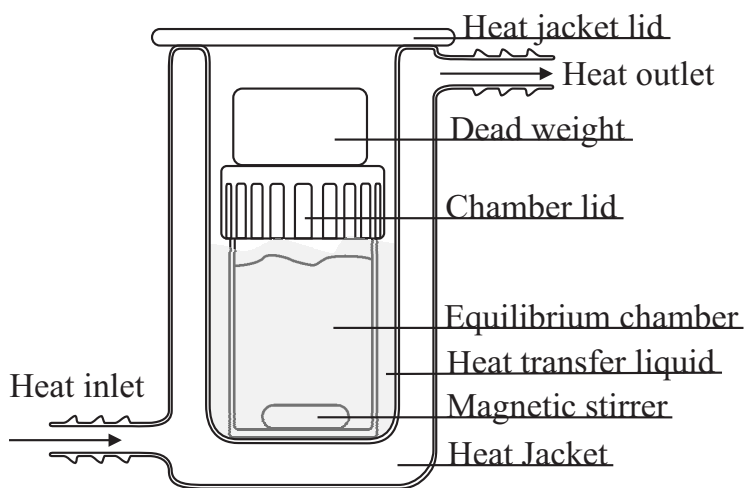
Figure 23: Sketch of a SLE equilibrium cell.

The saturated solutions were analyzed by potentiometric titration using an autoburette, ABU93 triburette, from Radiometer. The pH electrodes were an Orion 617500 and a Metrohm 6.0228.000 connected to a ThermoOrion 635 unit and a Metrohm 694 pH meter respectively.

Figure 24: The analysis unit consisting of to titration cells in the left part of the picture and the computer on the right for data acquisition and burette control. The ABU unit is seen behind the titration cells.

The two electrodes are seen in the titration process in figure 24, the Orion unit at the left and the Metrohm unit at the right of the black ABU unit in the back. The computer for data acquisition and burette control is seen in the right part of the picture. The ABU unit allows up to three simultaneous titrations but only two were used. Software to control the ABU unit with respect to the measured pH was developed. The software allowed for high precision titrations to be performed close to the equivalence points.

7.3 Experimental procedure

The chemicals were mixed from the pure chemicals listed in table 5 and a magnet was added to the equilibrium chamber. Containers were kept closed until sampling. The size of the vapour phase was kept low and assumed to consist mainly of air. Solutions were stirred at approximately 500 rpm and set to equilibrate over a period of 16 h to 78 h. The time necessary for equilibration was determined to be a few hours.

The pressure was maintained at 1 *atm* ± 0.05 *atm* and the temperature was measured in the heat transferring liquid just before sampling at an accuracy of ±0.05*K*. The *CO₂* pressure was not measured but assumed to correspond to the atmospheric background of approximately 0.0004 bar.

The liquid was filtered before sampling by one of four methods. Preferably a cone shaped filter paper was put into the equilibrium chamber and the liquid was allowed to flow inside the filter. If this method did not produce a sample large enough for analysis, the content of the equilibrium chamber was filtered through a conically shaped paper filter on top of small beaker. If these two procedures failed to produce enough liquid for analysis, saturated liquid was absorbed with a known amount of paper towel inside a cone shaped filter, similar to method one. Finally, liquids of high glycol concentrations were vacuum filtered using ceramic filters because they only wet the surface of the paper filters poorly.

Samples were obtained by micropipette when possible at a volume of 100 to 1000 μL and weighed. Samples were between 0.1 *g* and 1.3 *g*. Samples were taken in triple from each equilibrium chamber. The saturated liquid was allowed to stand no more than 5 minutes before being weighed. The densities of the samples were determined as weight per volume sample at system temperature.

Samples were stored up to 3 days after sampling in closed weighing containers similar to the equilibrium chambers and titrated by 0.1 *M HCl*. Approximately 15 *g* of water was added to the samples prior to the automatic titration which took 30 minutes on average and samples were stirred at 400 rpm while titrating. The titration was configured so that a stable *pH* was obtained over a period of 10 seconds before the next addition of *HCl*. Titrations required between 1.5 *mL* and 25 *mL HCl*. The diluted *HCl* was produced from concentrated *HCl* and standardized by *Na₂CO₃*.

The solid phases were analysed when in doubt by powder X-ray diffraction to determine the type of solid phase. This was done by decanting the liquid and analysing the solid within 30 minutes after separation.

7.3.1 Previous work on analysis for sodium and carbonate

Solubility in the *CO₂-Na₂O-H₂O* system has been thoroughly studied in the open literature. Table 6 gives a summary of the used experimental methods in the literature.

The methods were used for solubility determination in aqueous systems and may similarly be used for the solubility determination in the mixed solvent Na_2CO_3-$NaHCO_3$-MEG-H_2O system.

The techniques fall into two categories, one for determining carbon species, another for determining sodium content. The measurements are always converted to solubility of solid Na_2CO_3, $NaHCO_3$ or $NaOH$, and rarely tabulated as ionic species.

Table 6: Overview of analytical methods used in the literature for analysing the CO_2-Na_2O-H_2O system.

#	Method	Determines	Used by reference
1	Acid titration	Total alkalinity (sodium) or total carbon or bicarbonate or carbonate.	Alkali: 15,16,17,18,19,20,21 HCO_3^- and CO_3^{2-} : 22,23,6,24 Only HCO_3^- : 25,26,27,28,29 Only CO_3^{2-} : 30, 31,32
2	Acid + absorbed CO_2	Total carbon content	16,17,18,33,19,34,29,20
3	Winklers method	Carbonate and Bicarbonate or Carbonate and hydroxide	35,36,20,29
4	Gravimetrical precipitation by $BaCl_2$	Total carbon (as $BaCO_3$)	35,29
5	Triple Acetate method	Total Sodium	37, 38, 39, 29, 24, 20
6	Drying	Total Sodium (as $NaCl$ or Na_2CO_3)	$NaCl$: 33,40,41. Na_2CO_3: 21,19
7	ICP-AES	Total Sodium	5

The solubility of a salt in the Na_2CO_3-MEG-H_2O or in the $NaHCO_3$-MEG-H_2O system may be determined by using one or more of the methods mentioned in table 6. A second or third analysis only serves to check the result of the first. If the precipitating salt is a hydrate, the *water-MEG* ratio is changed from its initial value. This ratio needs to be determined separately.

The determination of solubility of salts in a Na_2CO_3-$NaHCO_3$-MEG-H_2O solution requires the use of at least two different methods from table 6, one for determining sodium content and another for determining carbon content. From these results, the composition of the solution can be determined. Again, if a salt hydrate precipitates from the initial solution, the *water-MEG* ratio is changed from its initial value.

The first method mentioned in table 6 is titration. It is a well-known method for analysing carbonate mixtures which is also applied in this study. The solution is titrated using a strong acid. Interpreting the equivalence points however is not a trivial task.

In the second approach, total carbon content is determined by adding an excess of strong acid to a sample to convert carbonates and bicarbonates to CO_2. It is stripped off with nitrogen. The vapour must be dried and the total carbon is determined by adsorption of CO_2 or by the weight loss of the solution. This method requires relatively big sample sizes and very accurate weights. It has been used by many authors over the years despite the difficulties[16,17,18,29,20,33,19,34]. This method was also tested in this study, but consistent results were not obtained.

Winklers method[42] may be applied in two different ways; either for analysing mixtures of carbonate and hydroxide or mixtures of carbonate and bicarbonate. In both cases the total sodium is determined by a preliminary titration. Hydroxide in a

carbonate/hydroxide solution is determined by precipitating carbonate as $BaCO_3$ and titration of hydroxide to the equivalence point[35]. The bicarbonate in a carbonate/bicarbonate solution is determined by adding a known excess of $NaOH$, precipitating the existing and formed carbonate as $BaCO_3$ and back-titrating the excess hydroxide. The amount of bicarbonate is calculated from the difference of the added and back-titrated $NaOH$[36,29,20].

In a fourth method, aqueous $BaCl_2$ is added to precipitate carbonates as $BaCO_3$. The total carbon is determined gravimetrically or by titration of the precipitated $BaCO_3$[35,29]. The gravimetrical determination may require big samples and careful filtration. Barium requires special handling in the laboratory.

The total amount of sodium may be determined by either of the three following methods or by titration. Titration is used in this work.

One method is the triple acetate method, in which sodium is precipitated as the triple uranyl acetate salt and weighed gravimetrically as $(UO_2)_3 ZnNa(CH_3COO)_9 \cdot 6H_2O$.

Small amounts of sodium can be determined, due to the large molecular mass of triple uranyl acetate. A description is given by Barber and Kolthoff[38] and Salit[37], but the method has limitations[39] and the uranium makes the solutions hazardous.

Another method in which total sodium is determined is drying of the liquid phase. By adding excess amounts of HCl, CO_2 vaporizes and sodium is determined as precipitated $NaCl$ by drying[33,40,41]. If carbonate is the only anion it may be determined by drying and weighing as Na_2CO_3[21,19]. Drying is problematic in solutions containing bicarbonate which decomposes at temperatures above 60 °C by

$$2NaHCO_3 \rightarrow Na_2CO_3 + CO_2(g) + H_2O(g) \qquad (217)$$
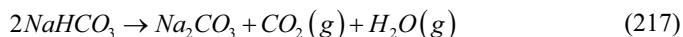
This method is also problematic when used for Na_2CO_3-$NaHCO_3$-MEG-H_2O solutions because of the low vapour pressure of MEG.

The third method of determining total sodium is ICP-AES (Inductively Coupled Plasma - Atomic Emission Spectrometry). This method was used by Oosterhof *et al.*[5]

7.3.2   Interpreting the titration results

Very few authors have reported the complete compositions of the solvents of the saturated solutions. The solvent composition may change significantly if solvent molecules precipitate together with the salts. According to equations (209) to (212) Na_2CO_3, can precipitate with various amounts of hydrate water. The amount of solid phase precipitated must therefore be known in order to determine the new solvent composition. This is a general problem in mixed solvent electrolyte systems. Oosterhof *et al.*[5] solved this problem by applying a total organic carbon method (TOC) for their poly ethylene glycol mixtures. Unfortunately they did not apply this method for their *MEG* mixtures. Instead they assumed the amount of precipitated solvent to be negligible. The solvent compositions they reported are therefore not accurate. In this work a method is presented to solve this problem. It may also be applied to other similar mixed solvent electrolyte systems.
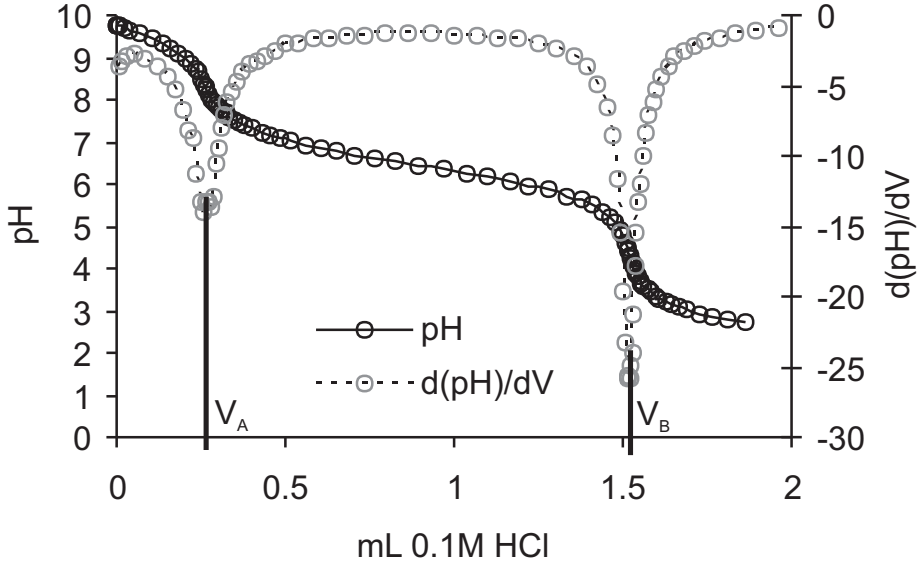
Figure 25: A regular titration curve of a 0.3 g sample saturated with *NaHCO₃* in a 63 *wt% MEG* solution at 25 °C.

Figure 25 shows a typical titration curve of a saturated solution from the Na_2CO_3-$NaHCO_3$-MEG-H_2O mixture obtained in this work. Volumes of titrant at the two equivalence points are V_A and V_B. The interpretation of the titration curves is not straight forward. Three different methods for interpreting this type of measurements are found in published scientific papers giving significantly different results. The methods depend on the concentration of the titrant, C_{HCl}, and the sample size in kilo grams, m_{sample}. Equation (218) to (220) represent the three methods and give the liquid phase composition in *mol/kg* solution of component *i*, S_i. Method I provide both the composition of carbonate and bicarbonate, whereas method II and III only give the total carbon, *TC*, or total sodium, *TNa*:

Method I: $$S_{CO_3^{2-}} = C_{HCl}V_A / m_{sample} \ , \qquad S_{HCO_3^-} = C_{HCl}\left(V_B - 2V_A\right) / m_{sample} \qquad (218)$$

Method II: $$S_{TC} = S_{CO_3^{2-}} + S_{HCO_3^-} = C_{HCl}\left(V_B - V_A\right) / m_{sample} \qquad (219)$$

Method III: $$S_{TNa} = C_{HCl}V_B / m_{sample} \qquad (220)$$

Method I and method II both depend on V_A. Our results show that V_A can not be accurately determined. The reasons are due to the evaporation of an unknown amount of carbon dioxide, difference in titration and equilibrium temperatures, and the degree of dilution of the sample during titration. A typical accuracy of 5 % to 10 % is obtained, which is unacceptable, see table 7 column $S_{CO_3^{2-}}$.

In method I it is assumed that the moles of carbonate and bicarbonate are determined from the titration volumes at the two equivalence points. This method apparently reveals HCO_3^- and CO_3^{2-} content and no more analysis is needed. This is a

misinterpretation. Figure 25 illustrate the problem, it shows a titration curve and its gradient for the titration of a saturated solution of *NaHCO₃*. It is determined that $V_A >$ 0 which indicates that the solution contains a considerable amount of carbonate. The *NaHCO₃* salt was checked for *NaOH* and *Na₂CO₃* impurities by X-ray diffraction and titration and showed no impurities. The carbonate must originate from the hydrolysis of bicarbonate to carbon dioxide and carbonate. Apparently carbon dioxide is evaporating even though the cell was filled and closed during the experiments. Interpreting the titration curve using method I results in an amount of *Na₂CO₃*, even though nothing was present. If the same practice is carried out for a solution with an infinitesimal amount of *Na₂CO₃* added, an erroneous high amount of carbonate is determined and equivalently an erroneous low amount of *NaHCO₃*. The procedure has unfortunately been used by some authors[6,22,23,24] and should be avoided.

Method II gives the amount of carbon as $HCO_3^- + CO_3^{2-}$. An additional analysis is required in order to fully determine the liquid composition. Method III is similar to method II, but method III is more accurate since it is independent of V_A.

Method III is used for determining the total sodium or total alkali. The acid titration gives the amount of "alkali", $OH + HCO_3^- + 2\,CO_3^{2-}$ -H^+. The H^+ concentration is negligible in the pH range used here. Na^+ is therefore the only counter ion. Total sodium can therefore be calculated from (220). Some authors state that the amount of CO_3^{2-} [30,31,32] in a solution of carbonates or HCO_3^- [6,25,26,27,28,29] in a solution of bicarbonate is determined this way. In reality they determined the amount of sodium ion.

Typically, method III is used for analysing solutions of a single salt. For analyzing solutions containing two salts, method I is used and it is assumed that this method gives the amounts of carbonate and bicarbonate. As described above, this is not correct and a discontinuity in solubility is observed due to the switching between the two analysis methods. Switching to method I at the first addition of *Na₂CO₃* after measuring *NaHCO₃* solubility creates a non-continuous solubility curve in the limit of $n_{Na_2CO_3} \to 0$. The discontinuity amounts to several *wt%*. Some authors are aware of this and they support their analysis by the *CO₂* absorption method to get a fully determined liquid phase[15,16,17,18,19,20,21].

In this work we determined total sodium by titration. Afterwards, we calculated the liquid composition using the "reverse Schreinemakers method" outlined below.

7.3.3   The reverse Schreinemakers method

Schreinemakers method[1] was originally developed as a graphical method for determining a solid phase from the compositions of the initial and the saturated solutions. The method was also applied to multi solvent systems through a more complicated graphical method[2]. The method requires two different initial compositions from which the same solid precipitates. By drawing levers through the points marking the initial composition and the composition of the saturated liquid the solid phase can be identified at the intersection between the levers.
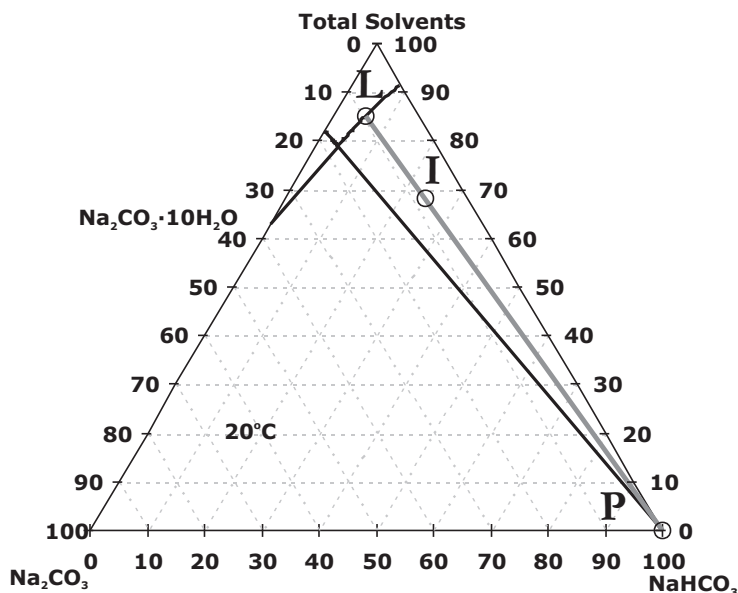
Figure 26: Phase diagram and the lever rule used in the reverse Schreinemakers method. *L*(saturated liquid), *P*(solid precipitate), and *I*(initial solution). The diagram shows the area marked by black lines in figure 21.

Here a method is developed in which Schreinemakers method is used in reverse. Figure 26 shows the principle. From the guessed or known precipitating solid (*P*) and initial composition (*I*) a lever may be drawn through the two points to determine the saturated solution (*L*). Only one lever is drawn but the length of the lever is determined by the amount of *mol sodium/kg total* determined by titration. The method is applicable for 2 salts and *n* solvents.

One solvent may precipitate from the solution together with a salt. For example *Na$_2$CO$_3$·10H$_2$O* may precipitate from the quaternary *Na$_2$CO$_3$-NaHCO$_3$-MEG-H$_2$O* system. The amount of precipitated hydrate is usually unknown and the *MEG/H$_2$O* ratio is therefore different from the ratio in the initial solution. The method requires four criteria to be fulfilled for a quaternary solution:

- ▫ Initial composition must be known
- ▫ Only one solid precipitates
- ▫ The identity of the solid is known or guessed
- ▫ One common ion exists

The weight fraction of solids in the saturated liquid phase is determined by the lever rules formulated in equations (221) and (222) and the sodium mole balance (223).

This requires the solution of three equations of three unknowns. The equations are generally applicable and may be used in an *n* solvent system.

$$\text{Salt 1: } fw_{1L} + (1-f) w_{1P} = w_{1I} \tag{221}$$

$$\text{Salt 2: } fw_{2L} + (1-f) w_{2P} = w_{2I} \tag{222}$$

$$\text{Sodium balance: } n_{Na,L} = v_1 n_{1L} + v_2 n_{2L} \tag{223}$$

w_{im} is the weight fraction of compound *i* in point *m*. Point *m* can be one of the following points marked in figure 26: *L(Liquid solution)* ,*P(solid precipitate), or I(initial solution)*. Compound *i* can be one of the following four, 1: *NaHCO_3*, 2: *Na_2CO_3*, 3: *H_2O* and 4: *MEG*. w_{iP} is assumed known or guessed and w_{iI} is known from weighing. v_i is the stoichiometric coefficient of the sodium ion in the solid phase. $n_{Na,L}$ is the total amount of sodium in the saturated solution, *L*, and *f* is the lever factor. The unknowns are *f* and w_{iL}.

The titration result given in this work is calculated by equation (220) as S_{TNa} in *mol sodium/kg sample*. S_{TNa} may be expressed in terms of the mass of a liquid sample, m_{sample} , in kilo grams, and $n_{Na,sample}$, the number of moles of sodium ions in the liquid sample using equation (223):

$$\Rightarrow S_{TNa} = \frac{n_{Na,sample}}{m_{sample}} = v_1 \frac{w_{1L}}{M_1} + v_2 \frac{w_{2L}}{M_2} \tag{224}$$

M_i *(kg/mol)* is the molar mass of compound *i*. The mass fraction of *NaHCO_3* in the liquid sample solution, w_{1L}, is derived from equation (224) and w_{2L} is the only unknown:

$$\Leftrightarrow w_{1L} = \frac{S_{TNa} \cdot M_1}{v_1} - v_2 w_{2L} \frac{M_1}{M_2} \tag{225}$$

Equation (221) and (222) can be rearranged by elimination of *f*.

$$(w_{1I} - w_{1P}) w_{1P} = w_{1L} (w_{2I} - w_{2P}) + w_{1I} w_{2P} - w_{1P} w_{2I} \tag{226}$$

After inserting (225) in (226) and rearranging, the weight fraction of *Na_2CO_3* in the mixed solvent system, w_{2L}, can be expressed as:

$$\Leftrightarrow w_{2L} = \frac{S_{TNa} M_1 (w_{2I} - w_{2P})/v_1 + w_{1I} w_{2P} - w_{1P} w_{2I}}{w_{1I} - w_{1P} + v_2 \frac{M_1}{M_2} (w_{2I} - w_{2P})} \tag{227}$$

The solubility of *NaHCO_3* in weight fraction, w_{1L}, is calculated by equation (225) and the solubility of *Na_2CO_3*, w_{2L}, by equation (227).

The initial mass of water, m_{3I}, is distributed between the saturated liquid (*L*) and the solid phase (*P*). The water mass balance is:

$$m_{3I} = m_{3P} + m_{3L} \tag{228}$$

The mass of water in the solid, m_{3P}, is determined from the moles of water in the solid, m_{3P}/M_3, which is related to the ratio $\nu_{WNa,P}$ of moles water to the moles of sodium, $n_{Na,P}$, in the solid:

$$m_{3P} = \nu_{WNa,P} \cdot n_{Na,P} M_3 \tag{229}$$

$\nu_{WNa,P}$ is known from X-ray analysis of the solid or guessed. It is obtained from the stoichiometric composition of the solid, examples are $\nu_{WNa,P}=0$ for $NaHCO_3$, $\nu_{WNa,P}=5$ for $Na_2CO_3 \cdot 10H_2O$ and $\nu_{WNa,P}=\frac{2}{3}$ for trona. $\nu_{WNa,P}$ may be guessed and a correct value of $\nu_{WNa,P}$ gives a continues saturation line by repeated samples. An incorrect value results in a discontinuous saturation line. $n_{Na,P}$ is determined from a sodium mol balance:

$$n_{Na,I} = n_{Na,L} + n_{Na,P} \tag{230}$$

where $n_{Na,I}$ is the initial total amount of sodium which can be expressed from the initial kilo grams of $NaHCO_3$, m_{1I}, and Na_2CO_3, m_{2I}:

$$n_{Na,I} = \nu_1 \frac{m_{1I}}{M_1} + \nu_2 \frac{m_{2I}}{M_2} \tag{231}$$

The stoichiometric coefficients of sodium in $NaHCO_3$ and Na_2CO_3, $\nu_1=1$ and $\nu_2=2$, are the same as those used in (223). The moles of sodium in the sample, $n_{Na,L}$, is calculated from the mass of solvents:

$$n_{Na,L} = m_{solvents,L} \cdot J \tag{232}$$

where $m_{solvents,L}$ is the total kilo grams of solvent in the saturated liquid, $H_2O + MEG$. J is the number of moles of sodium per kilo gram solvents defined by:

$$J = \frac{n_{Na,sample}}{m_{solvents,sample}} \tag{233}$$

J is determined by sampling the liquid L and determining the moles of sodium in the sample, $n_{Na,sample}$, by titration. It is divided by the mass of solvents in the sample, $m_{solvents,sample}$, which is calculated by:

$$m_{solvents,sample} = w_{solvents,L} \cdot m_{sample} \tag{234}$$

The sample mass, m_{sample}, is known from weighing of the sample. The total solvents mass fraction, $w_{solvents,L}$, is calculated from equations (225) and (227):

$$w_{solvents,L} = 1 - w_{1L} - w_{2L} \tag{235}$$

The total mass of solvent in the saturated liquid (L), $m_{solvents,L}$, is calculated by the following relation

$$m_{solvents,L} = m_{3L} + m_{4L} \tag{236}$$

For a *n* solvent system the above equation is given as a sum over all solvents. It is assumed that *MEG* does not precipitate and stays in solution and m_{4L} is therefore determined by:

$$m_{4L} = m_{4I} \tag{237}$$

where m_{4I} is the initial amount of glycol, which is known. For the *n* solvent system the initial amount of all solvent are given similar to (237).

The only unknown in the above equations is the amount of water in the saturated liquid, m_{3L}. Contracting (228) to (236) to one equation by inserting (229) in (228), (230) in (229), (231) in (230), (232) in (230), (237) in (236), and (236) in (232) gives the final equation of water in the saturated liquid phase:

$$m_{3L} = \frac{m_{3I} - M_3 \nu_{Na,P} \left(\nu_1 \frac{m_{1I}}{M_1} + \nu_2 \frac{m_{2I}}{M_2} - Jm_{4I} \right)}{1 - M_3 \nu_{WNa,P} J} \tag{238}$$

For the *n* solvent system m_{4I} is the initial sum of all solvent in the system except water. All variables are known from the initial composition or the titration data since *J* is related to the solubility, S_{TNa}, by $J = S_{TNa}/(1-w_{1L}-w_{2L})$, derived from equations (224), (233), (234), and (235). Values of the initial compositions and S_{TNa} are found in table 7.

The total mass of the saturated liquid, m_L, is calculated using equation (225), (227), (235), (237), and (238) by

$$m_L = \frac{m_{3L} + m_{4L}}{w_{solvents}} \tag{239}$$

For the *n* solvent system m_{4L} is the sum of all solvents except water. The weight fraction of solvents, $H_2O(3)$ and *MEG*(4), in the liquid phase (*L*) may now be calculated by:

$$w_{4L} = \frac{m_{4L}}{m_L}, \qquad w_{3L} = \frac{m_{3L}}{m_L} \tag{240}$$

The mass of solid, m_P, is determined from a total mass balance:

$$m_I = m_L + m_P \tag{241}$$

By using the equations presented here, the identity of the solid phase and the composition of the liquid phase can be determined from the titration results. This method may be called a reverse Schreinemakers method. This is a general method not only applicable to the Na_2CO_3-Na_2CO_3-MEG-H_2O system. It is valid for an *n* solvent system and allows for the full determination of the identity of the solid phase and the composition of the saturated liquid phase from a small amount of information. The method is restricted to single salt precipitation and requires a common ion (in this case the sodium ion) to calculate the composition. The method has not been extended to systems in which more than one solid phase is in equilibrium with the same liquid.

7.4   Experimental results

The solubility of Na_2CO_3 and $NaHCO_3$ has been determined in the mixed solvent *MEG*-H_2O at atmospheric pressure between 2 and 60 °C. Table 7 gives the experimental initial compositions, titration results, and densities, together with the compositions of the saturated solutions, and the identity of the solid phases determined by the reverse Schreinemakers method.

The initial composition is listed as amounts of pure compounds in grams. The titration results are listed in *mol/kg total* as described above. Every measurement was repeated three times and the deviation is given. The $S_{CO_3^{2-}}$ is listed in table 7. It may be used together with the intial composition and Schreinemakers method to get an idea of the identity of the solid phase. The standard deviation is high and reflects the difficulties in determining V_B accurately. Some solution could only be measured once and the deviation is missing.

The density measurements were difficult to reproduce and the deviations are high. In some cases, the determination of density failed completely due to one or more reasons. Either the micropipette took in air, it was not completely emptied, or too small samples were used. In a few cases the density could not be measured, in other cases only one measurement could be made, and the standard deviation could not be determined. The sampling technique was refined over time and the measurements of the density of solutions saturated with Na_2CO_3, which were measured last, are therefore more accurate than the corresponding data for solutions saturated with *NaHCO_3*.

The titration data were interpreted using the reverse Schreinemakers method. The results are given in table 7 as *wt% Na_2CO_3*, *NaHCO_3* and *MEG*. The standard deviation is very low and shows the high reproducibility obtained by this method.

The reverse Schreinemakers method developed in this work can not be used for interpreting titration results for solutions with two solid phases in equilibrium with the same liquid. The titration results for such solutions were therefore not converted to *wt%* in table 7.

The identities of selected solid phases were determined by X-ray diffraction to verify the results of the reverse Schreinemakers method.

Table 7: Experimental initial composition, equilibrium composition, results of the reverse Schreinemakers method and solid phase information from the Na_2CO_3-Na_2CO_3-MEG-H_2O system at 1 bar and 2 °C to 60 °C.

T^a °C	$\tilde{w}_{MEG}^{b}$ %	m_{H_2O} g	m_{MEG} g	m_{NaHCO_3} g	$m_{Na_2CO_3}$ g	S_{TNa} mol/kg	dev %	$S_{CO_3^{2-}}$ mol/kg	dev %	$\rho_{sat.liquid}$ g/cm³	dev %	$w_{Na_2CO_3}$ %	$\sigma_{Na_2CO_3}$ %	w_{NaHCO_3} %	σ_{NaHCO_3} %	m_{H_2O} g	w_{MEG} %	P_1^{f}	P_2^{f}
		Initial^c						**Equilibrium^d**						**Reverse Schreinemakers^e**					
2.45	15.60	26.1109	4.8273	4.6238	0.0000	0.733	0.38	0.115	11.57	1.057	-	0		6.16	0.024	26.1109	14.642	B	
2.55	42.22	17.2869	12.6312	3.3322	0.0000	0.475	-	0.085	-	-	-	0		3.992	-	17.2869	40.534	B	
2.35	63.21	9.9027	17.0171	2.4722	0.0000	0.375	1.24	0.095	24.69	-	-	0		3.15	0.039	9.9027	61.223	B	
10.20	0.00	10.0318	0.0000	1.0104	0.0000	0.962	0.31	0.054	16.08	1.049	0.09	0		8.08	0.025	10.0318	0.000	B	
10.55	0.00	10.0009	0.0000	1.9083	0.0000	1.009	1.33	0.104	12.62	1.044	0.24	0		8.47	0.11	10.0009	0.000	B	
10.35	3.08	9.7773	0.3109	1.0030	0.0000	0.910	0.49	0.071	11.22	1.048	-	0		7.64	0.037	9.7773	2.846	B	
10.40	3.15	9.6940	0.3156	1.9070	0.0000	0.963	1.02	0.118	11.16	1.045	-	0		8.09	0.082	9.6940	2.898	B	
10.05	14.96	8.4850	1.4924	1.6265	0.0000	0.792	1.12	0.112	6.02	1.047	-	0		6.65	0.075	8.4850	13.963	B	
10.20	15.32	8.5744	1.5507	0.9111	0.0000	0.747	0.07	0.074	3.42	1.055	0.27	0		6.278	0.0046	8.5744	14.354	B	
10.15	28.05	7.2142	2.8118	1.3677	0.0000	0.634	0.88	0.118	11.41	1.066	2.24	0		5.33	0.047	7.2142	26.551	B	
10.20	28.12	7.2232	2.8261	0.7926	0.0000	0.607	0.55	0.063	2.57	1.069	0.21	0		5.10	0.028	7.2232	26.688	B	
10.35	42.22	20.3200	14.8473	3.5293	0.0000	0.477	5.33	0.100	-	-	-	0		4.01	0.21	20.3200	40.526	B	
10.05	53.05	4.7262	5.3404	0.6002	0.0000	0.441	-	0.037	-	1.091	1.17	0		3.702	-	4.7262	51.087	B	
10.10	53.13	4.6877	5.3131	1.1178	0.0000	0.447	0.97	0.079	6.63	1.072	-	0		3.75	0.036	4.6877	51.133	B	
10.25	63.21	14.0064	24.0690	2.5329	0.0000	0.382	0.32	0.088	37.49	-	-	0		3.21	0.010	14.0064	61.183	B	
10.20	77.89	2.2212	7.8272	0.5056	0.0000	0.308	0.20	0.024	2.40	1.117	0.05	0		2.589	0.0052	2.2212	75.879	B	
10.45	78.10	2.1872	7.7994	1.1120	0.0000	0.340	1.09	0.053	8.98	-	-	0		2.86	0.031	2.1872	75.868	B	
10.30	100.00	0.0000	9.9890	1.3650	0.0000	0.647	1.58	0.083	15.75	-	-	0		5.44	0.086	0.0000	94.564	B	
20.15	0.00	10.0660	0.0000	1.8708	0.0000	1.088	0.86	0.163	2.37	1.065	0.09	0		9.14	0.079	10.0660	0.000	B	
20.00	0.00	9.9966	0.0000	1.9238	0.0000	1.117	0.08	0.217	0.14	1.072	1.15	0		9.383	0.0076	9.9966	0.000	B	
20.10	2.70	9.6800	0.2684	1.8776	0.0000	1.049	2.15	0.153	0.30	1.042	0.34	0		8.81	0.19	9.6850	2.459	B	
20.00	2.93	9.7341	0.2942	1.1232	0.0000	1.036	0.12	0.190	1.59	1.048	0.28	0		8.71	0.010	9.7341	2.678	B	
20.10	3.21	9.6970	0.3215	1.8969	0.0000	1.072	0.04	0.206	0.79	1.065	0.42	0		9.003	0.0037	9.6970	2.920	B	
20.00	15.09	8.5923	1.5275	2.0342	0.0000	0.919	0.21	0.170	0.65	1.083	0.61	0		7.72	0.017	8.5923	13.928	B	
20.10	15.12	8.5210	1.5173	1.5716	0.0000	0.867	0.17	0.129	2.33	1.064	-	0		7.28	0.012	8.5210	14.014	B	
20.00	15.43	8.4692	1.5448	1.1100	0.0000	0.847	0.31	0.169	-	1.068	0.39	0		7.12	0.022	8.4692	14.328	B	
20.10	27.89	7.2172	2.7908	1.3003	0.0000	0.697	1.38	0.089	9.53	1.079	0.04	0		5.86	0.081	7.2172	26.253	B	
20.00	28.42	7.1993	2.8586	1.3270	0.0000	0.701	0.23	0.126	10.52	1.080	0.67	0		5.89	0.013	7.1993	26.748	B	
19.60	42.22	20.3200	14.8473	3.5293	0.0000	0.568	0.02	0.141	26.93	-	-	0		4.7747	0.00093	20.3200	40.203	B	
20.10	52.82	4.7172	5.2816	1.1088	0.0000	0.478	1.24	0.045	0.63	1.094	0.41	0		4.02	0.050	4.7172	50.701	B	
20.00	52.99	4.7049	5.3028	1.0919	0.0000	0.480	0.27	0.077	2.32	1.097	0.21	0		4.03	0.011	4.7049	50.853	B	
20.10	60.02	4.0003	6.0058	0.9790	0.0000	0.444	0.43	0.057	2.32	1.101	0.32	0		3.73	0.016	4.0003	57.782	B	
19.60	63.21	14.0064	24.0690	2.5329	0.0000	0.435	4.81	0.093	35.50	-	-	0		3.65	0.18	14.0064	60.905	B	
20.10	67.44	3.2574	6.7474	1.0456	0.0000	0.411	0.94	0.060	9.29	1.098	0.59	0		3.46	0.032	3.2574	65.111	B	

T^a	$\tilde{w}_{MEG}^b$	m_{H_2O}	m_{MEG}	m_{NaHCO_3}	$m_{Na_2CO_3}$	S_{TNa}	dev	$S_{CO_3^{2-}}$	dev	$\rho_{sat.liquid}$	dev	$w_{Na_2CO_3}$	$\sigma_{Na_2CO_3}$	w_{NaHCO_3}	σ_{NaHCO_3}	m_{H_2O}	w_{MEG}	P_1^f	P_2^f
20.10	75.01	2.4977	7.4957	0.9924	0.0000	0.388	1.34	0.055	8.48	1.110	0.64	0		3.26	0.044	2.4977	72.563	B	
20.00	78.07	2.2024	7.8396	1.1731	0.0000	0.383	1.43	0.057	2.70	1.117	0.98	0		3.22	0.046	2.2024	75.554	B	
20.10	82.48	1.7574	8.2719	0.9970	0.0000	0.373	0.30	0.047	0.06	1.117	0.53	0		3.137	0.0094	1.7574	79.890	B	
20.10	90.02	0.9995	9.0123	1.0003	0.0000	0.401	0.28	0.046	5.48	1.128	0.14	0		3.372	0.0094	0.9995	86.981	B	
20.10	97.42	0.2592	9.7689	0.9833	0.0000	0.572	0.16	0.051	6.21	1.146	0.02	0		4.804	0.077	0.2592	92.735	B	
20.10	100.00	0.0000	10.0005	1.2820	0.0000	0.744	0.10	0.045	3.58	1.160	0.04	0		6.249	0.0065	0.0000	93.751	B	
20.00	100.00	0.0000	9.9970	1.3853	0.0000	0.772	0.08	0.086	11.11	1.151	-	0		6.482	0.0051	0.0000	93.518	B	
24.40	42.22	20.3200	14.8473	3.5293	0.0000	0.594	0.34	0.095	8.22	1.084	-	0		4.99	0.017	20.3200	40.113	B	
24.60	63.21	14.0064	24.0690	2.5329	0.0000	0.435	1.03	0.076	2.49	-	-	0		3.66	0.038	14.0064	60.903	B	
29.80	0.00	10.0320	0.0000	1.3015	0.0000	1.262	1.84	0.105	13.05	1.071	0.03	0		10.60	0.20	10.0320	0.000	B	
29.90	2.87	9.6877	0.2858	1.3034	0.0000	1.181	0.34	0.116	9.97	1.070	0.04	0		9.92	0.034	9.6877	2.581	B	
29.90	2.93	9.7167	0.2936	1.5166	0.0000	1.196	0.04	0.149	2.44	1.074	0.16	0		10.043	0.0042	9.7167	2.639	B	
30.00	15.01	8.5444	1.5094	1.1944	0.0000	1.030	0.25	0.139	4.99	1.085	2.10	0		8.65	0.022	8.5444	13.715	B	
29.90	15.43	8.4689	1.5447	1.4930	0.0000	0.986	0.17	0.135	6.93	1.080	0.57	0		8.28	0.014	8.4689	14.148	B	
30.00	28.11	7.2252	2.8258	1.0006	0.0000	0.796	0.49	0.135	6.24	1.082	-	0		6.69	0.033	7.2252	26.235	B	
30.00	52.81	4.7268	5.2907	0.6992	0.0000	0.517	0.98	0.065	9.79	1.110	1.42	0		4.34	0.043	4.7268	50.523	B	
30.00	77.33	2.2914	7.8158	0.6260	0.0000	0.367	0.31	0.031	5.77	1.116	0.21	0		3.087	0.0096	2.2914	74.942	B	
30.00	100.00	0.0000	10.0247	0.9025	0.0000	0.810	0.09	0.059	2.41	1.161	0.11	0		6.806	0.0060	0.0000	93.194	B	
34.90	0.00	10.0139	0.0000	1.8971	0.0000	1.346	0.08	0.262	2.48	1.110	0.34	0		11.311	0.0086	10.0139	0.000	B	
34.70	3.36	9.7142	0.3375	1.9009	0.0000	1.261	0.11	0.261	3.52	1.108	0.74	0		10.60	0.012	9.7142	3.002	B	
34.90	14.96	8.5202	1.4989	1.6346	0.0000	1.100	0.12	0.238	18.79	1.100	0.31	0		9.24	0.011	8.5202	13.578	B	
32.70	15.60	26.1109	4.8273	4.6238	0.0000	1.077	0.37	0.314	-	-	-	0		9.05	0.034	26.1109	14.191	B	
34.90	28.01	7.1995	2.8007	1.3540	0.0000	0.863	0.09	0.174	23.11	1.114	1.21	0		7.248	0.0063	7.1995	25.977	B	
32.70	42.22	17.2869	12.6312	3.3322	0.0000	0.658	0.49	0.212	17.48	-	-	0		5.53	0.027	17.2869	39.884	B	
34.90	52.88	4.7139	5.2903	1.1031	0.0000	0.570	0.18	0.089	7.09	1.109	0.17	0		4.787	0.0085	4.7139	50.349	B	
33.00	63.21	9.9027	17.0171	2.4722	0.0000	0.509	0.35	0.148	3.46	-	-	0		4.27	0.015	9.9027	60.513	B	
34.90	78.17	2.1880	7.8359	1.1269	0.0000	0.420	0.06	0.081	19.86	1.123	0.77	0		3.532	0.0020	2.1880	75.411	B	
34.90	100.00	0.0000	10.0162	1.4230	0.0000	0.871	1.12	0.140	43.44	1.149	2.61	0		7.32	0.082	0.0000	92.680	B	
39.90	0.00	10.0165	0.0000	1.4127	0.0000	1.414	0.23	0.120	12.37	1.093	0.98	0		11.88	0.028	10.0165	0.000	B	
39.40	2.97	9.7180	0.2975	1.3060	0.0000	1.343	0.10	0.152	8.71	1.084	-	0		11.28	0.011	9.7180	2.635	B	
39.80	3.04	9.7116	0.3048	1.9159	0.0000	1.378	0.04	0.238	3.03	1.115	0.24	0		11.579	0.0051	9.7116	2.691	B	
39.95	15.13	8.4968	1.5145	1.1928	0.0000	1.147	0.11	0.162	3.70	-	-	0		9.63	0.011	8.4968	13.670	B	
39.60	15.34	8.3722	1.5168	1.9049	0.0000	1.139	1.60	0.236	4.47	1.122	-	0		9.57	0.15	8.3722	13.871	B	
40.50	15.60	26.1109	4.8273	4.6238	0.0000	1.107	0.23	0.083	-	1.071	-	0		9.30	0.021	26.1109	14.152	B	
39.90	27.85	7.2561	2.8009	1.0128	0.0000	0.890	1.48	0.112	1.77	1.103	1.47	0		7.47	0.11	7.2561	25.769	B	
40.00	42.22	17.2869	12.6312	3.3322	0.0000	0.677	3.81	0.113	31.01	1.090	1.00	0		5.69	0.22	17.2869	39.818	B	
39.90	53.03	4.7096	5.3171	0.7055	0.0000	0.579	0.19	0.070	2.58	1.111	-	0		4.866	0.0093	4.7096	50.449	B	
40.60	63.21	9.9027	17.0171	2.4722	0.0000	0.516	0.31	0.078	1.34	-	-	0		4.33	0.014	9.9027	60.476	B	

T^a	$\tilde{w}_{MEG}^{\,b}$	m_{H_2O}	m_{MEG}	m_{NaHCO_3}	$m_{Na_2CO_3}$	S_{TNa}	dev	$S_{CO_3^{2-}}$	dev	$\rho_{sat.liquid}$	dev	$w_{Na_2CO_3}$	$\sigma_{Na_2CO_3}$	w_{NaHCO_3}	σ_{NaHCO_3}	m_{H_2O}	w_{MEG}	$P_1^{\,f}$	$P_2^{\,f}$
39.90	70.01	3.2669	7.6250	0.5313	0.0000	0.456	0.38	0.041	19.90	-	-	0		3.83	0.014	3.2669	67.323	B	
39.60	75.09	2.4916	7.5101	0.5415	0.0000	0.413	0.22	0.032	16.30	1.117	0.51	0		3.472	0.0076	2.4916	72.481	B	
39.80	78.10	2.1983	7.8386	0.6093	0.0000	0.410	0.11	0.037	7.39	1.125	0.25	0		3.447	0.0037	2.1983	75.406	B	
39.90	82.44	1.7665	8.2936	0.5126	0.0000	0.422	0.73	0.043	0.74	1.129	0.27	0		3.54	0.026	1.7665	79.521	B	
39.90	89.81	1.0243	9.0243	0.5135	0.0000	0.426	0.22	0.032	7.14	1.136	0.19	0		3.578	0.0077	1.0243	86.593	B	
39.90	97.51	0.2487	9.7557	0.6277	0.0000	0.613	0.44	0.061	45.41	1.149	0.13	0		5.15	0.023	0.2487	92.493	B	
39.85	100.00	0.0000	10.0544	0.9057	0.0000	0.856	0.62	0.036	12.61	1.164	0.23	0		7.19	0.045	0.0000	92.806	B	
49.90	0.00	10.0034	0.0000	1.5841	0.0000	1.603	0.14	0.207	1.55	1.140	-	0		13.47	0.019	10.0034	0.000	B	
48.65	2.89	9.7089	0.2885	1.6013	0.0000	1.479	0.90	0.187	10.34	1.139	2.39	0		12.42	0.11	9.7089	2.527	B	
48.70	3.04	9.6849	0.3040	1.9179	0.0000	1.580	0.30	0.294	9.41	1.126	0.60	0		13.27	0.039	9.6849	2.639	B	
49.85	14.74	8.5482	1.4778	1.2886	0.0000	1.317	0.10	0.197	5.86	1.129	1.98	0		11.06	0.011	8.5482	13.110	B	
49.00	15.34	8.4856	1.5374	1.9052	0.0000	1.323	6.11	0.304	21.19	-	-	0		11.12	0.68	8.4856	13.633	B	
49.80	27.86	7.1944	2.7780	1.2150	0.0000	1.036	0.21	0.151	1.30	1.114	0.38	0		8.70	0.019	7.1944	25.433	B	
49.80	53.02	4.6912	5.2946	0.8969	0.0000	0.660	0.18	0.072	1.40	1.113	0.93	0		5.544	0.0097	4.6912	50.082	B	
49.75	78.05	2.1902	7.7858	0.7096	0.0000	0.458	0.34	0.042	4.37	1.131	0.29	0		3.85	0.013	2.1902	75.041	B	
49.70	100.00	0.0000	10.0219	0.8838	0.0000	0.832	0.57	0.055	5.57	1.166	0.68	0		6.99	0.040	0.0000	93.015	B	
56.85	3.16	9.7463	0.3179	0.5975	0.0000	1.701	0.26	0.216	3.12	1.105	0.46	0		14.29	0.037	9.7463	2.707	B	
59.65	0.00	10.0668	0.0000	1.7070	0.0000	1.808	0.14	0.214	8.23	1.152	-	0		15.19	0.021	10.0668	0.000	B	
59.75	14.93	8.5408	1.4984	1.4310	0.0000	1.524	0.30	0.239	0.64	1.121	0.92	0		12.81	0.038	8.5408	13.014	B	
59.60	27.93	7.2290	2.8021	1.3035	0.0000	1.186	0.09	0.181	5.77	1.122	8.01	0		9.959	0.0094	7.2290	25.152	B	
59.60	53.05	4.7048	5.3158	0.9456	0.0000	0.744	1.27	0.065	85.38	1.125	2.78	0		6.25	0.080	4.7048	49.731	B	
59.50	77.91	2.2126	7.8048	0.7067	0.0000	0.510	0.21	0.050	4.27	1.132	0.24	0		4.283	0.0090	2.2126	74.575	B	
59.40	100.00	0.0000	10.0630	0.9045	0.0000	0.874	1.51	0.075	3.05	1.155	0.25	0		7.34	0.11	0.0000	92.655	B	
10.20	0.00	10.0134	0.0000	0.0000	2.5072	2.236	0.95	1.109	0.88	1.123	0.32	11.85	0.11	0		7.4558	0.000	D	
10.15	3.04	9.6966	0.3043	0.0000	4.2919	2.298	0.00	0.942	4.41	-	-	12.17933	0.000020	0		3.2361	7.549	D	
10.40	3.94	9.7279	0.3990	0.0000	2.7720	2.083	2.08	1.030	2.86	1.105	0.84	11.04	0.23	0		6.4640	5.172	D	
10.20	14.93	8.5053	1.4925	0.0000	2.2930	1.772	3.63	0.876	3.64	1.142	1.14	9.39	0.34	0		5.9132	18.262	D	
10.20	27.93	7.2202	2.7978	0.0000	2.1673	1.643	-	0.796	-	1.144	2.10	8.708	-	0		4.7621	33.786	D	
10.20	54.34	4.7315	5.6305	0.0000	1.7704	2.223	0.33	1.104	0.61	1.191	0.36	11.78	0.038	0		4.6642	48.251	M	
10.20	77.95	2.2120	7.8197	0.0000	1.7773	1.131	0.22	0.557	1.61	1.142	1.16	5.99	0.013	0		2.0165	74.733	M	
10.20	100.00	0.0000	10.0181	0.0000	1.7743	0.974	0.17	0.427	0.60	1.118	2.22	5.160	0.0085	0		0.0000	94.840	C	
15.20	0.00	9.9952	0.0000	0.0000	2.8448	2.807	0.31	1.399	0.47	1.153	0.09	14.87	0.046	0		7.3395	0.000	D	
15.20	3.10	9.7155	0.3112	0.0000	2.8648	2.641	0.69	1.311	0.41	1.143	0.46	13.99	0.097	0		6.8177	3.754	D	
15.20	9.10	9.1058	0.9111	0.0000	2.0813	2.438	0.14	1.213	0.47	1.128	0.59	12.92	0.019	0		7.7536	9.156	D	
15.10	14.97	8.4855	1.4940	0.0000	2.1267	2.241	0.44	1.109	1.17	1.131	0.31	11.88	0.052	0		6.7621	15.947	D	
15.20	36.50	6.3496	3.6500	0.0000	2.0555	2.291	1.52	1.131	1.53	1.164	0.62	12.14	0.18	0		4.8530	37.716	D	
15.20	44.87	5.5182	4.4917	0.0000	2.5300	2.820	0.36	1.398	0.88	1.210	1.47	14.95	0.054	0		5.3831	38.688	M	
15.20	78.11	2.1900	7.8164	0.0000	0.8600	1.118	0.15	0.549	0.15	1.145	0.55	5.924	0.0090	0		2.1505	73.778	M	

T^a	$\tilde{w}_{MEG}^b$	m_{H_2O}	m_{MEG}	m_{NaHCO_3}	$m_{Na_2CO_3}$	S_{TNa}	dev	$S_{CO_3^{2-}}$	dev	$\rho_{sat.liquid}$	dev	$w_{Na_2CO_3}$	$\sigma_{Na_2CO_3}$	w_{NaHCO_3}	σ_{NaHCO_3}	m_{H_2O}	w_{MEG}	P_1^f	P_2^f
15.20	100.00	0.0000	10.0145	0.0000	0.8703	0.869	0.10	0.410	0.85	1.159	0.90	4.603	0.0045	0		0.0000	95.397	C	
20.10	0.00	10.0175	0.0000	0.0000	2.5408	3.497	0.26	1.735	0.32	1.176	0.57	18.53	0.049	0		9.2920	0.000	D	
20.10	3.07	9.7043	0.3075	0.0000	2.5149	3.357	0.08	1.663	0.08	1.170	0.43	17.79	0.014	0		8.7673	2.786	D	
20.10	8.98	9.1021	0.8975	0.0000	2.5114	3.109	0.09	1.541	0.06	1.163	0.59	16.47	0.014	0		7.7236	8.695	D	
20.10	15.26	8.5166	1.5333	0.0000	2.5043	2.919	0.17	1.441	0.12	1.163	0.76	15.47	0.027	0		6.8753	15.414	D	
20.10	21.02	7.9181	2.1070	0.0000	2.5518	2.828	0.14	1.397	0.07	1.170	0.36	14.99	0.022	0		6.0142	22.056	D	
20.10	28.13	7.2056	2.8202	0.0000	2.5101	2.876	0.10	1.417	1.06	1.189	0.26	15.24	0.014	0		6.1353	26.691	H	
20.10	39.99	6.0083	4.0036	0.0000	2.5520	3.144	0.16	1.558	0.11	1.166	0.22	16.66	0.026	0		5.9115	33.650	M	
29.90	15.43	8.4562	1.5425	0.0000	4.5921	4.917	0.20	2.446	0.73	1.283	1.15	26.06	0.052	0		8.2630	11.632	M	
39.80	0.00	9.9823	0.0000	0.0000	5.7611	6.537	0.40	3.283	0.61	1.330	1.34	34.64	0.14	0		9.8945	0.000	M	
39.80	3.04	9.6958	0.3043	0.0000	4.6687	5.813	0.10	2.902	0.59	1.367	1.93	30.81	0.030	0		9.6560	2.114	M	
39.50	3.06	9.7113	0.3068	0.0000	5.7592	6.087	0.18	3.031	0.16	1.307	1.83	32.26	0.057	0		9.5285	2.113	M	
40.00	15.11	8.4945	1.5115	0.0000	4.9300	5.018	0.15	2.514	0.47	1.232	0.92	26.59	0.039	0		8.2582	11.357	M	
39.50	15.34	8.4566	1.5322	0.0000	4.6623	4.826	0.32	2.391	0.54	1.246	2.28	25.57	0.082	0		8.2346	11.675	M	
40.00	27.94	7.2336	2.8046	0.0000	4.2938	3.886	0.26	1.931	0.46	1.225	0.81	20.60	0.053	0		6.9331	22.870	M	
40.00	52.90	4.7177	5.2990	0.0000	1.7583	1.950	0.19	0.966	0.44	1.160	1.70	10.34	0.020	0		4.6131	47.934	M	
39.90	78.45	2.2158	8.0670	0.0000	1.1124	0.935	2.65	0.453	2.36	1.112	1.48	4.96	0.13	0		2.1170	75.287	M	
39.90	100.00	0.0000	10.0301	0.0000	1.1395	1.128	1.92	0.549	2.66	1.143	-	5.98	0.12	0		0.0000	94.021	C	
49.60	0.00	9.9849	0.0000	0.0000	5.5709	6.273	0.59	3.127	1.23	1.303	3.67	33.24	0.20	0		9.8738	0.000	M	
48.85	2.74	9.6756	0.2729	0.0000	5.8053	5.935	0.14	2.963	0.46	1.258	2.96	31.45	0.045	0		9.4468	1.925	M	
49.80	15.04	8.5359	1.5107	0.0000	4.1711	4.822	0.44	2.409	0.97	1.321	0.87	25.55	0.11	0		8.4055	11.342	M	
49.60	15.34	8.4741	1.5353	0.0000	4.6669	4.701	1.72	2.289	3.38	1.306	1.47	24.92	0.43	0		8.2318	11.803	M	
49.70	27.76	7.2678	2.7930	0.0000	3.3213	3.687	0.73	1.832	1.13	1.238	1.57	19.54	0.14	0		7.1121	22.689	M	
49.70	52.72	4.7511	5.2973	0.0000	1.5709	1.819	0.79	0.862	2.98	1.178	2.30	9.64	0.076	0		4.6647	48.049	M	
49.70	77.30	2.2837	7.7780	0.0000	0.7996	0.972	1.78	0.479	2.32	1.147	14.19	5.15	0.092	0		2.2403	73.640	M	
49.70	100.00	0.0000	10.0678	0.0000	0.8105	0.705	2.68	0.317	3.99	1.151	0.46	3.74	0.10	0		0.0000	96.264	C	
59.55	0.00	10.0055	0.0000	0.0000	5.8730	6.054	1.61	3.038	2.97	1.367	-	32.08	0.52	0		9.7938	0.000	M	
58.20	2.97	9.6703	0.2955	0.0000	5.7978	5.817	0.49	2.907	1.35	1.351	1.66	30.83	0.15	0		9.4209	2.104	M	
59.75	15.16	8.5310	1.5248	0.0000	4.2020	4.675	0.48	2.320	1.05	1.340	3.87	24.77	0.12	0		8.3707	11.592	M	
59.65	27.92	7.1741	2.7784	0.0000	3.2790	3.527	0.70	1.747	0.36	1.267	1.98	18.69	0.13	0		6.9988	23.106	M	
59.55	53.13	4.6970	5.3252	0.0000	1.5942	1.756	0.51	0.853	3.63	1.149	0.81	9.30	0.048	0		4.5991	48.666	M	
59.55	77.53	2.2641	7.8099	0.0000	0.7861	0.802	0.38	0.389	0.19	1.166	0.40	4.25	0.016	0		2.2060	74.662	M	
59.45	100.00	0.0000	9.7490	0.0000	0.8038	0.454	4.60	0.215	4.76	1.122	2.22	2.41	0.11	0		0.0000	97.594	C	
10.15	3.04	9.7296	0.3054	1.0819	0.1704	1.152	2.61	0.303	1.87	1.083	0.05	1.549	0.0043	7.22	0.26	9.7296	2.776	B	
10.50	3.04	9.7031	0.3046	1.7053	0.4846	1.579	0.40	0.523	8.04	1.068	0.49	4.322	0.0027	6.41	0.057	9.7031	2.716	B	
10.30	3.04	9.6998	0.3044	1.0567	0.7047	1.889	0.43	0.716	6.42	1.104	1.20	6.181	0.0050	6.07	0.076	9.6998	2.670	M	
10.30	3.04	9.7057	0.3046	1.2318	1.1119	2.375	1.01	0.946	2.76	1.147	3.19	9.51	0.024	4.88	0.24	9.7057	2.605	B	
10.25	3.04	9.6945	0.3043	0.1307	2.3848	2.299	0.98	0.996	1.68	-	-	11.24	0.12	1.499	0.0072	7.3067	3.489	D	

T [a]	$\tilde{w}_{MEG}$ [b]	m_{H_2O}	m_{MEG}	m_{NaHCO_3}	$m_{Na_2CO_3}$	S_{TNa}	dev	$S_{CO_3^{2-}}$	dev	$\rho_{sat.\,liquid}$	dev	$w_{Na_2CO_3}$	$\sigma_{Na_2CO_3}$	w_{NaHCO_3}	σ_{NaHCO_3}	m_{H_2O}	w_{MEG}	P_1 [f]	P_2 [f]
10.10	3.04	9.7080	0.3047	0.0614	2.3601	2.042	0.24	0.960	0.54	1.093	2.77			0.7295	0.00073	7.1789	3.620	D	D
10.30	3.04	9.6841	0.3040	1.4853	3.3331	2.491	1.73	0.928	1.71	-		10.36	0.027					B	
10.20	15.34	8.4994	1.5399	1.0136	0.2222	1.038	0.16	0.305	-	1.057	2.14	2.0468	0.00032	5.48	0.015	8.4994	14.185	B	
10.15	15.34	8.4642	1.5335	1.1697	0.4706	1.374	0.51	0.469	0.22	1.084	2.19	4.282	0.0029	4.76	0.064	8.4642	13.952	B	
10.30	15.34	8.4954	1.5392	1.0409	0.5814	1.517	0.11	0.558	-	1.064	2.87	5.2330	0.00081	4.45	0.015	8.4954	13.854	B	
10.15	15.34	8.4546	1.5318	1.2177	0.9746	2.064	0.38	0.854	2.40	1.118	-	8.555	0.0068	3.78	0.076	8.4546	13.447	B	
10.20	15.34	8.4820	1.5368	0.0619	2.3604	1.741	1.84	0.794	0.83			8.73	0.17	0.780	0.0047	5.6488	19.352	D	
15.10	15.34	8.4844	1.5372	1.4805	3.3366	1.949	0.29	0.747	0.21									B	D
15.10	3.19	9.7140	0.3205	0.3268	2.1216	2.879	0.21	1.267	0.95	1.156	0.97	13.30	0.034	3.101	0.0045	8.4903	3.041	D	
15.20	3.05	9.7010	0.3048	0.1588	2.0646	2.756	0.03	1.288	0.46	1.145	0.15	13.657	0.0044	1.5063	0.00028	8.6391	2.891	D	
15.20	15.46	8.5047	1.5553	0.1837	2.0719	2.402	0.37	1.088	0.46	1.154	0.51	11.54	0.049	1.881	0.0036	6.8987	15.928	D	
15.20	14.98	8.4929	1.4963	0.0961	2.0797	2.341	0.18	1.106	0.91	1.134	0.76	11.78	0.023	1.0007	0.00089	6.8802	15.581	D	
20.10	2.93	9.7292	0.2940	1.1381	0.1453	1.186	0.12	0.263	-	1.066	0.35	1.3164	0.00018	7.88	0.013	9.7292	2.664	B	
20.00	2.93	9.6991	0.2931	1.1647	0.5314	1.661	0.32	0.521	1.45	1.088	0.40	4.723	0.0025	6.47	0.049	9.6991	2.605	B	
20.00	2.93	9.7237	0.2939	1.2183	0.9686	2.207	0.11	0.822	0.09	1.120	0.43	8.349	0.0020	5.30	0.023	9.7237	2.533	B	
20.00	2.93	9.7171	0.2937	1.2884	1.5513	2.912	0.25	1.219	0.93	1.166	0.53	12.87	0.010	4.05	0.078	9.7171	2.437	B	
20.00	2.93	9.7268	0.2940	1.3226	1.9235	3.358	0.18	1.467	0.13	1.180	0.81	15.52	0.011	3.60	0.069	9.7268	2.373	B	
20.10	3.01	9.7138	0.3013	0.3269	2.5787	3.627	0.14	1.641	0.49	1.186	0.19	17.38	0.029	2.911	0.0043	8.6482	2.683	D	
20.10	2.99	9.6938	0.2986	0.1626	2.5346	3.488	0.14	1.660	0.30	1.169	0.16	17.56	0.026	1.463	0.0020	8.7037	2.686	D	
20.00	2.93	9.7010	0.2932	1.4289	2.8880	3.470	0.19	1.537	0.21	1.197	0.56							B	T
20.00	2.93	9.7060	0.2933	1.4271	2.8647	3.451	0.23	1.532	0.35	1.193	0.40							T	B
20.10	2.93	9.7172	0.2937	1.3712	2.3268	3.483	0.18	1.532	0.54	1.195	0.29							B	T
20.10	15.43	8.4512	1.5415	1.1279	0.1213	0.987	0.22	0.232	6.52	1.072	0.31	1.1212	0.00023	6.51	0.019	8.4512	14.249	B	
20.00	15.43	8.4543	1.5421	1.1652	0.4610	1.413	0.18	0.464	0.98	1.096	0.15	4.177	0.0010	5.24	0.023	8.4543	13.973	B	
20.00	15.43	8.4606	1.5432	1.2227	0.9750	2.086	0.23	0.833	0.75	1.128	0.09	8.525	0.0041	4.01	0.046	8.4606	13.493	B	
20.00	15.43	8.4529	1.5418	1.2485	1.2541	2.443	0.23	1.026	0.65	1.156	0.80	10.763	0.0063	3.46	0.057	8.4529	13.232	B	
20.00	15.43	8.4598	1.5431	1.4300	2.8600	2.741	0.02	1.242	0.27	1.169	0.50	12.807	0.0019	2.727	0.0019	7.9783	13.689	T	
20.00	15.43	8.4677	1.5445	1.4939	3.3353	3.067	0.04	1.443	0.46	1.172	0.65	15.079	0.0034	1.860	0.0038	7.9178	13.558	T	T
20.10	15.21	8.5024	1.5257	0.1515	2.1462	3.098	0.10	1.467	0.68	1.166	0.53	15.57	0.017	1.344	0.0011	7.8365	13.540	D	
20.10	14.95	8.5242	1.4983	0.3177	2.1697	3.158	0.11	1.477	0.55	1.173	0.31							D	
20.00	15.43	8.4715	1.5452	1.2890	1.5319	2.550	0.10	1.083	-	1.152	0.10							B	
20.10	15.43	8.4610	1.5433	1.3521	2.1621	2.510	0.17	1.065	0.35	1.149	0.66							B	
29.80	2.93	9.7021	0.2932	1.1946	0.7175	2.033	0.13	0.657	0.24	1.107	0.90	6.214	0.0016	7.23	0.024	9.7021	2.539	B	T
30.00	2.93	9.7264	0.2939	1.5389	3.8482	3.956	0.28	1.832	0.41	1.203	1.50	19.19	0.033	2.81	0.041	9.2133	2.412	T	T
30.00	2.93	9.7254	0.2939	1.6170	4.5138	4.408	0.35	2.115	0.60	1.245	0.34	22.22	0.043	1.80	0.062	9.1278	2.370	T	T
29.90	2.93	9.7080	0.2934	1.3653	2.2428	3.467	0.12	1.490	0.32	1.192	1.59							T	
29.80	15.43	8.4709	1.5451	1.1963	0.7237	1.850	0.26	0.648	0.44	1.110	0.34	6.372	0.0030	5.44	0.045	8.4709	13.604	B	
30.00	15.43	8.4575	1.5427	1.4907	3.3510	3.148	0.04	1.478	0.30	1.203	0.37	15.400	0.0035	2.037	0.0039	7.9183	13.463	T	T

T^a	$\tilde{w}_{MEG}^b$	m_{H_2O}	m_{MEG}	m_{NaHCO_3}	$m_{Na_2CO_3}$	S_{TNa}	dev	$S_{CO_3^{2-}}$	dev	$\rho_{sat.liquid}$	dev	$w_{Na_2CO_3}$	$\sigma_{Na_2CO_3}$	w_{NaHCO_3}	σ_{NaHCO_3}	m_{H_2O}	w_{MEG}	P_1^f	P_2^f
30.00	15.43	8.4640	1.5439	1.6168	4.5217	4.168	0.29	2.056	0.48	1.215	3.78	21.59	0.034	0.79	0.049	7.8114	12.810	T	
29.90	15.43	8.4631	1.5437	1.3154	1.6136	2.514	2.26	1.029	1.97	1.176	1.39	-	-	-	-	-	-	B	T
30.00	15.43	8.4584	1.5429	0.4061	5.5990	4.900	0.26	2.441	0.91	1.268	1.44	-	-	-	-	-	-	T	M
39.90	0.00	10.0081	0.0000	0.2910	4.4064	5.566	0.93	2.771	1.51	1.250	2.54	29.22	0.12	0.43	0.25	9.9096	0.000	T	
39.60	3.04	9.7036	0.3046	1.2050	0.8367	2.253	0.55	0.750	0.62	1.109	0.62	7.127	0.0092	7.63	0.12	9.7036	2.594	B	
39.80	3.04	9.6833	0.3039	1.5510	3.8741	4.074	0.26	1.873	0.47	1.226	2.24	19.60	0.032	3.16	0.040	9.1846	2.474	T	
39.80	3.04	9.7284	0.3053	1.6437	4.7442	4.600	0.05	2.221	0.10	1.233	0.37	23.343	0.0062	1.641	0.0094	9.1117	2.432	T	
39.70	3.04	9.6826	0.3039	1.3556	2.3409	3.527	0.14	1.459	0.53	1.236	1.97	-	-	-	-	-	-	B	
39.80	3.04	9.7064	0.3047	0.4710	5.0355	5.802	0.10	2.881	0.45	1.324	0.79	-	-	-	-	-	-	T	M
39.90	3.86	9.7241	0.3905	0.2979	3.5821	4.889	0.66	2.404	1.15	1.289	2.27	25.09	0.084	1.30	0.14	9.6724	2.857	T	
39.20	15.34	8.4632	1.5333	1.1500	0.3445	1.515	0.16	0.418	1.31	1.123	0.65	3.0696	0.00071	7.86	0.021	8.4632	13.663	B	
39.80	15.34	8.4733	1.5352	1.2068	0.8436	2.178	0.21	0.783	0.88	1.186	1.86	7.244	0.0034	6.81	0.044	8.4733	13.183	B	
39.60	15.34	8.4627	1.5332	1.4300	2.8565	2.943	0.25	1.293	0.43	1.204	0.68	13.45	0.024	3.40	0.024	8.0168	13.350	T	
39.90	15.03	8.5264	1.5086	0.2587	2.8435	4.081	0.06	1.984	0.25	1.250	1.05	20.975	0.0072	1.04	0.010	8.4723	11.788	T	
39.90	14.95	8.5100	1.4961	0.2762	2.8792	4.075	0.18	1.972	0.04	1.222	1.16	21.02	0.021	0.91	0.029	8.4410	11.754	T	
39.90	28.13	7.2394	2.8331	0.3182	1.7991	2.696	0.95	1.278	0.84	1.165	1.76	13.50	0.081	1.25	0.087	7.1660	24.154	T	
39.80	54.19	4.7356	5.6010	0.2300	0.7296	1.211	1.68	0.515	1.51	1.119	2.61	5.60	0.070	1.29	0.061	4.6982	50.634	T	
39.90	77.61	2.2556	7.8178	0.2096	0.3681	0.675	0.79	0.255	2.11	1.138	0.30	2.71	0.019	1.37	0.015	2.2271	74.652	T	
49.70	3.04	9.7088	0.3047	1.2223	0.9949	2.625	0.11	0.907	5.07	1.164	1.48	8.223	0.0025	9.01	0.028	9.7088	2.519	B	
49.75	3.04	9.7056	0.3046	1.4822	3.3377	4.002	0.06	1.766	0.48	1.240	1.25	18.043	0.0073	5.021	0.0081	9.3398	2.430	T	
49.70	3.04	9.6974	0.3044	1.5275	3.6444	4.163	0.14	1.876	0.17	1.260	0.31	19.26	0.017	4.43	0.020	9.2812	2.423	T	
48.80	15.34	8.4761	1.5357	1.0151	0.3467	1.607	0.44	0.407	1.31	1.137	0.96	3.057	0.0021	8.66	0.062	8.4761	13.542	B	
49.60	15.34	8.4610	1.5330	1.1913	0.7143	2.093	0.65	0.659	1.74	1.167	2.20	6.148	0.0086	7.83	0.13	8.4610	13.194	B	
49.75	15.34	8.4607	1.5329	1.4304	2.8570	3.804	0.26	1.800	0.24	1.108	0.93	18.76	0.010	2.21	0.065	8.4607	12.121	W	
49.70	15.34	8.4660	1.5338	1.5161	3.6380	4.540	0.18	2.207	0.37	1.228	6.89	23.205	0.0055	1.35	0.059	8.4660	11.572	W	
49.40	15.34	8.4716	1.5349	1.5757	4.1760	4.519	0.08	2.099	9.72	1.291	1.75	-	-	-	-	8.4660	-	W	M

[a] equilibrium temperature in °C. [b] $\tilde{w}_{MEG}$, salt-free weight percent of MEG in the initial composition, $m_{MEG}/(m_{MEG}+m_{H_2O})$. [c] The weight of the initial composition in grams, m_i, of component i. [d] The equilibrium composition determined by titration. S_{TNa} is calculated by equation (220) as $mol\ sodium/kg\ total$ and $S_{CO_3^{2-}}$ by equation (218) in $mol\ CO_3^{2-}/kg\ total$. $\rho_{sat.\,liquid}$ is the density of the saturated liquid at equilibrium temperature in g/cm^3. The deviation of S_{TNa}, $S_{CO_3^{2-}}$, and $\rho_{solution}$ (dev) is calculated as the standard deviation, σ, divided by the mean of the samples times hundred. [e] The result of the reverse Schreinemakers method. w_i is the weight percent of component i per kilogram of total solution calculated by equation (225), (227) and (240). m_{H_2O} is the grams of water in the saturated liquid phase at equilibrium calculated by equation (238). σ_i is the standard deviation of the weight fraction i. [f] P_1 and P_2 is the precipitated solid phases. B: $NaHCO_3$, C: Na_2CO_3, M: $Na_2CO_3 \cdot H_2O$, H: $Na_2CO_3 \cdot 7H_2O$, D: $Na_2CO_3 \cdot 10H_2O$, T: trona, and W: wegscheiderite.

7.4.1   Meta stable solutions

A challenge when measuring solubility in the *Na₂CO₃-NaHCO₃-MEG-H₂O* system at lower temperature is the formation of meta-stable solutions. Several different meta-stable phases may form depending on the initial concentration and the added seed crystals.
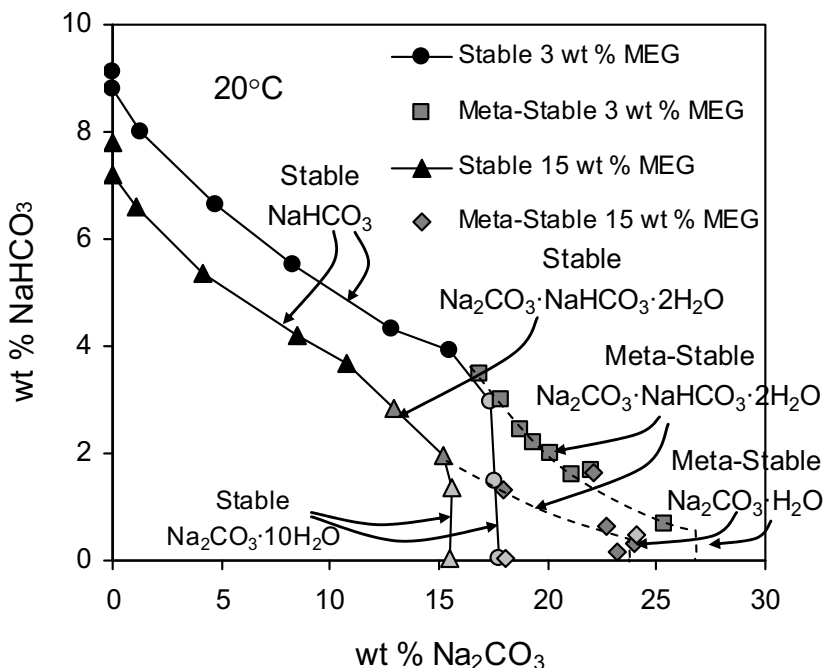
Figure 27: Stable and meta-stable data at 20 °C in the *Na₂CO₃-NaHCO₃-MEG-H₂O* system. ●,▲: *NaHCO₃*. ▲,■,◆: Trona. △,◉: *Na₂CO₃·10H₂O*. ◇: *Na₂CO₃·H₂O*. Dotted line: meta-stable trend.

In this study meta-stable solutions have a tendency to form below 35 °C from initial solutions from which salt hydrates were expected to precipitate. For example *Na₂CO₃* solutions may stand for several days at very high super-saturation at 10 °C to 25 °C without solids precipitating. By seeding, precipitation occurs instantly. Seeding an aqueous *Na₂CO₃* solution at 10 °C by *Na₂CO₃* will make *Na₂CO₃·H₂O* precipitate, but seeding using *Na₂CO₃·10H₂O* initiates *Na₂CO₃·10H₂O* precipitation. The equilibrium experiments related to *Na₂CO₃* were carried out by supersaturating a solution by a few *wt% Na₂CO₃*, seeding, and determining the composition by the reverse Schreinemakers method. *Na₂CO₃·7H₂O* was not used as a seeding crystal, but the reverse Schreinemakers method revealed that one solution precipitated *Na₂CO₃·7H₂O*. Table 8 shows the meta-stable data determined in this study. The columns correspond to those of table 7. Figure 27 shows a selection of meta-stable data from table 8 determined in this study. The *stable* branches of the isotherms consist of a *NaHCO₃* branch, a trona branch and a *Na₂CO₃·10H₂O* branch. The trona branch at 3 *wt% MEG* is very short. The *meta-stable* isotherms have longer trona branches and the

Na$_2$CO$_3$·10H$_2$O branch is replaced by a *Na$_2$CO$_3$·H$_2$O* branch. The meta-stable solutions in equilibrium with trona can easily be reproduced and it is difficult to get the stable phase of *Na$_2$CO$_3$·10H$_2$O* without using seed crystals.

The long meta-stable trona branch in 3 *wt% MEG* indicates that trona can be produced consistently at 20 °C even though *Na$_2$CO$_3$·10H$_2$O* is expected to precipitate. On the other hand if impurities of *Na$_2$CO$_3$·10H$_2$O* are present in the crystallizer, then *Na$_2$CO$_3$·10H$_2$O* precipitates immediately.

Seed crystals of *Na$_2$CO$_3$·10H$_2$O* can be stored at room temperature in a saturated *Na$_2$CO$_3$* solution. The crystals grow to big hydrates over a few days. *Na$_2$CO$_3$·10H$_2$O* may not be stored in open air since it quickly loses water. A test was made where an amorphous single $0.25cm^3$ crystal was stored in air. It decomposes in a few hours due to evaporation of water. It forms crystals of lower *Na$_2$CO$_3$* hydrates and becomes white.

Table 8: Experimental initial composition, meta-stable composition, results of the reverse Schreinemakers method and solid phase information from the Na_2CO_3-Na_2CO_3-MEG-H_2O system at 1 bar and 20 °C to 30 °C.

T^a °C	$\tilde{w}_{MEG}^b$ %	m_{H_2O} g (Initial^c)	m_{MEG} g	m_{NaHCO_3} g	$m_{Na_2CO_3}$ g	S_{TNa} mol/kg (Meta-stable solution^d)	dev %	$S_{CO_3^{2-}}$ mol/kg	dev %	$\rho_{sat.\,liquid}$ g/cm³	dev %	$w_{Na_2CO_3}$ % (Reverse Schreinemakers^e)	$\sigma_{Na_2CO_3}$ %	w_{NaHCO_3} %	σ_{NaHCO_3} %	m_{H_2O} g	w_{MEG} %	P_1^f	P_2^f
30.00	2.93	9.7162	0.2936	0.0000	4.9251	4.429	0.11	2.207	0.01	1.259	0.28	23.472	0.0033	0		9.3835	2.322	M	
29.90	2.93	9.7317	0.2941	0.0000	4.5903	5.421	0.60	2.696	0.31	1.301	1.22	28.73	0.088	0		9.6315	2.112	M	
30.00	15.17	8.5091	1.5221	0.0000	2.8568	3.403	1.16	1.692	0.90	1.198	0.29	18.04	0.16	0		8.3944	12.581	M	
29.90	15.43	8.4678	1.5445	0.0000	4.7036	4.935	2.86	2.484	3.14	1.303	1.27	26.15	0.82	0		8.2586	11.635	M	
29.80	15.43	8.4507	1.5414	0.0000	4.5941	5.101	0.24	2.531	0.12	1.306	0.63	27.03	0.031	0		8.2888	11.442	M	
29.90	27.93	7.2273	2.8006	0.0000	2.5354	2.704	1.07	1.337	0.75	1.173	0.45	14.33	0.11	0		7.0772	24.289	M	
20.00	2.93	9.7135	0.2936	0.9606	2.7433	3.563	0.36	1.594	0.15	1.203	0.79	16.76	0.016	3.36	0.018	9.4781	2.400	T	
20.00	2.93	9.7023	0.2932	0.7427	2.6877	3.685	0.60	1.675	0.07	1.207	0.49	17.735	0.0078	2.843	0.0092	9.5346	2.370	T	
20.00	2.93	9.7021	0.2932	0.5215	2.6353	3.804	0.65	1.767	0.22	1.203	0.24	18.7	0.025	2.31	0.031	9.6027	2.340	T	
20.10	2.93	9.7144	0.2936	0.3914	2.5992	3.871	0.10	1.804	0.24	1.227	0.46	19.23	0.027	2.04	0.034	9.6570	2.323	T	
20.00	2.93	9.7253	0.2939	0.4096	2.7680	3.993	0.33	1.874	0.30	1.232	0.05	20.01	0.034	1.83	0.045	9.6495	2.310	T	
20.00	2.93	9.7234	0.2939	1.6334	4.5144	4.312	0.52	2.075	0.03	1.255	2.23	21.901	0.0034	1.506	0.0049	9.1021	2.395	T	
20.00	2.93	9.7055	0.2933	0.4132	2.9801	4.148	0.01	1.982	0.14	1.236	0.63	21.07	0.017	1.45	0.023	9.6077	2.295	T	
20.10	2.93	9.7235	0.2939	0.7449	4.1752	4.832	0.13	2.387	0.11	1.258	0.46	25.3	0.013	0.49	0.023	9.4314	2.242	T	
20.00	2.93	9.7249	0.2939	0.4399	4.0581	4.530	0.23	2.201	0.17	1.253	0.47	-	-	-	-	-	-	M	T
20.00	15.43	8.4662	1.5443	1.6138	4.5150	4.334	0.24	2.138	0.21	1.267	0.20	22.04	0.029	1.48	0.041	7.8518	12.571	T	
20.10	15.43	8.4573	1.5427	1.5409	3.8445	3.509	2.68	1.703	2.63	1.187	1.64	17.86	0.28	1.17	0.35	7.8550	13.292	T	
20.00	15.43	8.4614	1.5434	0.0603	3.3499	4.556	0.19	2.246	0.01	1.277	0.41	23.85	0.045	0.4578	0.00034	8.4261	11.717	M	
20.00	15.43	8.4606	1.5433	0.5692	3.5209	4.319	0.50	2.117	-	1.269	0.48	-	-	-	-	-	-	T	
20.00	15.43	8.4653	1.5441	0.1216	3.3729	4.511	0.21	2.230	0.47	1.273	0.99	22.61	0.059	0.45	0.089	8.2410	12.136	T	M
20.00	15.43	8.4678	1.5446	0.1742	3.3933	4.537	0.50	2.232	0.68	1.278	0.37	-	-	-	-	-	-	T	M
20.10	15.43	8.4698	1.5449	0.2601	3.4191	4.517	0.75	2.228	0.70	1.280	0.76	-	-	-	-	-	-	T	M
20.00	15.43	8.4623	1.5435	0.4161	3.4759	4.353	0.19	2.144	0.23	1.272	0.25	-	-	-	-	-	-	T	M
20.00	15.43	8.4635	1.5438	0.7440	4.1814	4.723	0.39	2.355	-	1.268	0.41	-	-	-	-	-	-	T	M
30.00	2.93	9.7058	0.2933	0.0275	4.6715	5.997	0.51	2.981	0.47	1.355	1.03	31.66	0.042	0.1875	0.00015	9.7010	2.000	M	
29.80	2.93	9.7129	0.2935	0.5414	4.9622	5.423	0.62	2.682	0.49	1.287	0.93	-	-	-	-	-	-	T	
29.90	2.93	9.7225	0.2938	0.1836	4.6845	4.488	0.34	2.183	0.04	1.265	0.51	-	-	-	-	-	-	M	T
30.00	15.43	8.4640	1.5439	0.5630	3.0946	3.811	0.32	1.856	0.08	1.227	0.02	19.93	0.0088	0.42	0.012	8.2446	12.563	T	
29.90	15.43	8.4597	1.5431	0.0280	4.6156	4.745	0.15	2.359	0.35	1.270	1.59	25.01	0.088	0.2142	0.00031	8.2309	11.805	M	
30.00	15.43	8.4630	1.5437	0.1868	4.6814	3.330	0.85	1.631	0.90	1.215	0.06	-	-	-	-	-	-	D	T

a system temperature in °C. b,c,e,f see table 7. d The meta-stable composition determined by titration. Symbols defined in table 7.

7.5 Parameter fitting

The parameter estimation routines used in this study consist of four parts. A thermodynamic model, a speciation routine for calculating the equilibrium composition in the liquid and the gas phase, a set of routines for calculating specific properties and a parameter optimisation routine. The modelling extends the previous work by Thomsen and co-workers[7,8,9,43].

An object function is calculated for the optimisation routine in which experimental and calculated properties are compared. The value of the object function, and thereby the difference between calculated and experimental properties, is minimized by varying the parameters of the extended UNIQUAC model using a combination of Nelder-Mead and Marquardt-Levenberg minimization routines. The extended UNIQUAC parameters are constrained by a penalty function in the objective function. The volume and surface parameters, r_i and q_i, are constrained to the interval from 0.05 to 15, the interaction parameters, u_{ij}^o, to the interval from -2500 to 2500 and the

temperature gradients of the interaction parameters, u_{ij}^t, to the interval from -20 to 20.

If parameters were determined to have a value corresponding to one of these boundaries, it was taken as an indication that either the parameter was unnecessary, some data were wrong, or that a parameter was given a bad initial value. Maximum step sizes were used for the parameters to avoid extreme values. The objective function is given by

$$
\begin{aligned}
S = &\sum_{VLE\,data} \left(\frac{P_{calc} - P_{exp}}{0.05\left(P_{total,exp} + 0.01\right)} \right)^2 \\
&+ \sum_{H^{Ex}\,data} \left(\frac{H_{calc}^{Ex} - H_{exp}^{Ex}}{14.4R} \right)^2 \\
&+ \sum_{\Delta_{sol}H\,data} \left(\frac{\Delta_{sol}H_{calc} - \Delta_{sol}H_{exp}}{120.3R} \right)^2 \\
&+ \sum_{Lit.\,SLE\,data} \left(\frac{1}{0.05}\left(\Delta_r G^o/RT + \sum_i \nu_{ir}\ln a_i\right) \right)^2 \\
&+ \sum_{Our\,SLE\,data} \left(5\left(S_{TNa,exp} - S_{TNa,calc}\right) \right)^2
\end{aligned}
\tag{242}
$$

The first term is related to the binary and ternary VLE data. The bubble point pressure is calculated for a given solution. The weighting factor of 0.05 is used to make a relative deviation of 5 % contribute by 1 in the objective function. The residual at low pressures may become very high when dividing by $P_{total,exp}$. This is overcome by adding 0.01 bar, and therefore pressures below 0.01 *bar* receive little weight. The bubble point pressures of the solutions considered here were between 0.0002 and 5 *bar*. The weighted residuals calculated with the optimized parameters are in the range from -3 to 3.

Absolute deviations are used for calculating the contribution of excess enthalpy data to the object function. A difference of $14.4 \cdot R = 120$ *J/mol* between calculated and

experimental excess enthalpy corresponds to $\left(H^{Ex}_{calc} - H^{Ex}_{exp}\right)\big/(14.4R) = 1$ and therefore contributes by 1 to the object function. The weighted residuals for excess enthalpy data calculated by the optimized parameters are in the range from -1 to 1. The contribution of heat of solution data to the objective function are also calculated from absolute differences. A difference of 120.3·R=1000*J/mol* between calculated and measured heats of solution gives $\left(\Delta_{sol}H_{calc} - \Delta_{sol}H_{exp}\right)\big/(120.3R) = 1$ and therefore contributes by 1 to the objective function. The weighted residuals of this type calculated with the optimized parameters are in the range from -0.2 to 0.2.

The deviation of SLE data was added to the objective function by determining the logarithm of the saturation index, $\ln(SI_k) = \ln\left(\prod_{i \text{ in } k}\left(a_i\right)^{v_{ik}}\Big/K_{T,P_o,k}\right) = \Delta_k G^o_{T,P_o}\big/RT +$

$\sum_i v_{ik} \ln a_i$ for reaction k with equilibrium constant K_k and stoichiometric coefficients v_{ik} of the i'th component with activity a_i. The experimental data define which salts saturate the liquid and $\ln(SI)$ of those salts are returned in the objective function and should be 0 when parameters are optimized. The weighting factor of 0.05 scales the contribution of SLE data to be 1 if the calculated $\ln(SI)$ is 0.05. A penalty is added if a "wrong salt" precipitates compared to salts determined by the dataset. SLE data of ice formation are weighted 100 times higher because this type of data are usually very accurate. The weighted residuals of SLE data calculated with the optimized parameters are in the range from -10 to 10.

The equilibrium data measured in this work are represented by the last term of the objective function, (242). The equilibrium routine was set up to use the initial composition, the identity of the solid phase, and the temperature to calculate *mol sodium/kg total*, $S_{TNa,calc}$, The calculated value was compared to the measured value. The weighting was set to give a contribution of 1 when the deviation is 0.2 *mol sodium/kg total*. The weighted residuals calculated with the optimized parameters are in the range from -2 to 2. Results of the reverse Schreinemakers method were only used for plotting and were not used in the fitting process. Therefore the two-salt saturation points are not represented in the figures even though they were used in the fitting process.

350 VLE data, 192 thermal property data and 209 SLE data were used in the fitting process. All literature values used were taken from original articles. Data collections were deliberately not used in order to avoid printed errors and misinterpretations. Two *MEG* specific parameters and 12 *MEG* related interaction parameters were optimized by minimizing the objective function in equation (242).

An average relative deviation, ARD, was calculated in order to compare experimental and calculated values. The calculated ARD is defined by

$$ARD = \frac{1}{n_{exp}}\sum_{i=1}^{n_{exp}}\frac{\left|u_{exp} - u_{calc}\right|}{u_{exp}} \tag{243}$$

u is an arbitrary calculated or experimental value and n_{exp} is the number of experimental data.

7.5.1   Parameter estimation procedure

Binary, ternary, and quaternary data were used in the fitting process. In the parameter estimation procedure the initial UNIQUAC volume and surface area parameters for *MEG*, r_{MEG} and q_{MEG}, were given guesses of 5. Interaction parameters were given initial values of 500 with a temperature gradient of 0.5.

The fitting process was divided into five steps. First the *MEG-MEG* and *MEG-H_2O* interaction parameters were fitted to the binary VLE, H^{Ex}, and freezing point depression data for the *MEG-H_2O* system. Freezing point depression data were only used for ice precipitation up to 55 *wt% MEG* since thermodynamic properties of *MEG·H_2O(s)* and *MEG(s)* were unknown. Second the *CO_2-MEG* interaction parameters were fitted to the *CO_2-MEG-H_2O* data. In the third step *r*, *q*, and *MEG-Na^+*, *MEG-HCO_3^-* and *MEG-CO_3^{2-}* interaction parameters were fitted to SLE data for the *$NaHCO_3$-MEG-H_2O* and *Na_2CO_3-MEG-H_2O* systems. In the last step, all these parameters were simultaneously fitted to all the binary, ternary, and quaternary *Na_2CO_3-$NaHCO_3$-MEG-H_2O* data. The parameters were gradually refined by repeating this procedure a few times until a low objective function value was obtained. Finally the standard state property for *MEG·H_2O(s)* and *MEG(s)* were fitted to SLE data for the *MEG-H_2O* system in the whole composition range.

The *MEG-OH⁻* interaction was not fitted in this study due to the lack of data. It was therefore given the fixed value $u^o_{OH-MEG} = 2500$ and $u^t_{OH-MEG} = 0$ equivalent to no interaction. The *OH⁻* concentrations in the solutions studied are up to 10^{-3} *molal*. Therefore interaction has little or no effect on the thermodynamics of the solutions studied here. The *MEG-H^+* interaction parameter is defined in accordance with the systematic approach defined by Thomsen[7], see appendix D.3.

7.6   Results and discussion

7.6.1   Correlation of density

The densities measured in this study are reported in table 7. It was found that the density data for solutions containing H_2O, *MEG*, $NaHCO_3$, Na_2CO_3, and *NaCl* could be correlated using the simple, empirical equation:

$$\rho_{sol} = \rho_{H_2O} + \Delta\rho_{MEG} + \Delta\rho_{NaHCO_3} + \Delta\rho_{Na_2CO_3} + \Delta\rho_{NaCl} \qquad (244)$$

The density of water, ρ_{H_2O} *(g/cm³)*, was calculated by the Kell[44] correlation:

$$
\begin{aligned}
\rho_{H_2O} = \big(& 0.99983952 + 16.945176 \cdot 10^{-3} t - 7.9870401 \cdot 10^{-6} t^2 \\
& -46.170461 \cdot 10^{-9} t^3 + 105.56302 \cdot 10^{-12} t^4 \\
& -280.54253 \cdot 10^{-15} t^5 \big) \big/ \big(1 + 16.87985 \cdot 10^{-3} t \big)
\end{aligned}
\qquad (245)
$$

where *t* is the temperature in °C. The contribution from glycol, $\Delta\rho_{MEG}$ *(g/cm³)*, was fitted to the following equation:

$$\Delta\rho_{MEG} = \tilde{w}_{MEG}\left(d_1 \cdot \tilde{w}_{MEG} + d_2 + d_3\left(t - 25°C\right)^2 + d_4\left(t - 25°C\right)\right) \qquad (246)$$

$\tilde{w}_{MEG}$ is the salt-free weight fraction of *MEG*, tilde indicate salt-free solution. d_1 and d_2 were fitted to data at 25 °C of Hayduk and Malik[45] and Huot *et al.*[46] as shown in figure 28. d_1 and d_2 are found in table 9.
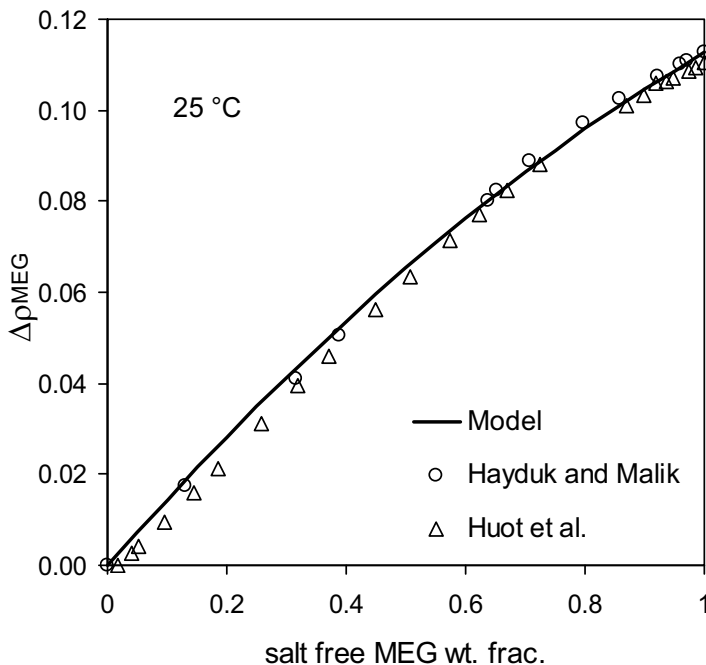
Figure 28: Density of *MEG-H₂O* solutions. $\Delta\rho_{MEG}$ as function of salt-free *MEG* wt. fraction.

Mol fraction of *MEG* was not used in this study since fitting $\Delta\rho_{MEG}$ as a polynomial function of *MEG* mol fraction requires more parameters. A small refinement of the model was made by fitting the temperature dependence of $\Delta\rho_{MEG}$, d_3 and d_4, to data from Kapadi *et al.*[47], Sakurai[48], George and Sastry[49], Cocchi *et al.*[50], and Douheret and Hoiland[51]. The calculated density was compared to Gallant's graph[52] and the agreement is good as shown in figure 29. The density measured by Yang *et al.*[53] were deliberately not used since they diverge compared to the remaining data. d_3 and d_4 are found in table 9.

The densities of solutions containing 0 to 15 *wt% MEG*, saturated in one or both salts of *Na₂CO₃* and *NaHCO₃*, are shown in figure 30. The plot shows a linear trend of the density as function of S_{TNa}. The trend is also observed by looking at the two salts separately, which is not shown here. Densities of solutions containing higher *MEG* concentrations are also linear, but have a higher density compared to densities in figure 30.
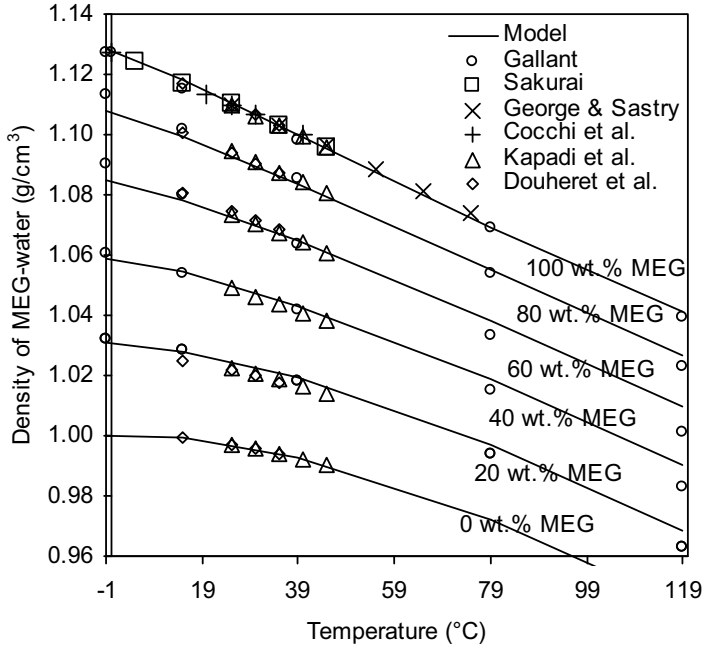
Figure 29: Density of *MEG-H₂O* solution as function of temperature and salt-free *MEG* wt. fraction.

From these results it is assumed that contributions from salts, $\Delta\rho_{NaHCO_3}$, $\Delta\rho_{Na_2CO_3}$, and $\Delta\rho_{NaCl}$, in *g/cm³* in (244) follows a linear dependence by:

$$\Delta\rho_{NaHCO_3} = d_5 \cdot w_{NaHCO_3}$$

$$\Delta\rho_{Na_2CO_3} = d_6 \cdot w_{Na_2CO_3} \tag{247}$$

$$\Delta\rho_{NaCl} = d_7 \cdot w_{NaCl}$$

The parameters d_5 and d_6 were fitted to the experimental data from table 7 calculated using the reverse Schreinemakers method. This indicate that the experimental densities were fitted using the measured experimental compositions of the liquid phase. The result is shown in figure 31 and 32. The calculated density shown in figure 31 is lower than the experimental density at high *MEG* concentrations. The deviation is related to the accuracy of the extended UNIQUAC model.

Figure 32 shows a curvature below 40 *wt% MEG* at low temperature. This is due to the precipitation of *Na₂CO₃·10H₂O* also shown by figure 45. The density has a very distinct temperature dependence which is reproduced by the model.
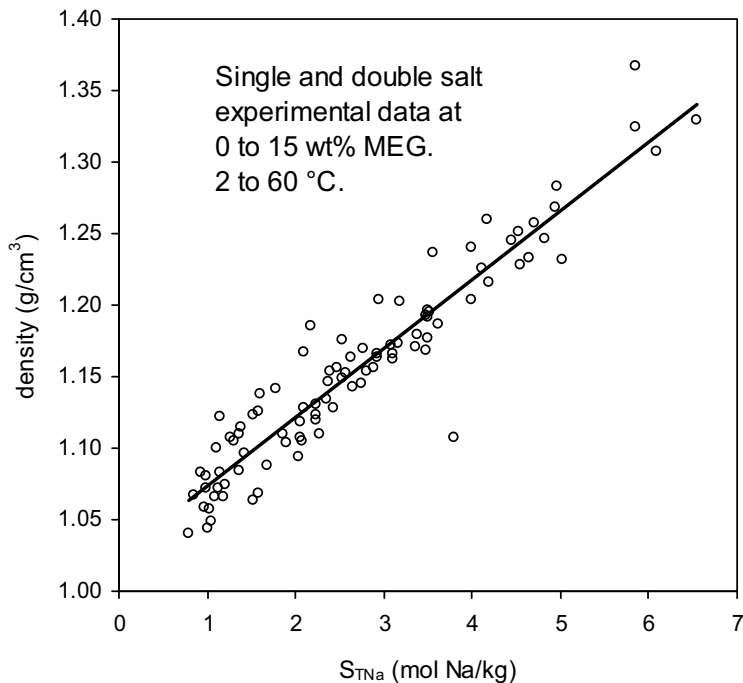
Figure 30: Density of *Na₂CO₃-NaHCO₃-MEG-H₂O* solution as function of sodium content.
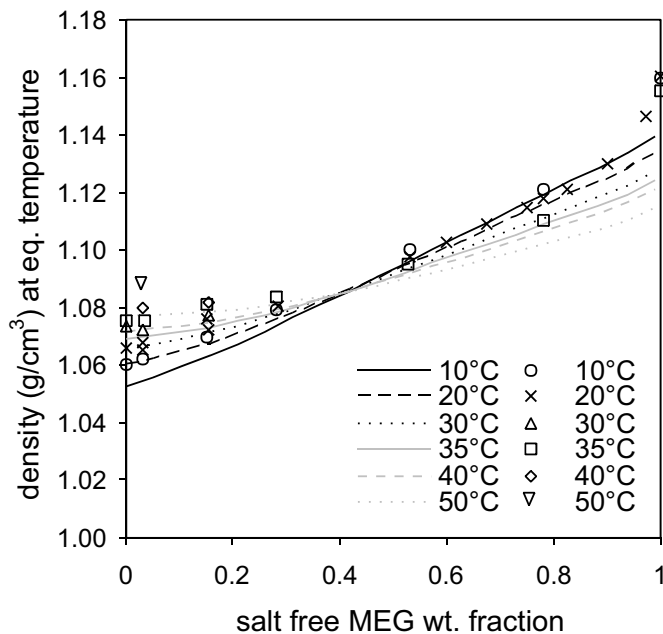
Figure 31: Density of saturated *NaHCO₃-MEG-H₂O* solution determined using equation (244). Composition of the saturated solution determined using the extended UNIQUAC model.

d_7 was fitted to the un-saturated *NaCl-MEG-H_2O* data of Sandengen and Kaasa[54]. A comparison is shown in figure 33. The linear trend with respect to wt. fraction of *NaCl* is obvious. The parameters d_5 to d_7 are found in table 9.

No temperature dependence of $\Delta\rho_{NaHCO_3}$, $\Delta\rho_{Na_2CO_3}$, and $\Delta\rho_{NaCl}$ was included since the above correlations reproduce the experimental results satisfactory in the used temperature range. This is for example verified by looking at figure 33. The result is predicted equally well at 25 and 50 °C with no temperature correction.
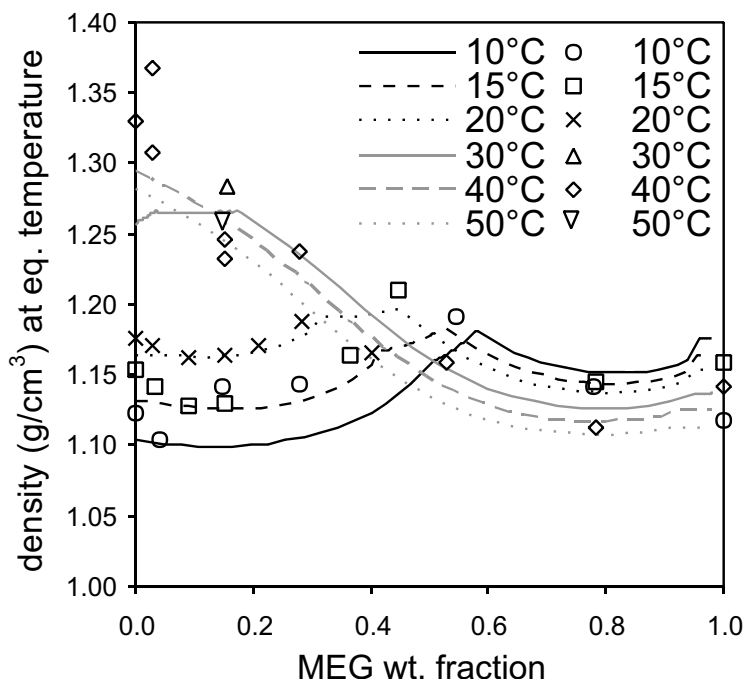
Figure 32: Density of saturated *Na_2CO_3-MEG-H_2O* solution determined using equation (244). Composition of the saturated solution determined using the extended UNIQUAC model.

The average relative deviation (ARD) between experimental densities and densities calculated with equation (244) was used as objective function. The ARD obtained was 0.79 % which is within the experimental error. The data are scattered but the model reproduces the temperature dependence even though there is no temperature dependence of the salts in the model.

Equation (244) is also valid for salt-free systems and may be used for calculating water, *MEG*, or *MEG-H_2O* density between 0 and 100 °C. It must be emphasized that the model gives an engineering approach to calculating the density and is only accurate down to 0.01 *g/cm³*. Figure 34 shows a comparison of experimental and calculated densities in the salt solutions. There is no tendency to either over- or under predict. The plot shows that outliers are approximately 5% which is related to the quality of the density measurement.
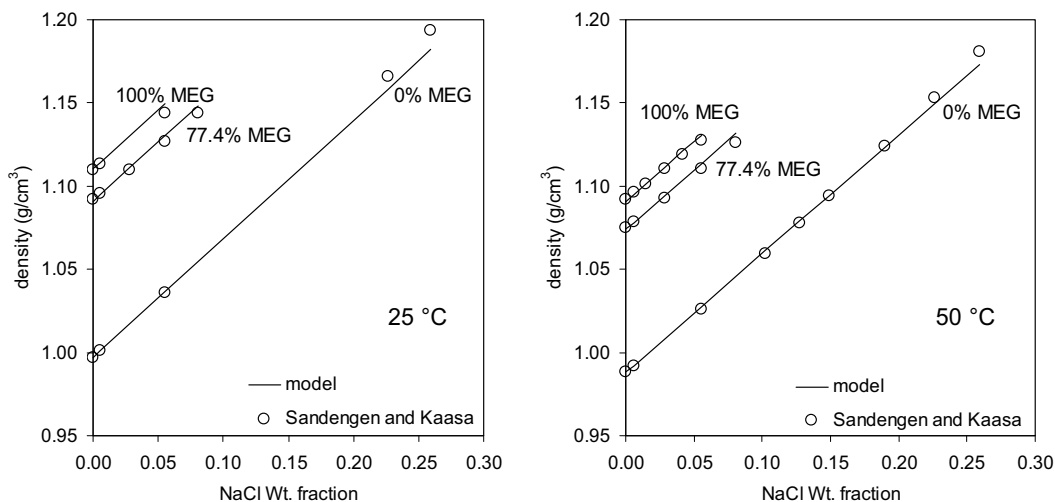
Figure 33: Density of *NaCl-MEG-H_2O* solutions determined by equation (244) at 25 and 50 *°C*.
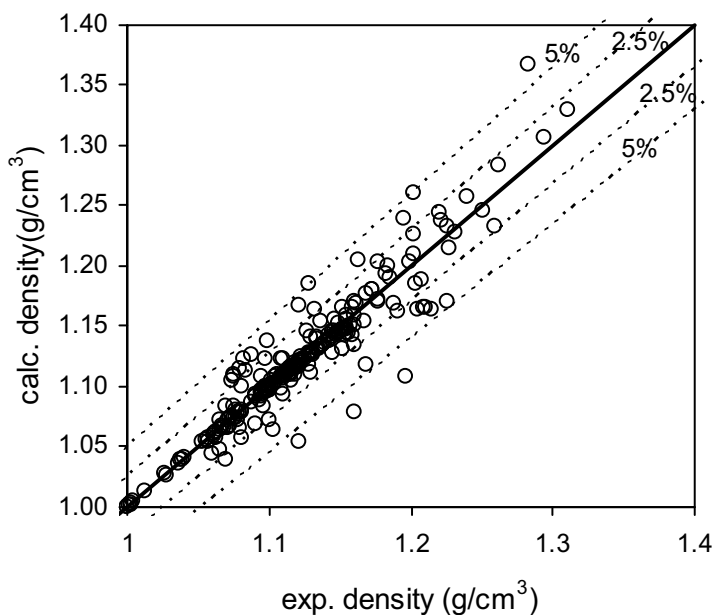
Figure 34: Comparison of calculated and experimental density of *NaCl-Na_2CO_3-$NaHCO_3$-MEG-H_2O* solutions between 2 to 60 °C.

The density model presented by (244) has certain similarities to the model of Sandengen and Kaasa[54]. Their model uses three parameters per salt, and is only valid at 15 and 20 *°C*. (244) uses one parameter per salt and is valid in a broader temperature range. The model by Sandengen and Kaasa[54] was fitted to the *NaHCO₃-NaCl-MEG-H_2O* system and not for systems with *Na_2CO_3*. In our model *Na_2CO_3* and

NaHCO₃ was only fitted to data for saturated solutions but works satisfactory for unsaturated solutions. This was evaluated by comparing our correlation to the dilute *NaHCO₃* solutions of Sandengen and Kaasa[54]. At 20 °C it gives an ARD of 0.14 %. The model by Sandengen and Kaasa[54] gives an ARD of 0.12 % for the same data and the agreement is good. Comparing the models to our data at 20 °C for solutions of *NaHCO₃* give an ARD of 0.44 % for equation (244) and 0.47 % for the model by Sandengen and Kaasa[54]. This is understandable since their data were not used in our fitting process. Equation (244) gives an ARD of 0.19 % for the *NaCl* related data at 20 °C and the model by Sandengen and Kaasa[54] gives an ARD of 0.02 %. It shows that their model performs better for the *NaCl-MEG-H₂O* system at 20 °C. Our model performs equally well at 50 °C which the correlation by Sandengen and Kaasa[54] does not.

Table 9: Correlation parameters for equation (246) and (247).

Parameter	d_1 (g/cm^3)	d_2 (g/cm^3)	d_3 (g/cm^3K^2)	d_4 (g/cm^3K)	d_5 (g/cm^3)	d_6 (g/cm^3)	d_7 (g/cm^3)
	-0.0358	0.149	$3.41 \cdot 10^{-6}$	$-495.9 \cdot 10^{-6}$	0.921	0.714	0.714

The density model represented in equation (244) uses few parameters and is valid at concentrations up to saturation of the two salts at temperatures between 2 and 60 °C. It is expected that the model can be used in a wider temperature range with good accuracy. The parameters of the correlation are found in table 9.

Salt contribution for *Na₂CO₃* and *NaHCO₃* can alternative be calculated by $\Delta\rho_{NaHCO_3} + \Delta\rho_{Na_2CO_3} = S_{TNa} \cdot 0.0509 \, kg/mol$. This is a simplified approach and gives an ARD of 1.04%, where the contribution to *NaHCO₃* is not as accurately calculated.

7.6.2 Model of the Na₂CO₃-NaHCO₃-MEG-H₂O system

Eight species are assumed to be present in the liquid phase as shown in table 10. Two parameters sets were determined in this work, denoted set *A* and *B*. Table 10, 11, 12, and 13 give the used standard state properties and the regressed interaction parameters.

Parameter set *A* contains mainly standard state properties from NIST[12] and a few of such properties regressed in this and in a previous study[8] as shown in table 10 and 11. The interaction parameters were determined by Thomsen *et al.*[13,8] and Garcia *et al.*[55] except for the *MEG* parameters determined in this study.

Set *B* include most of the liquid phase parameters used in set *A*, but part of the standard state properties of the solid species were optimised, as seen in table 11. The interaction parameters $Na^+ - CO_3^{2-}$, $Na^+ - HCO_3^-$, and $OH^- - CO_3^{2-}$ were also optimised to get a better representation of the properties of the aqueous *Na₂CO₃-NaHCO₃-H₂O* system as well as of the mixed solvent system, *Na₂CO₃-NaHCO₃-MEG-H₂O*.

Figure 35 shows the solubility of *Na₂CO₃* in pure water. The *A* parameters give an offset at T>35 °C. The same is the case for the *NaHCO₃* solubility, not shown here. The improvement is related to better values of the standard state enthalpies of *Na₂CO₃·H₂O* and *Na₂CO₃(s)*, and better interaction parameters.
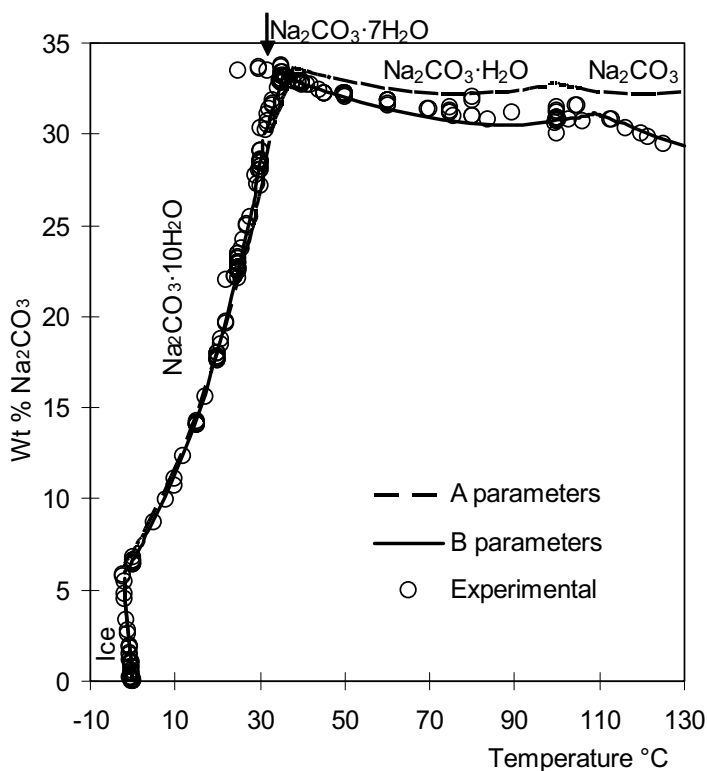
Figure 35: The temperature dependence of Na_2CO_3 solubility in water. Lines calculated with the A and the B parameters. Experimental data points are from the IVC-SEP database[10].

Figure 36 shows the temperature dependence of the two salt saturation lines in the Na_2CO_3-$NaHCO_3$-H_2O system, they also represent ternary univariant compositions. The y-axis corresponds to the salt fraction $n_{Na_2CO_3}/\left(n_{Na_2CO_3} + n_{NaHCO_3}\right)$ in the saturated solution. The ternary invariant points are shown and represent the points where three solid phases are in equilibrium with a liquid and a gas phase. The binary invariant points are shown on the top and bottom axes where salt fraction is zero or one, and two solid phases are in equilibrium. It is shown how set B gives a better representation of the two salt lines, especially the $NaHCO_3$-trona $(Na_2CO_3 \cdot NaHCO_3 \cdot 2H_2O)$ line, but also a better transition temperature between $Na_2CO_3 \cdot H_2O(s)$ and $Na_2CO_3(s)$.
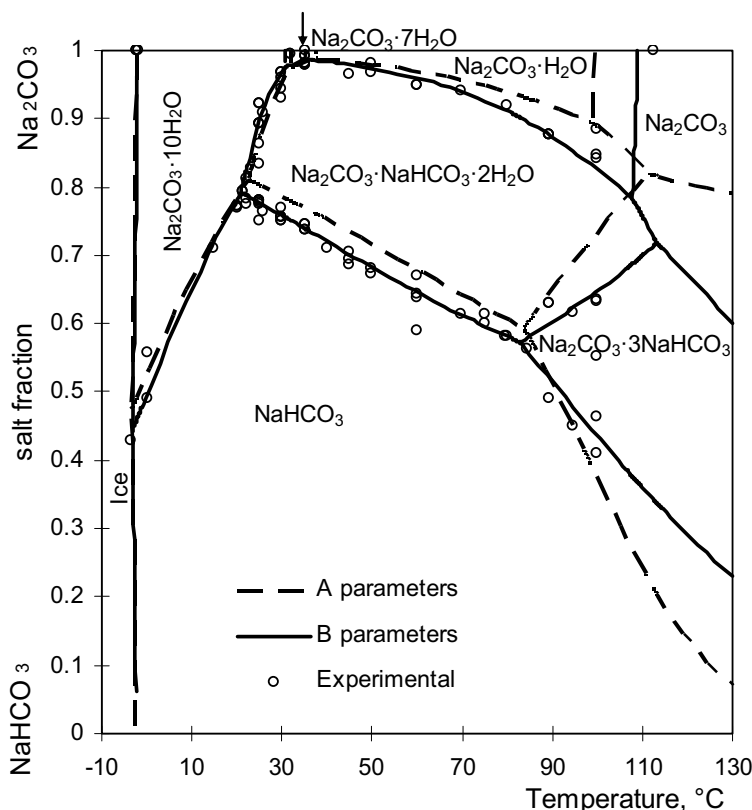
Figure 36: Temperature dependence of the two-salt lines in the aqueous $Na_2CO_3 - NaHCO_3$ system. Phase lines calculated with the *A* and the *B* parameters. Experimental data points are from the IVC-SEP database[10].

A comparison of the standard state properties used in set *A* and *B*, reveals that a change of less than 1 % in these properties gives a better result as shown in table 11. The significant difference, is the change in $\Delta_f H^o_{Na_2CO_3(s)}$. Parameter set *B* is not compatible with the previously determined parameters, such as those of Iliuta *et al.*[9] and Thomsen *et al.*[43].

The standard state properties of *MEG(s)* and *MEG·H₂O(s)* were determined in this study. The values are almost identical between set *A* and *B* and the differences are within the confidence intervals of the properties as shown by table 11.

The rational symmetrical standard state properties $\Delta_f G^o_{MEG(l)}$ and $\Delta_f H^o_{MEG(l)}$, were obtained from the NIST tables[12] as listed in table 11 and the extended UNIQUAC model were used in the conversion of *MEG(l)* to *MEG(aq)*. *MEG(aq)* is assumed to be the only liquid glycol compound in solution. The calculated molal unsymmetrical standard state properties $\Delta_f G^*_{MEG(aq)}$ and $\Delta_f H^*_{MEG(aq)}$, are listed in table 10. These values were calculated by the method given by Iliuta *et al.*[9]. The values are $\Delta_f G^*_{MEG(aq)}$=-335.1±0.3*kJ/mol* and $\Delta_f H^*_{MEG(aq)}$=-461.6±1.1*kJ/mol*, calculated using parameter set A. The heat capacity of *MEG(aq)*, $C^*_{p,MEG(aq)}$, is calculated by using the

DIPPR heat capacity correlation of *MEG(l)*, $C^o_{p,MEG(l)}$, and the extended UNIQUAC model. The conversion is performed by a linear interpolation of $C^*_{p,MEG(aq)}$ between 0 and 110 °C giving the correlation parameters for *MEG(aq)* shown in table 10 for equation (215). Heat capacity correlation parameters of other compounds are given in table 10 and 11. The UNIQUAC volume and surface area parameters for *MEG*, $r_{MEG(aq)}$ and $q_{MEG(aq)}$, were determined in this work by fitting to data. The values are shown in table 10. They are different from those obtained by the calculation method of Abrams and Prausnitz[56] and Bondi[57], $r_{MEG(l)}$=2.4088 and $q_{MEG(l)}$=2.248, as given by Skjold-Jørgensen *et al.*[58] and later by Chiavone-Filho *et al.*[59,60], Lancia *et al.*[61], and Horstmann *et al.*[62]. Our regressed values are considerably higher, but they are comparable to values determined by Iliuta *et al.*[9] who obtained *r*=3.3 and *q*=3.7 for methanol, and Thomsen *et al.*[43] who got *r*=*q*=5.9 for ethanol and *r*=10.3, *q*=9.5 for 1-butanol. Since the *MEG* molecule is larger than methanol it should have higher *r*, and *q* values than methanol and comparable or higher values than ethanol but less than 1-butanol, which it also has.

The extended UNIQUAC interaction parameters are summarized in table 12 and 13. The most noteworthy difference between set *A* and *B* is found in table 13. The temperature gradient of the *MEG-MEG*, *MEG-Na^+*, and *MEG-HCO_3^-* interaction energy parameters are similar in numerical size but have opposite sign. The temperature gradient of the Na^+-HCO_3^- interaction parameter is noticeable different in the two parameter sets. The improved temperature dependence of the bicarbonate solubility might be related to this difference.

Table 10: Molar mass, M, extended UNIQUAC parameters of set A and B, standard state formation properties and correlation parameter for the heat capacity equation (215) for liquid species.

Unit	Set	M g/mol	r_i	q_i	$\Delta_f G^{*\,f}$ kJ/mol	$\Delta_f H^{*\,f}$ kJ/mol	a_i J/(mol·K)	b_i J/(mol·K^2)	c_i J/mol
$H_2O(l)^a$	A and B	18.01528	0.9200	1.4000	-237.129	-285.83	58.36952	0.03896110	523.8794
$MEG(aq)^c$	A	62.06844	5.4996	7.0797	-334.9996[d]	-461.7981[d]	55.90368[d]	0.3134489[d]	0
	B	62.06844	4.0060	5.4610	-334.7257[d]	-461.3862[d]	72.35423[d]	0.2843604[d]	0
$CO_2(aq)^b$	A and B	44.00980	5.7410	6.0806	-385.98	-413.8	243.0000	0	0
$Na^+(aq)^a$	A and B	22.98977	1.4034	1.1990	-261.905	-240.12	600.6158	-1.100623	-23231.92
$H^+(aq)^a$	A and B	1.007940	0.13779	$1\cdot10^{-16}$	0	0	0	0	0
$OH^-(aq)^a$	A and B	17.00734	9.3973	8.8171	-157.2481[e]	-230.2433[e]	1418.157	-3.445769	-51473.13
$CO_3^{2-}(aq)^b$	A and B	60.00920	10.828	10.769	-527.81	-677.14	894.6877	-2.827237	-21149.44
$HCO_3^-(aq)^b$	A and B	61.01714	8.0756	8.6806	-586.77	-691.99	-0.6770971	0.2737451	-10089.51

[a] r_i, q_i, a_i, b_i, and c_i determined/defined by Thomsen et al.[7,13] [b] r_i, q_i, a_i, b_i, and c_i determined by Thomsen and Rasmussen[8]. [c] Parameters determine in this study. [d] Calculated using the extended UNIQUAC model from $MEG(l)$ properties. [e] Determined by Kaj Thomsen, previously unpublished. [f] Obtained from NIST[12] if not stated otherwise.

Table 11: Standard state properties of set *A* and *B*. Correlation parameter for the heat capacity equation (215). Values not marked are from NIST[12].

Set	M g/mol	$\Delta_f G^o$ (25 °C, 1 bar) kJ/mol		$\Delta_f H^o$ (25 °C, 1 bar) kJ/mol		$a_i, b_i=c_i=0$ J/(mol·K)	
		A	B	A	B	A	B
Na₂CO₃(s)	105.9887	-1044.44	-1045.387[b]	-1130.68	-1121.155[b]	112.3	
Na₂CO₃·10H₂O(s)	286.1415	-3427.66	-3428.800[b]	-4081.32	-4078.249[b]	550.32	
Na₂CO₃·H₂O(s)	124.004	-1285.31	-1287.599[b]	-1431.26	-1426.673[b]	145.6	
Na₂CO₃·7H₂O(s)	232.0957	-2714.2	-2715.602[b]	-3199.97	-3197.269[b]	300[c]	303.31[a]
Ice	18.01528	-236.538[f]		-292.624[f]		47.89955[f]	
NaHCO₃(s)	84.00691	-851	-851.352[b]	-950.81	-947.6426[b]	87.61	
Na₂CO₃;NaHCO₃;2H₂O(s)	226.0262	-2379.85[c]	-2382.157[b]	-2684.9	-2676.566[b]	349.7375[c]	245.51[a]
Na₂CO₃;3NaHCO₃(s)	358.0095	-3599,73[c]	-3606.270[b]	-3982.7	-3979.125[b]	781.5798	358.23[a]
H₂O(g)	18.01528	-228.572		-241.818		33.577	
CO₂(g)	44.0098	-394.359		-393.509		37.11	
MEG(s)	62.06844	-321.4179±0.8[b]	-321.4198±0.6[b]	-467.4966±3.1[b]	-467.4533±2.5[b]	93.98[a]	
MEG·H₂O(s)	98.099	-558.298±1.1[b]	-557.9913±0.8[b]	-764.9524±3.7[b]	-766.1036±2.7[b]	122.52[a]	
MEG(l)	62.06844	-323.08		-454.8			e

[a] Value calculated using Kopps modified rule[14]. [b] Estimated in this work. [c] Estimated in a previous study by Thomsen and Rasmussen[8]. [d] Properties of *MEG(l)* is used for estimating *MEG(aq)*. [e] DIPPR correlation: $C^o_{p,MEG}$ $(J/(mol K)) = 35.53 + 0.43678T - 1.8486 \cdot 10^{-4} T^2$ (T in Kelvin). [f] Estimated by Kaj Thomsen. Not previously published.

Table 12: $u_{ij}^o = u_{ji}^o$ in K, extended UNIQUAC parameters for parameter set A and B

set	H_2O		$MEG(aq)$		$CO_2(aq)$	$Na^+(aq)$		$H^+(aq)$	$OH^-(aq)$		$CO_3^{2-}(aq)$	$HCO_3^-(aq)$
	A	B	A	B	A and B	A	B	A and B	A	B	A and B	A and B
H_2O	0^a		-		-	-		-	-		-	-
$MEG(aq)$	249.7378^c	241.2451^c	339.9663^c	350.4045^c	-	-		-	-		-	-
$CO_2(aq)$	41.07171^b		174.5583^c	173.2765^c	40.51756^b	-		-	-		-	-
$Na^+(aq)$	733.2863^b		292.9922^c	496.3903^b	1788.825^b	0^a		-	-		-	-
$H^+(aq)$	$1·10^{4a}$		$1·10^{9a}$		$1·10^{9a}$	$1·10^{9a}$		0^a	-		-	-
$OH^-(aq)$	600.4952^b		2500^a		2500^a	1398.137^b		$1·10^{9a}$	1562.881^b		-	-
$CO_3^{2-}(aq)$	361.3877^b		671.8906^c	566.6611^c	2500^a	547.9543^b	454.124^c	$1·10^{9a}$	1588.025^b	1423.716^c	1458.344^b	-
$HCO_3^-(aq)$	577.0502^b		676.5772^c	616.8792^c	651.045^b	1101.92^b	979.940^c	$1·10^{9a}$	2500^a		800.0081^b	771.0377^b

[a] Defined as a reference or no data available to fit this parameter. [b] Determined by Thomsen and Rasmussen[8]. [c] Determined in this study.

Table 13: $u_{ij}^t = u_{ji}^t$ in K^2, extended UNIQUAC interaction energy parameters for parameter set A and B

set	H_2O		$MEG(aq)$		$CO_2(aq)$	$Na^+(aq)$		$H^+(aq)$	$OH^-(aq)$		$CO_3^{2-}(aq)$	$HCO_3^-(aq)$
	A	B	A	B	A and B	A	B	A and B	A	B	A and B	A and B
H_2O	0^a		-		-	-		-	-		-	-
$MEG(aq)$	0.71268^c	0.18095^c	0.56247^c	-0.21916^c	-	-		-	-		-	-
$CO_2(aq)$	7.5184^b		5.0355^c	4.4442^c	13.629^b	-		-	-		-	-
$Na^+(aq)$	0.48719^b		3.9323^c	-3.5685^c	-0.22080^b	0^a		-	-		-	-
$H^+(aq)$	0^a		0^a		0^a	0^a		0^a	-		-	-
$OH^-(aq)$	8.5455^b		0^a		0^a	20.278^b	2.7887	0^a	2.7496^d	5.6169^b	-	-
$CO_3^{2-}(aq)$	3.3516^b		2.1482^c	4.2392^c	0^a	3.7820^b	2.7887^c	0^a	2.7496^d	3.6426^c	-1.3448^b	-
$HCO_3^-(aq)$	-0.38795^b		-0.50597^c	0.65204^c	2.7730^b	1.8290^b	-0.040973^c	0^a	0^a		1.7241^b	-0.019813^b

[a] Defined as a reference or no data available to fit this parameter. [b] Determined by Thomsen and Rasmussen[8]. [c] Determined in this study. [d] Determined by Garcia et al.[55]

The result of the *MEG-H₂O* VLE data correlation is illustrated in figure 37. It shows the bubble point pressure as a function of liquid composition. The trend indicates that *MEG* behaves ideal since the pressure is linear with composition. This is only the case for the *MEG-H₂O* system and not for the ternary and quaternary salt solubility.
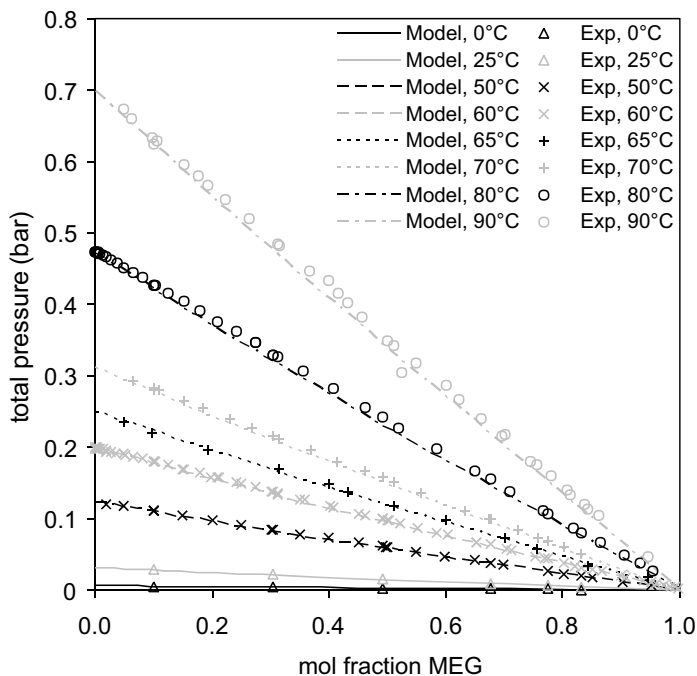
Figure 37: Total vapor pressure of the mixed solvent *MEG-H₂O* system, lines calculated using the model and parameter set *B*. References for the used experimental data points are listed in table 14.

Table 14 summarizes the experimental VLE data used for parameter estimation in this study. Column *T*, *P* gives the temperature and pressure interval of the data. *N* signifies the number of data used and the number of data points found in each paper. The temperature interval 0 °C to 90 °C is the focus of this study. In this temperature range the vapour pressure of *MEG* is insignificant compared to the vapour pressure of water and *CO₂*. Therefore we did not use vapour-liquid equilibrium data for pure *MEG*. Trimble and Potts[63] and Sokolov *et al.*[64] made measurements in a broad temperature interval but only data from the lower temperatures were included here. Villamanan[65] published a collection of data, but they were not used in this study since they had previously been published by Gonzalez *et al.*[66] and Villamanan *et al.*[67]. The data by Skripach and Temkin[68] were not used since they were too scattered as noted by Kumar *et al.*[69]. The data from a few authors were not included because they only measured a few data at high temperatures[70,71,72,73,74,75,69,61]. Liu *et al.*[76] did not report the equilibrium pressure and their data are not suited for thermodynamic modelling. The thorough study of Gallant[52] shows useful graphs but no tabulated experimental values. The study was therefore only used for comparison.

The VLE performance of parameter set *A* and *B* is shown in table 14. The average relative deviation in the total pressure of set *B* is slightly better than *A*. Figure 38.1 and 39.1 shows the predictions by the model and the two set perform very similar.

Table 14: Used experimental *MEG-H₂O* and *CO₂-MEG-H₂O* VLE data.

Author	P interval bar	T interval °C	# data used (actual # data)	P Deviation % (ARD) Parameter set	
				A	B
MEG-H₂O data					
Villamanan et al.[67]	0.01 - 0.19	60	21(24)	4.4	3.7
Gonzalez et al.[66]	0.006 - 0.12	50	20(21)	4.3	3.6
Horstmann et al.[62]	0.003 - 0.47	60, 80	60(84)	8.1	7.4
Chiavone-Filho et al.[59]	0.06 - 0.66	70, 90	38(40)	4.0	3.5
Trimble and Potts[63]	0.30, 0.57	72 - 89	15(79)	1.7	1.8
Nath and Bender[77]	0.02 - 0.67	65, 77, 90	36(42)	5.2	4.9
Sokolov et al.[64]	0.01, 0.03, 0.06, 0.13	18 - 87	41(51)	10.0	10.0
Mokbel et al.[11]	0.0002 - .62	-15 - 90	97(106)	5.6	4.9
Villamanan[65]	0.0001 - 0.2	50,60	0(48)	-	
Skripach and Temkin[68]	0.1	47 - 136	0(11)	-	
Efremova et al.[70]	1.01325	103 - 170	0(9)	-	
Frolova et al.[71]	1.01325	102 - 183	0(11)	-	
Ramanujam and Laddha[72]	1.01325	107, 118, 136	0(3)	-	
Ogorodnikov et al.[73]	1.01325	103 - 197	0(10)	-	
Liu[74]	1.0138	103 - 195	0(10)	-	
Kireev and Popov[75]	1.01325	100 - 189	0(18)	-	
Kumar et al.[69]	0.97	99 - 197	0(7)	-	
Lancia at al.[61]	0.4 - 1.5	98, 110, 122	0(42)	-	
Liu et al.[76]	Not given	103 - 195	0(10)	-	
Gallant[52]	1 - 35	0 - 240	0(0)	-	
CO₂-MEG-H₂O data					
Hayduk et al.[45]	1.01325	25	10(13)	23.5	15.0
Davis et al.[78]	5	0, 25, 60	7(18)	31.3	29.5
Won et al.[79]	1.01325	25	3(3)	25.1	12.3
Kobe and Mason[80]	1.01325	25	0(3)	-	
Sandengen[4 a]	1	4, 22	0(3)	-	

[a] The data of Sandengen were measured in the system *CO₂-NaHCO₃-MEG-H₂O*. pH was the only dependent variable measured.
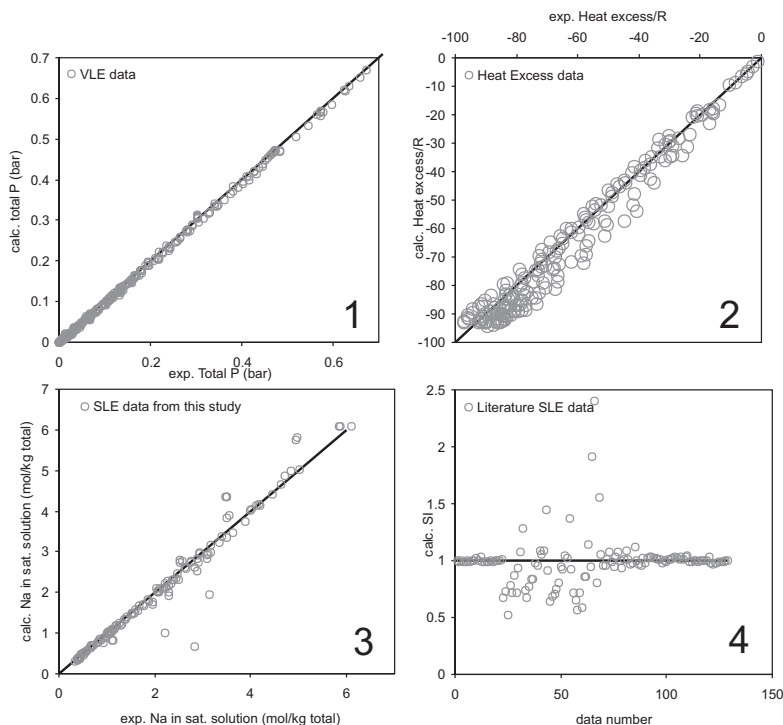
Figure 38: Comparison of experimental and calculated properties using parameter set *A*. 1: Comparison of VLE data. 2: Comparison of excess enthalpy. 3: Our SLE data compared to predictions by the model. 4: Model prediction of literature data.

The extended UNIQUAC model is also capable of calculating the excess enthalpy within reasonable accuracy. The excess enthalpy in the binary *MEG-H_2O* system is related to the surface area parameter q_{MEG} and the *MEG-H_2O* and *MEG-MEG* interaction parameters. The volume parameter r_{MEG} does not influence the excess enthalpy calculation. It is therefore crucial that q_{MEG} is used as a fitting parameter to model the excess enthalpy.
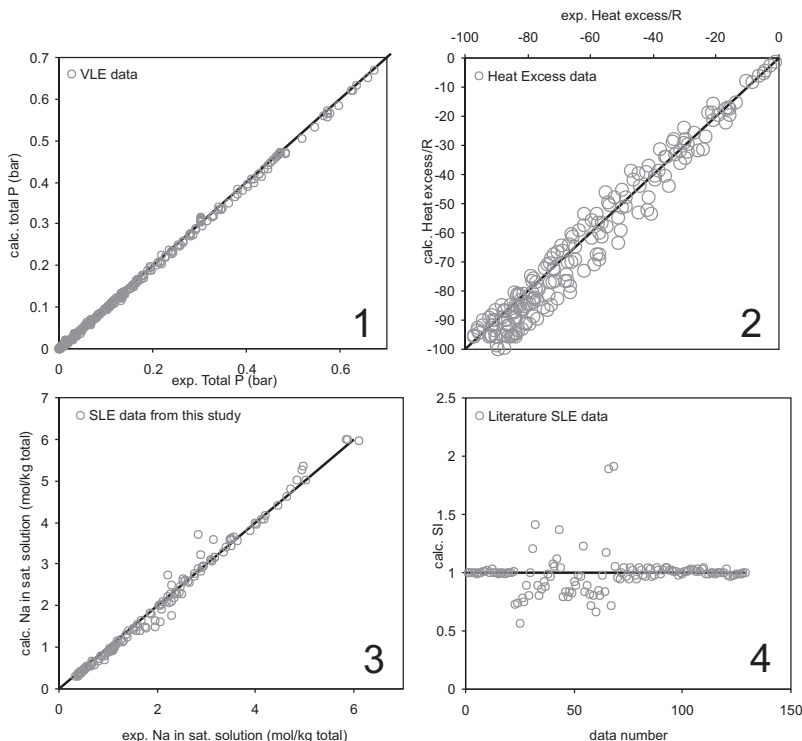
Figure 39: Comparison of experimental and calculated properties using parameter set *B* 1: Comparison of VLE data. 2: Comparison of excess enthalpy. 3: Our SLE data compared to predictions by the model. 4: Model prediction of literature data.

Table 15 outlines the used literature sources for excess enthalpy data. Kracht *et al.*[81] are clearly the most valuable contributors. The data from Könnecke *et al.*[82] were excluded as these data are even more scattered than those in figure 40. Wang *et al.* [83] made an experimental study but did not publish the experimental values. Figure 40 shows the calculated and experimental excess enthalpy as a function of solvent composition. The data at 25 °C are very scattered and the model represents the data within the experimental error. The model also reproduces the temperature dependence of the excess enthalpy, which increase with increasing temperature in accordance with the experimental data.
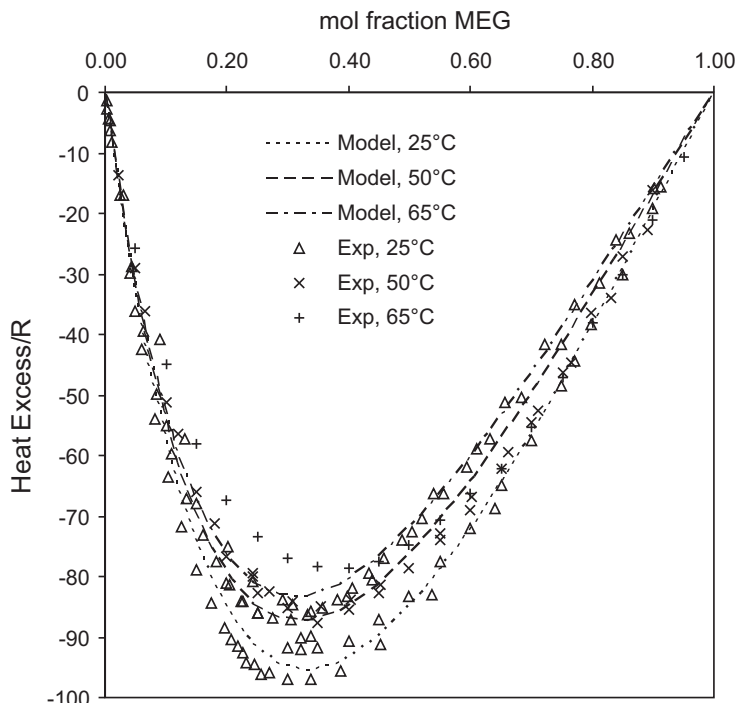
Figure 40: Excess enthalpy for the mixed solvent *MEG-H_2O* system, lines calculated using the model and parameter set *B*. The shown experimental data points are obtained from references in table 15.

Table 15: Used experimental *MEG-H_2O* data on heat excess and heat of solution.

Author	MEG interval wt%			T interval °C	# data used (actual # data)	Deviation % (ARD)	
						Parameter set	
Heat excess (H^{Ex})						A	B
Villamanan et al.[67]	7.0	-	96.6	50	18(20)	7.6	7.2
Kracht et al.[81]	15.3	-	98.5	12.5, 25, 35, 50, 65	90(93)	5.8	7.1
Matsumoto at al.[84]	2.3	-	97.3	25	31(33)	9.7	10.6
Dohnal et al.[85]	0.6	-	3.5	25	5(5)	3.0	2.7
Gallego[86]	9.9	-	96.9	25	18(18)	18.5	19.7
Biros et al.[87]	12.6	-	92.0	25	22(22)	5.0	4.0
Rehm and Bittrich[88]	62.0	-	63.6	25	3(3)	2.4	5.3
Könnecke et al.[82]	18.0	-	95.1	25, 35, 45	0(21)	-	
Wang et al.[83]		-		-	0(0)	-	
Heat of solution							
Manin et al.[89]	0.3	-	0.6	25	2(2)	1.9	6.5
Batov et al.[90]	0.2			25	3(3)	3.5	2.6
Nakayama[91]	Not given			25, 40	0(2)	-	
Nichols et al.[92]	Not given			20, 25, 30	0(3)	-	

Table 15 shows the capability of the model to reproduce the experimental data. The performance is good and parameter set *B* reproduces the data better than *A*. The difference between the two parameter sets is not obvious when comparing figure 38.2 and 39.2, but the temperature dependence of set *B* is significantly better than *A*. The data by Gallego[86] gives a very high deviation and the work may be erroneous, but the data were still included in the fitting process.
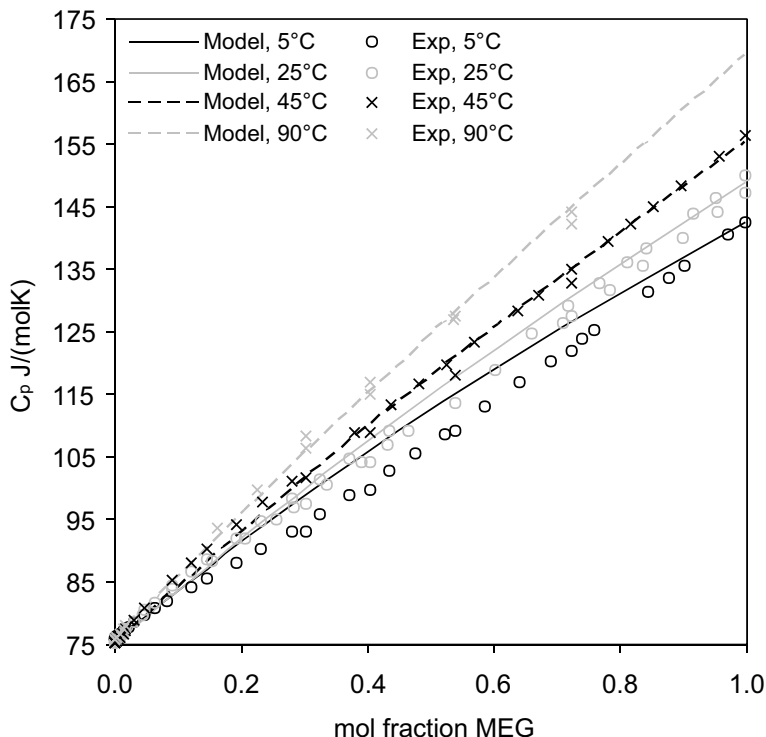
Figure 41: Model predictions (lines) and experimental heat capacity data points for the mixed solvent *MEG-H$_2$O* system. Data were obtained from various authors[93,94,46,53,51]. Table 11 shows the parameters of the used heat capacity correlation (215). Mixture properties calculated using parameter set *B*.

A few data of heat of solution were included in the objective function. Nakayama[91] and Nichols *et al.*[92] published studies on the subject but did not report the composition. Their work can therefore not be used for determining model parameters. Table 15 shows how well the heat of solution is predicted. Set *A* performs better but this may be due to the few number of data and the relative low weight they obtained in the objective function.

The parameters of the extended UNIQUAC model are consistent. This is proved by the result in figure 41 which shows the predicted *MEG-H$_2$O* heat capacity. It was not used in the parameter fitting process but the model resembles the measured values[93,94,46,53,51] closely. The ARD is 1.0 %, which is acceptable. The model over-predicts slightly at 5 °C, but it is still satisfactory. The apparent molal heat capacity below 30 *mol% MEG* is not shown here, but it is predicted less accurately, and deviation up to 20 % can be expected at infinite dilution. This is acceptable since

experimental determination of apparent molal heat capacity is very challenging and requires high precision equipment. The deviation may be related to the experimental data and not to the model.

The freezing point depression of *MEG* in water is shown in figure 42. The result is very satisfactory. Only the ice precipitation up to 55 *wt% MEG* data was used for determining model parameters of *MEG(aq)*. The data for the precipitation of solid *MEG* hydrate and pure *MEG* were used to determine the standard state properties of *MEG·H₂O(s)* and *MEG(s)*. The experimental data used for parameter estimation are listed in table 16. The few data points not used, are the freezing point of pure water and solutions in meta-stable equilibrium with *MEG·H₂O(s)*. Zinchenko and Zinchenko[95] did a very thorough investigation of the SLE behaviour, but unfortunately they did not tabulate their data, and their work was not included in this study. Table 16 reveals that parameter set *A* and *B* performs equally well for solid – liquid equilibrium calculation in this system and a very low deviation in the saturation index (*SI*) is observed. The calculated deviation of *SI* may be examined by looking data point 23-88 in figure 38.4 and 39.4. There is an amount of scatter, but the correlation is generally good. The freezing point data are less scattered as shown by data point 1-22. The remaining freezing point data above 55 *% MEG* are represented by data point 89-129. These two last series show low scatter.
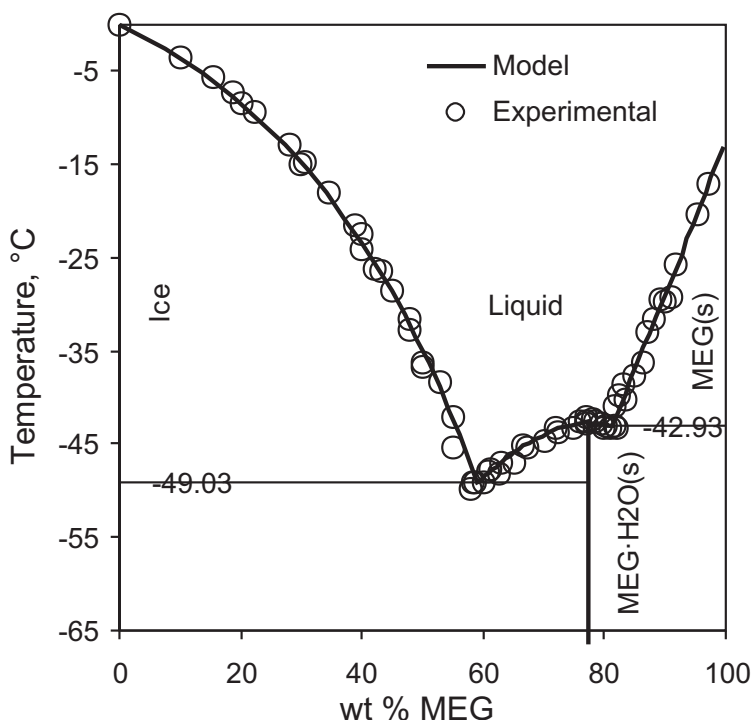
Figure 42: SLE curve for the mixed solvent *MEG-H₂O* system. Circles represent experimental values obtained from references in table 16 and line calculated using the model and parameter set *B*.

Only scarce amount of equilibrium data are available for the ternary *CO₂-MEG-H₂O* system as shown by table 14. Hayduk *et al.*[45], Won *et al.*[79], and Kobe and Mason[80] all tabulated the solubility in *mol/L*. The individual density measurements were used in

order to eliminate the volume dependence if possible. Kobe and Mason[80] did not report density and their data were not used since our density correlation was not available at the time of fitting the data. One data point of Hayduk *et al.*[45] seemed to be an outlier and two other data points at high glycol concentration were not used. Most of the scattered data at low temperature by Davis *et al.*[78] were not used. Sandengen's data[4] were not included as they were not available to us during the parameter estimation. Binary CO_2-*MEG* data[96,97] were not included in the fitting process. Result of the fitting is also shown in table 14. Parameter set B performs somewhat better than set *A*. But still a relatively high deviation is observed for this kind of data. Figure 43 shows that the curvature corresponding to the experimental data is not reproduced by the model. The overall temperature and pressure dependence is reproduced satisfactory. The deviation may be related to the standard data of the carbonate species or the volume and surface parameter of the CO_2 compound. It was not attempted to improve the CO_2 parameters.
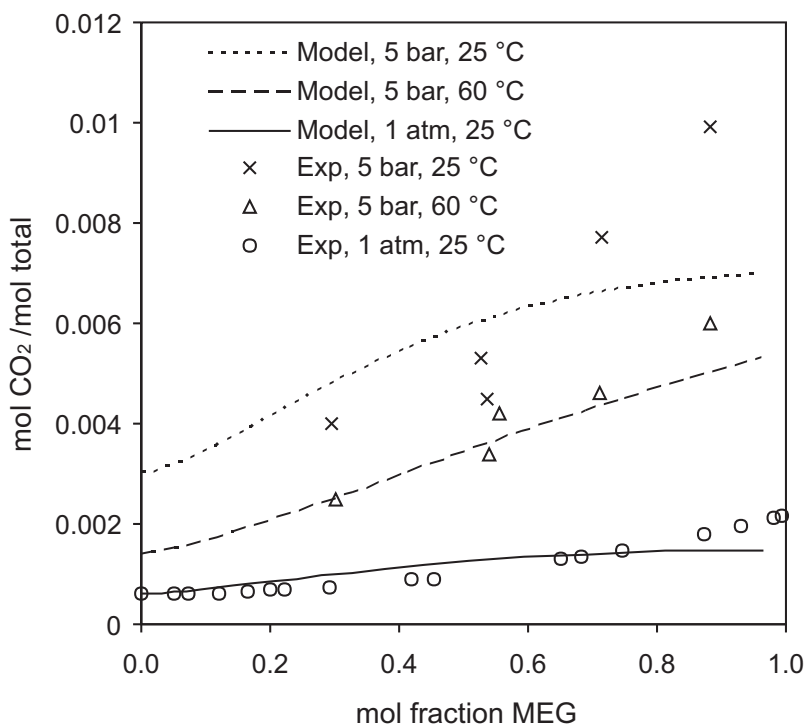
Figure 43: CO_2 solubility in the mixed solvent *MEG-H₂O* system. The points represent experimental data from references in table 14 and lines were calculated using the model and parameter set *B*.

Data for salt solubility in *MEG* are needed in order to fit the *MEG*- HCO_3^- and *MEG*- CO_3^{2-} interaction parameters. As the solubility is relatively low in these systems, data for salt solubility in the ternary *salt-MEG-H₂O* system are used instead. Quaternary *salt₁-salt₂-MEG-H₂O* solubility data were also included. As the model only contains binary interaction parameters, only ternary data are strictly needed. Quaternary data are needed if a solid precipitate which consist of *salt₁-salt₂-MEG-H₂O*. It is not the case for the systems in this work.

Oosterhof et al.[5], Gärtner et al.[6], Dugstad[98], Sandengen[4], and Atakhodzhaev and Dzhuraev[99] have all published SLE data related to the *Na₂CO₃-NaHCO₃-MEG-H₂O* system, see table 17. Atakhodzhaev and Dzhuraev [99] only show their experimental *NaHCO₃-MEG-H₂O* results in graphs and their results were therefore not used in this study. Dugstad[98] lists a volume dependent solubility. Density is not given, and our density model was not available at the time of fitting. The data were therefore not usable for modelling. Sandengen[4] reports a few data which were not used since they were unavailable at the time of fitting. Oosterhof et al.[5] did a very useful study on *Na₂CO₃* solubility in *MEG-H₂O*. They made a very consistent analysis of the liquid phase but did not analyse the solid phase. The missing information is of key importance when reporting solubility data. This is especially true in the carbonate system where several different hydrates may precipitate. Their study was fortunately carried out at relatively high temperature where *Na₂CO₃* and *Na₂CO₃·H₂O* are the only possible solid phases. Gärtner et al.[6] did a comprehensive study on the *Na₂CO₃-NaHCO₃* solubility in the mixed solvent. They briefly analysed the solubility of *NaHCO₃* in the mixed solvent, but the main part of their data are quaternary solubility data. The measurements were done in solutions with a high glycol content, >50 *wt% MEG* (22 *mol%*).

The ternary data of Gärtner et al.[6] are comparable to our results and were used in this study. None of their quaternary data were included, since Gärtner et al.[6] determined solubility by a method that may be based on an inaccurate interpretation of the titration experiments. The inaccuracy is in our experience in the order of 0.5 to 2.0 *wt%*. Besides, they list only the salt-free glycol concentration in the initial solutions and assumed that the solvent composition did not change due to precipitation of salt hydrates or evaporation of water at the high temperatures.
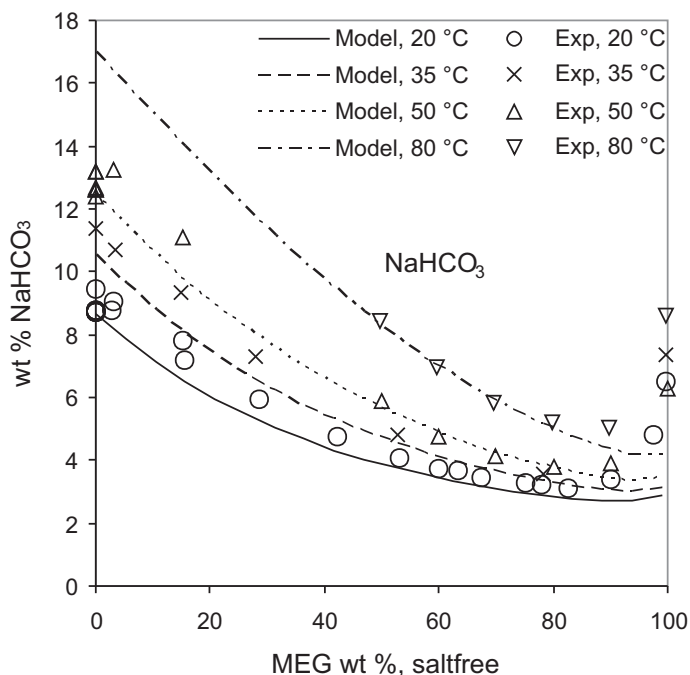
Figure 44: Solubility of *NaHCO₃* in the mixed solvent *MEG-H₂O* system. The points represent experimental data from references in table 17 and model lines calculated using parameter set *B*.

The result of modelling the ternary SLE system *NaHCO₃-MEG-H₂O* is shown in figure 44. The experimental data points are mainly from this study, but some are from Gärtner *et al.*[6]. The data for solubility of *NaHCO₃* in pure water were obtained from the IVC-SEP electrolyte data bank and were only used in set *B* for fitting the standard state properties. *NaHCO₃* is the only solid phase that precipitates in this system above the freezing point. An unusual increase in the solubility of *NaHCO₃* is observed in solutions with more than 85 *wt%* MEG. The phenomenon is unexpected and was validated several times in this study. It was also confirmed by powder X-ray diffraction, that the solid phase is pure *NaHCO₃* and not a complex or solid solution formed by *MEG* and *NaHCO₃*. Gärtner *et al.*[6] suggested that the solubility increase may be explained by the presence of a liquid complex. It may rather be explained by the increase in *CO₂* solubility at high *MEG* concentrations, shown in figure 43, and the dissociation of bicarbonate to *CO₂*. Comparing figure 43 and 44 shows that the model predicts a too low *CO₂* solubility at high *MEG* concentrations and equivalently a too low solubility of *NaHCO₃*.
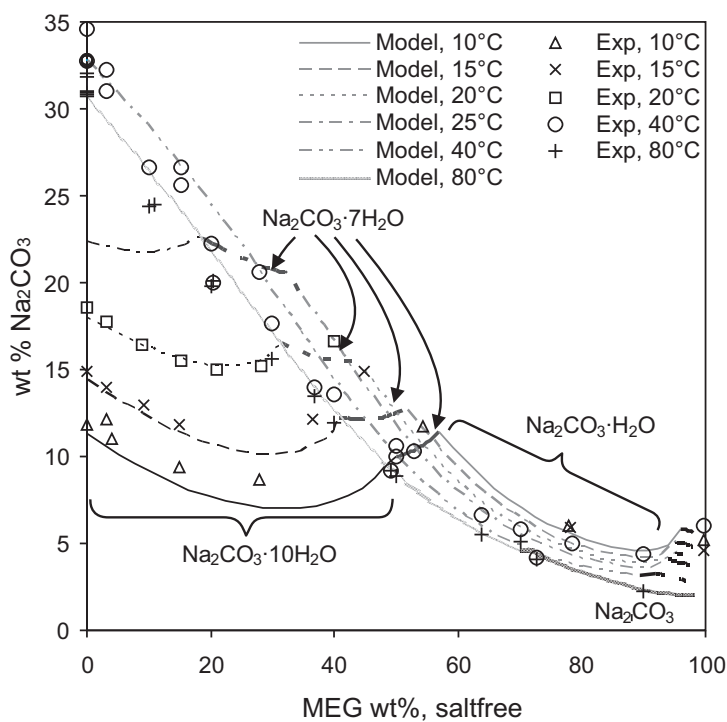
Figure 45: Solubility of *Na₂CO₃* in the mixed solvent *MEG-H₂O* system. The points represent experimental data from references in table 17 and model lines calculated using parameter set *B*. Thin black: *Na₂CO₃·10H₂O*. Thick grey: *Na₂CO₃·7H₂O*. Thin grey: *Na₂CO₃·H₂O*. Thick black: *Na₂CO₃*.

The solubility of *Na₂CO₃* in the mixed solvent system is shown in figure 45. Most of the shown experimental values were produced in this work. Some of the data at 40 °C and 80 °C are from Oosterhof *et al.*[5]. *Na₂CO₃·H₂O* and *Na₂CO₃* precipitate at these temperatures and the solubility decrease linearly with *MEG wt%*. Figure 45 shows that the model predicts a high solubility compared to their experimental values at

these temperatures. Apparently Oosterhof *et al.*[5] did not correct for solvent composition change even though water precipitated in $Na_2CO_3 \cdot H_2O$. Therefore *MEG* concentration is higher at equilibrium then at initial conditions. Their solubility data of $Na_2CO_3 \cdot H_2O$ is lower compared to our values since their *MEG* concentration in reality was higher than expected. Figure 45 shows the solubility profile plotted as a function of the initial *MEG wt%* on a salt-free basis. $Na_2CO_3 \cdot 10H_2O$ precipitates at low temperature and low *MEG* concentration followed by a small $Na_2CO_3 \cdot 7H_2O$ branch, a $Na_2CO_3 \cdot H_2O$ branch and finally a Na_2CO_3 branch. The model predicts the $Na_2CO_3 \cdot 7H_2O$ precipitation and it was only supported by one experimental data point.
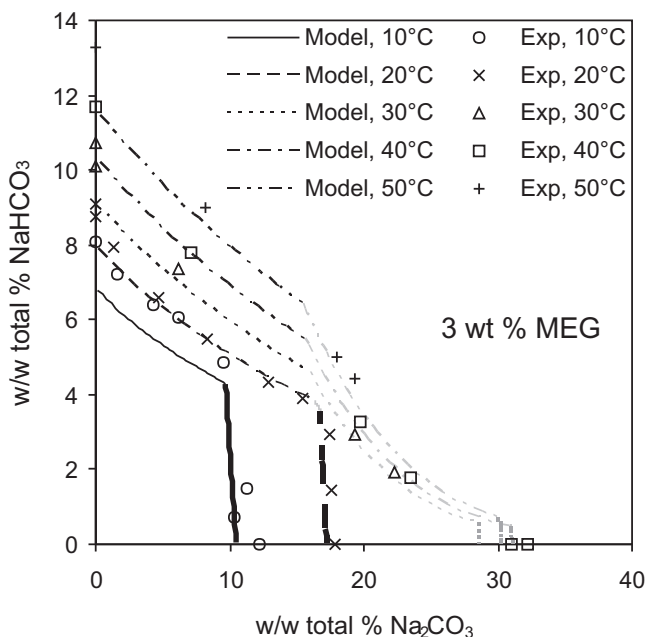
Figure 46: Experimental and calculated solubility of Na_2CO_3 and $NaHCO_3$ in the mixed solvent system *MEG-H₂O* with 3 *wt% MEG*. Experimental data points were obtained in this study. Lines were calculated using the model and parameter set *B*. Thin black lines: $NaHCO_3$. Thick black: $Na_2CO_3 \cdot 10H_2O$. Thin grey: trona. Thick grey: $Na_2CO_3 \cdot H_2O$.

Table 16: Used experimental freezing point depression data of *MEG-H₂O*.

Author	MEG interval wt%		T interval °C		# data used (actual # data)	SI Deviation % [c]	
Parameter set						A	B
Cordray *et al.*[100]	10.0	- 90.9	-49.9	- -3.6	33(34)	0.06[a], 1.6[b]	0.4[a], 1.6[b]
Ott *et al.*[101]	15.6	- 97.2	-49.0	- -5.7	25(27)	-0.7[a], -0.6[b]	-0.3[a], -0.6[b]
Baudot and Odagescu[102]	40.0	- 50.0	-36.2	- -22.4	5(5)	-0.2	0.2
Zinchenko and Zinchenko[95]	5	- 100	-50	- 0	0(0)	-	

[a] <55 *wt% MEG*. [b] >55 *wt% MEG*. [c] % deviation in the saturation index, SI, calculated as dev. % = $100 \cdot \sum (SI - 1) / n_{exp}$

Not all the data of Oosterhof *et al.*'s[5] were used in this study, since it is unclear what the solid phases were. Most of the solid phases were determined by Gärtner *et al.*[6] but still some phases are ambiguous at higher *MEG* concentration.

Parameter set *A* and *B* does not perform equally well for calculating *Na₂CO₃* solubility. Figure 45 shows the predictions using parameter set *B*. Set *A*, not shown here, does not perform as well at *MEG* concentrations >80 *wt%*. This is mainly related to the improved thermodynamic properties of *Na₂CO₃·H₂O* in set *B*.
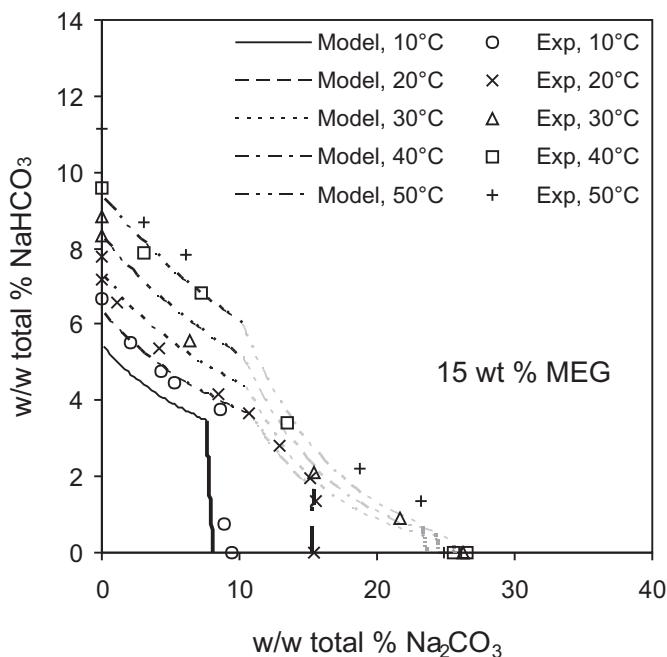
Figure 47: Experimental and calculated solubility of *Na₂CO₃* and *NaHCO₃* in the mixed solvent system *MEG-H₂O* with 15 *wt% MEG*. Experimental data points were obtained in this study. Lines were calculated using the model and parameter set *B*. Thin black lines: *NaHCO₃*. Thick black: *Na₂CO₃·10H₂O*. Thin grey: trona. Thick grey: *Na₂CO₃·H₂O*.

Table 17: Used experimental salt solubility data in *Na₂CO₃-NaHCO₃-MEG-H₂O*

Author	*T* interval °C	# data used (actual # data)	Deviation %	
			A	*B*
This study	2 - 50	133(212)	-0.04[a]	-0.04[a]
Oosterhof *et al.*[5]	40 - 90	46(58)	-6.1[b]	-4.7[b]
Gärtner *et al.*[6]	50 - 90	20(159)	0.6[b]	-0.05[b]
Dugstad[98]	20, 124	0(3)	-	
Sandengen[4]	4	0(2)	-	
Atakhodzhaev and Dzhuraev[99]	18	0(0)	-	

[a] deviation in ARD of calculated using *mol Na/kg total*. [b] % deviation in the saturation index calculated as $dev\ \% = 100 \cdot \sum (SI - 1)/n_{exp}$.

The predicted solubility in the quaternary Na_2CO_3-$NaHCO_3$-MEG-H_2O system is depicted in figure 46, 47, and 48. Figure 46 gives the solubility in a solvent consisting of 3 *wt%* (1 *mol%*) *MEG* on a salt-free basis. Figure 47 shows solubility in a solvent consisting of 15 *wt%* (5 *mol%*) *MEG*, salt-free basis. Figure 48 shows the change in the composition by addition of *MEG* for solutions saturated with two salts. Adding MEG makes it a quaternary system and the ternary invariant points shown in figure 36 become univariant and therefore dependent on MEG concentration. Invariant points in the quaternary system exist where four solid phases are in equilibrium, none are shown for the specific MEG concentration in figure 48.
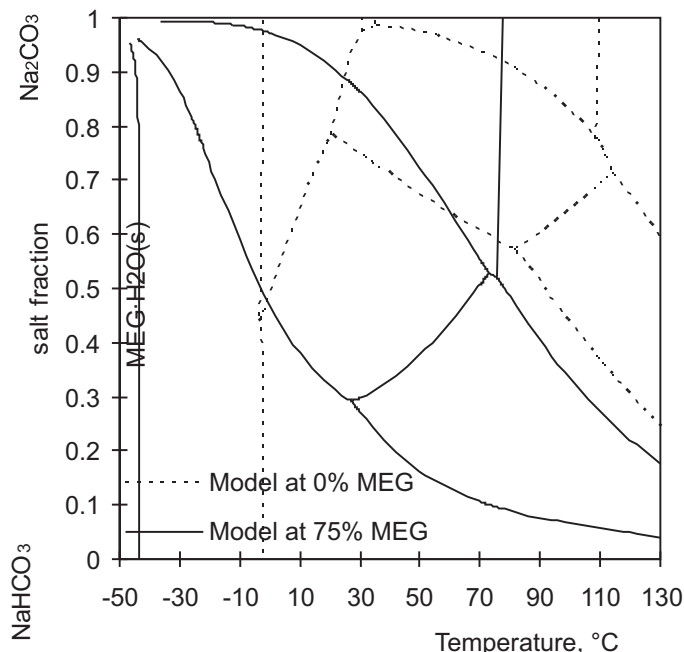
Figure 48: The influence of temperature and *MEG* concentration on the precipitation fields in the *Na₂CO₃-NaHCO₃-MEG-H₂O* system. Description of areas given in figure 36. The ternary invariant points move to lower temperatures by addition of *MEG*.

The deviation observed between experimental and calculated values in figure 46 and 47 is due to two reasons. The *MEG* concentration and temperature used in model calculations are constant. But the experiments were performed at slightly different temperatures, and the *water – MEG* ratio was not constant due to precipitation of hydrated salts. Table 7 shows the exact experimental temperatures and *MEG*-concentrations plotted in figure 46 and 47. Comparing the 20 °C isotherm in figures 46 and 47, shows how trona *(Na₂CO₃·NaHCO₃·2H₂O)* breaks through by the addition of *MEG*. This is similar to the breakthrough of wegscheiderite at 50 *wt%* and 50 °C to 90 °C measured by Gärtner et al.[6]. Additionally it can bee seen how the trona area widens by increased temperature. The residuals of the SLE data are summarised in figure 38.3, 38.4, 39.3, and 39.4. The data by Oosterhof et al.[5] and Gärtner et al.[6] are data number 23 to 88 and a lower scatter is seen when using parameter set *B*. The model predicts the *Na₂CO₃-NaHCO₃-MEG-H₂O* solubility satisfactory. The results of

set *A* and *B* are similar at 3 *wt% MEG* but the result at 15 *wt% MEG* is slightly better described by parameter set *B*. Table 17 compares the correlation of SLE data using parameter set *A* and *B*. The performance of set *B* is better. Table 17 shows that not all our experiments were used for modelling. Data in pure water were not used and a collection of data was produced after the modelling to verify part of the system.
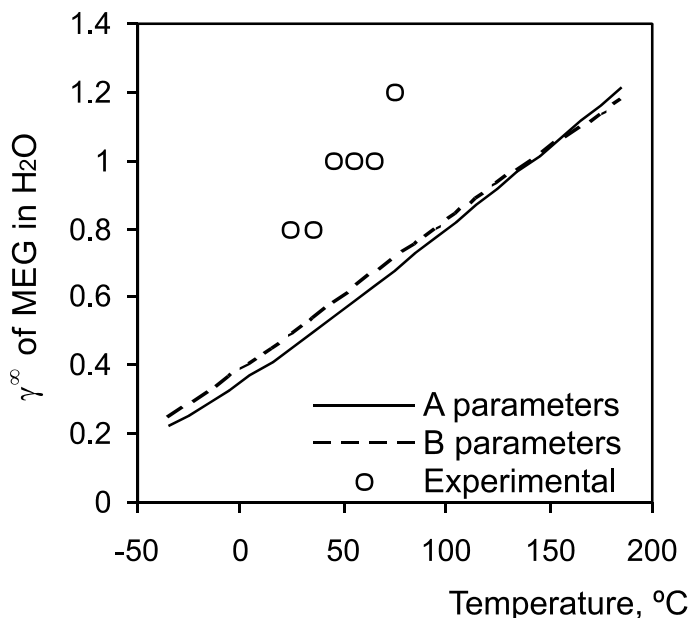
Figure 49: The calculated infinite dilution activity coefficient of *MEG* in water compared to literature values of Suleiman and Eckert[103].

Figure 48 shows a plot similar to figure 36, but for the mixed solvent system. The two-salt invariant lines move towards lower temperatures by adding 75 *wt% MEG*. It shows how glycol changes the water activity and displaces the precipitation fields of this system The trona area has moved to the temperature range from -40 °C to 70 °C instead of 20 °C to 115 °C. The wegscheiderite area has similarly moved to lower temperatures and wegscheiderite may precipitate at 0 °C. The trend has changed above 80 °C. Instead of a broad area of *NaHCO$_3$*, a broad area of *Na$_2$CO$_3$* is observed. All the binary and ternary invariant points have moved 30 to 50 °C down and the solid phases *Na$_2$CO$_3$·7H$_2$O* and *Na$_2$CO$_3$·10H$_2$O* are no longer present. The same phenomenon was observed in figure 44 and 45. At low temperature *MEG·H$_2$O* is precipitating at approximately -44 °C instead of ice at approximately –3 °C. These temperatures are lower than the freezing point of the *MEG-H$_2$O* system, shown in figure 42, since the solutions are saturated with *Na$_2$CO$_3$* and *NaHCO$_3$*. Comparing the results of figure 46 and 47 to 48 shows that *MEG* has the tendency to widen the trona, wegscheiderite, *Na$_2$CO$_3$·H$_2$O*, and the *Na$_2$CO$_3$* fields, but to narrow the *NaHCO$_3$* field at isothermal conditions. For example trona may precipitate at salt fractions 0.7 to 0.97 at 40 °C in pure water whereas it has widened to 0.5 to 0.97 at 0 °C in 75 *wt% MEG*. Table 34 and 35 in appendix D.1 show the correlation matrix and the confidence interval of the parameters fitted in parameter set *A*. Table 36 and 37 give

the same, for parameter set *B*. The tables show indications of correlation between $u^o_{MEG,MEG} \sim u^o_{MEG,H_2O}$ and $u^t_{MEG,MEG} \sim u^t_{MEG,H_2O}$. These parameters are related to the VLE data shown in figure 37 and freezing point depression data shown in figure 42. The correlation indicates that the system may be slightly over parameterized. Table 35 and 37 shows on the other hand that $u^o_{MEG,MEG}$ and u^o_{MEG,H_2O} have a low confidence interval. $u^t_{MEG,MEG}$ and u^t_{MEG,H_2O} could probably be fixed but were nonetheless fitted. There is also a correlation between $u^o_{MEG,CO_3^{2-}} \sim u^o_{MEG,HCO_3^-}$ which is expected due to the speciation equilibria given by (201).

The $u^o_{MEG,MEG}$ and u^o_{MEG,CO_2} parameters are related to the *CO₂-MEG-H₂O* equilibria shown in figure 43. The two parameters show a minor correlation, possibly due to the low amount of available data. The low confidence interval of u^o_{MEG,CO_2} shown in table 35 and 37 indicates that u^o_{MEG,CO_2} is necessary in the fitting process.

The infinite dilution activity coefficient of *MEG* in the binary *MEG-H₂O* system is shown in figure 49. The calculation is shown for both parameter set *A* and *B*. The sets predict almost the same values. It is a coincidence that the two follow the same trend. The calculations are carried out using the extended UNIQUAC model applying the surface and volume parameters *r* and *q*, of *MEG (M)* and *water* (W):

$$\ln \gamma_M^\infty = \ln \frac{r_M}{r_w} - \frac{r_M}{r_w} + 1 - 5q_M \left(\ln \frac{r_M q_w}{r_w q_M} - \frac{r_M q_w}{r_w q_M} + 1 \right)$$
$$+ q_M \left(1 + \frac{u_{wM} - u_{MM}}{T} - \exp \frac{u_{ww} - u_{Mw}}{T} \right) \tag{248}$$

r and *q* are obtained from table 10. The interaction parameters of the *MEG-H₂O*, are calculated by the linear temperature relation:

$$u_{ij} = u^o_{ij} + u^t_{ij} \left(T - 298.15 \right) \tag{249}$$

where u^o_{ij} and u^t_{ij} are given in table 12 and 13. Figure 49 shows the comparison of the model to the work by Suleiman and Eckert[103]. Studying their work shows that the experimental value of the infinite dilution coefficient were determined at a very low precision. Therefore the calculated values are significantly different compared to the experimental values.

Comparison of predicted and experimental solubility data of Gärtner *et al.*[6] are shown in Figure 50 for 50 *wt% MEG* from 50 to 90 °C. The solid lines represent the calculated solubility using parameter set *B*. The coloured areas indicate the solubility of a single salt. The interfaces between two areas correspond to the 2-salt solubility points. The experimental data are offset compared to the predicted values. For example the ternary solubility of *NaHCO₃* and *Na₂CO₃·H₂O* is experimentally higher than the calculated values as shown by *A* which is also observed for the quaternary solubility of trona as shown by *B*. The 2-salt interface between *NaHCO₃* and *Na₂CO₃·3NaHCO₃* is offset as shown by *C* and similarly the *Na₂CO₃·NaHCO₃·2H₂O-Na₂CO₃·H₂O* interface, indicated by *D*.
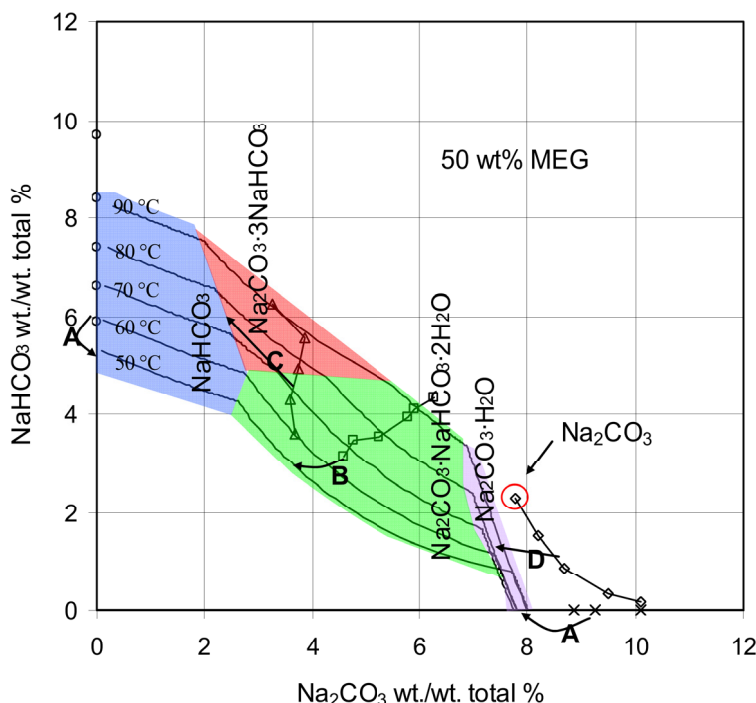
Figure 50: Comparison of predicted and experimental solubility of Gärtner *et al.*[6] between 50 and 90 °C in 50 wt% *MEG*. Deviation indicated by ABCD. ○: Exp. *NaHCO₃* solubility. ×: Exp. *Na₂CO₃·H₂O* solubility. △: Exp. 2-salt solubility of *NaHCO₃*-wegscheiderite. □: Exp. single salt trona solubility. ◇: Exp. 2-salt solubility of trona-*Na₂CO₃·H₂O*. Red circle: Exp. Trona-*Na₂CO₃* solubility.

The red circle signify *Na₂CO₃* was experimentally determined to be the solid phase and the model predicted *Na₂CO₃·H₂O*. The red area indicates that wegscheiderite may exists down to 60 °C. The experiments show how wegscheiderite exist at least at 50°C. The deviations are related to the experimental method used by Gärtner *et al.*[6]. Their titration method tends to give solubilities which are up to 2 *wt%* off compared to the actual solubility as mentioned before. The discrepancy in the predicted solid phases may be explained by the deviation in the experimental solvent composition due to evaporation or precipitation of water.

7.7   Conclusion

An experimental study was conducted for the *NaHCO₃-Na₂CO₃-MEG-H₂O* system in order to improve the experimental description of this system. The experimental work showed that trona and the hydrates of *Na₂CO₃* easily form meta-stable phases.
Ternary mixtures of *Na₂CO₃-MEG-H₂O* and *NaHCO₃-MEG-H₂O* both show unusual solubility profiles. The solubilities of the salts seem to go through local minima and increase toward higher *MEG* concentrations.
A literature study has shown that titration alone may not be used for carbonate and bicarbonate determination. It may only be used for determination of alkalinity and a second method may support the titration. For this purpose the reverse Schreinemakers method was derived in order to determine the composition of the saturated liquid from little experimental information. The method has not yet been extended to solutions saturated with more than one salt.
Based in part on the new experimental data, parameters in an activity coefficient model were determined with the purpose to improve *CO₂* corrosion models, scale prediction programs, or gas drying simulators in the mixed solvent electrolyte system of *CO₂-NaHCO₃-Na₂CO₃-MEG-H₂O*.
The extended UNIQUAC model was shown to be a suitable model for reproducing and predicting a number of properties of the *CO₂-NaHCO₃-Na₂CO₃-MEG-H₂O* and its binary, and ternary sub-systems. This is done using only binary interaction parameters with linear temperature dependence. For the particular system 751 SLE, VLE, and excess enthalpy data points were fitted satisfactory using 12 ion specific interaction parameters and two UNIQUAC volume and surface parameters for *MEG*. The model predicts the heat capacity with good accuracy even though it was not used in the parameter regression. The model predicts solubility in the quaternary system based on parameters fitted to data for binary and ternary systems. It is expected that the model predicts activity coefficients equally well in saturated and un-saturated solutions since both types of data were used in the fitting process.
The activity coefficient model with the parameters determined in this work is not only valid for modelling corrosion or similar processes, but may as well be used for *CO₂* capture, scale prediction, gas drying or similar processes involving *CO₂* and *MEG*.
A simple engineering correlation which reproduces the density of *NaHCO₃-Na₂CO₃-MEG-H₂O* solutions was presented. The correlation reproduces the density data within the experimental error using only one salt specific parameter for each salt in the whole concentration and temperature interval studied.
There is a general lack of experimental data for CO_2 solubility in MEG-H_2O, NaHCO₃-H_2O, and Na₂CO₃-H_2O systems. These could improve the current modelling of the system.

7.8   Literature cited

[1]   Schreinemakers, F.A.H. Graphical deductions from the solution isotherms of a double salt and its components. Z. Physik. Chem., 1893, 11, 75-109.

[2]   Schreinemakers, F.A.H.; van Dorp, W.A.; Cocheret, D.H.; Filippo, H.; Waal, A.J.C. Quaternary equilibrium systems. Z. Physik. Chem., 1907, 59, 641-669.

[3]   Kaasa, B. Prediction of pH, mineral precipitation and multiphase equilibria during oil recovery. Ph.D. Thesis no. IUK 103, NTNU, 1998.

[4]   Sandengen, Kristian. Prediction of mineral scale formation in wet gas condensate pipelines and in MEG (mono ethylene glycol) regeneration plants. PhD thesis, NTNU, Norway, 2006.

[5]   Oosterhof H.; Witkamp, G.J.; van Rosmalen, G.M. Some antisolvents for crystallisation of sodium carbonate. Fluid Phase Equilibria, 1999, 155, 219-227.

[6]   Gärtner, R.S.; Seckler, M.M.; Witkamp, G.-J. Solid Phases and Their Solubilities in the System Na_2CO_3 + $NaHCO_3$ + Ethylene Glycol + Water from (50 to 90)°C. J. Chem. Eng. Data, 2004, 49, 116-125.

[7]   Thomsen, K. Aqueous Electrolytes, model parameters and process simulation. Ph.D. Thesis, IVC-SEP, Technical University of Denmark, 1997.

[8]   Thomsen, K; Rasmussen, P. Modeling of Vapor-liquid-solid equilibrium in gas-aqueous electrolyte systems. Chemical Engineering Science, 1999, 54, 1787-1802.

[9]   Iliuta, M.; Thomsen, K.; Rasmussen, P. Extended UNIQUAC model for correlation and prediction of vapor-liquid-solid equilibria in aqueous salt systems. Chemical Engineering Science, 2000, 55, 2673-2686.

[10]   http://www.ivc-sep.kt.dtu.dk. IVC-SEP, Center for phase equilibria and separation processes, Electrolyte database, 2007.

[11]   Mokbel, I.; Porcedda, S.; Guetachew, T.; Marongiu, B.; Jose, J. Static measurements of the total vapor pressure of ethane-1,2-diol + water mixtures at temperatures from 258 K to 363 K. The International Electronic Journal of Physico-Chemical Data, Eldata, 1999, 5(2), 79-84.

[12]   Wagman, D.D.; Evans, W.H.; Parker, V.B.; Schumm, R.H.; Halow, I.; Bailey, S.M. Journal of Physical and Chemical Reference Data, Vol. 11, Suppl. No. 2: The NBS Tables of Chemical Thermodynamic Properties. Selected Values for Inorganic and C1 and C2 Organic Substances in SI Units. J. Phys. Chem. Ref. Data, 1982, 11 Supplement No. 2.

[13]   Thomsen, K.; Rasmussen, P.; Gani, R. Correlation and prediction of thermal properties and phase behaviour for a class of electrolyte systems. J. Chem. Eng. Science, 1996, 51, 3675-83.

[14]   Hurst, J.E.; Harrison, B.K. Estimation Of Liquid And Solid Heat Capacities Using A Modified Kopp's Rule. Chemical Engineering Communication, 1992, 112, p 21-30.

[15]   Oglesby, N.E. A Study Of The System Sodium Bicarbonate-Potassium Bicarbonate-Water. J. Am. Chem. Soc., 1929, 51, 2352-2362.

[16]   Waldeck, W.F.; Lynn, G.; Hill, A.E. Aqueous solubility of salts at high temperatures II. The ternary system Na_2CO_3-$NaHCO_3$-H_2O from 100 – 200. J. Am. Chem. Soc., 1934, 56, 43-47.

[17]   Hill, A.E.; Bacon, L.R. Ternary Systems VI. Sodium Carbonate, Sodium Bicarbonate and Water. J. Am. Chem. Soc., 1927, 49, 2487-95.

[18]   Hill, A.; Smith, S. Equilibrium between the carbonates and bicarbonates of sodium and potassium in aqueous solution at 25C. J. Am. Chem. Soc., 1929, 51, 1626-1636.

[19]   Hill, A. Double salt formation among the carbonates and bicarbonates of sodium and potassium. J. Am. Chem. Soc., 1930, 52, 3813-17.

[20]   Green, S.J.; Frattali, F.J. The system Na_2CO_3-Na_2SO_4-NaOH-H_2O at 100C. J. Am. Chem. Soc., 1946, 68, 1789-1794.

[21] Itkina, L.S.; Chaplygina, N.M. The solubility isotherm in the $2Li^+$, $2Na^+$. CO_3^{2-}, $2OH^- + H_2O$ system at 50C. Russ. J. Inorg. Chem., 1963, 8(6), 768-772.

[22] Morozova, V. A.; Rzhechitskii, E. P. Solubility in The sodium fluoride-sodium bicarbonate-water, sodium fluoride-sodium sulfate-water, and sodium fluo. Russ. J. Inorg. Chem., 1977, 22, 485-486.

[23] Ellingboe, J. L.; Runnels, J. H. Solubilities of Sodium Carbonate and Sodium Bicarbonate in Acetone-Water and Methanol-Water Mixtures. J. Chem. Eng. Data, 1966, 11, 323-324.

[24] Sedel'nikov, G.S.; Trofimovich, A.A. The reciprocal system $2K^+$, $2Na^+$, $2HCO_3^-$, CO_3^{2-}, H_2O at 75C. Russ. J. Inorg. Chem., 1959, 4(6), 649-652.

[25] Fedotieff, P.P.; Koltunoff, J. Another form of ammonia-soda process. Z. anorg. allg. Chemie, 1914, 85, 247-260.

[26] Bogoyavlensky, P.S.; Manannikova, A.S. The $NaCl$-$NaHCO_3$-H_2O system (Carlsbad salt) at 25 and 38C. J. Applied Chemistry, USSR, 1955, 28, 225-28.

[27] Ponizovskii, A.M.; Vladimirova, N.M.; Gordon-Yanovskii, F.A. Solubility in the Na Mg Cl HCO_3 - H_2O system at 0C with carbon dioxide at 4 and 10 kg/cm^2. Russ. J. Inorg. Chem., 1960, 5, 1250-2.

[28] Sukmanskaya, G.V.; Bogoyavlenskii, P.S. Solubility in the Sodium Sulfate - Sodium Bicarbonate - Sodium Chloride - Water system. Russ. J. Inorg. Chem., 1960, 5, 468-71.

[29] Trypuc, M.; Kielkowska, U. Solubility in the NH_4HCO_3 + $NaHCO_3$ + H_2O System. J. Chem. Eng. Data, 1998, 43, 201-204.

[30] Plyushchev, V.E.; Kurtova, L.V. The Li^+,Na^+//CO_3^{2-}, NO_3^--H_2O system. Russ. J. Inorg. Chem., 1965, 10, 800-803.

[31] Waldeck, W.F.; Lynn, G.; Hill, A.E. Aqueous solubility of salts at high temperatures. I Solubility of Sodium Carbonate from 50 to 348C. J. Am. Chem. Soc., 1932, 54, 928-936.

[32] Wells, R.C.; McAdam, D.J. Phase Relations Of The System: Sodium Carbonate And Water. J. Am. Chem. Soc., 1907, 29, 721-727.

[33] Morey, G.W.; Burlew, J.S. Studies of solubility in systems containing alkali and water IV. J. Phys. Chem., 1964, 68, 1706-1712.

[34] Freeth, F.A. The system Na_2O-CO_2-$NaCl$-H_2O considered as two four component systems. Phil.Trans.Roy.Soc.(London), ser A., 1922, 223, 35-87.

[35] Itkina, L.S.; Kokhova, V.F. Solubility and composition of solid phases in the Na_2SO_4-Na_2CO_3-NaOH - H_2O system between 25 and 150C. Russ. J. Inorg. Chem., 1960, 5, 622-626.

[36] Wegscheider, R.; Mehl, J. The system sodium carbonate-sodium bicarbonate-water and the region of existence of trona, $Na_2CO_3.NaHCO_3.2H_2O$. Monatshefte Chem. Österreichische Akademi der Wissenschaften, 1928, 49, 283-315.

[37] Salit, P.W. A New Triple Acetate Method For Sodium Determinations In Biological Materials. J. Biol. Chem., 1932, 96(3), 659.

[38] Barber, H. H.; Kolthoff, I. M. A Specific Reagent For The Rapid Gravimetric Determination of Sodium. J. Am. Chem. Soc., 1928, 50, 1625.

[39] Ervin, G.J.; Giorgi, A.L.; McCarthy, C.E. The system Potassium Carbonate-Sodium Carbonate-Water at 100 and 150C. J. Am. Chem. Soc., 1944, 66, 384-7.

[40] Kremann, K.; Zitek, A. The Formation of Saltpeter from Sodium Nitrate and Potash from the Standpoint of the Phase Rule. Monatshefte für Chemie, 1909, 30, 311-340.

[41] Osaka, J. On Sodium Potassium Carbonates. Mem. Coll. Sci. Eng. (Kyoto), 1911, 3, 55-61.

[42] Skoog, D.A.; West, D. M.; Holler, F. J. Fundamentals of Analytical Chemistry, 7th edition, Sounders college publishing, 1996.

[43] Thomsen, K.; Iliuta, M.; Rasmussen, P. Extended UNIQUAC model for correlation and prediction of vapor-liquid-liquid-solid equilibria in aqueous salt systems containing non-

electrolytes. Part B. Alcohol (Ethanol, Propanols, Butanols) - water - salt systems. Chemical Engineering Science, 2004, 59, 3631-3647.

[44] George, S. K. Density, thermal expansivity, and compressibility of liquid water from 0° to 150°. Correlations and tables for atmospheric pressure and saturation reviewed and expressed on 1968 temperature scale. J. Chem. Eng. Data, 1975, 20, 97-105.

[45] Hayduk, W.; Malik, V. K. Density, Viscosity, and Carbon Dioxide solubility and diffusivity in aqueous ethylene glycol solutions. J. Chem. Eng. Data, 1971, 16(2), 143-146.

[46] Huot, J. Y.; Battistel, E.; Lumry, R.; Villeneuve, G.; Lavallee, J. F.; Anusiem, A.; Jolicoeur, C. A Comprehensive Thermodynamic Investigation Of Water-Ethylene Glycol Mixtures At 5,25, And 45°C. Journal Of Solution Chemistrym, 1988, 17(7), 601-636.

[47] Kapadi, U. R.; Hundiwale, D. G.; Patil, N. B.; Patil, P. R.; Lande, M. K. Densities, excess molar volumes, viscosities of binary mixtures of ethanediol with water at various temperatures. Journal Of The Indian Chemical Society, 2000, 77(7), 319-321.

[48] Sakurai, M. Partial Molar Volumes Of Ethylene-Glycol And Water In Their Mixtures. Journal Of Chemical And Engineering Data, 1991, 36(4), 424-427.

[49] George, J.; Sastry, N. V. Partial excess molar volumes, partial excess isentropic compressibilities and relative permittivities of water + ethane-1,2-diol derivative and water + 1,2-dimethoxyethane at different temperatures. Fluid Phase Equilibria, 2004, 216(2), 307-321.

[50] Cocchi, M.; Marchetti, A.; Pigani, L.; Sanna, G.; Tassi, L.; Ulrici, A.; Vaccari, G.; Zanardi, C. Density and volumetric properties of ethane-1,2-diol plus di-ethylen-glycol mixtures at different temperatures. Fluid Phase Equilibria, 2000, 172(1), 93-104.

[51] Douheret, G.; Pal, A.; Hoeiland, H.; Anowi, O.; Davis, M. I. Thermodynamic Properties Of (Ethan-1,2-Diol + Water) At The Temperature 298.15-K .1. Molar Volumes, Isobaric Molar Heat-Capacities, Ultrasonic Speeds, And Isentropic Functions. Journal Of Chemical Thermodynamics, 1991, 23(6), 569-580.

[52] Gallant, R. W. Physical properties of hydrocarbons. XIII. Ethylene glycols. Hydrocarbon Processing (1966-2001), 1967, 46(4), 183-96.

[53] Yang, C.; Ma, P.; Jing, F.; Tang, D. Excess Molar Volumes, Viscosities, and Heat Capacities for the Mixtures of Ethylene Glycol + Water from 273.15 K to 353.15 K. Journal of Chemical and Engineering Data, 2003, 48(4), 836-840.

[54] Sandengen, K.; Kaasa, B. Estimation of Monoethylene Glycol (MEG) Content in Water + MEG + NaCl + NaHCO₃ Solutions. J. Chem. Eng. Data, 2006, 51 (2), 443 -447.

[55] Garcia, A.V.; Thomsen, K.; Stenby, E.H. Prediction of mineral scale formation in geothermal and oilfield operations using the extended UNIQUAC model Part II. Carbonate scaling minerals. Geothermics, 2006, 35, 239-284.

[56] Abrams, D.S.; Prausnitz, J.M. Statistical thermodynamics of liquid mixtures: A new expression for the Gibbs excess energy of partly or complete miscible systems. AIChE Journal, 1975, 21, 116-128.

[57] Bondi, A. Physical Properties of Molecular Crystals, Liquids and Glasses, 1968, Wiley. New York,

[58] Skjold-Jørgensen, S.; Kolbe, B., Gmehling, J., Rasmussen, P. Vapor-Liquid-Equilibria By Unifac Group Contribution - Revision And Extension. Industrial & Engineering Chemistry Process Design And Development, 1979, 18(4), 714-722.

[59] Chiavone-Filho, O.; Proust, P.; Rasmussen, P. Vapor-Liquid-Equilibria For Glycol Ether Plus Water-Systems. Journal Of Chemical And Engineering Data, 1993, 38(1), 128-131.

[60] Chiavone-Filho O.; Rasmussen P. Modeling of salt solubilities in mixed solvents, Brazilian Journal Of Chemical Engineering, 2000, 17(2), 117-131

[61] Lancia, A.; Musmarra, D.; Pepe, F. Vapour liquid equilibria for mixtures ethylene glycol, propylene glycol, and water between 98C and 122C. Journal of Chemical Engineering of Japan, 1996, 29(3), 449-455.

[62]   Horstmann, S.; Gardeler, H.; Wilken, M.; Fischer, K.; Gmehling, J. Isothermal Vapor-Liquid Equilibrium and Excess Enthalpy Data for the Binary Systems Water + 1,2-Ethanediol and Propene + Acetophenone. Journal of Chemical and Engineering Data, 2004, 49(6), 1508-1511.

[63]   Trimble, H. M.; Potts, W. Glycol-water mixtures. Vapor pressure-boiling point-composition relations. Ind. Eng. Chem., 1935, 27(1), 66-68.

[64]   Sokolov, N. M.; Tsygankova, L. N.; Zhavoronkov, N. M. Liquid-vapor phase equilibrium in water-ethylene glycol and water-1,2-propylene glycol systems at various pressures. Teor. Osn. Khim. Tekhnol., 1971, 5, 900-904.

[65]   Villamanan, M. A. Liquid-vapor equilibrium. 1,2-Ethanediol - water system. International DATA Series, Selected Data on Mixtures, Series A: Thermodynamic Properties of Non-Reacting Binary Systems of Organic Substances, 2004, 32(3), 189.

[66]   Gonzalez, C.; Van Ness, H. C. Excess thermodynamic functions for ternary systems. 9. Total-pressure data and GE for water/ethylene glycol/ethanol at 50C. J. Chem. Eng. Data, 1983, 28, 410.

[67]   Villamanan, M.A.; Gonzalez, C.; van Ness, H.C. Excess thermodynamic properties for water/ethylene glycol. J. Chem. Eng. Data, 1984, 29(4), 427-429.

[68]   Skripach, T. K.; Temkin, M. I. Studies of the equilibrium liquid-vapor in the systems: water-ethylene glycol, water-diethylene glycol, ethylene glycol-diethylene glycol, diethylene glycol-triethylene glycol. Zhurnal Prikladnoi Khimii (Sankt-Peterburg, Russian Federation), 1946, 19, 180-6.

[69]   Kumar, P.; Sudhakar, K.; Rao, D. Phaneswara. A study of vapor-liquid equilibrium from isobaric boiling-point data for the monoethylene glycol-diethylene glycol-water system. Indian Chemical Engineer (1959-1993), 1982, 24(2), 14-16.

[70]   Efremova, S. A.; Komarova, L. F.; Garber, Yu. N.; Tikhanovich, E. V. Study of phase equilibria in binary subsystems of the acetone-ethanol-water-methylcellosolve-ethylene glycol system. Zhurnal Prikladnoi Khimii (Sankt-Peterburg, Russian Federation), 1988, 61(11), 2579-81.

[71]   Frolova, E. A.; Ershova, T. P.; Stepanova, V. A.; Pavlov, S. Yu. Separation of mixtures from the synthesis of ethylene glycol dimethacrylate. Osnov. Organ. Sintez i Neftekhimiya, (Leningrad), 1979, 11, 90-5.

[72]   Ramanujam, M.; Laddha, G. S. Vapour liquid equilibria for ethanol-water-ethylene glycol system. Chemical Engineering Science, 12(1), 1960, 65-68.

[73]   Ogorodnikov, S. K.; Kogan, V. B.; Morozova, A. I. Liquid-vapor equilibrium in the system ethylene glycol-water. Zh. Prikl. Khim., 1962, 35, 685.

[74]   Liu, F. Mathematical modelling and indentification in extractive distillation of alcohol-water with glycol and diethylene glycol. J. east china. inst. chem. techn., 1993, 19(3), 254.

[75]   Kireev, V. A.; Popov, A. A. Equilibria in mixtures of liquids and solutions. I. Boiling points and the composition of aqueous solutions of ethylene glycol and ethylene oxide. Zhurnal Prikladnoi Khimii (Sankt-Peterburg, Russian Federation), 1934, 7, 489-94.

[76]   Liu, F.; Zhang, C.; Huang, F.; Zhang, C. Studies on separation of alcohols and water by extractive distillation. Fuel Science & Technology International, 1993, 11(11), 1537-50.

[77]   Nath, A.; Bender, E. Isothermal Vapor Liquid Equilibria Of Binary And Ternary Mixtures Containing Alcohol, Alkanolamine, And Water With A New Static Device. Journal Of Chemical And Engineering Data, 1983, 28(4), 370-375.

[78]   Davis, P.M.; Clark, P.D.; Fitzpatrick, E.; Lesage, K.L.,; Svrcek, W.Y.; Satyro, M. The impact of sulfur species on glycol dehydration - a study of the solubility of certain gases and gas mixtures in glycol solutions at elevated pressures and temperatures. Gas Processors Association, Research report 183, 2002.

[79]   Won, Y. S.; Chung, D. K.; Mills, A. F. Density, viscosity, surface tension, and carbon dioxide solubility and diffusivity of methanol, ethanol, aqueous propanol, and aqueous ethylene glycol at 25 °C. Journal of Chemical and Engineering Data, 1981, 26(2), 140-1.

[80] Kobe, K.A.; Mason, G.E. Aqueous Solutions of Alcohols as Confining Liquids for Gas Analysis. Industrial and Engineering Chemistry, Analytical Edition, 1946, 18, 78 – 79.

[81] Kracht, C.; Ulbig, P.; Schulz, S. Measurement and correlation of excess molar enthalpies for (ethanediol, or 1,2-propanediol, or 1,2-butanediol plus water) at the temperatures (285.65, 298.15, 308.15, 323.15, and 338.15) K. Journal Of Chemical Thermodynamics, 1999, 31(9), 1113-1127.

[82] Könnecke, H. G.; Steinert, H.; Leibnitz, E. Heats of mixing of binary systems on the example benzene/water and water/glycols. Z. Phys. Chem. (leipzig), 1958, 208, 147-156.

[83] Wang, S.; Luo, B.; Zheng, D. Study of the relationship between heat of mixing and vapor-liquid equilibrium for binary aqueous solutions of glycols. Beijing Huagong Xueyuan Xuebao, Ziran Kexueban, 1992, 19(3), 1-9.

[84] Matsumoto, Y.; Touhara, H.; Nakanishi, K.; Watanabe, N. Molar excess enthalpies for water + ethanediol, + 1,2-propanediol, and + 1,3-propanediol at 298.15 K. Journal of Chemical Thermodynamics, 1977, 9(8), 801-5.

[85] Dohnal, V.; Roux, A. H.; Hynek, V. Limiting partial molar excess enthalpies by flow calorimetry: some organic solvents in water. Journal of Solution Chemistry, 1994, 23(8), 889-900.

[86] Arroyo, G. A. Excess enthalpy of binary mixtures of water with mono-, di-, tri-, and tetraethylene glycols. Anales de Quimica, Serie A: Quimica Fisica e Ingenieria Quimica, 1988, 84(2), 179-82.

[87] Biros, J.; Pouchly, J.; Zivny, A. A calorimetric investigation of interactions in aqueous solutions of poly(oxyethylene). 1. Heats of mixing of oligomeric models. Makromolekulare Chemie, 1987, 188(2), 379-94.

[88] Rehm, K.; Bittrich, H.-J. Heats Of Mixing Of Binary Liquid Systems Using Thermometric Titration. Z. Phys. Chem (leipzig), 1972, 251, 104.

[89] Manin, N.G.; Antonova, O.A.; Korolev, V.P. Thermochemical study of the solvation of ethylene glycol, glycerine and formamide in water-tert-butanol mixed solvent. Russian journal of general chemistry, 1996, 66(2), 204-211.

[90] Batov, D. V.; Antonova, O. A.; Egorova, N. G.; Korolev, V. P. Enthalpies of ethyleneglycol, 1,4-butyleneglycol, 2,3-butyleneglycol, glycerine and 2-ethoxyethanol solution in water-methanol mixed solvent. Russian journal of general chemistry, 1996, 66(8), 1331-1234.

[91] Nakayama, H. Temperature dependence of the of solution of poly(ethylene glycol) and of related compounds. Bull. Chem. Soc. jpn., 1970, 43(6), 1683.

[92] Nichols, N.; Skjold, R.; Sprink, C.; Wadso, I. Thermochemistry of solutions of biochemical model compounds 6. alpha,omega-dicarboxylic acids, -diamines, and -diols in aqueous solution. J. Chem. Thermodyn., 1976, 8(10), 993-999.

[93] Zhaodong, N.; Liu, B.P.; Zhicheng T. Calorimetric investigation of excess molar heat capacities for water plus ethylene glycol from T=273.15 to T=373.15 K. Journal Of Chemical Thermodynamics, 2002, 34 (6), 915-926.

[94] Origlia-Luster, M.L.; Patterson, B.A.; Woolley, E.M. Apparent molar volumes and apparent molar heat capacities of aqueous ethane-1,2-diol, propane-1,2-diol, and propane-1,3-diol at temperatures from 278.15 K to 393.15 K and at the pressure 0.35 MPa. Journal Of Chemical Thermodynamics, 2002, 34(4), 511-526.

[95] Zinchenko, A. V.; Zinchenko, V. D. On phase transitions in the water-ethylene glycol system at subzero temperatures under non-isothermal conditions. Cryo-Letters, 2001, 22(3), 191-198.

[96] Jou, F.Y.; Deshmukh, R.D.; Otto, F.D.; Mather, A.E. Vapor-Liquid-Equilibria of H₂S and CO₂ and ethylene-glycol at elevated pressures. Chemical Engineering Communications, 1990, 87, 223-231.

[97] Da-Qing, Z.; Wen-Dong, M.; Rei, W.; Tian-Min, G. Solubility study of methane, carbon dioxide and nitrogen in ethylene glycol at elevated temperatures and pressures. Fluid Phase Equilibria, Volume, 1999, 155(2), 277-286.

[98]   Dugstad, A.; Seiersten, M. pH-stabilisation, a Reliable Method for Corrosion Control of Wet Gas Pipelines. SPE, 2004, paper 87560.

[99]   Atakhodzhaev, A. K.; Dzhuraev, B. Solubility sodium bicarbonate in mixed alcohol-water solvents. Doklady Akademii Nauk USSR, 1988, (7), 39-40.

[100]   Cordray, D.R.; Kaplan, L.R.; Woyciesjes, P.M.; Kozak, T.F. Solid-liquid phase diagram for ethylene glycol + water. Fluid Phase Equilibria, 1996, 117(1-2), 146-152.

[101]   Ott, J.B.; Goates, J.R.; Lamb, J.D. Solid-liquid phase equilibria in water + ethylene glycol. J.Chem.Thermodynamics, 1972, 4, 123-126.

[102]   Baudot, A.; Odagescu, V. Thermal properties of ethylene glycol aqueous solutions. Cryobiology, 2004, 48(3), 283-294.

[103]   Suleiman, D.; Eckert, C.A. Limiting Activity-Coefficients of Diols on Water by a Dew-Point Technique. Journal Of Chemical And Engineering Data, 1994, 39(4), 692-696.

8 Review and recommended thermodynamic properties of FeCO₃ corrosion films

8.1 Introduction

CO_2 corrosion or sweet corrosion has been known for a long time and continues to be a problem in the process industry. Properties of $FeCO_3$ are important in order do understand $FeCO_3$ stability. The solubility constant of $FeCO_3$ may for example be used for calculating the solubility of $FeCO_3$ and to show how $FeCO_3$ precipitates with respect to pH or temperature. It may also be used in kinetic models for calculating the precipitation rate and thereby the scale build-up. These calculations require high precision of the equilibrium constant.

$FeCO_3$ is not only observed in CO_2 corrosion systems, it is also found in other systems which contain iron: The availability of aqueous Fe^{2+} is frequently controlled by the solubility of $FeCO_3$ and the iron concentration follows the saturation by $FeCO_3$. The calculated iron concentration is dependent on the thermodynamic properties of $FeCO_3$ and inaccurate properties will influence the calculated concentrations. Using an erroneous solubility constant of $FeCO_3$ may lead to false conclusions. This is especially important in geological systems as shown by Jensen *et al.*[1,2]. Iron also influences the production of crops and Schwab and Lindsay[3] has shown how $FeCO_3$ control the chemistry in agriculture. Previously Flügge[4] discussed how to produce $FeCO_3$ for human consumption. It is also related to ground water[5,6], aeration of ground water[7,8] and natural waters[9,10]. The water transported in pipes receives an amount of iron from the dissolved transport equipment which gives a contribution to iron in tap water as examined by Tillmans and Klarmann[11]. $FeCO_3$ has an economical aspect since it occurs naturally as technical pure crystals and is used for iron and steel production[12,13]. Consequently iron has leaked into ground waters and it has become an environmental problem which also has been addressed[14]. The prehistoric high temperature and pressure ore formation has also been examined by French[15], Weidner[16], and Rosenberg[17].

Recently authors have studied the crystals for a Mars evolution theory[18], but also in scenarios of fuel cells[19]. As an alternative to existing CO_2 capture processes Palandri and Kharaka[20] have discussed $FeCO_3$ in a process for underground sequestration of CO_2 from flue gas.

Since then many contributors have published and discussed the $FeCO_3$ properties used for corrosion modelling. Properties have been used for Pourbaix stability plots by several authors[21,22,7,23,14,24,25,26]. Properties have also been used in kinetic models to predict the rate of $FeCO_3$ precipitation and dissolution. Johnson and Tomson[27,28,29] and Hunnik *et al.*[30] published two of the most cited models, other models have been published[11,31,32,33,34,14,35,36] even recently by Golubev *et al.*[37]. The kinetic models continue to be the focus of the corrosion literature. Some of the newer applications were made by Dugstad[38], Nesic *et al.*[39,40], Sun *et al.*[41], Sun and Nesic[42], and Gulbrandsen[43].

Two reviews have previously been published by Grauer[44] and Preis and Gamsjäger[45] which focused mainly on the solubility constant and the enthalpy of formation of $FeCO_3$. In this study a comprehensive collection of $FeCO_3$ properties are reviewed. This includes entropy, enthalpy of formation and Gibbs energy of formation, heat

capacity, aqueous solubility and solubility constants. Properties of Fe^{2+} have also been collected since they are closely related to $FeCO_3$. Works on thermal decomposition of $FeCO_3$ are presented and an overview of synthesis of $FeCO_3$ is given.

The focus of this study is mainly related to aqueous systems between 0 and 100 $°C$ and pressures up to 50 bar CO_2. A few high temperature salt systems are discussed in order to show how low temperature properties may be determined from high temperature measurements. Much literature has been published on using $FeCO_3$ properties to predict other properties. In this study only works related to measured $FeCO_3$ properties has been included. An extensive review of entropy, enthalpy of formation and Gibbs energy of formation, heat capacity, aqueous solubility and solubility constant of $FeCO_3$ is given. A consistent set of thermodynamic properties for $FeCO_3$ and relevant aqueous species is selected and recommended for use. Speciation schemes for aqueous $FeCO_3$ are reviewed and evaluated. Issues related to supersaturation of $FeCO_3$ are discussed. Works on the thermal decomposition of $FeCO_3$ are presented and an overview of measured solubility and synthesis of $FeCO_3$ is given. Measurements of non-aqueous systems are not discussed here.

8.2   Standard state properties of FeCO₃

8.2.1   Databases of standard state formation properties

Standard state properties of *FeCO₃* have been collected in several databases. Table 18, 19 and 20 give an overview of the available properties of CO_3^{2-}, Fe^{2+}, and *FeCO₃* respectively which will be discussed in the following subsections. The database collections of thermodynamic properties are also discussed and require special attention since they have been used in many studies. The databases by the United States Geological Survey (USGS)[46,47,48] and Nordstrom *et al.*[49] were used in a range of ground water and geological studies. The book by Latimer[50] was used in the past as a source of properties and was therefore included in several works. Also the smaller iron database by Langmuir[51] was typically used since it covers many iron species. The collections by Barin *et al.*[52] and Martell and Smith[53] were used less and the collections by Wagman *et al.*[54], NIST[55], and Stumm[22] have rarely been used. The first carbonate property database was compiled by Kelley and Anderson[56]. The properties of *FeCO₃* were estimated but not measured. The result of their work has been used by almost all later data collections and their assumptions have spread into many of the later data collections, which is discussed below. This assessment is based on all references to databases with standard thermodynamic properties for *FeCO₃* encountered in this study.

The data collections by CODATA[57,58] related to *Fe*(II) properties and the book by Baes and Mesmer[59] related to hydroxide properties, are also used in the discussion of *FeCO₃* properties below.

8.2.2   Standard state heat capacity of FeCO₃

The standard state heat capacity, C_p°, was measured and tabulated by Anderson[60] and Robie *et al.*[61]. Kelley and Anderson[56] gave an approximate linear correlation which was estimated using the heat capacity of iron, oxygen and carbon valid at room temperature. The correlation has apparently been adopted by many authors through time. Some authors refer to Kelley[62] as the origin, but the work originates from Kelley and Anderson[56] even though Kelley[62] states it was derived by Anderson[60]. *FeCO₃* has a Néel transition temperature between 30 K and 40 K which was not recognised by Anderson[60]. The Néel transition temperature is a second order magnetic phase transition which is observed as a spike in the heat capacity. This was determined by Kalinkina[63], Kostryukov and Kalinkina[64], Kalinkina and Kostryukov[65], and Robie *et al.*[61]. Robie *et al.*[61] measured the low temperature heat capacity more accurately and refined the correlation. Figure 51 shows the two correlations compared to the measured heat capacities. The values by Anderson[60] were measured in the interval 54 K to 296 K and are therefore only plotted at low temperature. Kalinkina[63] and Anderson[60] gave a Debye and Einstein correlation of the heat capacity, which may be used for calculating the heat capacity at low temperature.

Table 20 shows the literature values of the standard state heat capacity of *FeCO₃* at 25 °C. Only small variations are observed through time and a good agreement between authors is found. A recommended value of the heat capacity at 298.15 K is $82.25\, kJ/(molK)$ obtained from the correlation given by Robie *et al.*[61].
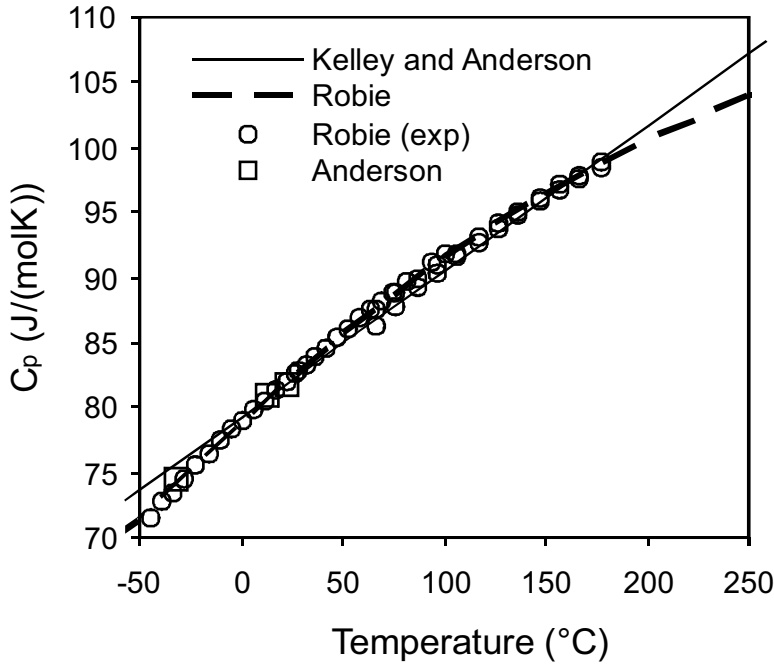
Figure 51: The standard state heat capacity of *FeCO₃(s)* as function of temperature.

8.2.3   Standard state entropy of FeCO₃

Table 20 lists the standard state entropy of *FeCO₃*, *S°*. The entropy follows the third law of thermodynamics which states that S^o (T=0 °C, 1bar)=0 *J/(mol·K)*. It is calculated by integrating the standard state heat capacity, C_p^o, and the sum of heat of phase changes, $\Delta_{trs}H^o$, by:

$$S^o_{298.15K} = \int_{0K}^{298.15K} \frac{C_p^o\left(T,1bar\right)}{T}dT + \sum_{trs}\frac{\Delta_{trs}H^o}{T_{trs}} \tag{250}$$

Anderson[60] and Kostryukov and Kalinkina[64] estimated the entropy from the measured heat capacity. The value by Anderson[60] has been used by many authors and the value is still listed in the NIST[55] database, see table 20. The value was revised by Robie[66], re-evaluating the work by Anderson[60] using a rough correction. It is not likely that the new value is more accurate then the Anderson[60], but the value was used in the data collections by Robie *et al.*[47], Robie and Waldbaum[46], and Helgeson *et al.*[67], see table 20. French[15] determined a new value by extrapolation from high temperature using the heat capacity correlation by Kelley and Anderson[56] even though the correlation is not valid in the applied temperature interval. This explains the deviation as indicated by French[15]. Robie *et al.*[61] improved the heat capacity measurements as explained above and estimated a more reliable entropy. Still it may be improved since the measured *FeCO₃* crystals were not pure. A recommended value of the standard state

entropy of *FeCO₃* is $S^o_{FeCO_3}$ =95.47*J/(mol·K)*, obtained by Robie *et al.*[61], which is consistent with their measured value of the heat capacity.

The entropy listed in table 20 is the standard state entropy of *FeCO₃*, $S^o_{FeCO_3}$ is significantly different from the entropy of formation, $\Delta_f S^o_{FeCO_3}$. $\Delta_f S^o_{FeCO_3}$ is calculated from the entropy of iron carbonate, crystalline iron, graphite, and gaseous oxygen. For example, using the NIST[55] and Robie *et al.*[61] standard state entropies of:

$$
\begin{array}{ccccc}
Fe(\alpha,s)+ & C(s)+ & \tfrac{3}{2}O_2(g) & \rightleftarrows & FeCO_3(s) \\
S^o = \quad 27.28 & 5.74 & \tfrac{3}{2}205.138 & & 95.47 \quad J/(molK)
\end{array}
\tag{251}
$$
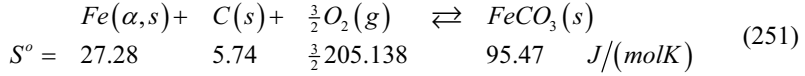
gives $\Delta_f S^o$ =-245.26*J/(mol·K)*. Using the *FeCO₃* entropy of Anderson[60] gives $\Delta_f S^o_{FeCO_3}$ =-247.8*J/(mol·K)*, a 1 % difference. Kelley and Anderson[56] actually used the value of Anderson[60], but listed a value of $\Delta_f S^o_{FeCO_3}$ =-247.7*J/(mol·K)*. This value was obtained by using other values of the standard state entropies of iron, graphite, and oxygen. $\Delta_f S^o_{FeCO_3}$ thus depends not only on properties of *FeCO₃*.

8.2.4   Fe²⁺ and CO₃²⁻ standard state properties

The standard state properties of Fe^{2+} and CO_3^{2-} are often used in the calculation of the *FeCO₃* properties. CO_3^{2-} properties have remained constant over the years as shown by table 18, but Fe^{2+} properties have varied as shown in table 19.

Table 18: Standard state properties of CO_3^{2-} listed in databases related to *FeCO₃* at 298.15K and 1 bar.

Authors	Year	$\Delta_f H°$ (kJ/mol)	$\Delta_f G°$ (kJ/mol)	$S°$ (J/(mol·K))
Robie and Waldbaum[46]	1968		-527.9	
Wagman *et al.*[68]	1969	-677.14	-527.90	-56.9
Robie *et al.*[47]	1978	-677.14	-527.9	-56.9
NIST[55]	1982	-677.14	-527.81	-56.9
CODATA[58]	1989	-675.23		-50.0
Robie and Hemingway[48]	1995	-675.2	-527	-50

The controversy was discussed by Tremaine *et al.*[69], Tremaine and LeBlanc[70], and Parker and Khodakovskii[57]. They showed that the discrepancies between the determined $\Delta_f G^o_{Fe^{2+}}$ are related to the contamination by oxygen and hydrogen. The value by Randall and Frandsen[71], see table 19, is often used and was obtained in an atmosphere contaminated by oxygen as discussed by Patrick and Thompson[72]. Randall and Frandsen[71] measured the standard state potential of iron, $\Delta E^o = 0.4402V$, and calculated the Gibbs energy of formation, $\Delta_f G^o_{Fe^{2+}} = -nF\Delta E^o$ =-84.9*kJ/mol*.

In the oxygen free environment, two different $\Delta_f G^o_{Fe^{2+}}$ values have been obtained. Patrick and Thompson[72] obtained a higher value in vacuum, $\Delta_f G^o_{Fe^{2+}}$ =-78.9 *kJ/mol*, and Larson *et al.*[73] obtained a lower value in a hydrogen atmosphere, $\Delta_f G^o_{Fe^{2+}}$ =-91.2 *kJ/mol*, see table 19. The high value was accepted by NIST[55]. The lower value was

accepted by Langmuir[51] and has therefore been used in many studies. Johnson and Bauman[74] support the NIST[55] value, but the value by Parker and Khodakovskii[57] was recently evaluated and accepted by Preis and Gamsjäger[45,75]. Langmuir[51], Preis and Gamsjäger[45], and Gamsjäger *et al.*[76] indicated also that the value by NIST[55] could be improved. They showed that it could be inconsistent with the enthalpy of *FeCO₃*, even though it is physically more correct. This is presumed since it was measured in vacuum and not contaminated by hydrogen of oxygen.

Table 19: Frequently used standard state properties of Fe^{2+} at 298.15K and 1 bar.

Author	Year	$\Delta_f H°$ (kJ/mol)	$\Delta_f G°$ (kJ/mol)	$S°$ (J/(mol·K))
Randall and Frandsen[71]	1932		-84.98	
Latimer[50]	1952	-87.86	-84.94	-113.4
Patrick and Thompson[72]	1953		-78.9	
Robie and Waldbaum[46]	1968		-84.94	
Larson *et al.*[73]	1968	-92.5	-91.2	-107.1
Langmuir[51]	1969		-91.2 [a]	
Wagman *et al.*[54]	1969	-89.1	-78.9	-137.7
Robie *et al.*[47]	1978	-89.1	-78.87	-138
Tremaine and LeBlanc[70]	1980		-88.92	-107.1 [a]
NIST[55]	1982	-89.1	-78.9	-137.7
Parker and Khodakovskii[57]	1995	-90.0	-90.53	-101.6
Robie and Hemingway[48]	1995	-91.1	-90.0	-107.1 [a]

[a] Obtained without refitting from Larson *et al.*[73]

$\Delta_f H^o_{Fe^{2+}}$ remained reasonably constant between studies, see table 19, but it has been determined in many different ways. For example, Larson *et al.*[73] estimated $S^o_{Fe^{2+}}$ from the entropy of iron sulphate and from this calculated $\Delta_f H^o_{Fe^{2+}}$. NIST[55] used the opposite approach where $S^o_{Fe^{2+}}$ was calculated $\Delta_f H^o_{Fe^{2+}}$ and $\Delta_f G^o_{Fe^{2+}}$. A relatively low value of $S^o_{Fe^{2+}}$ was found. $S^o_{Fe^{2+}}$ determined by Larson *et al.*[73] was recently accepted and included in the work by Robie and Hemingway[48].

Since $\Delta_f G^o_{Fe^{2+}}$ is scattered and $\Delta_f H^o_{Fe^{2+}}$ has remained relatively constant, the calculated values of $S^o_{Fe^{2+}}$ are also scattered as shown in table 19.

It is not possible to recommend a reliable set of thermodynamic properties of Fe^{2+}, due to the observed scatter. The NIST[55] or Parker and Khodakovskii[57] values are equally good from a physical point of view even though they are significantly different.

8.2.5 Gibbs energy of formation of FeCO₃

The standard state Gibbs energy of formation of *FeCO₃*, $\Delta_f G^o_{FeCO_3}$, has been determined by several authors. Table 20 lists the available values and a noteworthy interval between -697*kJ/mol* and -666*kJ/mol* is observed. We have found that all except Robie and Hemingway[48] and Barin *et al.*[52] calculated $\Delta_f G^o_{FeCO_3}$ from one of the following three reactions named "sp" (solubility product), "psp" (pressure solubility product), and "therm" (thermal decomposition):

sp:
$$FeCO_3(s) \rightleftarrows Fe^{2+} + CO_3^{2-} \qquad (252)$$

psp:
$$FeCO_3(s) + 2H^+ \rightleftarrows Fe^{2+} + CO_2(g) + H_2O(l) \qquad (253)$$

therm:
$$3FeCO_3(s) \rightleftarrows Fe_3O_4 + 2CO_2(g) + CO(g) \qquad (254)$$
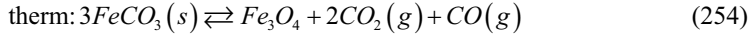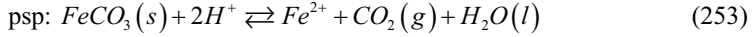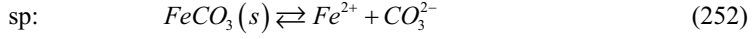
The equilibrium constant of reaction k is symbolized by K_k. It is related to the Gibbs energy of reaction, $\Delta_{r,k}G^o$, the stochiometric coefficient, ν_i, and the Gibbs energy of formation, $\Delta_f G_i^o$, of component i in reaction k by:

$$\Delta_{r,k}G^o = \sum_{i \ in \ k} \nu_i \Delta_f G_i^o = -RT \ln K_k \qquad (255)$$

$\Delta_{r,k}$ is the change of any property related to reaction k. $\Delta_{r,sp}H$ is for example the enthalpy of reaction (252). The negative base-ten logarithm to the equilibrium constant is $-logK_k = pK_k$, and written for reaction (252) is denoted by pK_{sp}. Reaction (252) is most frequently used in the open literature, but both of the above reactions have been used for determining $\Delta_f G_{FeCO_3}^o$. This is done using equation (255) which written for reaction (252), (253), and (254) gives:

$$\Delta_f G_{FeCO_3}^o = RT \ln K_{sp} + \Delta_f G_{CO_3^{2-}}^o + \Delta_f G_{Fe^{2+}}^o \qquad (256)$$

$$\Delta_f G_{FeCO_3}^o = RT \ln K_{psp} + \Delta_f G_{H_2O}^o + \Delta_f G_{CO_2(g)}^o + \Delta_f G_{Fe^{2+}}^o - 2\Delta_f G_{H^+}^o \quad (257)$$

$$3\Delta_f G_{FeCO_3}^o = RT \ln K_{therm} + \Delta_f G_{Fe_3O_4}^o + 2\Delta_f G_{CO_2(g)}^o + \Delta_f G_{CO(g)}^o \qquad (258)$$

The equilibrium constant of reaction (256) and (257) are determined at low temperature in aqueous media while (258) is determined through decomposition of *FeCO₃* at high temperature.

Equation (256) and (257) demonstrates how $\Delta_f G_{FeCO_3}^o$ is a linear function of $\Delta_f G_{Fe^{2+}}^o$. This is problematic, since $\Delta_f G_{Fe^{2+}}^o$ varies significantly between databases as shown by section 8.2.4. The same is true for $S_{FeCO_3}^o$ which depends on the $S_{Fe^{2+}}^o$. It illustrates the importance of knowing which Fe^{2+} properties were used in the calculation. This problem was also noted by Preis and Gamsjäger[45].

The issue may be avoided by tabulating the equilibrium constant of reaction (252) or (253) instead of $\Delta_f G_{FeCO_3}^o$, since they are independent of the Fe^{2+} properties.

$\Delta_f G_{FeCO_3}^o$ determined at high temperature is independent of the Fe^{2+} properties. It is determined using equation (258) at approximately 1000K and extrapolated to 298.15K using the heat capacity of *FeCO₃*. This is a drawback since the extrapolation involves an amount of uncertainty. To demonstrate this, consider $\Delta_f H_{FeCO_3}^o$ determined by Holland[77], see table 20. He used the heat capacity correlation of Robie *et al.*[61]. The obtained enthalpy is low compared to other works, see table 20. It can be shown that this value is too low by calculating $\Delta_f G_{FeCO_3}^o$ by:

$$\Delta_f G^o_{FeCO_3} = \Delta_f H^o_{FeCO_3} - T\Delta_f S^o_{FeCO_3} \qquad (259)$$

Table 20: Standard state formation properties of *FeCO₃* at 298.15K and 1 bar.

Authors	Year	$\Delta_f H°$ (kJ/mol)	$\Delta_f G°$ (kJ/mol)	$S°$ (J/(mol·K))	$C_p°$ (J/(mol·K))
Anderson[60]	1934			92.9(D)	83.35(x,D,M)
Kelley and Anderson[56]	1935	-747.60(T)	-673.75(T,xᵃ)	92.9 ᵇ	82.09(T)
Latimer[50]	1952	-744.8	-673.88	92.9	
Wilcox and Bromley[78]	1963	-748.9(xᶜ)			
Kostryukov and Kalinkina[64]	1964			96.1(M)	
Robie[66]	1965			105.0(*,xᵈ)	
Robie and Waldbaum[46]	1968	-743.965	-673.749 ᵉ	105.0	
Langmuir[51]	1969		-679.44(xᵃ)		
Wagman *et al.*[54]	1969	-740.57	-666.72	92.9	82.13
Singer and Stumm[6]	1970		-671.53		
French[15]	1971	-775.71*ᶠ	-697.05*	74.1*	
Barin *et al.*[52]	1973	-740.57(M)	-768.26(xᵍ,M)	92.9(M)	82.08(T)
Helgeson *et al.*[67]	1978	-749.656(xᵏ)	-679.440ʰ	105.0	82.09(T)
Robie *et al.*[47]	1978	-736.985	-666.698(xᵃ)	105.0	
Reiterer *et al.*[79,80]	1980		-669.02(xⁱ,M,D)		
NIST[55]	1982	-740.57	-666.67(xᵃ)	92.9	82.13
Robie *et al.*[61]	1984	-753.22(xᵏ)	-680.03(xʲ)	95.47	82.44(M,D) 82.25(x,T)
Stubina and Toguri[81]	1989	-749(xᶠ)			
Holland[77]	1990	-761.18(xᶠ)	-688.04(xˡ)	95.50	82.27(T)
Chai and Navrotsky[82]	1994	-750.6(xᶠ)			
Robie and Hemingway[48]	1995	-755.9	-682.8ᵐ	95.47	82.27(*,T,M)
Preis and Gamsjäger[45]	2002	-752.0	-678.9	95.47	

* ~ Rough estimate due to scatter in data, extrapolation or guess, x ~ calculated, T ~ temperature correlation given, D ~ experimental data given, M ~ properties at several temperatures given. ᵃ calculated from equilibrium constant of *FeCO₃* and properties of *Fe²⁺* and CO_3^{2-}. ᵇ they calculated $\Delta_f S^o$ =-247.7. ᶜ estimated by a group contribution method. ᵈ a corrected value of the $S^o_{FeCO_3}$ by Anderson[60]. ᵉ obtained directly from Kelley and Anderson[56] without refitting. ᶠ determined from the high temperature measurements. ᵍ the listed $G^o_{FeCO_3}$ value is not identical to $\Delta_f G^o_{FeCO_3}$. It is not comparable to other $\Delta_f G^o_{FeCO_3}$ values. ʰ obtained directly from Langmuir[51] without refitting. ⁱ corrected to 25 °C from 50 °C. ʲ calculated from equilibrium constant of *FeCO₃* and properties of CO_3^{2-} using Larson *et al.*[73] properties of *Fe²⁺*. ᵏ calculated from $\Delta_f G^o_{FeCO_3}$ and $\Delta_f S^o_{FeCO_3}$. ˡ calculated using $\Delta_f H^o_{FeCO_3}$ and $\Delta_f S^o_{FeCO_3}$. $\Delta_f S^o_{FeCO_3}$ was calculated using Hollands[77] own properties, see text. ᵐ The value is erroneous which is identified by calculating K_{sp}, see text.

Which is carried out using an entropy of formation of $\Delta_f S^o_{FeCO_3}$ =-245.32 *J/(mol·K)*, calculated from Holland's[77] own data. The obtained Gibbs energy is very low, see table 20, which indicates that the measured enthalpy is similarly too low. This can be further illustrated by using $\Delta_f G^o_{FeCO_3}$ to calculate the equilibrium constant of reaction (252). Using the NIST[55] properties of Fe^{2+} and CO_3^{2-}, reveals pK_{sp} =12.45 and similarly using Robie and Hemingway[48] ion properties reveals pK_{sp} =14.25. Both equilibrium constants, K_{sp}, are several orders of magnitude too low compared to literature values, see table 21 and figure 52. French[15] likewise determined $\Delta_f G^o_{FeCO_3}$ which was even lower than the value by Holland[77], see table 20. This value is inaccurate and the calculated K_{sp} would be four orders of magnitude different compared to literature.

Robie and Hemingway[48] also applied equation (259) while determining $\Delta_f G^o_{FeCO_3}$. They used the reaction enthalpy of *FeCO₃* dissolution of Nordstrom *et al.*[49], $\Delta_{r,sp} H^o$ =-10.4 *kJ/mol*, and the entropy of Robie *et al.*[61] and obtained a $\Delta_f G^o_{FeCO_3}$ comparable to other works, see table 20. Unfortunately they obtained pK_{sp} =11.53 which is very high compared to other works, see table 21 and figure 52.

Barin *et al.*[52] determined a $G^o_{FeCO_3}$. It was calculated from $\Delta_f H^o_{FeCO_3}$ and $S^o_{FeCO_3}$ using equation (259). $S^o_{FeCO_3}$ was used instead of $\Delta_f S^o_{FeCO_3}$ and the $G^o_{FeCO_3}$ value obtained is not identical to $\Delta_f G^o_{FeCO_3}$.

A consistent value of $\Delta_f G^o_{FeCO_3}$ is given during the final discussion.

8.2.6   Enthalpy of formation of FeCO₃

The standard state enthalpy of formation of *FeCO₃* is given in the literature and determined by two different methods. Either calculated at 298.15K by

$$\Delta_f H^o_{FeCO_3} = \Delta_f G^o_{FeCO_3} + T\Delta_f S^o_{FeCO_3} \qquad (260)$$

or extrapolated from high temperature to 298.15K. Barin *et al.*[52] and Robie and Hemingway[48] are exceptions. They used other approaches as described above. The variation in the enthalpy is shown in table 20, the value span -775.7 *kJ/mol* to -737.0 *kJ/mol*.

In the first approach $\Delta_f H^o_{FeCO_3}$ is calculated through equation (260) using $\Delta_f G^o_{FeCO_3}$. $\Delta_f G^o_{FeCO_3}$ is determined from the equilibrium constant of reaction (252) or (253) using $\Delta_f G^o_{Fe^{2+}}$ through equation (256) or (257). $\Delta_f G^o_{Fe^{2+}}$ is uncertain due to the variation in $\Delta_f G^o_{Fe^{2+}}$ and therefore $\Delta_f H^o_{FeCO_3}$ is uncertain. Approximately $\Delta_f H^o_{FeCO_3}$ =-740 *kJ/mol* is obtained by using the $\Delta_f G^o_{Fe^{2+}}$ of Patrick and Thompson[72] as NIST[55] does or -750 *kJ/mol* if the value by Parker and Khodakovskii[57] is used. Accordingly -745 *kJ/mol* is obtained by using the $\Delta_f G^o_{Fe^{2+}}$ of Randall and Frandsen[71]. Small variations are related to differences in the used entropy of *FeCO₃* given by either Anderson[60], Robie[66], or Robie *et al.*[61].

In the second approach French[15], Stubina and Toguri[81], Holland[77], and Chai and Navrotsky [82] all extrapolated $\Delta_f H^o_{FeCO_3}$ from high temperature down to 298.15K. The variation is notable as shown in table 20, which indicates that the procedure is difficult. It is valuable that the extrapolation procedure is independent of the variation in $\Delta_f G^o_{Fe^{2+}}$. A value in the lower range of the enthalpy interval is typically obtained. Stubina and Toguri[81] and Chai and Navrotsky [82] obtained an enthalpy of approximately -750 *kJ/mol* similar to studies using the $\Delta_f G^o_{Fe^{2+}}$ of Parker and Khodakovskii[57] shown above. Either their value is more correct or the high temperature experiments were polluted by hydrogen or oxygen as indicated by Patrick and Thompson[72]. Preis and Gamsjäger[45] made a critical evaluation of the enthalpy and obtained a similar value pointing out the problems shown here. They argued that the enthalpy of reaction (253) is only consistent with the Parker and Khodakovskii[57] enthalpy of Fe^{2+}.

A recommended value of $\Delta_f H^o_{FeCO_3}$ is difficult to determine since it varies with the values used for the properties of Fe^{2+}, similar to $\Delta_f G^o_{FeCO_3}$. It must be pointed out which properties of Fe^{2+} and CO_3^{2-} were used in the calculation of $\Delta_f H^o_{FeCO_3}$ to obtain consistency.

8.2.7 Solution enthalpy of FeCO₃, reaction (252)

The enthalpy of reaction (252) or (253) are linear function of $\Delta_f H^o_{FeCO_3}$, $\Delta_f H^o_{CO_2}$, $\Delta_f H^o_{Fe^{2+}}$ and $\Delta_f H^o_{CO_3^{2-}}$. $\Delta_f H^o_{Fe^{2+}}$ and $\Delta_f H^o_{CO_3^{2-}}$ vary only slightly between studies as shown in table 18 and 19, contrary to $\Delta_f H^o_{FeCO_3}$ as discussed. The enthalpy of solution written for reaction (252) is:

$$\Delta_{r,sp} H^o = \Delta_f H^o_{Fe^{2+}} + \Delta_f H^o_{CO_3^{2-}} - \Delta_f H^o_{FeCO_3} \qquad (261)$$

also $\Delta_{r,sp} H^o$ varies between studies as shown in table 21 with values in the range between -30.14 *kJ/mol* and -9.46 *kJ/mol*. It is important to point out that both $\Delta_f G^o_{Fe^{2+}}$ and $\Delta_f H^o_{Fe^{2+}}$ are used in the calculation of $\Delta_{r,sp} H^o$ even though $\Delta_f G^o_{Fe^{2+}}$ is not found explicitly in equation (261). This is due to $\Delta_f G^o_{Fe^{2+}}$ is used in the calculation of $\Delta_f H^o_{FeCO_3}$ as explained previously.

Most authors used consistent values of $\Delta_f G^o_{Fe^{2+}}$ and $\Delta_f H^o_{Fe^{2+}}$ and it seems that the variation in $\Delta_{r,sp} H^o$ is not connected to the variation observed in $\Delta_f G^o_{Fe^{2+}}$. Some irregularities were introduced by for example Langmuir[51] who used $\Delta_f H^o_{FeCO_3}$ from Robie and Waldbaum[46] calculated on the basis of Randall and Frandsen's[71] $\Delta_f G^o_{Fe^{2+}}$. Langmuir[51] used the $\Delta_f H^o_{Fe^{2+}}$ of Larson *et al.*[73]. Table 19 shows that Randall and Frandsen[71] and Larson *et al.*[73] are not consistent.

A similar combination was used by Nordstrom *et al.*[49] who used $\Delta_f H^o_{FeCO_3}$ of Robie *et al.*[61] who again used $\Delta_f G^o_{Fe^{2+}}$ from Larson *et al.*[73], while Nordstrom *et al.*[49] used the $\Delta_f H^o_{Fe^{2+}}$ from NIST[55]. Table 19 shows that the Larson *et al.*[73] and NIST[55] properties of Fe^{2+} are inconsistent. $\Delta_{r,sp}H^o$ given by Nordstrom *et al.*[49] has unfortunately been implemented in some later studies e.g. Ptacek and Blowes[12], Robie and Hemingway[48], and Marion *et al.*[18].

Helgeson[83] also used $\Delta_f H^o_{FeCO_3}$ of Robie and Waldbaum[46] who used $\Delta_f G^o_{Fe^{2+}}$ of Randall and Frandsen[71]. Helgeson[83] used the $\Delta_f H^o_{Fe^{2+}}$ from Latimer[50] and therefore obtained a more consistent value since the Latimer[50] value is compatible with Randall and Frandsen[71].

Greenberg and Tomson[33], Johnson and Tomson[27,28,29], and Preis and Gamsjäger[45] all fitted the enthalpy and obtained this way internal consistency of their data.

Preis and Gamsjäger[45] showed the temperature dependence of reaction (253) and concluded that the Fe^{2+} properties of Parker and Khodakovskii[57] are better than those given by NIST[55]. Preis and Gamsjäger[45] determined $\Delta_{r,psp}H^o$ which correspond to $\Delta_{r,sp}H^o$ =-13.2 *kJ/mol*. They also showed that using the NIST[55] properties for Fe^{2+} results in a biased temperature dependence of $FeCO_3$. This indicates that the solubility experiments were either polluted by oxygen or that the Parker and Khodakovskii[57] Fe^{2+} properties are more consistent than the NIST[55] properties.

It is recommended to either fit $\Delta_{r,sp}H^o$ or $\Delta_f H^o_{FeCO_3}$ to obtain a consistent property set, or to use properties of $\Delta_f H^o_{FeCO_3}$ and $\Delta_f H^o_{Fe^{2+}}$ from the same data collection which are consistent.

8.2.8   Solubility constants of FeCO₃

Reaction (252) and (253) define the two solubility constants of *FeCO₃* discussed in the open literature. Table 21 and figure 52 gives an overview of the published values and correlations of pK_{sp} of reaction (252) while table 22 gives an overview of pK_{psp} of reaction (253). pK_{sp} has primarily been examined in the literature. The 25 *°C* value range between 10.24 and 11.53 as observed in figure 52. The lower value gives a solubility constant, K_{sp}, which is twenty times higher than K_{sp} calculated from the upper value.

The equilibrium constants are much easier to compare between works compared to standard state properties. The reason is that pK_{sp} is independent of Fe^{2+} properties which vary between studies. This gives a direct way to identify why some authors obtained their standard state property values.

The equilibrium constant has still not been determined accurately due to few misinterpretations which have accumulated in data collections through time as discussed in the following sections.

Table 21: Literature, $\Delta_{r,sp}H°$, speciation scheme, and pK_{sp}, of reaction (252) at 25 °C and 1 bar.

Authors	Year	$\Delta_{r,sp}H°$ (kJ/mol)	Speciation scheme	pK_{sp}
Smith[84]	1918		No extra species	10.46 (30 °C)
Tillmans and Klarmann[11]	1924		No extra species	9.57 (18 °C)
Kelley and Anderson[56]	1935		No extra species	10.67 (x[a]), 10.50 (30 °C)
Latimer[50]	1952	-19.37	No extra species	10.68 [b]
Robie and Waldbaum[46]	1968		No extra species	10.67 [b]
Langmuir[51]	1969	-25.20	$FeOH^+$, $Fe(OH)_2(aq)$, $Fe(OH)_3^-$, $Fe(OH)_4^{2-}$	10.55 (T, M)
Helgeson[83]	1969	-21.05 [c]	No extra species	10.69 (M,x) [b]
Singer and Stumm[6]	1970	-19.37 [d]	No extra species	10.24 (M)
Martell and Smith[53]	1976		No extra species	10.68 [b]
Bardy and Péré[85]	1976			10.46 (M)
Serebrennikov[86]	1977		$FeHCO_3^+$, $FeCO_3(aq)$	10.54 (x)
Robie et al.[47]	1978	-29.26(x)	No extra species	10.50 [b]
Reiterer et al.[79,80]	1980		No extra species	10.91 (x[e])
NIST[55]	1982	-25.67	$FeOH^+$	10.50 (x) [b]
Robie et al.[61]	1984			10.60
Greenberg[32]	1986	-22.8	$FeHCO_3^+$, $FeCO_3(aq)$, $FeOH^+$, $Fe(OH)_2(aq)$	10.56 (x[f])
Greenberg and Tomson[33]	1986	-22.9	$FeHCO_3^+$, $FeCO_3(aq)$, $FeOH^+$, $Fe(OH)_2(aq)$	10.605(T,D,M), 10.58 (x)
Nordstrom et al.[49]	1990	-10.38	$FeHCO_3^+$, $FeCO_3(aq)$, $FeOH^+$	10.89, 10.45 [g]
Haarberg et al.[87]	1990		No extra species	10.37 (x,T)
Johnson and Tomson[27,28,29]	1991	-30.14	$FeHCO_3^+$, $FeOH^+$	10.45 (T)
Braun[35]	1991		No extra species	10.99(x[*,h],M,T)
Ptacek and Reardon[88]	1992		$FeHCO_3^+$, $FeCO_3(aq)$, $FeOH^+$	11.06
Ptacek[13]	1992		$FeHCO_3^+$, $FeCO_3(aq)$, $FeOH^+$	11.0-11.2 (D)
Greenberg and Tomson[36]	1992	-9.46	$FeHCO_3^+$, $FeCO_3(aq)$, $FeOH^+$	10.78
Bruno et al.[24]	1992		$FeCO_3(aq)$, $Fe(CO_3)_2^{2-}(aq)$	10.8
Ptacek and Blowes[12]	1994	-10.38 [i]	$FeHCO_3^+$, $FeCO_3(aq)$, $FeOH^+$	11.03 (M)
Robie and Hemingway[48]	1995	-10.4 [i,j]	Unknown	11.53 (x[k])
Garber et al.[89]	1996		Unknown	10.66 (x,T)
Grauer[44]	1999		$FeCO_3(aq)$, $Fe(CO_3)_2^{2-}(aq)$	10.8 [b,l]
	2002		$FeHCO_3^+$, $FeCO_3(aq)$, maybe $FeOH^+$	11.03, 10.43 (D)[m]
Preis and Gamsjäger[45]	2002	-13.23(x)	$FeCO_3(aq)$, $Fe(CO_3)_2^{2-}(aq)$	10.59 (x)
Silva et al.[90]	2002		$FeCO_3(aq)$ maybe more	10.9 (*)

Authors	Year	$\Delta_{r,sp}H°$ (kJ/mol)	Speciation scheme	pK_{sp}
Marion *et al.*[18]	2003		$FeCO_3\,(aq),\ FeOH^+$	11.06 (T^n)
Sun and Nesic[91]	2004		Unknown	10.59 (x)

* ~ Rough estimate due to scatter in data, extrapolation or guess, x ~ calculated by regressed correlation or similar, T ~ temperature correlation given, D ~ experimental data given, M ~ properties at several temperatures given. [a] calculated from $\Delta_{r,sp}G^o = 60.92$ *kJ/mol* given in their work. [b] the value was obtained from Kelley and Anderson[56]. [c] a value of $\Delta_{r,sp}S^o_{FeCO_3}$ =-275.3 *J/(mol·K)* was given. [d] obtained from Latimer[50]. [e] calculated using NIST[55] properties of Fe^{2+} and CO_3^{2-}. [f] calculated by their given correlation. [g] 10.89 is calculated consistently with the remaining speciation. 10.45 is an evaluation of Smith[84] measurements. [h] The value is calculated at a ionic strength of 0.1. [i] obtained from Nordstrom *et al.*[49]. [j] a value of $\Delta_f S^o_{FeCO_3}$ =-252.6 *J/(mol·K)* was given. [k] The value is calculated from the given thermodynamic properties. [l] obtained from Bruno *et al.*[24]. [m] 11.53 of dry crystals and 10.43 of wet crystals. [n] Temperature dependence obtained from $\Delta_{sp}H^o$ of Nordstrom *et al.*[49].

Speciation Schemes

A speciation scheme refers to the number of liquid compounds assumed to be present in a liquid phase. It is usually assumed that $H_2O(l)$, H^+, OH^-, Fe^{2+}, $CO_2(aq)$, HCO_3^-, and CO_3^{2-} are present in a system saturated with $FeCO_3$. In the following sections this is classified as a basic speciation scheme. It could also be assumed that a liquid iron complex is formed and the total iron is distributed between several liquid iron species for example $FeHCO_3^+$ in addition to Fe^{2+}. This will be known as an extended speciation scheme.

Table 21 gives an overview of the various liquid iron species used in the calculation of pK_{sp}. Fe^{2+} is a compound in all calculation of pK_{sp} and therefore not mentioned in table 21. The difference between using a basic and an extended speciation scheme, is the calculated amount of free Fe^{2+} ions. To illustrate this, take two similar solutions of iron. Assume all iron is Fe^{2+} in one solution. In the second solution the same amount of iron is distributed between Fe^{2+} and $FeCO_3(aq)$. Evidently the amount of free Fe^{2+} is reduced if $FeCO_3(aq)$ is present. Accordingly the value of K_{sp} will decrease since the concentration of Fe^{2+} is reduced. The consequence is an observed increase in the pK_{sp} value. It is therefore important that the speciation scheme is carefully chosen equivalent to the scheme for which pK_{sp} was calculated. In the following it is illustrated, how the choice of speciation schemes influence the resulting value of pK_{sp}.

Solubility constant of Reaction (252)

Smith[84] was the first to determine the equilibrium constant of $FeCO_3$. This was done by measuring the total iron and CO_2 content in the liquid phase at anaerobe conditions and at various CO_2 pressures. The value was determined by setting up the mass action laws for the CO_2-H_2O system and reaction (252) assuming the solid phase is in its standard state:

$$K_{CO_2(aq)} = \frac{a_{H^+} a_{HCO_3^-}}{a_{CO_2} a_{H_2O}} \tag{262}$$

$$K_{HCO_3^-} = \frac{a_{H^+} a_{CO_3^{2-}}}{a_{HCO_3^-}} \tag{263}$$

$$K_{sp} = a_{Fe^{2+}} a_{CO_3^{2-}} \tag{264}$$

Fe^{2+}, HCO_3^-, and $Fe(HCO_3)_2(aq)$ were assumed to be the species in the liquid phase. Smith[84] tabulated the total concentration of iron as $Fe(HCO_3)_2(aq)$. The molality of Fe^{2+}, $b_{Fe^{2+}}$, was calculated by:

$$b_{Fe^{2+}} = \alpha \cdot b_{Fe(HCO_3)_2(aq)} \tag{265}$$

α is the degree of ionization. The above relation is an uncommon approach since the total iron is expected to be $b_{T,Fe} = b_{Fe^{2+}} + b_{Fe(HCO_3)_2(aq)} = (1+\alpha)b_{Fe(HCO_3)_2(aq)}$. This way Smith[84] assumed that the total amount of iron is *(1+α)* times higher than the measured value $b_{Fe(HCO_3)_2(aq)}$. This indicates that some inconsistency was introduced. Smith[84] wrote an electroneutrality balance in order to calculate the bicarbonate concentration. It was assumed that only Fe^{2+} and HCO_3^- were present and therefore

$$2b_{Fe^{2+}} = b_{HCO_3^-} \tag{266}$$

K_{sp} was determined by inserting (262) and (263) in (264) to remove a_{H^+} and $a_{CO_3^{2-}}$ from the equation:

$$K_{sp} = \frac{K_{HCO_3^-}}{K_{CO_2(aq)}} \cdot \frac{a_{HCO_3^-}^2 a_{Fe^{2+}}}{a_{CO_2(aq)} a_{H_2O}} \tag{267}$$

Rearranging and substituting (265) and (266) in the above, while assuming solute activities equal to molalities and a water activity of $a_{H_2O} = 1$, gives:

$$K \equiv \frac{\left(\alpha b_{Fe(HCO_3)_2}\right)^3}{b_{CO_2(aq)}} = \frac{K_{CO_2(aq)} K_{sp}}{4 K_{HCO_3^-}} \tag{268}$$

K is defined by the left hand side of the equation. Smith[84] assumed $\alpha \approx 0.9$ and determined K from experimental measurements of iron ($b_{Fe(HCO_3)_2}$) and CO_2 ($b_{CO_2(aq)}$). He obtained $\sqrt[3]{K} = 4.04 \cdot 10^{-3}$ and K_{sp} was determined from (268) by:

$$K_{sp} = \frac{K_{HCO_3^-} K}{4 K_{CO_2(aq)}} \tag{269}$$

using a set of approximated $K_{HCO_3^-}$ and $K_{CO_2(aq)}$ values. Smith[84] obtained $K_{sp} = 3.453 \cdot 10^{-11}$ at 30 °C which is equivalent to $pK_{sp}(30^o C) = 10.46$. He stated that the solubility at zero *CO₂* pressure would be $C_{Fe^{2+}} \approx \sqrt{K_{sp}} \approx 5.8 \cdot 10^{-6}$ *mol/L*. Taking Smiths[84] data, setting $\alpha = 1$ and $b_{T,Fe} = b_{Fe(HCO_3)_2(aq)}$ results in $pK_{sp} = 10.32$ at 30 °C. Tillmans and Klarmann[11] used the same approach using $\alpha = 1$ and arrived at $\sqrt[3]{K} = 7.05 \cdot 10^{-3}$ for their data at 18 °C. They also used approximate values of $K_{HCO_3^-}$ and $K_{CO_2(aq)}$ and calculated $pK_{sp}(18^o C) = 9.57$. This value is very low compared to other later works as shown in figure 52 which may be related to the applied values of $K_{HCO_3^-}$ and $K_{CO_2(aq)}$. The work by Tillmans and Klarmann[11] has not been used in any

later works, but the experimental data by Smith[84] has been reinterpreted numerous times.
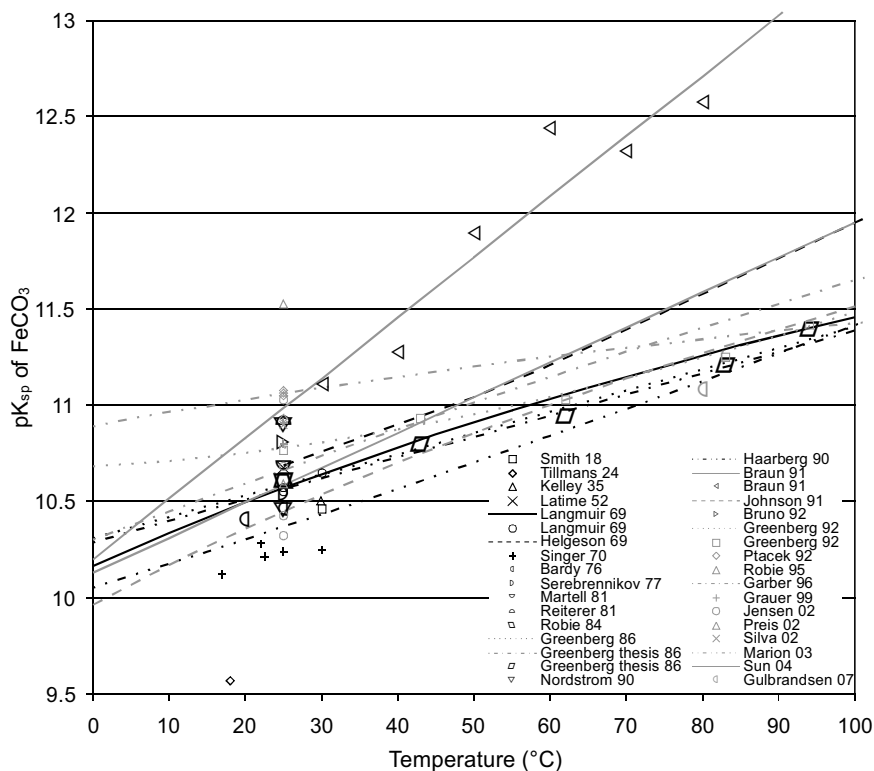
Figure 52: Negative base-ten logarithm to the equilibrium constant, *pK$_{sp}$*, of reaction (252) as function of temperature determined by various authors in the literature. Lines are correlations, symbols are single values.

Kelley and Anderson[56] made an evaluation of the work by Smith[84]. This evaluation is central in the literature, since it was and is still included in many data collections. Kelley and Anderson[56] used the measured $\sqrt[3]{K}=4.04\cdot 10^{-3}$ by Smith[84] at 30 °C using a different set of $K_{HCO_3^-}$ and $K_{CO_2(aq)}$ and obtained $pK_{sp}\left(30^{o}C\right)=10.50$ which correspond to a Gibbs energy of reaction of $\Delta_{r,sp}G\left(30^{o}C\right)=60.92\,kJ/mol$. They corrected K_{sp} to the temperature 25 °C; even though the method is not described as noted by Singer and Stumm[6]. Their conversion reveals a value of $pK_{sp}\left(25^{o}C\right)=10.67$. The result may only be obtained by assuming $\Delta_{r,sp}G\left(30^{o}C\right)=\Delta_{sp}G\left(25^{o}C\right)$ which is a rough approach. $pK_{sp}\left(25^{o}C\right)=10.67$ has unfortunately been adopted by many data collections: Latimer[50], Helgeson[83], Martell and Smith[53], Garber *et al.*[89], Palmer and Eldik[92], Högfeldt[93], Zhuk[94], and Stumm and Lee[22]. Even the $pK_{sp}\left(30^{o}C\right)=10.50$ at 30 °C was adopted by NIST[55] and Robie *et al.*[47] as the value at 25 °C. The correlation by Sun and Nesic[91] seems to originate from

the values given by Helgeson[83]. This may be recognised by comparing the two works in figure 52.

Singer and Stumm[6] were aware of the discrepancies between works. They showed how the biased pK_{sp} has led to numerous wrong interpretations of the $FeCO_3$ solubility and wrong conclusion of supersaturation also noted by Ghosh[95]. Singer and Stumm[6] conducted solubility measurements at four different temperatures between 17 and 30 °C and the solubility constant was re-evaluated. Unfortunately no experimental data were given. A temperature correction was employed by using the heat of solution from Latimer[50] and a value of $pK_{sp} = 10.24$ at 25 °C was obtained. The equilibrium constant is three times higher than the previous $pK_{sp} = 10.67$ by Kelley and Anderson[56].

Bardy and Péré[85] conducted experiments in order to resolve some of the disagreements. They performed solubility measurements of the pure Fe-CO_2-H_2O system, but also in systems of additional ions. pK_{sp} was estimated at zero ionic strength similar to the work by Singer and Stumm[6] using the activity coefficient correlation of Davies[96]. They determined pK_{sp} experimentally at 20 °C and calculated it at T=25 °C using the temperature correction of Singer and Stumm[6] and found $pK_{sp} = 10.46$. It is uncertain how high a precision they obtained from the assumptions they applied.

Many additional authors have determined the equilibrium constant of $FeCO_3$. There are three trends in the literature. One group uses an extended speciation scheme. Another group uses a basic speciation scheme similar to the works mentioned above. Finally a group uses any speciation scheme but base the calculations on scattered measurements and obtains an inaccurate high pK_{sp} value. The groups are discussed here.

Langmuir[51] collected properties of liquid iron species from different $FeCO_3$ related works. An evaluation of Smith[84] data was given even though the results were based on Langmuir's[51] own measurements. He found a relatively high, $pK_{sp} = 10.55$, and gave a temperature correlation using the van't Hoff law. The high value is probably due to the included $Fe(OH)_n^{(2-n)+}$ species. He stated that the properties of $Fe(OH)_2(aq)$ should be considered as tentative and the existence not adequately documented.

Wersin et al.[97] took another approach. They used the speciation scheme by Fouillac and Criaud[98], and added $FeOH^+$ without refitting. The same approach was used by Nordstrom et al.[49] who included the Fouillac and Criaud's[98] properties of $FeHCO_3^+$, the Langmuir[99] properties of $FeCO_3(aq)$, and $FeOH^+$ properties of Baes and Mesmer[59]. Nordstrom et al.[49] chose to give two different values of pK_{sp}. An evaluation of Smith[84] data, $pK_{sp} = 10.45$, and a recalculation which was consistent with the given speciation scheme, $pK_{sp} = 10.89$. This shows clearly the influence of using a different speciation scheme and a significantly higher pK_{sp} is obtained. The work by Nordstrom et al.[49] was later included in the computer models WATEQ4F, MINTEQA2, and PHREEQC, and in the collection by Stumm and

Morgan[100] which has since made their equilibrium constants widely used. Still, the database has room for improvements.

Greenberg and Tomson[36] applied the Nordstrom et al.[49] speciation scheme using activity coefficients correlation of Davies[96] and a relatively high equilibrium constant was found, $pK_{sp} = 10.78$. Johnson and Tomson[27,28,29] made a similar study on *FeCO₃*. The method is not described in detail but they determined a temperature correlation of the equilibrium constant using less speciation compared to Greenberg and Tomson[36]. Even with the amount of species included they found a low $pK_{sp} = 10.45$.

Previously Greenberg and Thomson[32,33] used another scheme and arrived at approximately $pK_{sp} = 10.6$. Their calculations are not clear and they used *CaCO₃* properties in their *FeCO₃* calculations. Ptacek et al.[88,12,13] adopted the speciation scheme from Nordstrom et al.[49] and refitted the equilibrium constant of *FeCO₃* using a Pitzer model and obtained approximately $pK_{sp} \approx 11$. Marion et al.[18] reinterpreted the data by Ptacek[13]. They arrived at more or less the same K_{sp} since they used a similar speciation scheme and many of the Nordstrom et al.[49] properties. It is unfortunate that they are missing crucial parameters of the liquid iron species and used parameters from *MgCO₃* assuming they were valid for *FeCO₃*. Figure 52 shows pK_{sp} used by Marion et al.[18] plotted together with pK_{sp} of other authors. The temperature dependence of the correlation by Marion et al.[18] is significantly different from other works. It should be seen as uncertain.

Jensen et al.[1] made a critical evaluation of pK_{sp}. They were aware of some of the problems described here, even though parts of the Nordstrom et al.[49] speciation scheme was used. Two different equilibrium constants of *FeCO₃* were determined for two types of measurements, a $pK_{sp} = 10.32$ and $pK_{sp} = 10.68$ were determined. The Fouillac and Criaud[98] equilibrium constant of $FeCO_3(aq)$ and $FeHCO_3^+$ was also used and two new equilibrium constants, $pK_{sp} = 10.43$ and $pK_{sp} = 11.03$, were found. The two scenarios clearly show the influence of using a different speciation scheme. The Fouillac and Criaud[98] scheme produces more $FeCO_3(aq)$ and $FeHCO_3^+$ and resulted in a lower equilibrium constant of $FeCO_3(s)$. If a simple speciation scheme had been used then evidently a smaller pK_{sp} was found.

An alternative speciation scheme was suggested by Davies and Burstein[101] in which $Fe(CO_3)_2^{2-}(aq)$ was presumed to exist. They referred to the work by Sidgwick[102] but Sidgwick[102] only mentioned $Fe(HCO_3)_2(aq)$. $Fe(CO_3)_2^{2-}(aq)$ was also taken up by Wieckowski et al.[103] and later by Bruno et al.[24] and Wersin[9] who determined the equilibrium constant of $Fe(CO_3)_2^{2-}(aq)$. Bruno et al.[24] gave a value of $pK_{sp} = 10.8$, which is relatively high due to the unusual speciation.

Grauer et al.[44] made a summary of some of the *FeCO₃* related works and chose to recommend the value of Bruno et al.[24]. The discussion is not elaborate and the value is recommended from a rough weighing of available works.

Recently $Fe(CO_3)_2^{2-}(aq)$ was included in the work by Preis and Gamsjäger[45] who made a critical study of *FeCO₃* properties and re-evaluated the data from Smith[84], Bruno et al.[24], Reiterer et al.[79,80], and Silva et al.[90]. They included a set of recalculated

equilibrium constants from Greenberg and Tomson[36] and included almost the same speciation scheme of Bruno et al.[24] and arrived at $pK_{sp} = 10.59$. This value is somewhat intermediate but indicates that the pK_{sp} may be lower if the Bruno et al.[24] speciation was not used. Even though the work by Preis and Gamsjäger[45] should be seen as consistent within the framework of their speciation scheme.

It is apparent from the overview given here that values of the equilibrium constants depend on the speciation considered. It must be emphasized that equilibrium constants from different studies should not be combined without a critical examination of the assumptions.

Some authors have chosen to keep a basic speciation scheme applying a low amount of iron species. One of the works was made by Haarberg et al.[87] who reinterpreted the experimental studies by Smith[84], Bardy and Péré[85], and Greenberg[32] using a basic speciation scheme and a Pitzer equation. Their result is consistent and they present a correlation of the pK_{sp} as function of temperature up to 200 °C. The calculated value at 25 °C $pK_{sp,25°C} = 10.37$ which is comparable to the equilibrium constant of Smith[84] and Singer and Stumm[6].

Robie et al.[61] also re-evaluated the data by Smith[84] together with a set of unpublished data. The speciation by Langmuir[51] was used and they obtained a $pK_{sp} = 10.60$, which is similar to the work of Langmuir[51], $pK_{sp} = 10.55$.

Braun[35] used a basic speciation scheme analogous to Haarberg et al.[87]. The obtained equilibrium constant was determined at an ionic strength of 0.1 *mol/kg H₂O* and they found a $pK_{sp} = 10.99$. This is a high value and may be explained by the applied ionic strength but also by the high scatter in their data. Their pK_{sp} was determined in the temperature interval 30 to 80 °C, but if the measurements are constrained between 40 and 60 °C, then $pK_{sp,25C} = 10.4$ is obtained. The same problems were introduced by Silva et al.[90]. They conducted an experimental study at 25 °C in *NaCl* solutions. Silva et al.[90] applied the equilibrium constants of Thurmond and Millero[104] using a Pitzer model by Millero et al.[105,10]. The Pitzer model was used with a speciation scheme similar to Bruno et al.[24], see table 21. The scheme is inconsistent with the original Bruno et al.[24] scheme since $FeCO_3(aq)$ was included. Their equations, figures and tables are in disagreement and the modelling should be seen as tentative. They arrive at an equilibrium constant of $pK_{sp} = 10.9$ due to the speciation used, but also due to the high scatter of their result. By removing two out of their nine data points used for their linear pK_{sp} correlation gives a $pK_{sp} = 10.4$. Their result is uncertain and may be improved.

Solubility constant of Reaction (253)

The solubility constant of *FeCO₃* represented by reaction (253) can be determined explicitly, since the equilibrium constants of the *CO₂-H₂O* system are not required. Instead it is obtained directly by the mass-action law:

$$K_{psp} = \frac{a_{Fe^{2+}} f_{CO_2} a_{H_2O}}{a_{H^+}^2} \qquad (270)$$

This is done by measuring *pH*, iron content and CO_2 pressure. Water is usually assumed ideal and the partial pressure of CO_2 is substituted for the fugacity of CO_2. Table 22 gives an overview of the authors who used this method. Reiterer *et al.*[79,80] were the first to use this approach for $FeCO_3$. $\Delta_f G^o_{FeCO_3,50°C}$ was determined and converted to $\Delta_f G^o_{FeCO_3,25°C}$ =-669.02 *kJ/mol*. Jensen *et al.*[1], Silva *et al.*[90] and Bruno *et al.*[24] stated that Reiterer *et al.*[79] found a value of $pK_{sp} = 11.20$, but it is unclear how they obtained this value. Reiterer *et al.*[79] did not publish this value but gave a $pK_{psp} = 7.61$ at 50 °C and an ionic strength of one. Using the NIST[55] standard thermodynamic properties of $Fe^{2+}(aq)$ and $CO_3^{2-}(aq)$ results in a pK_{psp} converted to $pK_{sp} = 10.9$. This value is high, which may be related to the high ionic strength and the difference in the used properties of $Fe^{2+}(aq)$. Reiterer *et al.*[79] did not correct the calculated pK_{psp} using an activity coefficient model even though they stated so.

Table 22: Literature, $\Delta_{r,psp}H°$, speciation scheme, and pK_{psp}, of reaction (253) at 25 °C and 1 bar.

Authors	Year	$\Delta_{r,psp}H°$ (kJ/mol)	Speciation scheme	pK_{psp}
Reiterer *et al.*[79,80]	1980		No extra species	-7.61 (50 °C, I=1molal)
Wersin[9]	1990		$FeCO_3(aq)$, $Fe(CO_3)_2^{2-}(aq)$	-7.69 (I=1M), -7.35 (I=0M)
Bruno *et al.*[24]	1992		$FeCO_3(aq)$, $Fe(CO_3)_2^{2-}(aq)$	-7.59 (I=1M), -7.65 (I=?)
Preis and Gamsjäger[45]	2002	-17.3	$FeCO_3(aq)$, $Fe(CO_3)_2^{2-}(aq)$	-7.56
Silva *et al.*[90]	2002		$FeCO_3(aq)$ maybe more	-6.95(*)

* ~ Rough estimate due to scatter in data, extrapolation or guess. I ~ Ionic strength.

Reiterer *et al.*[79] used a basic speciation scheme, opposite Wersin[9], Bruno *et al.*[24], and Preis and Gamsjäger[45] who all introduced $Fe(CO_3)_2^{2-}(aq)$, see table 22. Wersin[9] and Bruno *et al.*[24] determined pK_{psp} at an ionic strength of one and calculated the value at zero ionic strength using the SIT[106] model. Both authors obtained high values which are comparable to the value of Reiterer *et al.*[79]. Bruno *et al.*[24] obtained an unusual result; the pK_{psp} is lower at an ionic strength of one compared to an ionic strength zero which is opposite all other studies so far.

The work by Silva *et al.*[90] must be considered as uncertain since their method and speciation scheme is questionable as discussed previously.

8.2.9   Equilibrium constant of FeHCO₃⁺, FeCO₃(aq), and Fe(CO₃)₂²⁻

The existence of the three species, $FeHCO_3^+$, $FeCO_3(aq)$, and $Fe(CO_3)_2^{2-}(aq)$, has been widely debated in the literature. Some authors decided to include them; others have deliberately left them out of their speciation. Table 23, 24, and 25 give an overview of the authors who determined the related properties of the following reactions respectively:

$$FeCO_3(aq) \rightleftarrows Fe^{2+}(aq) + CO_3^{2-}(aq) \tag{271}$$

$$FeHCO_3^+ (aq) \rightleftarrows Fe^{2+}(aq) + HCO_3^- (aq) \qquad (272)$$

$$Fe(CO_3)_2^{2-}(aq) \rightleftarrows Fe^{2+}(aq) + 2CO_3^{2-}(aq) \qquad (273)$$
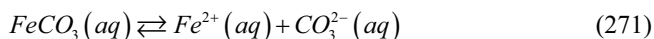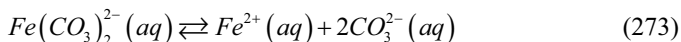
Table 21 to 25 gives an overview of all speciation schemes used. All three species are rarely included in combination. Usually only $FeCO_3(aq)$ and $FeHCO_3^+$ are used or $FeCO_3(aq)$ and $Fe(CO_3)_2^{2-}(aq)$. Very few of their properties were determined consistently, meaning that they were not found by the same authors by fitting to the same data simultaneously.

It has previously been shown that $CaHCO_3^+$ and $MnHCO_3^+$ could exist as compounds[6,107]. Larson[108] was the first to discuss how $FeHCO_3^+$ could explain supersaturation. Later Serebrennikov[86], Mattigod and Sposito[109], and Fouillac and Criaud[98] based their $FeHCO_3^+$ and $FeCO_3(aq)$ speciation on correlations of other works and extrapolated to the non investigated iron systems. Their results should be seen as approximate.

Table 23: Properties related to *FeCO₃(aq)*, reaction (271).

Authors	Year	Speciation scheme	pK
Serebrennikov[86]	1977	$FeHCO_3^+$, $FeCO_3(aq)$	-4*
Mattigod and Sposito[109]	1977	$FeHCO_3^+$, $FeCO_3(aq)$, $Fe(CO_3)_2^{2-}(aq)$, $FeOH^+$, $Fe(OH)_2(aq)$, $Fe(OH)_3^-$, $Fe(OH)_4^{2-}$	-6.57(*,x)
Turner et al.[112]	1981	$FeCO_3(aq)$, $FeOH^+$, $Fe(OH)_2(aq)$, $Fe(OH)_3^-$, $Fe(OH)_4^{2-}$	-4.73
Fouillac and Criaud[98]	1984	$FeHCO_3^+$, $FeCO_3(aq)$	-4.73 ª
Nordstrom et al.[49]	1990	$FeHCO_3^+$, $FeCO_3(aq)$, $FeOH^+$	-4.38 ᵇ
Bruno et al.[24]	1992	$FeCO_3(aq)$, $Fe(CO_3)_2^{2-}(aq)$	-5.5
Millero and Hawke[105]	1992	$FeHCO_3^+$, $FeCO_3(aq)$, $Fe(CO_3)_2^{2-}(aq)$, $FeOH^+$, $Fe(OH)_2(aq)$	-5.45 ᶜ
Silva et al.[90]	2002	$FeCO_3(aq)$ maybe more	-6.3(*)
Preis and Gamsjäger[45]	2002	$FeCO_3(aq)$, $Fe(CO_3)_2^{2-}(aq)$	-5.3

* ~ Rough estimate due to scatter in data, extrapolation or guess. x ~ calculated. ª $\Delta_f H^o_{FeCO_3(aq)}$=0.29 *kJ/mol*. ᵇ calculated by the oxalate correlation of Langmuir[99]. ᶜ obtained from Bruno et al.[24].

Nordstrom et al.[49] collected some of these properties. $FeHCO_3^+$ properties originated from Fouillac and Criaud[98] who did not include $FeOH^+$. This is noteworthy, since Nordstrom et al.[49] included it. The equilibrium constant of $FeOH^+$ was based on the work by Baes and Mesmer[59,110] and Sweeton and Baes[111]. They justified the existence of $FeOH^+$, $Fe(OH)_2(aq)$, and $Fe(OH)_3^-$ by the least square fitting of equilibrium

constants to the solubility data of *Fe(OH)₂* and *Fe₃O₄*. Nordstrom *et al.*[49] included only *FeOH⁺*. A consistent model would include all three complexes of iron. Nordstrom *et al.*[49] also included the $FeCO_3(aq)$ properties; they were not taken from the work of Fouillac and Criaud[98] as expected, similar to $FeHCO_3^+$, but from the oxalate correlation of Langmuir[99]. Nordstrom *et al.*[49] obtained some consistency by fitting one of the equilibrium constants similar to Silva *et al.*[90]. Bruno *et al.*[24] fitted all equilibrium constants to their data. Turner *et al.*[112] and Millero and Hawke[105] collected properties without refitting. Millero and Hawke[105] used the equilibrium constants of Bruno *et al.*[24] and extended the speciation scheme by $FeHCO_3^+$. This is noteworthy since Bruno *et al.*[24] and Wersin[9] determined that $FeHCO_3^+$ does not exist as species, even though Wersin *et al.*[97] used a speciation scheme which included this compound.

Marion *et al.*[18] stated that they re-estimated much of the thermodynamic properties of $FeCO_3(aq)$ and $FeOH^+$ even though they originate from Nordstrom *et al.*[49].

Table 24: Properties related to *FeHCO₃⁺(aq)*, reaction (272).

Authors	Year	Speciation scheme	pK
Serebrennikov[86]	1977	$FeCO_3(aq), FeHCO_3^+$	-2*
Mattigod and Sposito[109]	1977	$FeHCO_3^+, FeCO_3(aq), Fe(CO_3)_2^{2-}(aq),$ $FeOH^+, Fe(OH)_2(aq), Fe(OH)_3^-, Fe(OH)_4^{2-}$	-2.05(*,x)
Fouillac and Criaud[98]	1984	$FeCO_3(aq), FeHCO_3^+$	-2.17 [a]
Nordstrom *et al.*[49]	1990	$FeHCO_3^+, FeCO_3(aq), FeOH^+$	-2 [b]
Millero and Hawke[105]	1992	$FeHCO_3^+, FeCO_3(aq), Fe(CO_3)_2^{2-}(aq),$ $FeOH^+, Fe(OH)_2(aq)$	-1.47(*,xᶜ)

* ~ Rough estimate due to scatter in data, extrapolation or guess. x ~ calculated. [a] $\Delta_f H^o_{FeHCO_3^+}$ =4.35 *kJ/mol*. [b] obtained from the rough estimate by Fouillac and Criaud[98]. [c] extrapolated from other system from correlation of K_{sp}.

The question is whether $FeHCO_3^+$, $FeCO_3(aq)$, and $Fe(CO_3)_2^{2-}(aq)$ exist at all. Singer and Stumm[6] discussed this subject. They concluded that $FeHCO_3^+$ does not form and most likely not $FeCO_3(aq)$. The same was concluded by Johnson and Bauman[74]. Davies and Burstein[101] indicated on the other hand, that $Fe(CO_3)_2^{2-}(aq)$ exist, but not $FeOH^+$. This also contradicts Serebrennikov[86] who stated that $FeHCO_3^+$ could account for up to 50% of the total iron and should therefore be equivalent to the concentration of Fe^{2+}. In the speciation by Jensen[2], $FeHCO_3^+$ account for 26-41% and $FeCO_3(aq)$ for 1-5%.

Table 25: Properties related to *Fe(CO₃)₂²⁻(aq)*, reaction (273).

Authors	Year	Speciation scheme	pK
Mattigod and Sposito[109]	1977	$FeHCO_3^+$, $FeCO_3(aq)$, $Fe(CO_3)_2^{2-}(aq)$, $FeOH^+$, $Fe(OH)_2(aq)$, $Fe(OH)_3^-$, $Fe(OH)_4^{2-}$	-9.51(*,x)
Bruno et al.[24]	1992	$FeCO_3(aq)$, $Fe(CO_3)_2^{2-}(aq)$	-7.1
Millero and Hawke[105]	1992	$FeHCO_3^+$, $FeCO_3(aq)$, $Fe(CO_3)_2^{2-}(aq)$, $FeOH^+$, $Fe(OH)_2(aq)$	-7.17 [a]
Preis and Gamsjäger[45]	2002	$FeCO_3(aq)$, $Fe(CO_3)_2^{2-}(aq)$	-7.1 [a]

* ~ Rough estimate due to scatter in data, extrapolation or guess. x ~ calculated. [a] obtained from Bruno et al.[24].

It is unfortunate that species which have low experimental basis have been included in the highly cited works of for example Nordstrom et al.[49]. It is also notable that the critical evaluation by Preis and Gamsjäger[45] chose to include $Fe(CO_3)_2^{2-}(aq)$ even though it has a low experimental basis.

8.2.10 Supersaturation

The possible supersaturation of *FeCO₃* solutions has been widely debated in the literature and continues to be so. There are two groups which discuss this. One group used thermodynamic properties of *FeCO₃* where the calculated and the measured solubilities were different. They concluded that the solutions were supersaturated. Another group observed supersaturation due to improper handling of the liquid samples.

The reason why the first group observed supersaturation is basically due to inconsistency between equilibrium constants, speciation scheme and the measured solubilities. A group of studies were unaware of this problem. Bruno et al.[24] for example stated that supersaturation was observed and refer to the existence of $Fe(CO_3)_2^{2-}(aq)$. Similarly Larson[108] stated that supersaturation is related to the formation of $FeHCO_3^+$. Emerson[113] indicated that using an erroneous equilibrium constant resulted in a wrong calculated solubility. Still it was discussed that supersaturation could be related to $FeHCO_3^+$ formation. Ghosh[95] showed that using the correct equilibrium constant gives saturation and not supersaturation. An apparent supersaturation can be observed if an erroneous equilibrium constant of $FeCO_3(s)$ is used or if a constant which is inconsistent with the speciation scheme is used. The authors tend to include new unusual compounds in order to explain an observed supersaturation. This is also why the existence of $FeHCO_3^+$, $FeCO_3(aq)$, and $Fe(CO_3)_2^{2-}(aq)$ have been suggested. The reason is often that their equilibrium constants are fitted to experimental data in combination with other equilibrium constants of lower quality.

The other group which has discussed supersaturation were e.g. Hem[5] and Stumm and Singer[8]. Their discussions were related to ground-waters, but the issues are also

applicable to other systems. The problems were mainly related to improper or poor handling of the samples which could for example explain the supersaturation observed by Postma[114]. Problems were basically due to measurements at atmospheric laboratory condition, which did not resemble the reservoir conditions. Other problems could be related to the used equipment. The equilibrium measurements discussed by Gamsjäger[115] and Gamsjäger and Königsberger[116] showed that vigorous stirring could result in supersaturation due to carryover of solid to the measuring cells. Ghosh *et al.*[7] observed a 20 to 30 time supersaturation in their measurements, which may be explained by the pK_{sp} of *FeCO₃* at 25 °C, used at 10 °C. Jensen *et al.*[1,2]

observed continuous supersaturation, which could be related to leaking containers or due to the added *MnCl₂* and *CaCl₂* salt.

Other authors were unaware of supersaturation and have inadvertently published supersaturated results as equilibrium data. Tillmans and Klarmann[11] and Klarmann[117] state that a group of old works before 1900 did not recognise how *FeCO₃* may supersaturate before equilibrium. The time to reach equilibrium was shown experimentally by Müller *et al.*[118,119]. Equilibrium was attained within few hours at 50 atm *CO₂*. Dugstad[120] stated it could take 40 hours and Leybold[121] stated that equilibrium was not obtained within ten weeks at 1 atm *CO₂*. Jensen *et al.*[1] observed even longer equilibrium times. Wajon *et al.*[31] observed similar kinetics in *CaCO₃* solutions where equilibrium was not reached within six weeks.

In recent studies a soluble iron salt has been used to deliberately study the effect of supersaturation e.g. Dugstad[120] showed the importance of iron supersaturation on *CO₂* corrosion and the resulting corrosion protection and Dugstad and Drønen[122] discussed the influence of supersaturation on the morphology and structure of the corrosion scales. Their studies are ongoing and recently Gulbrandsen[43] discussed supersaturation to prevent corrosion from acetic acid in iron solutions.

Often the observed Fe^{2+} supersaturation is not appreciated and usually it is sought avoided. The above shows that "supersaturation" may be related to many different issues during measurements and calculation of results. The experimental equipment should be carefully setup in order to avoid erroneous measurements and the equilibrium constants should only be used in the speciation scheme that they were originally determined.

Other speciation schemes in the Fe-CO₂-H₂O system

A number of authors have applied speciation schemes for the *Fe-CO₂-H₂O* system which are not typical. Table 26 gives an overview of some of the species used in the various studies. Stumm and Lee[22] gave a review of iron chemistry. They used the K_{sp} of Kelley and Anderson[56] in combination with hydroxide properties. The resulting scheme is not accurate since hydroxides were not used by Kelley and Anderson[56]. Palmer and Eldik[92] followed the same approach but included the $FeHCO_3^+$ complex instead of hydroxides.

Table 26: Alternative speciation used for *FeCO₃* modelling.

Authors	Year	Speciation scheme
Stumm and Lee[22]	1960	$FeOH^+$, $Fe(OH)_2(aq)$, $Fe(OH)_3^-$
Langmuir[99]	1979	$FeHCO_3^+$, $FeCO_3(aq)$
Palmer and Eldik[92]	1983	$FeHCO_3^+$
Wersin et al.[97]	1989	$FeHCO_3^+$, $FeCO_3(aq)$, $FeOH^+$
Millero et al[123]	1995	$FeHCO_3^+$, $FeCO_3(aq)$, $Fe(CO_3)_2^{2-}(aq)$, $FeOH^+$, $Fe(OH)_2(aq)$
King[124]	1998	$FeHCO_3^+$, $FeCO_3(aq)$, $Fe(CO_3)_2^{2-}(aq)$, $FeCO_3(OH)^-$, $FeOH^+$, $Fe(OH)_2(aq)$
Jimenez-Lopez and Romanek[125]	2004	$FeHCO_3^+$, $FeCO_3(aq)$, $Fe(CO_3)_2^{2-}(aq)$, $FeOH^+$

A correlation between oxalate equilibrium constants were given by Langmuir[99]. The data were not fitted consistently but the study is important since it was used in a significant amount of speciation schemes, for example the one by Nordstrom et al.[49]. Wersin et al.[97] applied a speciation scheme almost equivalent to the later work by Nordstrom et al.[49]. They decided to change this scheme in the study of Bruno et al.[24]. Millero et al[123], King[124], and Jimenez-Lopez and Romanek[125] used an extended speciation scheme which included $FeHCO_3^+$, $FeCO_3(aq)$, and $Fe(CO_3)_2^{2-}(aq)$. All authors stated that the work was based on the speciation of Bruno et al.[24]. This is notable since Bruno et al.[24] stated explicitly that the existence of $FeHCO_3^+$ could not be justified.

Other questionable assumptions have been made. For example Millero et al[123] included a number of interaction parameters in their *FeCO₃* model which were fitted to the copper system. King[124] used the Pitzer model of Milllero and Hawke[105] unmodified. He added more species without refitting the equilibrium constants and the Pitzer parameters. It is stated that $FeCO_3(OH)^-$ could be justified by the modelling given by the following reaction:

$$Fe(CO_3)(OH)^-(aq) \rightleftarrows Fe^{2+} + OH^- + CO_3^{2-} \tag{274}$$
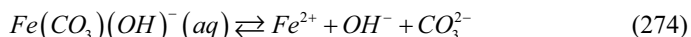
He stated that the equilibrium constant, $pK_{Fe(CO_3)(OH)^-}$, of the above reaction was -9.97. The effect of the new species is very small and less than the scatter in the experimental data. It is doubtful whether this compound exists. It is up for discussion whether the model is consistent, since constants and parameters of different models were used without refitting.

8.2.11 Comment on equilibrium constants of iron hydroxides

The iron hydroxide species, $Fe(OH)_n^{+2-n}$ n=0..4, have been discussed equivalent to $FeHCO_3^+$, $FeCO_3(aq)$, and $Fe(CO_3)_2^{2-}(aq)$.

Sweeton and Baes[111] studied the hydrolysis of iron which has been re-evaluated by Baes and Mesmer[59,110]. The properties were justified by fitting equilibrium constants to solubility measurements, and activity models were not applied. Table 27 gives an overview of the speciation used by the various authors. It shows how Baes and Mesmer changed the speciation scheme between studies. Baes and Mesmer[110] stated specifically that $Fe(OH)_4^{2-}$ could not be justified. The studies gave significantly different results. Equilibrium constants are 10 orders of magnitude different, and the speciation schemes and thermal properties vary significantly. The constants by Baes and Mesmer[59] are widely used since one was included in the work by Nordstrom *et al.*[49] and NIST[55]. But these works only included the properties of $FeOH^+$ and not the remaining three species.

The properties determined by Leussing and Kolthoff[126] were used in the collection by Langmuir[51] and have therefore also been used by a considerable number of authors. More recently Shock *et al.*[127] gave an alternative speciation scheme which included $FeO(aq)$ and $HFeO_2^-$. It has been shown that FeO is not stable at lower temperatures[128] and there are some disagreements between works. The same was suggested previously by Gayer and Woontner[129], who determined the solubility of $Fe(OH)_2(s)$ in $NaOH$ solutions. Their data indicate that $Fe(OH)_3^-$ and $Fe(OH)_4^{2-}$ are more likely to be $HFeO_2^-$ and FeO_2^{2-} which was also mentioned by Tremaine *et al.*[69]

Table 27: Speciation used by a selection of ferrous hydroxide studies.

Authors	Year	Speciation scheme
Gayer and Woontner[129]	1956	$FeOH^+$, $Fe(OH)_2(aq)$, $HFeO_2^-$, FeO_2^{2-}
Sweeton and Baes[111]	1970	$FeOH^+$, $Fe(OH)_2(aq)$, $Fe(OH)_3^-$
Baes and Mesmer[59]	1976	$FeOH^+$, $Fe(OH)_2(aq)$, $Fe(OH)_3^-$, $Fe(OH)_4^{2-}$
Tremaine *et al.*[69]	1977	$FeOH^+$, $HFeO_2^-$, FeO_2^{2-}
Tremaine and LeBlanc[70]	1980	$FeOH^+$, $Fe(OH)_2(aq)$, $Fe(OH)_3^-$
Baes and Mesmer[110]	1981	$FeOH^+$, $Fe(OH)_2(aq)$, $Fe(OH)_3^-$
Shock *et al.*[127]	1997	$FeOH^+$, $FeO(aq)$, $HFeO_2^-$

8.3   Experimental literature data on FeCO₃

8.3.1   Aqueous solubility

The solubility of *FeCO₃* has been determined a number of times. Table 28 summarises the works and outlines the used temperature, pressure, and ions. The ionic strength of the solution is often set deliberately. This is done in order to get a low liquid junction potential while measuring *pH* or to simplify the equilibrium constant calculations by fixing the ionic strength for the activity coefficient models. Frequently authors[6,85,79,80,24] assume the ions to be independent of the solvent medium. This indicates that there is no distinction between *FeCO₃* solubility in for example the *NaCl-H₂O* medium or in the *KNO₃-H₂O* medium. In reality activity coefficient are

different between the systems and ionic interaction are present. It is not advisable to set the ionic strength of the system, since the error related to the activity coefficient calculation can be significantly lowered by looking at the solubilities in the pure systems instead.

Recently some authors[24,1,90] applied more advanced methods to calculate activity coefficients which included the interaction between ions. Usually interaction parameters are not available, and occasionally these are used across systems[13]. This method is inconsistent and should be avoided.

Oxygen contamination was carefully eliminated by most authors and it should be, since oxygen rapidly oxidises Fe^{2+} to Fe^{3+}. Often this is done by purging the solutions using N_2 or CO_2.

The works shown in table 28 may be divided into two groups: Data that are either suitable or not suitable for thermodynamic modelling. Data that are not suitable for such use may be due to missing composition, missing temperature, missing information on CO_2 pressure, or ions were added to set the ionic strength.

Incomplete datasets were given by Langmuir[51], Singer and Stumm[6], Davies and Burstein[101], Braun[35], and Hunnik *et al.*[30]. Most of the data were shown in figures, but measured values were not tabulated. Similarly Robie *et al.*[61] used data which were never published.

In the works by Ehlert and Hempel[130], Leybold[121], Baylis[131], and Davies and Burstein[101] the equilibrium temperature was not measured. Lan and Jia[132] and Jensen *et al.*[1] did not focus on temperature control and their data are given with an accuracy of ±2.5 °C.

The works by Gould[133], Leybold[121], and Haehnel[134] are subject to some uncertainty and it is unclear if equilibrium was obtained. A kinetic study was performed by Johnson and Tomson[27,28,29]. The solubility was measured while changing the temperature and the temperature was kept constant 48h before and a few hours after the experiment. It is unclear if equilibrium was obtained within this time. Similarly Klarmann[117], discusses some of the previous works before 1900, which have not been included here, since it is also unclear if equilibrium was obtained.

Haehnel[134] and Dugstad[120] gave small datasets on $FeCO_3$ solubility but unfortunately listed the concentration in an undefined unit. The works by Brauns[135], Lyden[136] and Teodorovich[137] listed solubility of minerals but the salts were taken from nature and were not pure.

The CO_2 pressure has a significant influence on the $FeCO_3$ solubility. It affects the *pH* and the carbonate content in the liquid phase. Gould[133] and Leybold[121] used a high CO_2 pressure but neglected to measure the value, which is problematic. The same problem was introduced by Bardy and Péré[85]. They equilibrated CO_2 in oxygen free water at 20 °C and used the enriched CO_2 water for their $FeCO_3$ solubility experiments. The pressure was not measured, but the total carbon content was determined. Their data table lists the carbon content, but the unit is unfortunately missing.

Wells[138], Konz[139], and Lan and Jia[132] did not report the CO_2 content or pressure. The same was the case for Braun[35] who flushed the solutions by nitrogen; it is unclear if CO_2 evaporated. Johnson and Tomson[27,28,29] and Jensen *et al.*[1] used containers completely filled with liquid and used small gas phases. The CO_2 content was low and equal to the CO_2 pressure of aqueous $FeCO_3$ solutions.

Ions were used in some works to set the ionic strength of the solutions. Singer and Stumm[6], Reiterer *et al.*[79,80], and Wersin[9] used perchlorate to set the ionic strength

since it was believed not to form aqueous iron complexes. Bruno *et al.*[24] published the works of Wersin[9] and the two datasets are identical. Similarly Bardy and Péré[85] and Silva *et al.*[90] used other ions to set the ionic strength. Ehlert and Hempel[130], Konz[139], Babcan[140], Ptacek[13], and Jensen *et al.*[1] determined the solubility to show the effect of different ions. Braun[35] and Lan and Jia[132] added various *pH* buffers to set the *pH*. This complicates matters significantly, since the buffers contain several salts and the interactions are unknown. The work by Silva *et al.*[90] show the effect of *pH*, from their description it is unclear how they changed *pH* and exactly which ions were added to their mixtures.

Table 28: List of experimental literature data on aqueous *FeCO₃* solubility.

Authors	Year	Added salts	CO_2 Pressure	Temperature
Günzburg [141]	1911	None	1 atm	25 °C
Ehlert and Hempel[130]	1912	None or Na_2SO_4, $NaCl$, $MgCl_2$, $MgSO_4$	none and 2 atm	NA
Wells[138]	1915	None, sulphates	NA	15 °C
Smith[84]	1918	None	a	30 °C
Haehnel[134 b,c]	1924	None	1 and 56 atm	18 °C
Leybold[121 b]	1924	Tab water	NA (high)	NA
Tillmans and Klarmann[11]	1924	None	a	18 °C
Baylis[131]	1926	None or $NaOH$ and $Ca(OH)_2$	c	NA
Müller and Henecka[119]	1929	None	50 atm	20 °C
Müller and Harant[118]	1935	None	50 atm	40,60,80 °C
Konz[139]	1966	K_2CO_3, $KHCO_3$	NA	110 °C
Gould[133 b]	1968	None	NA (high)	23.9 °C
Langmuir[51 d]	1969	NA	NA	NA
Singer and Stumm[6 d]	1970	$NaHCO_3$ and $HClO_4$	a	22.5 °C
Babcan[140]	1974	$FeCl_2$, $MgCO_3$, $CaCO_3$, $NaCl$	2 to 22 atm	25 to 200 °C
Bardy and Péré[85 c]	1976	None or $NaClO_4$, $NaCl$, KNO_3, Na_2SO_4, $MgSO_4$, $CaSO_4$, $CaCl_2$, $MgCl_2$	NA (higher than 0)	20 °C
Reiterer and Gamsjäger[79,80]	1980	$NaClO_4 + HClO_4$	0.084, 0.84 bar	50 °C
Davies and Burstein[101]	1980	$KHCO_3$	NA	NA
Johnson and Tomson[27,28,29 b,d]	1991	None	None (low or 0)	35 °C, 79 °C
Braun[35 d]	1991	*pH* Buffers (I=0.1)	None (low or 0)	30 to 80 °C
Dugstad[120 c]	1992	None	1bar	15 to 72 °C
Bruno *et al.*[24] and Wersin[9]	1992	$NaClO_4$	0.01, 0.05 atm	25 °C
Ptacek[13]	1992	None or $NaCl$, $NaHCO_3$ or Na_2SO_4 or $FeSO_4$	0.0001 to 0.003 atm[a]	25 °C
Greenberg and Tomson[36]	1992	None	2.5-3.0 bar	25 to 94 °C
Andersen and Valle[142]	1993	NA	0.2-3.0 bar	20 to 80 °C
Hunnik *et al.*[30]	1996	NA	1-5.6 bar	40 to 106 °C
Lan and Jia[132]	1996	*pH* Buffers	NA	22.5°C±2.5°C
Jensen *et al.*[1]	2002	$CaCl_2$, $MnCl_2$, $NaHCO_3$	None (low or 0)	15 °C±1.5 °C
Silva *et al.*[90]	2002	$NaCl$, $NaHCO_3$	0.05 bar CO_2	25 °C

NA ~ Not stated. [a] CO_2 content in liquid phase determined. [b] Unclear if equilibrium was attained. [c] missing unit on a measured value. [d] no experimental data tabulated.

Another group of authors gave complete dataset and chose not to adjust the ionic strength. Smith[84] and Tillmans and Klarmann[11] measured the *FeCO₃* solubility and

determined the total carbon content in the liquid phase. Günzburg [141], Haehnel[134], Müller and Henecka[119], Müller and Harant[118], Dugstad[120], Greenberg and Tomson[36], and Andersen and Valle[142] measured the solubility and gave the CO_2 pressure. The measurements by Andersen and Valle[142] were briefly described and no experimental details were revealed. Ptacek[13] is the only author who determined both CO_2 pressure and the total carbon content in the liquid phase. The main part of Ptacek's[13] work is focused on mixtures of many salts, but seven data points were measured in pure water or the mixture of $NaHCO_3$-H_2O. A larger number of her data points were measured in the $NaHCO_3$-$NaCl$-H_2O salt mixture.

Müller and Henecka[119] performed their experiments in a broad temperature and pressure interval, but chose only to give the solubility at 20 °C and 50 atm. The work was continued by Müller and Harant[118]. The two works are comparable. Both works show a maximum in the solubility at approximately 60 °C, at 50 atm CO_2. Müller and Henecka[119] show how the solubility increases a factor 2 over the pressure range 20 to 50 atm CO_2. Müller and Henecka[119] made also a number of interesting experiments in the CO_2-$FeCO_3$-$NaOH$-H_2O system. Which show how $FeCO_3$ is partly converted to $Fe(OH)_2$.

8.3.2 Solid phases

The majority of the authors listed in table 28 determined the purity of $FeCO_3$ by X-ray diffraction before the solubility experiments. Only few authors took the effort to determine the precipitated solid phase after the solubility experiment. The two measurement do not necessarily give the same result and $FeCO_3$ may precipitate as $Fe(HCO_3)_2$ or as a hydrate of $FeCO_3$.

Singer and Stumm[6] and Reiterer[80] determined that crystalline $FeCO_3$ precipitated during their experiment. Jensen *et al.*[1] determined that several carbonate phases were in equilibrium with their solutions. This indicates the measurements by Jensen *et al.*[1] are in fact the 2-salt solubility of co-precipitated $FeCO_3$ and $CaCO_3$ and not the solubility of $FeCO_3$. This is important, since the solubility phenomena are different in the two cases. Berg and Buzdov[143] show that $FeCO_3$ does not form hydrates at 25 °C, but small inclusion of water may be expected. Reynolds[144] findings show that $FeCO_3 \cdot K_2CO_3 \cdot 4H_2O$ may be formed. This indicates that maybe other double carbonate salts of iron may form, for example double salts of Na_2CO_3 or similar. Rosenberg[17], Rosenberg and Foit[145], and Chai and Navrotsky[146] states that the double salt ankerite, $CaCO_3 \cdot FeCO_3$, may not form at low temperature but it will form solid solutions at high temperatures. Some indications show that it may form at lower temperatures[147]. Ghosh *et al.*[7] states that $Fe(OH)_2 \cdot FeCO_3$ may precipitate even though it is not experimentally proved. Other authors have recently made thorough investigations and determined experimentally that it exists[148,149,26,150,151,152,153]. Al-Hassan *et al.*[149] even stated that the precipitation of this solid phase could explain the unexpected CO_2 corrosion behaviour above 60 °C. Xia *et al.*[154] have also shown experimentally that $Fe(HCO_3)_2(s)$ may form as a intermediate meta-stable phase before it converts to the final $FeCO_3$ corrosion product.

8.3.3 Specific heat capacity of FeCO₃

The heat capacity of $FeCO_3$ was measured by Anderson[60] between 54K and 296K. The purity of the used $FeCO_3$ was 88% and the impurities were $CaCO_3$, $MnCO_3$, and

MgCO₃. Anderson[60] corrected the result for impurity, but the method was not described.

Robie *et al.*[61] measured the value more accurately between 5 K and 373 K; still the crystal had 4.4% impurities of *MnCO₃*. The measurements were improved at low temperature compared to the work by Anderson[60].

The heat capacity was also measured by Kalinkina[63], Kostryukov and Kalinkina[64], and Kalinkina and Kostryukov[65]. Kalinkina[64] stated that the used *FeCO₃* were 97% pure, which is an improvement compared to Robie *et al.*[61], but the measured values were only discussed and shown in figures and not tabulated.

These measurements may still be improved since the used crystals have not been pure even though the result is acceptable.

8.3.4   Thermal decomposition of FeCO₃

High temperature analysis of *FeCO₃* is not the focus of this study, but a number of groups have investigated the decomposition temperature and pressure of *FeCO₃* and the properties are given here. French[15] approached the subject and gave an outline of the previous work.

Berg and Buzdov[143,155] and Stubina and Toguri [81] found that *FeCO₃* decompose according to reaction (275) in low *CO₂* pressure atmosphere, close to vacuum at approximately 300 °C, to form magnetite, *Fe₃O₄* or *FeO·Fe₂O₃*[156]:

$$3FeCO_3 \rightarrow Fe_3O_4 + 2CO_2 + CO \qquad (275)$$

Powell[128] showed that the *CO:CO₂* ratio is not 1:2, in the initial part of the reaction. He suggests that *FeCO₃* decompose to wüstite, *FeO*, and *CO₂* is later reduced to *CO* by *FeO*. Berg and Buzdov[155] show that the *CO₂ + CO* pressure of *FeCO₃* is 10^{-18} atm at 25 °C. Reiterer[80] assumed that *FeO* was the reaction product and estimated the pressure to be 0.0003 atm.

The decomposition of *FeCO₃* is considerably more complicated in an oxygen atmosphere[143]. Berg and Buzdov[143] shows that oxygen oxidises magnetite to maghemite, $\alpha - Fe_2O_3$, with an intermediate form, $\gamma - Fe_2O_3$. Trace amount of oxygen and high *CO₂* pressure makes *FeCO₃* decompose at approximately 360 °C by the following reaction as studied by French[15]:

$$3FeCO_3 + \tfrac{1}{2}O_2 \rightarrow Fe_3O_4 + 3CO_2 \qquad (276)$$

He also showed that hematite, *Fe₂O₃*, may be produced as a side product. French[15] and Weidner[45] found that above 450 to 550 °C pure magnetite and graphite is always produced. The subject was also discussed by Chai and Navrotsky[82].

8.4   Synthesis of FeCO₃

FeCO₃ has been synthesised by different reaction paths. Nine patents have been obtained on *FeCO₃* synthesis, as shown in table 29. Table 30 gives an overview of the used reaction species and the colour of the produced *FeCO₃*. Babcan[157] gives an overview of the old literature on *FeCO₃* production and Ptacek[13] tested and compared some of the methods. The difference between reaction paths depends on the iron source, the carbonate source, and process condition of temperature and pressure.

A typical source of iron is iron powder, iron wire, or an iron salt of sulphate, chloride, chlorate or oxalate. The source of carbonate may either be gaseous CO_2 or a salt of bicarbonate, carbonate, oxalate or urea. Three types of process condition are used, room temperature and pressure, mid temperature and pressure and very high temperature and pressure.

The above conditions fall in four groups. They are all related to the reaction path for the carbonate formation.

One group uses very high temperature and pressure[15,16,82,158,146]. Iron oxalate is always used in these methods since it decomposes to CO_2 and carbonate. Ehrhardt *et al.*[158] show that a very high CO_2 pressure and temperature is needed to synthesise the desired quality. The method requires specialised high pressure equipment and only small samples may be produced.

Another approach uses pure gaseous CO_2 to form carbonate. CO_2 dissolves in water and dissociates to carbonate. Iron in the form of wire or powder dissolves and $FeCO_3$ precipitates[31,133,11]. The method is suited for producing high purity $FeCO_3$ since it does not require the interference from other ions as discussed by Gould[133]. The method is slow since it requires dissolution of the iron. Gaseous CO_2 has also been used with aqueous iron salt mixtures to precipitate $FeCO_3$[80,159]. This process requires high pressure equipment and a thorough deaeration of the setup. The same is true when using urea $((NH_2)_2CO)$[115,160]. Here ammonia is produced as a side product and the product may be impure. The work by Huxley and Fetchin[161] state that $FeCO_3$ may be produced in a CO_2-ammonia process, in reality they produce iron carbamate, $Fe(NH_2CO_2)_2$.

In a third process $FeCO_3$ may be precipitated from solutions of carbonate. This involves higher *pH* and the precipitate may be polluted by co-precipitated $Fe(OH)_2$. The precipitate is typically of lower quality and has been used in processes to remove iron as shown by Konz[139]. Sodium or potassium carbonate is typically used in this process[141,143,162,139,163,164,165,166] or calcium carbonate[168,167,128,169,157,140,81]. Ptacek[13] showed that $SrCO_3$ could alternatively be used as carbonate source. Reynolds[144] has shown on the other hand that the precipitated solid is most likely not iron carbonate. The key is the salt concentration. He explained that stable $FeCO_3$ only precipitates from the dilute solution. Concentrated solution also precipitate $FeCO_3$ but within minutes it reprecipitates as $FeCO_3 \cdot K_2CO_3 \cdot 4H_2O$. Another issue is that $CaCO_3$ may easily incorporate in the $FeCO_3$ crystal as discussed by Rosenberg and Foit[145].

The final method used by the majority of authors employs bicarbonate to precipitate $FeCO_3$. Iron sulphate is typically used as iron source[84,85,24,9,170,162,171,101], a few authors used perchlorate[6,125] or Mohrs salt $(FeSO_4 \cdot (NH_4)_2SO_4 \cdot 6H_2O)$[36,32,28,90,172,173]. Lyon[174] used iron chloride and the method is equivalent to Sharp[170]. Allison *et al.*[175] and Ptacek[13] are the only authors who suggest using a mixture of carbonate and bicarbonate. Allison *et al.*[175] even states that carbamate may be employed. Any of the setups applying a carbonate or bicarbonate salt were often supported by an atmosphere of CO_2 often at atmospheric conditions and room temperature. The method is popular since it is simple and requires less sophisticated equipment. The produced $FeCO_3$ were sometimes post treated in an anaerobic oven between 100 and 200 °C for drying.

Table 29: Patents on synthesis of *FeCO₃*.

Authors	Year	Short description of method	Colour
Hoy[162]	1899	*FeSO₄* with *K₂CO₃* or *NaHCO₃* at anaerobic conditions in glove box. Washed as same conditions.	NA
Parker[164]	1903	*NaHSO₄* and Iron to get *FeSO₄* precipitated as *FeCO₃*, *Fe(OH)₂* with carbonate or hydroxide.	NA
Flügge[171,176,4,177]	1905	*FeSO₄* and *Na/KHCO₃* to give *FeCO₃* which is washed in *CO₂-water* at anaerobic conditions.	Greenish-white [a]
Lilly[163]	1908	*FeSO₄* and *Na₂/K₂CO₃* in glycerine at anaerobe conditions under oil. States *Na₂/K₂CO₃* may be substituted by *CO₂+NaOH*.	NA
Gill[168]	1911	As part of their *Fe₂O₃* production, *CaCO₃* and *CO₂* are mixed with *FeCl₂* to get *FeCO₃*.	NA
Allison *et al.*[175]	1958	Ammonium bicarbonate or carbonate or carbamate with *FeSO₄*.	NA
Konz[139]	1966	*K₂CO₃* + *CO₂* precipitate *FeCO₃* by iron from the process equipment at anaerobe conditions.	
Gould[133]	1968	Iron wire and *CO₂* at anaerobic conditions.	NA
Lyon[174]	1987	*FeCl₂* and *NaHCO₃* (1:2) in a closed vessel at 200 °C (probably high *CO₂* pressure due to decomposition of *NaHCO₃*). Precipitate filtered in glove box.	Bluish grey, White or pale cream

[a] Ghosh *et al.*[7] states this may be due to oxidation

The colour of *FeCO₃* was often white, but beige is also typical. Krustinsons[167] mentions how *FeCO₃* precipitate as grey-white at 120 °C, which change to brow above 130 °C. Problems while performing the precipitation reveals green, blue or black precipitates. *FeCO₃* oxidises to red-brown magnetite and hematite. Baudisch and Welo[166] and Gayer and Woontner[178] show some of the difficulties observed when precipitating ferrous iron. The observed precipitate has various colours and they are not related to ferric iron. The colour scheme is similar to precipitation by mixing aqueous *FeCl₂* and *Na₂CO₃*: First dirty green, then black and finally red-brown. Gayer and Woontner[178] suggest the different colour are due to production of different hydrates of *Fe(OH)₂* and finally production of ferric iron. It must be underlined, that iron carbonate may only be produced at anaerobic condition where all oxygen has been strictly removed.

Table 30: Methods for synthesising $FeCO_3$ as published in the literature.

Authors	Year	Short description of method	Colour
Günzburg [141]	1911	$FeSO_4(NH_4)_2SO_4 \cdot ?H_2O$ and Na_2CO_3. O_2 avoided.	
Smith[84]	1918	$FeSO_4$ and $NaHCO_3$ in saturated CO_2 solution at 100 °C and 400psi (27.6bar) CO_2.	White
Tillmans and Klarmann[11]	1924	CO_2 and iron particles. O_2 avoided by vacuum and boiling.	White
Baudisch and Welo[166]	1925	$FeSO_4$ and Na_2CO_3 at anaerobic condition and room T.	White
Lemke and Biltz[160]	1934	$FeCl_2$ and Urea at 200 °C. Purity is low, 15%.	NA
Krustinsons[167]	1935	$FeCl_2$ and $CaCO_3$ in melted glass pipe for 20h, 120 °C.	Grey-white [a]
Sharp[170]	1960	$FeSO_4 \cdot 7H_2O$ and $NaHCO_3$ with $CO_{2(g)}$.	Yellow-brown [b]
Graf[165]	1961	$FeSO_4$ and Na_2CO_3 with $CO_{2(g)}$ at 143 °C or 300 °C.	NA
Berg and Buzdov[143]	1961	$FeSO_4$ and Na_2CO_3 at 25 °C at anaerobic conditions.	White
Powell[128]	1965	Excess $FeCl_2$ and $CaCO_3$, 170°C for 24h. O_2 avoided.	Grey
Johannes[169]	1968	$FeCl_2$ and $CaCO_3$ at 150 to 300 °C at 1000 bar.	NA
Singer and Stumm[6]	1970	$FeClO_4$ and $NaHCO_3$ with $HClO_4$ in N_2 flush.	NA
Babcan[157,140]	1970, 1974	$FeCl_2$ and $CaCO_3$ at 140 °C at low pressure. O_2 content unknown.	NA
Weidner[16], French[15], Chai and Navrotsky[82]	1971, 1994	$FeC_2O_4 \cdot 2H_2O$ heated in 97% CO_2/CO at 380 °C and 3kbars for 48h.	Tan (beige)
Bardy and Péré[85]	1976	$FeSO_4$ and $NaHCO_3$ in argon atmosphere at 80 °C, post washed.	NA
Gamsjäger and Reiterer[115]	1979	$FeCl_2$ with HCl, urea and CO_2 atmosphere of 40-80atm at 140-160 °C in autoclave, washed and dried at 80 °C.	NA
Reiterer[80]	1980	1: dry ice and $FeCl_2 \cdot 4H_2O$ in autoclave at 150 °C 2: CO_2 from bottle in $FeCl_2$ solution at 220 °C.	White
Ehrhardt et al.[158]	1980	$FeC_2O_4 \cdot 2H_2O$ heated at 470 °C and 3500bar CO_2.	Light-brown
Ehrhardt et al.[159]	1980	$FeSO_4 \cdot 7H_2O$ and CO_2 at 1200atm at 180 °C $Fe(OH)_2$ and CO_2 at 2500atm at 150 °C.	Colour-less
Davies and Burstein[101]	1980	$FeSO_4$ and $KHCO_3$ in N_2 atmosphere.	White, pale-green[c]
Wajon et al.[31]	1985	Fe wire and CO_2.	Green
Greenberg and Tomson[36,32,33]	1986	Mohrs salt and $NaHCO_3$ with CO_2 at room T, heated at 70-90 °C. Anaerobic conditions.	Light grey, white
Stubina and Toguri[81]	1989	Excess $FeCl_2 \cdot 4H_2O$ and $CaCO_3$ at 170 °C dried at 100 °C. Unclear if anaerobic conditions were obtained.	NA
Wersin et al.[97] and Wersin[9] used by Bruno et al.[24]	1990, 1992, 1989	$FeSO_4 \cdot 7H_2O$ with HCl and $NaHCO_3$ in autoclave at 100 °C and 19bar CO_2.	Beige
Johnson and Tomson[27,28,29]	1991	Mohrs salt and $NaHCO_3$ at anaerobic condition. Temperature unknown.	White
Ptacek[13]	1992	$FeCl_2 \cdot 4H_2O$ and 1:4 $Na_2CO_3/NaHCO_3$ at anaerobic conditions in glove box at room temperature. Removed Fe(III) and O_2 by precipitation. Heated at 160 °C.	White
Chai and Navrotsky[146]	1996	$FeC_2O_4 \cdot 2H_2O$ and CO_2 at 850 °C and 18kbars for 24h.	White
Heuer and Stubbins[173]	1999	Method by Johnson and Tomson[28] at room temperature post heated at 75 °C.	White
Silva et al.[90]	2002	Equivalent to Greenberg and Tomson[36,32,33] and details from Bruno et al.[24].	NA
Jimenez-Lopez And Romanek[125]	2004	$Fe(ClO_4)_2$ and $NaHCO_3$ at 25 °C and 1atm, 10% CO_2, at anaerobic conditions.	NA
Gogolev[172]	2006	$FeSO_4(NH_4)_2SO_4 \cdot 6H_2O$ and $KHCO_3$. O_2 avoided.	White

[a] Changed to brown while heated to 130-180°C. [b] The colour changed to Yellow-brown while drying. [c] Low concentration of $KHCO_3$: white, high $KHCO_3$: pale-green.

8.5   Discussion and conclusion

This study gives a review of available thermodynamic properties of *FeCO₃* found in the open literature. The heat capacity has been determined experimentally by a few authors. Until date the work by Robie *et al.*[61] is the most accurate. Their temperature correlation of heat capacity is also the most reliable. The standard state entropy, which obeys the third law of thermodynamics, was determined by Robie *et al.*[61] and is consistent with their measurements of heat capacity.

Based on the study performed in this work we recommend the properties given in table 31, 32 and 33. Two different alternatives are given. Table 31 contains a set of properties which are consistent with the NIST[55] thermodynamic properties. Table 32 presents properties which are consistent with the CODATA[57,58] thermodynamic properties. We consider these two alternatives to be of equal quality and consistent.

Table 31: Recommended standard state properties consistent with NIST[55] at 298.15K at 1 bar. Properties are from NIST if not stated otherwise.

	$\Delta_f G°$	$\Delta_f H°$	$S°$	$\Delta_f S°$ [a]
	kJ/mol	*kJ/mol*	*J/(mol·K)*	*J/(mol·K)*
Fe^{2+}	-78.9	-89.1	-137.7	-34.30
CO_3^{2-}	-527.81	-677.14	-56.9	-501.03
$FeCO_3$	-665.16 [b]	-738.28 [c]	95.47 [d]	-245.26

[a] Values were calculated using the NIST[55] standard entropies $S°_{Fe(s)}$ =27.28 *J/(mol·K)*, $S°_{C(s)}$ =5.74 *J/(mol·K)*, $S°_{O_2(g)}$ =205.138 *J/(mol·K)*, $S°_{H_2(g)}$ =130.684 *J/(mol·K)*, and $S°_{H^+(aq)}$ =0 *J/(mol·K)*. [b] Values were calculated consistently with $\Delta_f G°_{Fe^{2+}}$ and $\Delta_f G°_{CO_3^{2-}}$ using pK_{sp}=10.24 of Singer and Stumm[6]. [c] calculated using equation (260). [d] obtained from Robie *et al.*[61].

Table 32: Recommended standard state properties consistent with CODATA[57,58] at 298.15K at 1 bar.

	$\Delta_f G°$	$\Delta_f H°$	$S°$	$\Delta_f S°$ [a]
	kJ/(mol·K)	*kJ/(mol·K)*	*J/(mol·K)*	*J/(mol·K)*
Fe^{2+} [b]	-90.53	-90	-101.6	1.76
CO_3^{2-}	-527.90 [c]	-675.23 [d]	-50 [d]	-494.15
$FeCO_3$	-676.88 [e]	-750.01 [f]	95.47 [g]	-245.30

[a] Values were calculated using the CODATA[57,58] standard entropies $S°_{Fe(s)}$ =27.319 *J/(mol·K)*, $S°_{C(s)}$ =5.74 *J/(mol·K)*, $S°_{O_2(g)}$ =205.138 *J/(mol·K)*, $S°_{H_2(g)}$ =130.68 *J/(mol·K)*, $S°_{H^+(aq)}$ =0 *J/(mol·K)*. [b] Obtained from Parker and Khodakovskii[57]. [c] Calculated from $\Delta_f H°_{CO_3^{2-}}$ and $\Delta_f S°_{CO_3^{2-}}$. [d] Obtained from CODATA[58]. [e] Values were calculated consistently with $\Delta_f G°_{Fe^{2+}}$ and $\Delta_f G°_{CO_3^{2-}}$ using pK_{sp}=10.24 of Singer and Stumm[6]. [f] calculated using equation (260). [g] obtained from Robie *et al.*[61].

The two alternatives are different since there is a controversy regarding the thermodynamic properties of *Fe²⁺*. There are two sides in the literature, both being equally correct, but they give different results. The two opposing groups believe that the potential of *Fe²⁺* should be measured in vacuum or in hydrogen atmosphere. The discrepancies influence the standard state formation properties of *FeCO₃* which are shown in table 31 and 32. It can be concluded that the use of any *Fe²⁺* properties

should be done with care and properties must be evaluated before use. It is recommended never to combine properties from different data collections in the same work. It will eventually lead to inconsistencies between thermodynamic properties of Fe^{2+} and $FeCO_3$.

$S^{\circ}_{FeCO_3}$ was obtained from Robie *et al.*[61] and shown both in table 31 and 32. $\Delta_f S^{\circ}_{FeCO_3}$ is comparable in the two tables, since the standard state properties of the reference compounds are similar in NIST and CODATA.

The solubility constant of $FeCO_3$ can be determined experimentally and independently of the Fe^{2+} properties. At the same time it may be used to consistently determining the standard state formation properties of $FeCO_3$ from the Fe^{2+} properties. It has been determined by a considerable number of authors, but the work by Kelley and Anderson[56] is inaccurate and should not be used even though it is found in most property collections. The equilibrium constants determined by Singer and Stumm[6] or Haarberg *et al.*[87] on the other hand, are more consistent. These two works also apply a basic speciation scheme, opposite many other works. There is an ongoing debate on whether $FeHCO_3^+$, $FeCO_3(aq)$, $Fe(CO_3)_2^{2-}(aq)$, and $FeCO_3(OH)^-$ exist. The properties of these compounds are uncertain and they have unfortunately been included in many works recently. If these compounds are used, a relatively high solubility constant, pK_{sp}, of $FeCO_3$ is found. This is due to the lower observed free Fe^{2+} concentration in favour of the other iron species. If any of the species are included, then it is suggested to refit all equilibrium constants in order to obtain a consistent speciation scheme. Similarly the solubility constant of $FeCO_3$ must always be used in the speciation scheme that it was fitted to. It becomes inconsistent if properties from different data collections are combined.

Table 33 shows recommended standard state properties of $FeCO_3$ dissolution of reaction (252) and (253). Properties consistent with both NIST and CODATA are shown. The equilibrium constant was assumed to follow the calculated value by Singer and Stumm[6] of pK_{sp}=10.24.

Table 33: Recommended properties of reaction (252) and (253), consistent with NIST[55] or CODATA[57,58] at 298.15 K and 1 bar.

Reference	Reaction (k)	pK_k -	$\Delta_{r,k}H^{\circ}$ kJ/(mol·K)	$\Delta_{r,k}S^{\circ}$ J/(mol·K)
NIST[55]	(252) (sp)	10.24 [a]	-27.96 [b]	-289.81 [b]
CODATA[57,58]	(252) (sp)	10.24 [a]	-15.21 [b]	-247.05 [b]
NIST[55]	(253) (psp)	-7.92 [c]	-30.16 [d]	-50.55 [d]
CODATA[57,58]	(253) (psp)	-7.91 [c]	-19.32 [e]	-86.68 [e]

[a] Obtained from Singer and Stumm[6]. [b] Calculated from properties in table 31 and 32. [c] Calculated from $\Delta_{psp}H^{\circ}$ and $\Delta_{psp}S^{\circ}$ [d] Calculated from properties in table 31 and NIST: $\Delta_f H^{\circ}_{CO_2(g)}$=-393.509 kJ/mol, $\Delta_f H^{\circ}_{H_2O(l)}$=-285.83 kJ/mol, $S^{\circ}_{CO_2(g)}$=213.74 J/(mol·K), and $S^{\circ}_{H_2O(l)}$=69.91 J/(mol·K) [e] Calculated from properties in table 32 and CODATA: $\Delta_f H^{\circ}_{CO_2(g)}$=-393.51 kJ/mol, $\Delta_f H^{\circ}_{H_2O(l)}$=-285.83 kJ/mol, $S^{\circ}_{CO_2(g)}$=213.785 J/(mol·K), and $S^{\circ}_{H_2O(l)}$=69.95 J/(mol·K).

$\Delta_{r,sp}H^{\circ}$ was calculated from the enthalpies of formation of $FeCO_3$, CO_3^{2-}, and Fe^{2+} shown in table 31 and 32. The NIST value is an order of magnitude lower than the CODATA value. The value is uncertain but consistent with the remaining database

properties. The difference is related to the inequality of $\Delta_f G^\circ_{Fe^{2+}}$ between NIST and CODATA. Preis and Gamsjäger[45] discussed this problem and recommend the CODATA properties by evaluating $\Delta_{r,sp} H^\circ$. Unfortunately they included an extended speciation scheme in their calculations, using $FeCO_3 \left(aq \right)$ and $Fe\left(CO_3 \right)_2^{2-} \left(aq \right)$ despite the uncertainties outlined in the sections above. The discrepancy in $\Delta_{r,sp} S^\circ_{sp}$ and $\Delta_{r,psp} S^\circ$ between NIST and CODATA is also related to the $\Delta_f G^\circ_{Fe^{2+}}$. The pK_{psp} is calculated from the pK_{sp} value and the small difference between NIST and CODATA is related to the difference in the S° properties of the reference compounds.

An overview of experimental literature on $FeCO_3$ solubility measurements is given in this study. The majority of literature studies fix the ionic strength by adding another salt. The added ions will influence the solubility significantly. The best way to avoid errors is to keep the amount of unnecessary ions low. Some studies neglect to measure temperature or apply vague temperature control. CO_2 content in the system is an important parameter for $FeCO_3$ solubility and measurements should always include a CO_2 determination. Often measurements are misinterpreted as supersaturated due to improper use of equilibrium constants. In reality it has been shown, that $FeCO_3$ may form supersaturated solutions. It has also been shown that equilibrium is eventually attained.

$FeCO_3$ decompose at high temperature and a brief overview of the related literature is given in this study. A section on producing $FeCO_3$ is also given and many different methods may be used. Hydroxide concentration and oxygen contamination are two key parameters to control in order to prevent precipitation of $Fe(OH)_2$ and to avoid oxidation of Fe^{2+} to Fe^{3+}. Undesired reaction products may be obtained if oxygen is not carefully removed.

8.6   Literature cited

[1]   D.L. Jensen, J. K. Boddum, J. C. Tjell and T. H. Christensen: "The solubility of rhodochrosite ($MnCO_3$) and siderite ($FeCO_3$) in anaerobic aquatic environments", Applied Geochemistry, 2002, 17(4), 503-511.

[2]   D. L. Jensen: "Speciation of dissolved iron(II) and manganese(II) in a groundwater pollution plume", Environmental Science and Technology, 1998, 32(18), 2657-2664.

[3]   A. P. Schwab and W. L. Lindsay: "Effect of redox on the solubility and availability of iron", Soil Science Society of America Journal, 1983, 47(2), 201-5.

[4]   A. Flügge: "Process of making Ferrous Carbonate", US patent 842452, 1907.

[5]   J. D. Hem: "Restraints on Dissolved Ferrous Iron Imposed by Bicarbonate, Redox Potential, and pH", U. S. Geol. Surv. Water Supply, 1960, paper 1459-B.

[6]   P. C. Singer and W. Stumm: "The solubility of ferrous iron in carbonate-bearing waters", Journal - American Water Works Association, 1970, 62, 198–202.

[7]   M. M. Ghosh, J. T. O'connor and R. S. Engelbrecht: "Rate of precipitation of iron in aerated groundwaters", J. Sanit. Eng. Div. Am. Soc. Civil Engrs., 1996, 92(1), 199-213.

[8]   W. Stumm and P. C. Singer: "Precipitation of Iron in Aerated Groundwaters, discussion", J. San. Eng., ASCE, 1966, 92, 120.

[9]   P. Wersin: "The Fe(II)-CO_2-H_2O system in anoxic natural waters: Equilibria and surface chemistry", PhD dissertation, Swiss Fed. Inst. of Technol., Zürich, 1990.

[10]   F. J. Millero and D. Pierrot: "A chemical equilibrium model for natural waters", Aquatic Geochemistry 1998, 4(1), 153-199.

[11]   J. Tillmans and B. Klarmann: "The solution of iron by oxygen-free natural waters", Angewandte Chemie, 1924, 36, 94-7, 103-4, 111-5.

[12]   C. J. Ptacek and D. W. Blowes: "Influence of Siderite on the Pore-Water Chemistry of Inactive Mine-Tailings Impoundments", ACS Symposium Series, 1994, 550, 172-189.

[13]   C. J. Ptacek: "Experimental determination of siderite solubility in high ionic-strength aqueous solutions", Ph.D. thesis, University of Waterloo, Ontario, Canada, 1992.

[14]   P. E. Dresel: "The dissolution kinetics of siderite and its effect on acid mine drainage", Ph.D. thesis. Pennsylvania State University, 1989.

[15]   B. M. French: "Stability Relations of Siderite ($FeCO_3$) In System Fe-C-O", American Journal of Science, 1971, 271(1), 37-78.

[16]   J. R. Weidner: "Equilibria In System Fe-C-O .1. Siderite-Magnetite-Carbon-Vapor Equilibrium From 500 to 10,000 Bars", American Journal Of Science, 1972, 272(8), 735-751.

[17]   P. E. Rosenberg: "Subsolidus relations in the system $CaCO_3$-$FeCO_3$", Am. J. Sci., 1963, 261, 683-690.

[18]   G. M. Marion, D. C. Catling and J. S. Kargel: "Modeling aqueous ferrous iron chemistry at low temperatures with application to Mars", Geochimica Et Cosmochimica Acta, 2003, 67(22), 4251-4266.

[19]   G. H. Rau: "Possible use of Fe/CO_2 fuel cells for CO_2 mitigation plus H_2 and electricity production" Energy Conversion and Management, 2004, 45(13-14), 2143-2152.

[20]   J. L. Palandri and Y. K. Kharaka: Sequestration of CO_2 in redbeds: siderite precipitation from CO_2 and SO_2 waste gas. Water-Rock Interaction, Proceedings of the International Symposium on Water-Rock Interaction, 11th, Saratoga Springs, NY, United States, 2004, 1, 567-571.

[21]   E. Deltombe and M. Pourbaix: "Equilibrium potential-pH diagram for the system Fe-CO_2-H_2O at 25°", Proc. 6th Meeting Intern. Comm. Electrochem. Thermodynam. and Kinet., 1955, 124-32.

[22]   W. Stumm and G. F. Lee: "The chemistry of aqueous iron", Schweizerische zeitschrift für hydrologie, 1960, 22, 295-319.

[23]   J. D. Hem: "Equilibrium chemistry of iron in ground water", In "Principles and application of water chemistry ", (Ed. S.D. Faust and J.V. Hunter), 625; 1967, John Wiley and sons, inc., New York.

[24]   J. Bruno, P. Wersin, W. Stumm and F. Brandberg: "On the influence of carbonate in mineral dissolution: II. The solubility of FeCO₃(s) at 25°C and 1 atm total pressure", Geochim. Cosmochim. Acta., 1992, 56(3), 1149–1155.

[25]   B. Mishra, S. Al-Hassan, D. L. Olson and M. M. Salama: "Development of a predictive model for activation-controlled corrosion of steel in solutions containing carbon dioxide", Corrosion, 1997, 53(11), 852-859.

[26]   J. Dong, T. Nishimura and T. Kodama: "Corrosion behavior of carbon steel in bicarbonate (HCO₃⁻) solutions", Materials Research Society Symposium Proceedings, 2002, 713(Scientific Basis for Nuclear Waste Management XXV), 105-112.

[27]   M. L. Johnson and M. B. Tomson: "Ferrous carbonate precipitation kinetics and its impact CO₂ corrosion", CORROSION/91, NACE, 1991, paper 268.

[28]   M. B. Tomson and M. L. Johnson: "How Ferrous Carbonate Kinetics Impacts Oilfield Corrosion", Proceedings, International Symposium on Oilfield Chemistry, Anaheim, CA, SPE, 1991, Paper No. 21025, 257-264.

[29]   M. L. Johnson: "Ferrous Carbonate Precipitation Kinetics - A Temperature Ramped Approach", Ph. D. Thesis, Rice University, Houston, Texas, 1991.

[30]   E. Van Hunnik, B. F. M. Pots and E. L. J. A. Hendriksen: "The Formation of Protective FeCO₃ Corrosion Product Layers in CO₂ Corrosion", CORROSION/96, NACE, 1996, paper no. 6.

[31]   J. E. Wajon, G.-E. Ho and P. J. Murphy: "Rate of precipitation of ferrous iron and formation of mixed iron-calcium carbonates by naturally occurring carbonate materials", Water Research, 1985, 19(7), 831-7.

[32]   J. L. Greenberg: "High Temperature Kinetics of Precipitation and Dissolution of Ferrous Carbonate", M.S. Thesis. Rice University, Houston, Texas, 1986.

[33]   J.L. Greenberg and M. B. Tomson: "Kinetics of Precipitation and Dissolution of Ferrous Carbonate", International Symposium on Metals Speciation, Separation, and Recovery, (ed., J. W. Patterson), 1986, Lewis Publication, Inc., Chelsea, MI, pp. I-1/17.

[34]   G. I. Ogundele and W. E. White: "Some Observations on Corrosion of Carbon-Steel in Aqueous Environments Containing Carbon-Dioxide", Corrosion, 1986, 42(2), 71-78.

[35]   D. B. Robert: "Solubility of iron(II) carbonate at temperatures between 30 and 80°C", Talanta, 1991, 38(2), 205–211.

[36]   J. L. Greenberg and M. B. Tomson: "Precipitation and dissolution kinetics and equilibria of aqueous ferrous carbonate vs. temperature", Appl. Geochem., 1992, 7(2), 185–190.

[37]   S. V. Golubev, P. Bénézeth and J. Schott: "Siderite dissolution kinetics in acidic aqueous solutions from 60 to 100°C and 0 to 50 atm pCO₂", Geophysical Research Abstracts, 2007, 9, 04038.

[38]   A. Dugstad: "Mechanism of Protective Film Formation During CO₂ Corrosion of Carbon Steel", CORROSION/98, NACE, 1998, paper no. 31.

[39]   S. Nesic, M. Nordsveen, R. Nyborg and A. Stangeland: "A Mechanistic Model for CO₂ Corrosion with Protective Iron Carbonate Films", CORROSION/01, NACE, 2001, Paper No. 40.

[40]   M. Nordsveen, S. Nesic, R. Nyborg and A. Stangeland: "A mechanistic model for carbon dioxide corrosion of mild steel in the presence of protective iron carbonate films - Part 1: Theory and verification", Corrosion, 2003, 59(5), 443-456.

[41]   W. Sun, K. Chokshi and S. Nesic: "Iron Carbonate Scale Growth and the Effect of Inhibition in CO₂ Corrosion of Mild Steel", CORROSION/05, NACE, 2005, paper no. 285.

[42]   W. Sun, S. Nesic: "Basics Revisited: Kinetics of Iron Carbonate Scale Precipitation in CO_2 Corrosion", CORROSION/06, NACE, 2006, paper no. 365.

[43]   E. Gulbrandsen: "Acetic acid and carbon dioxide corrosion of carbon steel covered with iron carbonate", CORROSION/07, NACE, 2007, paper no. 322.

[44]   R. Grauer, Translation by: Urs Berner: "Solubility products of M(II) – Carbonates", PSI Bericht 99-04, Paul Scherrer Institute, Villigen, 1999.

[45]   W. Preis and H. Gamsjager: "Critical evaluation of solubility data: enthalpy of formation of siderite", Physical Chemistry Chemical Physics, 2002, 4(16), 4014-4019.

[46]   R. A. Robie and D. R. Waldbaum: "Thermodynamic properties of minerals and related substances at 298.15°K (25°C) and one atmosphere (1.013 bars) pressure and at higher temperatures", U.S. Geol. Survey Bull. 1259, 256 pages, 1968.

[47]   R. A. Robie, B. S. Hemingway and J. R. Fisher: "Thermodynamic properties of minerals and related substances at 298.15 K and 1 bar (10^5 pascals) pressure and at higher temperatures", U.S. Geol. Survey Bull. 1452, 456 pages, 1978.

[48]   R. A. Robie and B. S. Hemingway: "Thermodynamic properties of minerals and related substances at 298.15 K and 1 bar (10^5 Pascals) pressure and at higher temperatures", U.S. Geological Survey Bulletin 2131, Washington, 1995.

[49]   D. K. Nordstrom, L. N. Plummer, D. Langmuir, E. Busenberg, H. M. May, B. F: Jones and D. L. Parkhurst: "Revised chemical equilibrium data for major water-mineral reactions and their limitations", Chemical Modelling of Aqueous Systems II, ACS symposium series, 1990, 416, 398-413.

[50]   W. E. Latimer: "The Oxidation States of the Elements and Their Potentials in Aqueous Solutions", 2nd Ed., PrenticeHall Inc. Englewood Cliffs, N. J., 1952.

[51]   D. Langmuir: "The Gibbs free energies of substances in the system Fe-O_2-H_2O-CO_2 af 25 °C", U.S. Geol. Surv. Prof. Pap., 1969, 650B, p. 180-184.

[52]   I. Barin, O. Knacke and O. Kubaschewski: "Thermochemical Properties of Inorganic Substances", Berlin: Springer-Verlag. 1973 + Supplement 1977.

[53]   A. E: Martell and. R. M. Smith: "Critical stability constants. 4: Inorganic complexes", New York,N.Y., Plenum press., 1976 repr. 1981.

[54]   D. D. Wagman, W. H. Evans, V. B. Parker, I. Halow, S. M. Bailey and R. H. Schumm: "Selected values of chemical thermodynamic properties. Tables for elements 35 through 53 in the standard order of arrangement", Natl. Bur. standards Tech. Note 270-4, 154 pages, 1969.

[55]   D. D. Wagman, W. H. Evans, V. B. Parker, R. H. Schumm, I. Halow and S. M. Bailey: "NIST Chemical Thermodynamics Database Version 1.1", J. Phys. Chem. Ref. Data, 1982, 11 Supplement No. 2.

[56]   K. K. Kelley and C. T. Anderson: "Contributions to the data on theoretical metallurgy. IV. Metal carbonates: Correlations and applications of thermodynamic properties", U.S. Department of the Interior, Bureau of Mines, 1935, 384, 1-73.

[57]   V. B. Parker and I. L. Khodakovskii: "Thermodynamic properties of the aqueous ions (2+ and 3+) of iron and the key compounds of iron", Journal of Physical and Chemical Reference Data, 1995, 24(5), 1699-1745.

[58]   J. D. Cox, D. D. Wagman and V. A. Medvedev: "CODATA Key values for thermodynamics", Hemisphere Publishing Corp., New York, 1989.

[59]   C. F. Baes and R. E. Mesmer: "The Hydrolysis of Cations. Iron.", Wiley, New York, 226-237, 1976 repr. 1986.

[60]   C. T. Anderson: "The heat capacities of Magnesium, Zinc, Lead, Manganese and iron carbonate at low temperature", J. Am. Chem. Soc., 1934, 56, 849.

[61]   R. A. Robie, H. T. Haselton and B. S. Hemingway: "Heat-Capacities and Entropies of Rhodochrosite ($MnCO_3$) and Siderite ($FeCO_3$) Between 5K and 600K", American Mineralogist, 1984, 69(3-4), 349-357.

[62]   K. K. Kelley: "Contribution to the data on theoretical metallurgy. XIII High temperature heat content, heat capacity and entropy data for the elements and inorganic compounds", U.S. Bur. Mines Bull. 584, 1960.

[63]   I. N. Kalinkina: "Magnetic specific heat of antiferromagnetic Co, Ni, Mn, and Fe carbonates", Soviet Physics JETP, 1963, 16(6), 1432.

[64]   V. N. Kostryukov and I. N. Kalinkina: "Heat capacity and entropy for manganese, iron, cobalt, and nickel carbonates at low temperatures", Zhurnal Fizicheskoi Khimii, 1964, 38(3), 780-1.

[65]   I N. Kalinkina and V. N. Kostryukov: "Discontinuities of heat capacity in antiferromagnetic carbonates", Fizika Tverdogo Tela (Sankt-Peterburg), 1966, 8(1), 176-80.

[66]   R. A. Robie: "Heats and free energies of formation of troilite, herzenbergite, magnesite, and rhodochrosite calculated from equilibrium data", U.S. Geol. Survey Prof., 1965, paper 525-D, 65-72.

[67]   D. C. Helgeson, J. M. Delany, H. W. Nesbitt and D. K. Bird: "Summary and critique of the thermodynamic properties of rock-forming minerals", Amarican journal of science, 1978, 278A, 1-229.

[68]   D. D. Wagman, W. H. Evans, V. B. Parker, I. Halow, S. M. Bailey and R. H. Schumm: "Selected values of Chemical Thermodynamic Properties. Tables of the first 34 elements in the standard order of arrangement", Natl. Bur. standards Tech. Note 270-3, 268 pages, 1968.

[69]   P. R. Tremaine, R. Vonmassow and G. R. Shierman: "A Calculation of Gibbs Free-Energies for Ferrous-Ions - Solubility of Magnetite in H_2O and D_2O to 300 °C", Thermochim Acta, 1977, 19(3), 287-300.

[70]   P. R. Tremaine and J. C. LeBlanc: "The Solubility of Magnetite and the Hydrolysis and Oxidation of Fe^{2+} in Water to 300°C", Journal of Solution Chemistry, 1980, 9(6), 415-442.

[71]   M. Randall and M. Frandsen: "The standard electrode potential of iron and the activity coefficient of ferrous chloride", J. Am. Chem. Soc., 1932, 54, 47-54.

[72]   W. A. Patrick and W. E. Thompson: "Standard electrode potential of the iron-ferrous ion couple at 25°", Journal of the American Chemical Society, 1953, 75, 1184-7.

[73]   J. M. Larson, P. Cerutti, H. K. Garber and L. G. Hepler: "Electrode potential and thermodynamic data for aqueous ions. Copper, zinc, cadmium, iron, cobalt, and nickel", J. Phys. Chem., 1968, 72, 2902.

[74]   G. K. Johnson and J. E. Bauman: "Equilibrium-Constants for Aquated Iron(II) Cation", Inorg Chem, 1978, 17(10), 2774-2779.

[75]   W. Preis and H. Gamsjager: "Thermodynamic investigation of phase equilibria in metal carbonate-water-carbon dioxide systems", Monatshefte Fur Chemie, 2001, 132(11), 1327-1346.

[76]   H. Gamsjager, E. Konigsberger and W. Preis: "Solubilities of metal carbonates", Pure And Applied Chemistry, 1998, 70(10), 1913-1920.

[77]   T. J. B. Holland and R. Powell: "An enlarged and updated internally consistent thermodynamic dataset with uncertainties and correlations: the system K_2O-Na_2O-CaO-MgO-MnO-FeO-Fe_2O_3-Al_2O_3-TiO_2-SiO_2-C-H_2-O_2", J. of Metamorphic Geology, 1990, 8, 89-124.

[78]   D. E. Wilcox and L. A. Bromley: "Computer estimation of heat and free energy of formation for simple inorganic compounds", Journal of Industrial and Engineering Chemistry (Washington, D. C.), 1963, 55(7), 32-9.

[79]   F. Reiterer, W. Johannes, H. Gamjäger: "Semimicro determination of solubility constants: copper(II) carbonate and iron(II) carbonate", Mikrochimica Acta, 1981, 1, 63–72.

[80]   F. Reiterer: "Löslichkeitskonstanten und Freie Bildungsenthalpien neutraler Übergangsmetallcarbonate", Thesis, Montanuniversität Leoben, 1980.

[81]   N. M. Stubina and J. M. Toguri: "The decomposition pressure of synthetic siderite ($FeCO_3$)", Trans. Iron Steel Soc., 1989, 10, 87-90.

[82]   L. Chai and A. Navrotsky: "Enthalpy of formation of siderite and its application in phase equilibrium calculation", American Mineralogist, 1994, 79(9), 921-929.

[83]   H.C. Helgeson: "Thermodynamics of Hydrothermal Systems at Elevated Temperatures and Pressures", American journal of science, 1969, 267, 729.

[84]   H. J. Smith: "On Equilibrium in the system: ferrous carbonate, carbondioxide and water", Journal of the American Chemical Society, 1918, 40, 879–883.

[85]   J. Bardy and C. Péré: "Determination experimentale du coefficient de solubilite du carbonate ferreux en milieu aqueux", Tribune du CEBEDEAU, 1976, 387, 75.

[86]   V.S. Serebrennikov: "Redox conditions in the low caucasus carbonated mineral springs", Geochem. Int., 1977, 14, 925-945.

[87]   T. Haarberg, J. E. Jakobsen and T. Oestvold: "The effect of ferrous iron on mineral scaling during oil recovery", Acta Chemica Scandinavica, 1990, 44(9), 907-15.

[88]   C. J. Ptacek, E. J. Reardon: "Solubility of siderite (FeCO₃) in concentrated NaCl and Na₂SO₄ solutions at 25°C", Water-Rock Interaction, Proc. Int. Symp., 7th, 181–183, 1992.

[89]   J. D. Garber, R. S. Perkins, R. J. Vamshidhar and R. A. Rama: "Calculation of Downhole pH and Delta pH in the Presence of CO₂ and Organic Acids", CORROSION/96, NACE; 1996, paper no. 176.

[90]   C. A. R. Silva, X. W. Liu and F. J. Millero: "Solubility of siderite (FeCO₃) in NaCl solutions", Journal of Solution Chemistry, 2002, 31(2), 97-108.

[91]   Y. Sun, S. Nesic: "Parametric Study and Modeling on Localized CO₂ Corrosion in Horizontal Wet Gas Flow", CORROSION/04, NACE, 2004, paper no. 380.

[92]   D. A. Palmer and R. van Eldik: "The chemistry of metal carbonato and carbon dioxide complexes", Chemical Reviews, 1983, 83(6), 651–731.

[93]   E. Högfeldt: "Stability constants of metal-ion complexes - part A: inorganic ligands", IUPAC chemical data series volume 21, 1982.

[94]   N. P. Zhuk: "Thermodynamic constants of sulfates, carbonates, chromates, bromates, iodates, oxalates, and other salts slightly soluble in water", Zhurnal Fizicheskoi Khimii, 1954, 28, 1690-7.

[95]   M. M. Ghosh: "Oxygenation of ferrous iron(II) in highly buffered waters", In: "Aqueous-Environmental Chemistry of Metals ", (Ed. Rubin, A. J), Ann Arbor Science: Ann Arbor, 1974; 193-217.

[96]   C. W. Davies: "The Extent of dissociation of salts in water", Journal of the Chemical Society, 1938, 2, 2093-2100.

[97]   P. Wersin, L. Charlet, R. Karthein and W. Stumm: "From adsorption to precipitation: Sorption of Mn²⁺ on FeCO₃(s)", Geochim. Cosmochim. Acta., 1989, 53, 2787–2796.

[98]   C. Fouillac and A. Criaud: "Carbonate and bicarbonate trace metal complexes: critical reevaluation of stability constants", Geochem. J., 1984, 18, 297–303.

[99]   D. Langmuir: "Techniques of estimating thermodynamic properties for some aqueous complexes of geochemical interest", ACS Symposium Series, 1979, 93, 353-87.

[100]   W. Stumm and J. J. Morgan: "Aquatic chemistry : Chemical equilibria and rates in natural waters", 3.ed. New York,N.Y., Wiley., 1996.

[101]   D. H. Davies and G. T. Burstein: "The Effects of Bicarbonate on the Corrosion and Passivation of Iron", Corrosion, 1980, 36(8), 416-422.

[102]   N. W. Sidgwick: "The Chemical Elements and Their Compounds. Vols. II.", University Press, Oxford, 1952.

[103]   A. Wieckowski, E. Ghali, M. Szklarczyk and J. Sobkowski: "The behaviour of iron electrode in CO₂ saturated neutral electrolyte—I. Electrochemical study", Electrochimica Acta, 1983, 28(11), 1619.

[104] V. Thurmond and F. J. Millero: "Ionization of carbonic acid in sodium chloride solutions at 25°C", J. Solution Chem., 1982, 11(7), 447.

[105] F. J. Millero and D. J. Hawke: "Ionic Interactions of Divalent Metals in Natural-Waters", Marine Chemistry, 1992, 40(1-2), 19-48.

[106] I. Grethe, A. V. Plyasunov and K. Spahiu: "Estimations of Medium Effects on Thermodynamic Data", in: Modelling in Aqautic Chemistry, OECD NEA, Paris, 1997, 325-426.

[107] L. N. Plummer and E. Busenberg: "The Solubilities of Calcite, Aragonite and Vaterite in CO_2-H_2O Solutions Between 0-°C and 90 °C, and an Evaluation of the Aqueous Model for the System $CaCO_3$-CO_2-H_2O", Geochim. Cosmochim. Acta, 1982, 46, 1011-1040.

[108] T. E. Larson, "Oxidation of Metals and Ions in Solution", In "Principles and application of water chemistry", (Ed. S.D. Faust and J.V. Hunter), John Wiley and sons, inc., New York, 1967, p. 433.

[109] S. V. Mattigod nd G. Sposito: "Estimated Association Constants for Some Complexes of Trace-Metals With Inorganic Ligands", Soil Science Society of America Journal, 1977, 41(6), 1092-1097.

[110] C. F. Baes and R. E. Mesmer: "The Hydrolysis of Cations. Iron", American journal of science, 1981, 281, 935-962.

[111] F. H. Sweeton and C. F. Baes, Jr.: "The solubility of magnetite and hydrolysis of ferrous ion in aqueous solutions at elevated temperatures", Journal of Chemical Thermodynamics, 1970, 2(4), 479.

[112] D.R. Turner, M. Whitfield and A.G. Dickson: "The equilibrium speciation of dissolved components in freshwater and seawater at 25°C and 1atm pressure", Geochim. Cosmochim. Acta., 1981, 45, 855–881.

[113] S. Emerson: "Early diagenesis in anaerobic lake sediments: chemical equilibriums in interstitial waters", Geochimica et Cosmochimica Acta, 1976, 40(8), 925-34.

[114] D. Postma: "Pyrite and Siderite Formation in Brackish and Fresh-Water Swamp Sediments", American Journal of Science, 1982, 282(8), 1151-1183.

[115] H. Gamsjäger and F. Reiterer: "Investigation of equilibria involving carbon dioxide, carbonates and water", Environ. Internatl., 1979, 2, 419-424.

[116] H. Gamsjäger and E. Königsberger: "Solubility of sparingly soluble ionic solids in liquids", In "The experimental Determination of Solubilities", (Ed. Hefter and R.P.T. Tomkins), Wiley, 2003, 315.

[117] B. Klarmann: "Die Lösung von Eisen durch Kohlensäure", Zeitschrift für Angewandte Chemie, 1924, 37(34), 645-646.

[118] R. Müller and L. Harant: "Investigating the solubility of siderite and the electro-deposition of iron from these solutions", Berg und Huttenmannisches Jahrbuch, 1935, 83, 93-102.

[119] E. Müller and H. Henecka: "The action of carbon dioxide under high pressure on metallic iron", Z. anorg. allgem. Chem., 1929, 181, 159-71.

[120] A. Dugstad: "The Importance of $FeCO_3$ Supersaturation on the CO_2 Corrosion of Carbon Steels", CORROSION/92, NACE, 1992, paper no. 14.

[121] W. Leybold: "The solution of iron by carbonic acid", Angewandte Chemie, 1924, 37, 190-1.

[122] A. Dugstad and P.-E. Drønen: "Efficient Corrosion Control of Gas Condensate Pipelines by pH-Stabilisation", CORROSION/99, NACE, 1999, paper no. 20.

[123] F. J. Millero, Y. Wensheng, J. Aicher: "The speciation of Fe(II) and Fe(III) in natural waters", Marine Chem., 1995, 50(1-4), 21.

[124] D. W. King: "Role of carbonate speciation on the oxidation rate of Fe(II) in aquatic systems", Environmental Science & Technology, 1998, 32(19), 2997-3003.

[125]   C. Jimenez-Lopez and C. S. Romanek: "Precipitation kinetics and carbon isotope partitioning of inorganic siderite at 25°C and 1 atm", Geochimica et Cosmochimica Acta, 2004, 68(3), 557–571.

[126]   D. L. Leussing and I. M, Kolthoff: "The solubility of ferrous hydroxides and the ionisation of aquo-ferrous ion", J. am. chem. soc., 1953, 75, 2476.

[127]   E. L. Shock, D. C. Sassani, M. Willis, S. A. Sverjensky: "Inorganic species in geologic fluids: correlations among standard molal thermodynamic properties of aqueous ions and hydroxide complexes", Geochimica et Cosmochimica Acta, 1997, 61(5), 907-950.

[128]   H. E. Powell: "Thermal decomposition of siderite and consequent reactions", U.S. Bur. Mines Rept. Inv. 6643,44 p, 1965.

[129]   K. H. Gayer and L. Woontner: "The solubility of ferrous hydroxide and ferric hydroxide in acidic and basic media at 25°", Journal of Physical Chemistry, 1956, 60, 1569-71.

[130]   H. Ehlert and W. Hempel: "Über die löslichkeit einiger salze", Z. Elektrochem, 1912, 18, 727.

[131]   J. R. Baylis: "Factors other than dissolved oxygen influencing the corrosion of iron pipes", Journal of Industrial and Engineering Chemistry, 1926, 18(4) 370-80.

[132]   B. Lan and J. Jia: "Carbonate solubility in water at different pH values", Xi'an Dizhi Xueyuan Xuebao, 1996, 18(2), 80-86.

[133]   F. T. Gould: "Ferrous carbonate", US Patent 3416883, 1968.

[134]   O. Haehnel: "Solubilities and properties of the carbonates of strontium, barium, and heavy metals in water containing carbon dioxide under pressure", Journal fuer Praktische Chemie (Leipzig), 1924, 108, 187-93.

[135]   R. Brauns: "Chemische Mineralogie", Leipzig p. 398, 1896.

[136]   R. Lyden: "Studies on the solubilities of carbonate minerals and carbonates in carbonic acid solutions", Suomen Kemistiseuran Tiedonantoja, 1925, 34, 72-9.

[137]   G. I. Teodorovich and T. M. Shvedova: "Solubility of ferrous and other carbonate minerals in hydrochloric acid", Biull. Moskov. Obshchestva Ispytatelei Prirody, Otdel. Geol., 1960, 35(4), 100-4.

[138]   R. C. Wells: "The fractional precipitation of som ore-forming compounds at moderate temperatures", Geol. Surv. Bull. (U. S.) 609, 1915.

[139]   P.R. Konz: "Method of gas purification and removal of ferrous carbonate from the absorption solution", US patent 3264056, 1966.

[140]   J. Babcan: "Modelling of the low-temperature metasomatism of carbonates by siderite", Geologicky Zbornik--Geologica Carpathica, 1974, 25(1), 53-63.

[141]   J. Günzburg: "Über die Darstellung und die Eigenschaften von Ferrobikarbonatlösungen", Inaugural dissertation,Karlsruhe, 1911.

[142]   T. R. Andersen and A. Valle: "Prediction of top of the line corrosion in pipelines carrying wet CO₂ containing gas", CORROSION/93, NACE; 1993, paper no. 73.

[143]   L. G. Berg, and K. A. Buzdov: "Synthesis and thermal dissociation of iron(II) carbonate", Zhurnal Neorganicheskoi Khimii, 1961, 6, 2003-8.

[144]   W. C. Reynolds: "Chemical properties of concentrated solutions of certain salts. Part I. Double potassium carbonates", Journal of the Chemical Society, Transactions, 1898, 73, 262-267.

[145]   P. E: Rosenberg and F. F. Foit Jr.: "The stability of transition metal dolomites in carbonate systems: a discussion", Geochim. Cosmochim. Acta, 1979, 43, 951.

[146]   L. Chai and A. Navrotsky: "Synthesis, characterization, and energetics of solid solution along the dolomite-ankerite join, and implications for the stability of ordered CaFe(CO₃)₂", American Mineralogist, 1996, 81, 1141-1147.

[147]   P. M. Davidson: "Ternary iron, magnesium, calcium carbonates: a thermodynamic model for dolomite as an ordered derivative of calcite-structure solutions", American Mineralogist, 1994, 79(3-4), 332-9.

[148] E. Erdoe and H. Altorfer: "A basic iron carbonate similar to malachite as a corrosion product of steel", Werkstoffe und Korrosion, 1976, 27(5), 304-12.

[149] S. Al-Hassan, B. Mishra, D. L. Olson and M. M. Salama: "Effect of microstructure on corrosion of steels in aqueous solutions containing carbon dioxide", Corrosion, 1998, 54(6), 480-493.

[150] S. Music, I. Nowik, M. Ristic, Z. Orehovec and S. Popovic: "The effect of bicarbonate/carbonate ions on the formation of iron rust", Croatica Chemica Acta, 2004, 77(1-2), 141-151.

[151] W. Kamolpornwijit, L. Liang, G. R: Moline, T. Hart and O. R. West: "Identification and quantification of mineral precipitation in Fe0 filings from a column study", Environmental Science and Technology, 2004, 38(21), 5757-5765.

[152] R. de Marco, Z.-T. Jiang, B. Pejcic and E. Pionen: "An In Situ Synchrotron Radiation Grazing Incidence X-Ray Diffraction Study of Carbon Dioxide Corrosion", Journal of the Electrochemical Society, 2005, 152(10), B389-B392.

[153] R. de Marco, Z.-T. Jiang, D. John, M. Sercombe and B. Kinsella: "An in situ electrochemical impedance spectroscopy/synchrotron radiation grazing incidence X-ray diffraction study of the influence of acetate on the carbon dioxide corrosion of mild steel", Electrochimica Acta, 2007, 52(11), 3746-3750.

[154] Z. Xia, K. C. Chou and Z. Szklarska-Smialowska: "Pitting corrosion of carbon steel in carbon dioxide-containing sodium chloride brine", Corrosion, 1989, 45(8), 636-42.

[155] L. G: Berg, and K. A. Buzdov: "Determination of heat effects in the dissociation of FeCO₃", Zhurnal Neorganicheskoi Khimii, 1962, 7, 1773-8.

[156] H. Sontheimer, W. Kolle and V. Snoeyink: "The siderite model of the formation of corrosion resistant scales", American Water Works Association, 1981, 73, 572-579.

[157] J. Babcan: "Low-temperature synthesis of siderite", Geologicky Zbornik--Geologica Carpathica, 1970, 21(1), 89-97.

[158] H. Ehrhardt, H. C. Schober and H. Seidel: "Hochdrucksynthesen von Carbonaten. III. Darstellung von Carbonaten zweiwertiger Metalle durch Zersetzung ihrer Oxalate unter hohem CO₂-Druck", Z. Anorg. Allg. Chem., 1980, 465, 83.

[159] H. Ehrhardt, H. Schweer and H. Seidel: "Syntheses of some carbonates with carbon dioxide under high pressures", Zeitschrift fuer Anorganische und Allgemeine Chemie, 1980, 462, 185-98.

[160] A. Lemke and W. Biltz: "Zur Hydrothermalsynthese einiger Carbonate", Z. Anorg. all. Chem., 1934, 220, 312.

[161] E. E. Huxley and J. Fetchin: "Process for producing ferrous carbonate and removing oil from ammonia therewith", US patent, US3058810, 1962.

[162] C. Hoy: "Improvements in the manufacture of Iron carbonate", Great British patent, 7465, 1899.

[163] J. K. Lilly: "Production of ferrous carbonate", US patent 876366, 1908.

[164] C. L. Parker: "Improvements in & connected with the Production of Glauber Salts, Ferrous-carbonate, Ferrous-hydrate & Ammonia from Nitre-cake", Great British patent, 24639, 1903.

[165] D. L. Graf: "Crystallographic tables for the rhombohedral carbonates", Am. Mineralogist, 1961, 46, 1283-1316.

[166] O. Baudisch and L. A. Welo: "The aging of ferrous hydroxide and ferrous carbonate", Journal of Biological Chemistry, 1925, 64, 753-70.

[167] Von J. Krustinsons: "Dissociation of ferrous carbonate", Z. anorg. allgem. Chem. 1935, 225, 93-96.

[168] J. Gill: "Manufacture of Ferric oxide", US patent 842452, 1911.

[169]   W. Johannes: "Experimentelle Sideritbildung aus Calcit + FeCl₂", Contrib. Mineral, Petrology (Berlin), 1968, 17(2), 155-64.

[170]   W. E. Sharp: "The cell constants of artificial siderite", American Mineralogist, 1960, 45, 241-3.

[171]   A. Flügge: "Pure ferrous carbonate", Germany patent 178878, 1905.

[172]   A. V. Gogolev, E. V. Zakharova, N. I. Rodygina, A. M. Fedoseev, and V. P. Shilov: "Reduction of neptunium(V) and uranium(VI) with iron(II) in bicarbonate solutions", Radiochemistry, 2006, 48(3), 249-253.

[173]   J. K. Heuer and J. F. Stubbins: "An XPS characterization of FeCO₃ films from CO₂ corrosion", Corrosion Science, 1999, 41(7), 1231-1243.

[174]   W. G: Lyon: "Process for preparing ferrous carbonate", US patent 4657752, 1987.

[175]   C.F. Allison, GM. Dreher and C. A. Trathowen: "Production of ammonium sulfate and ferrous carbonate from ferrous sulfate-containing solutions", US patent 2845332, 1958.

[176]   A. Flügge: "Iron carbonate", Patent of France FR 371876, 1906.

[177]   A. Flügge: "An improvement of manufacture of Ferrous Carbonate in the cold", Great British Patent 27316, 1907.

[178]   K . H. Gayer, and L. Woontner: "The stability of iron(II) hydroxide", Journal of Chemical Education, 1957, 34, 178-9.

9 Improving diffusion models

The results of the thermodynamic modelling of the bulk phase are shown in section 7. This model may also be used for evaluating the thermodynamic factor, Γ_{ii}, used in the extended Nernst-Planck formulation defined by (62) and used in (114). The remaining thermodynamic factors Γ_{ij} for $i \neq j$ are not shown in this study since they are assumed to be negligible. In the result shown here only Γ_{ii} is illustrated. The reason is that including more thermodynamic factors complicates the equation scheme and the result can become difficult to interpret. This is illustrated by the following example: Equation (83) may be written for a binary system:

$$-\mathbf{d}_1 = \frac{RT}{x_1}\left(\Gamma_{11}\nabla x_1 + \Gamma_{1s}\nabla x_s\right) + z_1 F \nabla \phi = -\frac{RTx_s}{x_1 c_t \mathcal{D}_{1s}^\infty}\mathbf{J}_1^s \qquad (277)$$

Component 1 is the solute and component s is the solvent. The gradient of the solvent ∇x_s is often close to zero since the solvent composition is almost constant in the diffusion layer. Equation (277) shows that Γ_{1s} is related to the gradient of x_s. The diffusion problem has not been solved in the figures shown below and therefore ∇x_s has not been calculated. If Γ_{1s} is assumed to be zero, then Γ_{11} is the correction factor for the diffusivity at infinite dilution since the above rearranges to

$$\mathbf{J}_1^s = -\frac{c_t}{x_s}\mathcal{D}_{1,eff}\nabla x_1 - \frac{x_1 z_1 F}{RTx_s}\mathcal{D}_{1,eff}\nabla \phi \qquad (278)$$

Where the effective diffusivity is given by:

$$\mathcal{D}_{1,eff} = \mathcal{D}_{1s}^\infty \Gamma_{11} \qquad (279)$$

Γ_{ii} is therefore the correction factor of the diffusivity in order to account for non-ideality of the liquid phase.
The calculation of Γ_{ii} requires a thermodynamic activity coefficient model and a speciation routine. The thermodynamic model gives the activities and the derivatives with respect to T, P, and composition. The speciation routine calculates the equilibrium composition from the given T, P, and salt amount. In this study, parameter set B is used as determined in section 7. The rational symmetrical standard state is used for water and the rational unsymmetrical standard state for the other compounds.
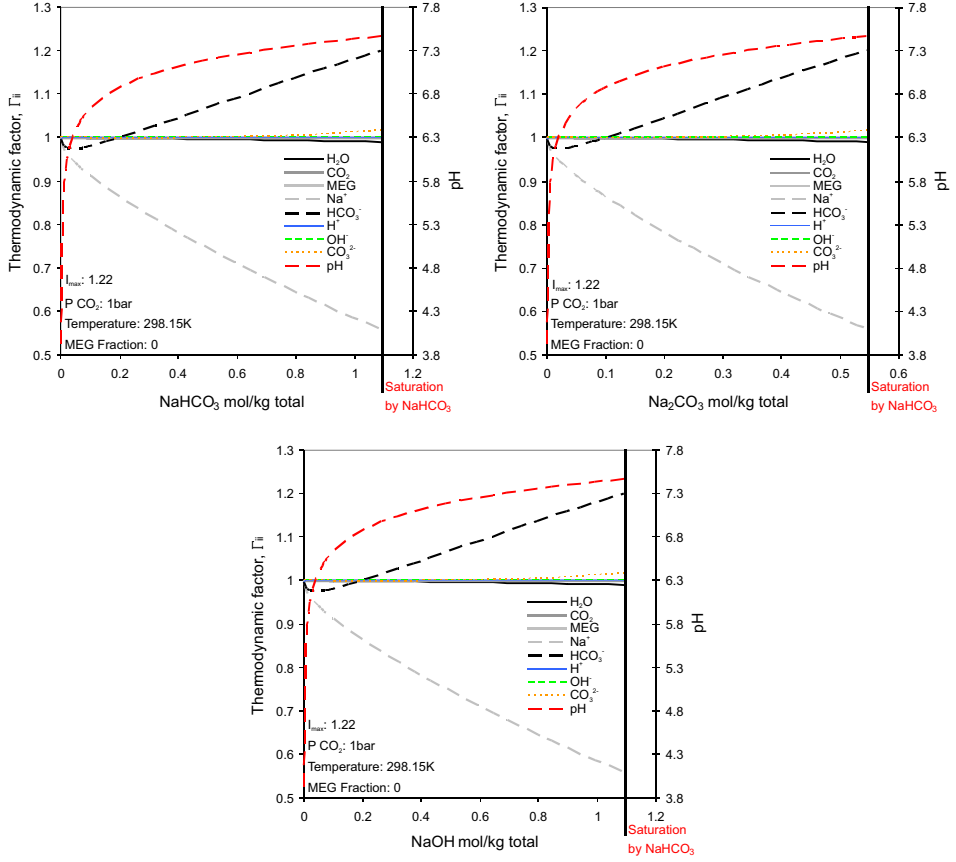
Figure 53: Thermodynamic factors, Γ_{ii}, as function of added *pH*-stabilizing salt, *NaOH, NaHCO₃*, and *Na₂CO₃*. The results of the three salts are equivalent since CO_2 reacts in the liquid phase. Saturation by *NaHCO₃* is reached in all three cases when salt concentration is high. I_{max} indicates the maximum ionic strength obtained at saturation.

Γ_{ii} will always approach one as the concentration goes to infinite dilution. Figure 53 shows Γ_{ii} and *pH* of the *Na₂CO₃-NaHCO₃-MEG-H₂O* system plotted for 1 bar partial pressure of CO_2 from zero concentration of the three salts *NaOH, NaHCO₃*, and *Na₂CO₃* at T=25°C to precipitation of a salt. *MEG* concentration is zero. *pH* is calculated using the molality of H^+, b_{H^+}, by:

$$pH = -\log\left(b_{H^+}\right) \tag{280}$$

CO_2 dissolves into the liquid phase and dissociates to HCO_3^- and CO_3^{2-} by the equilibria given by (201). The speciation routine is set up in order to calculate the liquid phase composition at a given temperature and CO_2 pressure at a specified amount of salt added. Comparing the three plots in figure 53 demonstrates that there is no difference between adding *NaOH, NaHCO₃* or *Na₂CO₃*.
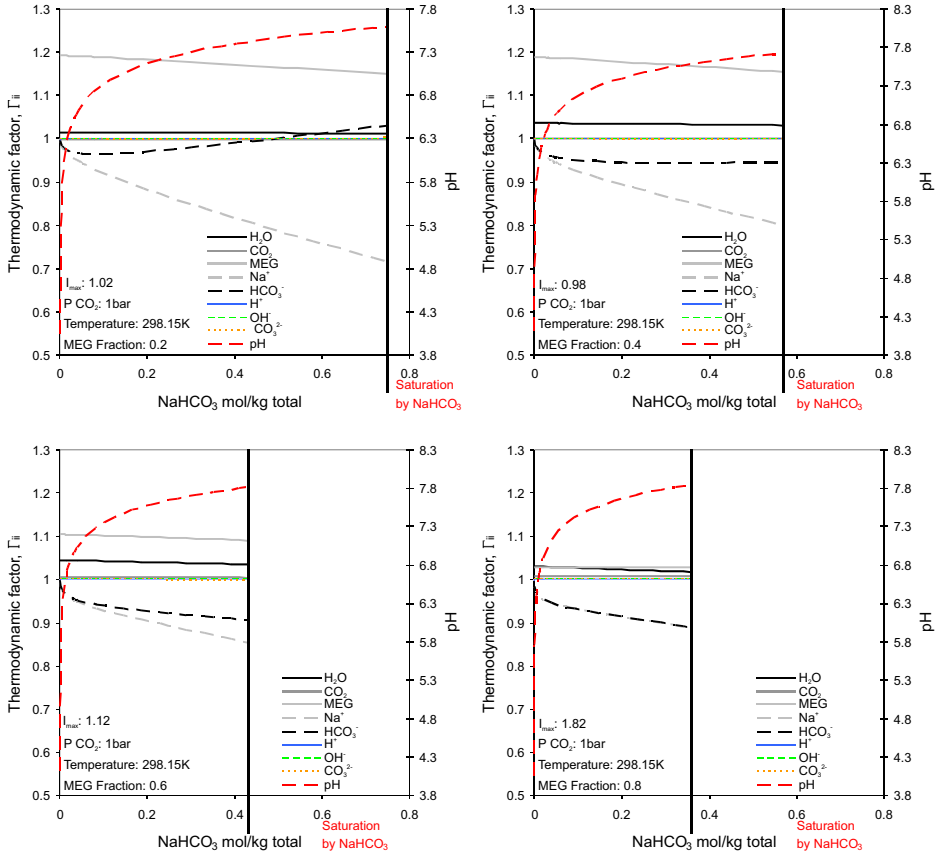
Figure 54: Setup is similar to figure 53 for increasing amount of *wt% MEG* on a salt-free basis.

The outcome of the calculation is the exact same result since the routine adds CO_2 until the defined pressure has been reached. This is similar to the real scenario in wet gas pipelines. The liquid phase is very small compared to the gas phase. CO_2 will dissolve the first few hours of production. New CO_2 is pumped through the pipeline and the partial pressure will quickly reach steady state and remain constant. The liquid phase becomes saturates with CO_2. The amount of CO_2 dissolved in the liquid is directly related to the added amount of *pH*-stabilizing salt. Figure 53 also shows that $NaHCO_3$ will precipitate if the concentration of *pH*-stabilizer is too high. The thermodynamic factors, Γ_{ii}, shown in figure 53 of $i = HCO_3^-$ is approximately one below 0.3 mol $NaHCO_3$/kg total. It illustrates that the effective diffusion coefficient is considerable different from the infinite dilution activity coefficient at higher concentration. It is 20% higher at saturation and the Γ_{ii} of $i = Na^+$ is 0.55 which indicates the effective diffusivity is 55% of the value at infinite dilution. The concentration of CO_3^{2-} is low in this solution, 0.01molal, and Γ_{ii} of $i = CO_3^{2-}$ is consequently also close to one, here 1.02. The concentration of the remaining components are close to infinite dilution and Γ_{ii} of these compounds are close to $\Gamma_{ii}=1$. The ionic strength, I_{max}, of the systems shown in figure 53 is approximately 1.2 *mol/kg H_2O* at saturation. This is an indication that the solutions behaves non-ideal.

Figure 54 demonstrates a calculation similar to figure 53. The effect of increasing amount of *MEG* is shown. Concentration of 20 *wt%* to 80 *wt% MEG* on a salt-free basis is given where figure 53 shows for 0 *wt% MEG*. It illustrates how Γ_{ii} of $i= HCO_3^-$ changes from 1.20 to 0.9 at saturation by addition of *MEG*. It also show that Γ_{ii} of $i=Na^+$ changes from 0.55 towards 0.9. This indicates the diffusion process is more "ideal" in the pure *MEG*. *MEG* lowers the activity of water and in addition it decreases the diffusivity of HCO_3^-, as figure 54 shows. This could explain why *MEG* reduces corrosion since the diffusion process of HCO_3^- is brought noticeably down.

The figure also shows that the effective diffusion coefficient of *MEG* it self in a 20 *wt% MEG* solution is 1.2, decreasing slightly with salt concentration. It is noteworthy that the ionic strength is 1.8 *mol/kg H_2O* at high *MEG* concentration due to the low amount of water present.
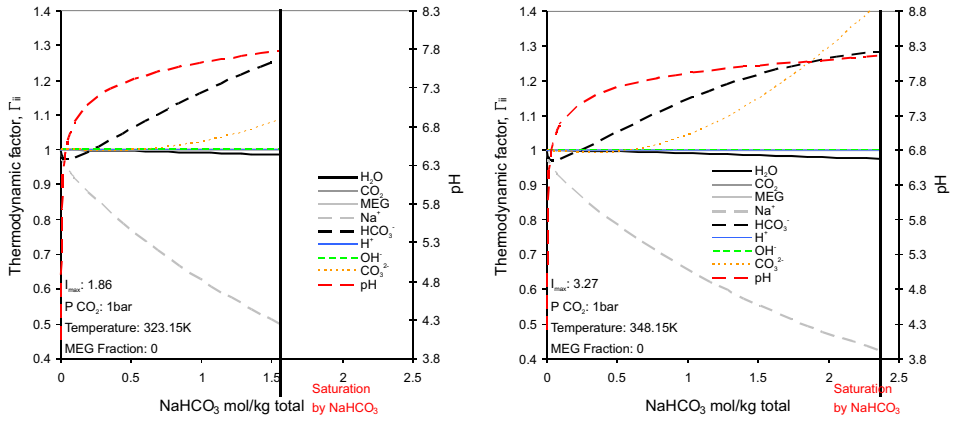
Figure 55: The effect of temperature on the thermodynamic factors, Γ_{ii}. Shown for 50 and 75°C. Solubility increases but profiles are almost unchanged.

Figure 55 reveals the effect of increasing temperature. The profiles are similar except that the solubility increases. By comparing figure 53 and the plots in 55 shows that the thermodynamic factor Γ_{ii} of $i= HCO_3^-$ and $i=Na^+$ are almost unchanged, but Γ_{ii} of $i= CO_3^{2-}$ increases with temperature. Figure 55 illustrates that the effective diffusivity of CO_3^{2-} at 75° is 1.4 at saturation. This indicates that carbonate diffuses much faster close to saturation at high temperature. The high transport of carbonate could have an unexpected influence on the build-up of protective $FeCO_3$ layers.
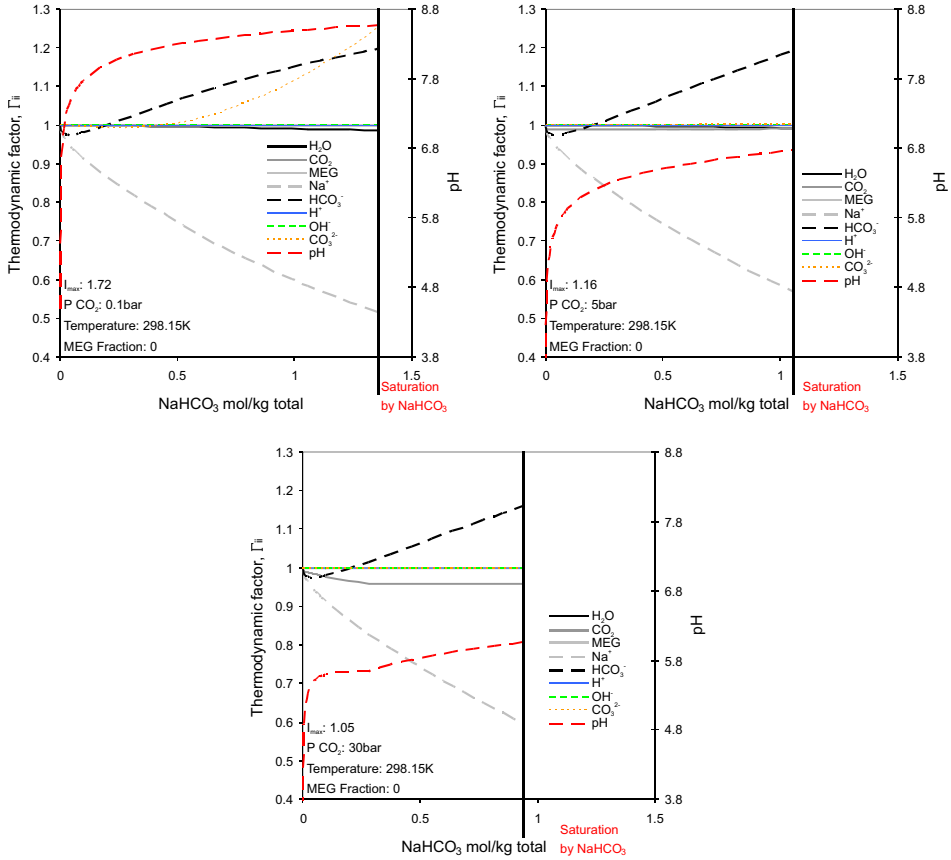
Figure 56: The effect of partial pressure of CO_2 on the thermodynamic factors, Γ_{ii}. High pressure lowers the thermodynamic factor of carbonate.

Figure 56 show the sensitivity to pressure. It compares to figure 53 at 1 bar CO_2. The high CO_2 pressure sours the liquid phase as observed on the *pH* axis. The *pH* is below 7 at p_{CO_2} =5 and 30 bar and therefore CO_3^{2-} has dissociates to HCO_3^- . Therefore Γ_{ii} of i=CO_3^{2-} decreases with increasing p_{CO_2} . Γ_{ii} of i= HCO_3^- and i=Na^+ remain almost unchanged. The high CO_2 pressure lowers the solubility limit since the activity of HCO_3^- has increased. The figure also shows that CO_2 pressure has a relatively high effect on Γ_{ii} at low pressures but limited effect at high pressure. At high pressure the change in the thermodynamic factor of CO_2 becomes noticeable.

The results shown here proves that a thermodynamic activity coefficient model can be used for evaluating the thermodynamic factors and thereby improving the results of a diffusion model. The correction factor of the diffusion coefficient is in the order of 0.4 to 1.6. It may be agued that this is within the experimental accuracy of the determined diffusion coefficients. If an activity coefficient is used for the bulk calculations, there is no reason not to include it in the diffusion model. One of the reasons why this is not done is probably because of the lack of theory. In this work a comprehensive set of

equations are presented which may be used for setting up the diffusion problem as function of the activity coefficient model.

10 Conclusion

The main objective of this work has been to improve the understanding of the CO_2 corrosion mechanism. The focus has mainly been wet gas pipelines for transportation of natural gas offshore.
An extensive mathematic theory is presented in order to improve existing mechanistic CO_2 corrosion models.
It is shown in brief how to perform a full thermodynamic bulk calculation.
A detailed scheme of the multi component electrolyte diffusion process is given. Several setups for implementation of the diffusion and thermodynamic models are given. The theory of extending the Nernst-Planck theory is given and expressed in terms of thermodynamic factors which have not been presented previously.
A precise representation of the electrochemical kinetics is given. Suggestions for enhancing the Stern and Geary theory is presented and thereby enhancement the theory behind linear polarization resistance and corrosion measurements. The alternative extensions of the Stern and Geary theory are compared. The result show that the original Stern and Geary theory is suited for normal activation controlled kinetics, but it over predicts considerably if the corrosion process is affected by limiting current densities.
An extensive review of CO_2 literature is presented and a review of existing mechanistic CO_2 corrosion models is given.
Literature has shown that $FeCO_3$ plays an important part in the corrosion process especially the solubility if $FeCO_3$. There is a lack of accuracy on existing thermodynamic properties of $FeCO_3$. This indicates that the calculated solubility and temperature dependence of the solubility has been imprecise. This is due to the properties of Fe^{2+}. These vary significantly depending of the atmosphere of either H_2 or vacuum. Existing properties are validated and a consistent set of $FeCO_3$ properties are given.
There are a great number of mechanistic CO_2 corrosion models in the open literature. The majority of models assume ideal thermodynamic condition. This is a crude assumption since the ionic strength is up to 10 *mol/kg H_2O* in certain pipelines. A thermodynamic model is build in order to improve the thermodynamic description. Parameters for the extended UNIQUAC model are presented for the extension to *MEG* calculations in the multi solvent electrolyte system: *CO_2-NaHCO₃-Na₂CO₃-MEG-wate*r. Parameters are regressed to literature values of SLE, VLE, heat excess, and validated for heat capacity data. 212 experimental SLE data points were measured in this work and used in the thermodynamic modelling. The determined parameters are valid between -50 and 90 °C. Measurements were conducted at 2 to 60 °C at atmospheric conditions. A method called the reverse Schreinemakers method was developed during the experimental work. It improves the accuracy of the solubility measurements and reduces the amount of experimental work needed since it gives almost the same information as a new experiment. The method may also be used for obtaining information on the unknown solid phase, just like the original Schreinemakers method.
A model of the density in the *NaCl-NaHCO₃-Na₂CO₃-MEG-wate*r system is given from literature values and experimental work measured in this study. The model is valid between 2 and 60℃.

The thermodynamic model is a general model and it is not restricted to the corrosion system. It may be used for calculating the activity coefficient in the CO_2-$NaHCO_3$-Na_2CO_3-MEG-*wate*r system. The system is for example found in some gas drying facilities and other closed CO_2 loops. The model may additionally be used for scale prediction CO_2 capture calculations. The representation of the phase equilibria by this model is good.

A database of approximately 3500 data points on phase equilibrium measurements in systems containing CO_2, CH_4, *MEG*, *DEG*, *TEG*, and *wate*r was collected and evaluated during the modelling.

The effect of applying the above thermodynamic model in a diffusion model is shown. The thermodynamic factors have been calculated in the system CO_2-$NaOH$-$NaHCO_3$-Na_2CO_3-MEG-*water*. The results show that the diffusivities of Na^+, HCO_3^-, CO_3^{2-}, *MEG*, and $CO_2(aq)$ may vary 60% up or down compared to the infinite dilute diffusivities. The outcome is independent of whether $NaOH$, $NaHCO_3$, or Na_2CO_3 is used. The effect on Na^+ diffusivity is high in all cases and *MEG* is affected at low *MEG* concentrations. Diffusivity of HCO_3^- is only affected by the *MEG* concentration. The system seems to perform more ideally in term of diffusion at high *MEG* concentrations. CO_3^{2-} diffusivity is a strong function of temperature and partial pressure of CO_2. Diffusivity of $CO_2(aq)$ is also effected at high CO_2 pressure.

The work done in this thesis has shown that all mechanistic CO_2 corrosion models may be improved by applying a thermodynamic model. It will involve some difficulties in the mathematical description. This will improve the capabilities of the models to predict corrosion and to extrapolate to unknown system at high ionic strength.

11 Future, short term – long term

The future work would be to include $FeCO_3$ in the extended UNIQUAC model. Fe^{2+} is already in the aqueous model, but the interaction between Fe^{2+}-CO_2, Fe^{2+}-HCO_3^-, Fe^{2+}-CO_3^{2-}, and Fe^{2+}-MEG needs to be fitted. Results for the effect of MEG on $FeCO_3$ would be interesting to investigate. This would require minimum work since the solubility of $FeCO_3$ was measured in this work both in water and in *MEG-water*, though not given in this thesis. This may show that the solubility of $FeCO_3$ is lower in *MEG* and *MEG* therefore enhances the corrosion protection.

It could be interesting to see the effect of *DEG* compared to *MEG*. Similarly the effect of methanol would be obvious to investigate since some of the industry is using the cheaper methanol. The extended UNIQUAC model has already been regressed for methanol. Showing the thermodynamic factors in the water system would be an interesting issue and to compare to *MEG*. It may involve a new regression of the methanol parameters since CO_2 has never been fitted to methanol.

Natural gas has been considered not to influence the equilibria in this study. It may be investigated by including CH_4 in the model. It would be an easy task since experimental data has already been collected in this work. The procedure is only interesting from a scientific point of view, since the effect of CH_4 is expected to be very low.

An obvious task would be to implement a full diffusion model which includes the extended UNIQUAC model. The objective would be to show the effect of the extended UNIQUAC model on the predicted corrosion rates. It would be interesting to see the effect of the thermodynamic model compared to the same corrosion model at ideal conditions. The OLI thermodynamic model has been used in a public study to create an advanced electrochemical model. It would be interesting to see the effect of implementing their model in a full diffusion scheme which include a thermodynamically correct bulk calculation and the thermodynamic factors in the diffusion model. This may be very difficult to obtain since OLI is very restrictive towards their internal computer code.

The electrochemical kinetics of CO_2 corrosion is understood to some extended, but there are still improvements to be made, especially the CO_2 corrosion mechanism in combination with H_2S, O_2 and acetic acid. The accuracy of the corrosion models always rely on the precision of the core electrochemical model. A mathematically model has still not been presented.

The corrosion literature and the thermodynamic property collections have reached a slight inconsistency level. The corrosion literature has accepted the existence of H_2CO_3, but it has been rejected by thermodynamic databases. This issue needs to be addressed in order to build consistent corrosion models.

The predictive CO_2 corrosion models are currently modelled as 1D discretized PDE's. The corrosion models of the future will and should be implemented in more general flow simulation scheme. One of the difficult tasks in the future will be to reliably and easily predict pitting and crevice corrosion. It would be a task to implement corrosion models directly in process simulators in order the quickly determine whether the equipment could withstand corrosion or which alloy would be optimal for the specific operating conditions.

12   List of figures and tables

12.1   Figures

12.2 Tables

13 Appendix

A. Theory of electrolyte thermodynamics

A.1 Converting between activity coefficient types

The following gives a general relation for the chemical potential from a combination of (23) and (13):

$$\mu_i = \mu_i^{\Theta s} + RT \ln \left(s_i \gamma_i^{\Theta s} / s_i^{\Theta} \right) \tag{281}$$

$$= \mu_i^{\circ x} + RT \ln \left(x_i \gamma_i^{\circ x} / x_i^{\circ} \right) \tag{282}$$

$$= \mu_i^{*x} + RT \ln \left(x_i \gamma_i^{*x} / x_i^{*} \right) \tag{283}$$

$$= \mu_i^{*m} + RT \ln \left(b_i \gamma_i^{*m} / b_i^{*} \right) \tag{284}$$

$$= \mu_i^{*c} + RT \ln \left(c_i \gamma_i^{*c} / c_i^{*} \right) \tag{285}$$

This section has its basis in eq. (282) to (285), here equations which relate $\gamma_i^{\circ x}$, γ_i^{*c}, γ_i^{*m} and γ_i^{*x} are derived.

The standard state concentration, s_i^{Θ}, is assumed 1 and therefore neglected in the following equations.

Only three relations are needed to convert between the four different activities. Four relations are given just to give a wider relation to other explicit variables. Equation (306) and (311) are in principal related and should be taken as two different representations of the same equation.

The equations derived in this appendix are listed here:

$$\gamma_i^{*x} = \frac{\gamma_i^{\circ x}}{\gamma_i^{\infty x}} \tag{290}$$

$$\gamma_i^{*m} = x_s \gamma_i^{*x} \tag{303}$$

$$\gamma_i^{*c} = \gamma_i^{*x} \frac{\rho_s}{M_s} \frac{\bar{M}_t}{\rho_t} \tag{306}$$

$$\gamma_i^{*c} = \gamma_i^{*m} \frac{\rho_s}{\rho_t} \frac{m_t}{m_s} \tag{311}$$

Nomenclature is found at the derived equations in the subsections below.
The above written as one gives:

$$\gamma_i^{*m} = x_s \gamma_i^{*x} = x_s \frac{\gamma_i^{\circ x}}{\gamma_i^{\infty x}} = x_s \gamma_i^{*c} \frac{\rho_t}{\rho_s} \frac{M_s}{\overline{M}_t} = \gamma_i^{*c} \frac{\rho_t}{\rho_s} \frac{m_s}{m_t} \qquad (286)$$

Remember that if a special standard state is applied which does not use a standard state concentration of $s_i^\Theta = 1[unit]$, then s_i^Θ will become part of the equations above.

A.1.1 Converting between rational symmetrical and rational unsymmetrical activity coefficients

From (282) and (283) by equalizing gives:

$$\mu_i = \mu_i^{\circ x} + RT \ln\left(x_i \gamma_i^{\circ x}\right) = \mu_i^{*x} + RT \ln\left(x_i \gamma_i^{*x}\right) \Leftrightarrow$$

$$\frac{\mu_i^{\circ x} - \mu_i^{*x}}{RT} = \ln\left(\frac{x_i \gamma_i^{*x}}{x_i \gamma_i^{\circ x}}\right) \Leftrightarrow \qquad (287)$$

$$\frac{\mu_i^{\circ x} - \mu_i^{*x}}{RT} = \ln\left(\frac{\gamma_i^{*x}}{\gamma_i^{\circ x}}\right)$$

At infinite dilution the rational unsymmetric activity coefficient approach one, $\gamma_i^{*x} \to 1$ for $x_i \to 0$. The rational symmetric activity coefficient is therefore very far from its ideal situation of $\gamma_i^{\circ x} \to 1$ for $x_i \to 1$. At infinite dilution it has a finite value, defined by:

$$\lim_{x_i \to 0} \gamma_i^{\circ x} \equiv \gamma_i^{\infty x} \qquad (288)$$

$\gamma_i^{\infty x}$ is the rational symmetric activity coefficient at infinite dilution in the solvent. At infinite dilution (287) is rewritten with (288) and $\gamma_i^{*x} \to 1$ to give:

$$\frac{\mu_i^{\circ x} - \mu_i^{*x}}{RT} = \ln\left(\frac{\gamma_i^{*x}}{\gamma_i^{\circ x}}\right) \to \ln\left(\frac{1}{\gamma_i^{\infty x}}\right) \quad for \quad x_i \to 0 \qquad (289)$$

Because (287) must be valid also at infinite dilution, (289) and (287) is combined to give:

$$\gamma_i^{*x} = \frac{\gamma_i^{\circ x}}{\gamma_i^{\infty x}} \Leftrightarrow$$

$$\ln\left(\gamma_i^{*x}\right) = \ln\left(\gamma_i^{\circ x}\right) - \ln\left(\gamma_i^{\infty x}\right) \qquad (290)$$

A.1.2 Converting between rational symmetrical and molal unsymmetrical activity coefficients

From eq. (282) and (284):

$$\mu_i = \mu_i^{\circ x} + RT \ln\left(x_i \gamma_i^{\circ x}\right) = \mu_i^{*m} + RT \ln\left(b_i \gamma_i^{*m}\right) \Leftrightarrow$$

$$\frac{\mu_i^{\circ x} - \mu_i^{*m}}{RT} = \ln\left(\frac{b_i \gamma_i^{*m}}{x_i \gamma_i^{\circ x}}\right) \tag{291}$$

The quantity b_i / x_i is found from:

$$\frac{b_i}{x_i} = \frac{n_i / (n_s M_s)}{n_i / n_t} = \frac{n_t}{n_s} \frac{1}{M_s} = \frac{1}{x_s M_s} \tag{292}$$

where n_i is the number of moles of i, n_s and M_s is the number moles and mol weight (*kg/mol*) of the solvent s. n_t is the total number of moles in the phase. At infinite dilution $x_s \approx 1$ which from (292) gives:

$$\frac{b_i}{x_i} = \frac{1}{x_s M_s} \rightarrow \frac{1}{M_s} \qquad for \qquad x_i \rightarrow 0 \tag{293}$$

at infinite dilution (291) and (293) gives a relation equivalent to (288) which is valid because $\gamma_i^{*x} \rightarrow 1$ for $x_i \rightarrow 0$:

$$\frac{\mu_i^{\circ x} - \mu_i^{*m}}{RT} = \ln\left(\frac{b_i \gamma_i^{*m}}{x_i \gamma_i^{\circ x}}\right) \rightarrow \ln\left(\frac{1}{M_s \gamma_i^{\infty x}}\right) \qquad for \qquad x_i \rightarrow 0 \tag{294}$$

From (291) and (294) the relation between unsymmetric molal and rational symmetrical activity coefficient is found because (291) must be valid also at infinite dilution, using (292) gives:

$$\frac{b_i \gamma_i^{*m}}{x_i \gamma_i^{\circ x}} = \frac{1}{M_s \gamma_i^{\infty x}} \Leftrightarrow$$

$$\gamma_i^{*m} = x_s \frac{\gamma_i^{\circ x}}{\gamma_i^{\infty x}} \tag{295}$$

the above could easily be used in combination of (290) to give (303).

A.1.3 Converting between rational symmetrical and molar unsymmetrical activity coefficients

From (282) and (285):

$$\mu_i = \mu_i^{\circ x} + RT \ln\left(x_i \gamma_i^{\circ x}\right) = \mu_i^{*c} + RT \ln\left(c_i \gamma_i^{*c}\right) \Leftrightarrow$$

$$\frac{\mu_i^{\circ x} - \mu_i^{*c}}{RT} = \ln\left(\frac{c_i \gamma_i^{*c}}{x_i \gamma_i^{\circ x}}\right) \tag{296}$$

The quantity c_i/x_i is found from:

$$\frac{c_i}{x_i} = \frac{n_i/V_t}{n_i/n_t} = \frac{n_t \rho_t}{m_t} = \frac{\rho_t}{\bar{M}_t} \tag{297}$$

c_i is the concentration in(*mol/L solution*). V_t is the total volume (L) of the phase and ρ_t is the total density in (*kg/L solution*) of the phase. m_t is the total mass of matter and $\bar{M}_t$ is the number average molecular weight of solution (*kg/mol*) calculated as $\bar{M}_t = \sum_i x_i M_i$ summed over all species in the phase.

At infinite dilution, the above reduces to the following as $V_t \rightarrow V_s$ for $x_i \rightarrow 0$:

$$\frac{c_i}{x_i} \rightarrow \frac{n_i/V_s}{n_i/n_s} = \frac{n_s \rho_s}{m_s} = \frac{\rho_s}{M_s} \qquad for \qquad x_i \rightarrow 0 \tag{298}$$

ρ_s is the density of pure solvent. An equivalent to (288) in combination with the above gives the following at infinite dilution:

$$\frac{\mu_i^{\circ x} - \mu_i^{*c}}{RT} = \ln\left(\frac{c_i \gamma_i^{*c}}{x_i \gamma_i^{\circ x}}\right) \rightarrow \ln\left(\frac{\rho_s}{M_s \gamma_i^{\infty x}}\right) \qquad for \quad x_i \rightarrow 0 \tag{299}$$

By (296), (297) and (299) the relation between the molar unsymmetrical and rational unsymmetrical activity coefficient is found.

$$\frac{c_i \gamma_i^{*c}}{x_i \gamma_i^{\circ x}} = \frac{\rho_s}{M_s \gamma_i^{\infty x}} \Leftrightarrow$$

$$\gamma_i^{*c} = \frac{\gamma_i^{\circ x}}{\gamma_i^{\infty x}} \frac{\rho_s}{\rho_t} \frac{\bar{M}_t}{M_s} \tag{300}$$

because (296) must be valid at infinite dilution. The above should be seen in relation to (290) and (306).

A.1.4 Converting between rational unsymmetrical and molal unsymmetrical activity coefficients

From (283) and (284):

$$\mu_i = \mu_i^{*x} + RT \ln\left(x_i \gamma_i^{*x}\right) = \mu_i^{*m} + RT \ln\left(b_i \gamma_i^{*m}\right) \Leftrightarrow$$

$$\frac{\mu_i^{*x} - \mu_i^{*m}}{RT} = \ln\left(\frac{b_i \gamma_i^{*m}}{x_i \gamma_i^{*x}}\right) \tag{301}$$

at infinite dilution by the use of (293):

$$\frac{\mu_i^{*x} - \mu_i^{*m}}{RT} = \ln\left(\frac{b_i \gamma_i^{*m}}{x_i \gamma_i^{*x}}\right) \rightarrow \ln\left(\frac{1}{M_s}\right) \qquad for \qquad x_i \rightarrow 0 \tag{302}$$

From the combination of (292), (301) and (302) the relation between the molal unsymmetrical and rational unsymmetric activity coefficient is found by:

$$\frac{b_i \gamma_i^{*m}}{x_i \gamma_i^{*x}} = \frac{1}{M_s} \Leftrightarrow$$

$$\gamma_i^{*m} = x_s \gamma_i^{*x} \tag{303}$$

because (301) must be valid at infinite dilution.
By taking a look at (290) it is obvious that (295) is the same as (303).

A.1.5   Converting between rational unsymmetrical and molar unsymmetrical activity coefficients

From (283) and (285):

$$\mu_i = \mu_i^{*x} + RT \ln\left(x_i \gamma_i^{*x}\right) = \mu_i^{*c} + RT \ln\left(c_i \gamma_i^{*c}\right) \Leftrightarrow$$

$$\frac{\mu_i^{*x} - \mu_i^{*c}}{RT} = \ln\left(\frac{c_i \gamma_i^{*c}}{x_i \gamma_i^{*x}}\right) \tag{304}$$

which reduces to the following by the combination of (298) at infinite dilution:

$$\frac{\mu_i^{*x} - \mu_i^{*c}}{RT} = \ln\left(\frac{c_i \gamma_i^{*c}}{x_i \gamma_i^{*x}}\right) \rightarrow \ln\left(\frac{\rho_s}{M_s}\right) \qquad for \quad x_i \rightarrow 0 \tag{305}$$

(304) and (305) gives the relation between the molar unsymmetric and rational unsymmetric activity coefficient using (297):

$$\gamma_i^{*c} = \gamma_i^{*x} \frac{\rho_s}{M_s} \frac{\bar{M}_t}{\rho_t} \tag{306}$$

because (304) must hold at infinite dilution.
By taking a look at (290) it is obvious that (300) is the same as (306).

A.1.6 Converting between molal unsymmetrical and molar unsymmetrical activity coefficients

From (284) and (285):

$$\mu_i = \mu_i^{*m} + RT \ln\left(b_i \gamma_i^{*m}\right) = \mu_i^{*c} + RT \ln\left(c_i \gamma_i^{*c}\right) \Leftrightarrow$$

$$\frac{\mu_i^{*m} - \mu_i^{*c}}{RT} = \ln\left(\frac{c_i \gamma_i^{*c}}{b_i \gamma_i^{*m}}\right) \tag{307}$$

the ratio c_i/b_i is calculated from the relation, where m_s is the mass of solvent and m_t is the total mass in the phase. ρ_t is the overall density of the phase:

$$\frac{c_i}{b_i} = \frac{n_i/V_t}{n_i/m_s} = \frac{m_s \rho_t}{m_t} \tag{308}$$

At infinite dilution the volume of the phase is $V_t \to V_s$ as $x_i \to 0$, which reduces the above to:

$$\frac{c_i}{b_i} \to \frac{n_i/V_s}{n_i/m_s} = \rho_s \qquad for \qquad x_i \to 0 \tag{309}$$

in combination with (307) at infinite dilution, this gives:

$$\frac{\mu_i^{*m} - \mu_i^{*c}}{RT} = \ln\left(\frac{c_i \gamma_i^{*c}}{b_i \gamma_i^{*m}}\right) \to \ln\left(\rho_s\right) \qquad for \qquad x_i \to 0 \tag{310}$$

From equalization of (307) and (310) the relation between the molar unsymmetrical and molal unsymmetrical activity coefficient is obtained:

$$\frac{c_i \gamma_i^{*c}}{b_i \gamma_i^{*m}} = \rho_s \Leftrightarrow$$

$$\gamma_i^{*c} = \gamma_i^{*m} \frac{\rho_s}{\rho_t} \frac{m_t}{m_s} \tag{311}$$

because (307) has to be true at infinite dilution.
m are the masses given in equation (308), which are related to the mole number and molecular weights by $m_s = n_s M_s$ and $m_t = n_t \bar{M}_t$.

A.2 Relations between standard state fugacities

A relation between the standard state fugacities f_i^{*m}, f_i^{*x}, f_i^{*c} and $f_i^{\circ x}$ is derived. Equation (282) to (285) and links to the original relation of chemical potential and

standard properties in (13) is used. The standard state concentration, s_i°, is assumed 1 and therefore neglected in the following equations.
The equations derived in this appendix are:

$$f_i^{*x} = f_i^{\circ x}\gamma_i^{\infty x} \tag{315}$$

$$f_i^{*m} = f_i^{\circ x} M_s \gamma_i^{\infty x} \tag{318}$$

$$f_i^{\circ x} = \frac{\rho_s f_i^{*c}}{M_s \gamma_i^{\infty x}} \tag{321}$$

Equation (324), (327) and (330) are linear combinations of the above three and may be derived from the above.
This section was originally written, in order to show the relation between Henry's law constants at different scales. The above equations allow for the use of Henry's law to determine the symmetrical standard state fugacity. The reader should remember that all the above equations are functions of (*T*,*P*) and there are a new standard state for every (*T*,*P*).
To summarize: The above equations written as one:

$$f_i^{*m} = M_s f_i^{*x} = \rho_s f_i^{*c} = M_s f_i^{\circ x}\gamma_i^{\infty x} \tag{312}$$

Remember that if a special standard state is applied which does not use a standard state concentration of $s_i^\circ = 1[unit]$, then s_i° will become part of the equations above.

A.2.1   Relation between rational symmetrical and rational unsymmetrical standard state fugacity

The chemical potential in the liquid phase can be expressed by the rational symmetrical and rational unsymmetrical standard state. The chemical potential has to be the same independent of the standard state. Using (13) for the same phase using different standard and substituting the solution fugacities in (23) by activity coefficients shows

$$\mu_i = \mu_i^{\circ x} + RT\ln\left(\frac{\hat{f}_i}{f_i^{\circ x}}\right) = \mu_i^{*x} + RT\ln\left(\frac{\hat{f}_i}{f_i^{*x}}\right)$$
$$= \mu_i^{\circ x} + RT\ln\left(x_i\gamma_i^{\circ x}/x_i^\circ\right) = \mu_i^{*x} + RT\ln\left(x_i\gamma_i^{*x}/x_i^\circ\right) \tag{313}$$

Rearranging (313) gives:

$$\frac{\mu_i^{\circ x} - \mu_i^{*x}}{RT} = RT\ln\left(x_i\gamma_i^{*x}\right) - RT\ln\left(x_i\gamma_i^{\circ x}\right) = RT\ln\left(\frac{\hat{f}_i}{f_i^{*x}}\right) - RT\ln\left(\frac{\hat{f}_i}{f_i^{\circ x}}\right) \Leftrightarrow$$
$$\frac{\gamma_i^{*x}}{\gamma_i^{\circ x}} = \frac{f_i^{\circ x}}{f_i^{*x}} \tag{314}$$

From (290) $\gamma_i^{*x}/\gamma_i^{\circ x}$ is substituted for $\gamma_i^{\infty x}$

$$f_i^{*x} = f_i^{\circ x}\gamma_i^{\infty x} \tag{315}$$

A.2.2 Relation between rational symmetrical and molal unsymmetrical standard state fugacity

Using (13) for the same phase using different standard states and substituting the solution fugacities in (23) by activity coefficients shows

$$
\begin{aligned}
\mu_t &= \mu_i^{\circ x} + RT\ln\left(\frac{\hat{f}_i}{f_i^{\circ x}}\right) = \mu_i^{*m} + RT\ln\left(\frac{\hat{f}_i}{f_i^{*m}}\right) \\
&= \mu_i^{\circ x} + RT\ln\left(x_i\gamma_i^{\circ x}\right) = \mu_i^{*m} + RT\ln\left(b_i\gamma_i^{*m}\right)
\end{aligned} \tag{316}
$$

which rearranges to:

$$
\begin{aligned}
\frac{\mu_i^{\circ x} - \mu_i^{*m}}{RT} &= RT\ln\left(b_i\gamma_i^{*m}\right) - RT\ln\left(x_i\gamma_i^{\circ x}\right) = RT\ln\left(\frac{\hat{f}_i}{f_i^{*m}}\right) - RT\ln\left(\frac{\hat{f}_i}{f_i^{\circ x}}\right) \Leftrightarrow \\
\frac{b_i\gamma_i^{*m}}{x_i\gamma_i^{\circ x}} &= \frac{f_i^{\circ x}}{f_i^{*m}}
\end{aligned} \tag{317}
$$

From (295) the above rearranges to

$$f_i^{*m} = f_i^{\circ x} M_s \gamma_i^{\infty x} \tag{318}$$

M_s is the molar mass of the solvent in *kg/mol*.

A.2.3 Relation between rational symmetrical and molar unsymmetrical standard state fugacity

Using (13) for the same phase using different standard states and substituting the solution fugacities in (23) by activity coefficients shows

$$
\begin{aligned}
\mu_t &= \mu_i^{\circ x} + RT\ln\left(\frac{\hat{f}_i}{f_i^{\circ x}}\right) = \mu_i^{*c} + RT\ln\left(\frac{\hat{f}_i}{f_i^{*c}}\right) \\
&= \mu_i^{\circ x} + RT\ln\left(x_i\gamma_i^{\circ x}\right) = \mu_i^{*c} + RT\ln\left(c_i\gamma_i^{*c}\right)
\end{aligned} \tag{319}
$$

this gives:

$$\frac{\mu_i^{\circ x} - \mu_i^{*c}}{RT} = RT \ln\left(c_i \gamma_i^{*c}\right) - RT \ln\left(x_i \gamma_i^{\circ x}\right) = RT \ln\left(\frac{\hat{f}_i}{f_i^{*c}}\right) - RT \ln\left(\frac{\hat{f}_i}{f_i^{\circ x}}\right) \Leftrightarrow$$

$$\frac{c_i \gamma_i^{*c}}{x_i \gamma_i^{\circ x}} = \frac{f_i^{\circ x}}{f_i^{*c}}$$

(320)

Using (300) the above results in

$$\frac{c_i \gamma_i^{*c}}{x_i \gamma_i^{\circ x}} = \frac{\rho_s}{M_s \gamma_i^{\infty x}} = \frac{f_i^{\circ x}}{f_i^{*c}} \Leftrightarrow$$

$$f_i^{\circ x} = \frac{\rho_s f_i^{*c}}{M_s \gamma_i^{\infty x}}$$

(321)

M_s is the molar mass of the solvent in *kg/mol* and ρ_s is the density of the pure solvent at (T,P) equal to the (T,P) at which the f_i^{*c}, $\gamma_i^{\infty x}$ and $f_i^{\circ x}$ are found.

A.2.4 Relation between rational unsymmetrical and molal unsymmetrical standard state fugacity

Using (13) for the same phase using different standard states and substituting the solution fugacities in (23) by activity coefficients shows

$$\mu_t = \mu_i^{*x} + RT \ln\left(\frac{\hat{f}_i}{f_i^{*x}}\right) = \mu_i^{*m} + RT \ln\left(\frac{\hat{f}_i}{f_i^{*m}}\right)$$

$$= \mu_i^{*x} + RT \ln\left(x_i \gamma_i^{*x}\right) = \mu_i^{*m} + RT \ln\left(b_i \gamma_i^{*m}\right)$$

(322)

Isolating $\left(\mu_i^{*x} - \mu_i^{*m}\right)/RT$ gives

$$\frac{\mu_i^{*x} - \mu_i^{*m}}{RT} = RT \ln\left(b_i \gamma_i^{*m}\right) - RT \ln\left(x_i \gamma_i^{*x}\right) = RT \ln\left(\frac{\hat{f}_i}{f_i^{*m}}\right) - RT \ln\left(\frac{\hat{f}_i}{f_i^{*x}}\right) \Leftrightarrow$$

$$\frac{b_i \gamma_i^{*m}}{x_i \gamma_i^{*x}} = \frac{f_i^{*x}}{f_i^{*m}}$$

(323)

From (303) this gives:

$$\frac{b_i \gamma_i^{*m}}{x_i \gamma_i^{*x}} = \frac{1}{M_s} = \frac{f_i^{*x}}{f_i^{*m}} \Leftrightarrow$$

$$f_i^{*m} = M_s f_i^{*x}$$

(324)

M_s is the molar mass of the solvent in *kg/mol*.

A.2.5 Relation between rational unsymmetrical and molar unsymmetrical standard state fugacity

Using (13) for the same phase using different standard states and substituting the solution fugacities in (23) by activity coefficients shows

$$
\mu_i = \mu_i^{*x} + RT \ln\left(\frac{\hat{f}_i}{f_i^{*x}}\right) = \mu_i^{*c} + RT \ln\left(\frac{\hat{f}_i}{f_i^{*c}}\right)
$$
$$
= \mu_i^{*x} + RT \ln\left(x_i \gamma_i^{*x}\right) = \mu_i^{*c} + RT \ln\left(c_i \gamma_i^{*c}\right)
$$
(325)

Finding $\left(\mu_i^{*x} - \mu_i^{*c}\right)/RT$ rearranges the above to:

$$
\frac{\mu_i^{*x} - \mu_i^{*c}}{RT} = RT \ln\left(c_i \gamma_i^{*c}\right) - RT \ln\left(x_i \gamma_i^{*x}\right) = RT \ln\left(\frac{\hat{f}_i}{f_i^{*c}}\right) - RT \ln\left(\frac{\hat{f}_i}{f_i^{*x}}\right) \Leftrightarrow
$$
$$
\frac{c_i \gamma_i^{*c}}{x_i \gamma_i^{*x}} = \frac{f_i^{*x}}{f_i^{*c}}
$$
(326)

Some reference to how $\rho s/M_s$ came about (see my master thesis)

$$
\frac{c_i \gamma_i^{*c}}{x_i \gamma_i^{*x}} = \frac{\rho_s}{M_s} = \frac{f_i^{*x}}{f_i^{*c}} \Leftrightarrow
$$
$$
f_i^{*x} = \frac{\rho_s}{M_s} f_i^{*c}
$$
(327)

M_s is the molar mass of the solvent in *kg/mol* and ρ_s is the density of the pure solvent at (T,P) equal to the (T,P) at which the f_i^{*c} is found.

A.2.6 Relation between molal unsymmetrical and molar unsymmetrical standard state fugacity

Using (13) for the same phase using different standard states and substituting the solution fugacities in (23) by activity coefficients shows

$$
\mu_i = \mu_i^{*m} + RT \ln\left(\frac{\hat{f}_i}{f_i^{*m}}\right) = \mu_i^{*c} + RT \ln\left(\frac{\hat{f}_i}{f_i^{*c}}\right)
$$
$$
= \mu_i^{*m} + RT \ln\left(b_i \gamma_i^{*m}\right) = \mu_i^{*c} + RT \ln\left(c_i \gamma_i^{*c}\right)
$$
(328)

This results in the following

$$\frac{\mu_i^{*m} - \mu_i^{*c}}{RT} = RT \ln\left(c_i \gamma_i^{*c}\right) - RT \ln\left(b_i \gamma_i^{*m}\right) = RT \ln\left(\frac{\hat{f}_i}{f_i^{*c}}\right) - RT \ln\left(\frac{\hat{f}_i}{f_i^{*m}}\right) \Leftrightarrow$$

$$\frac{c_i \gamma_i^{*c}}{b_i \gamma_i^{*m}} = \frac{f_i^{*x}}{f_i^{*m}}$$

(329)

From (311) this give

$$\frac{c_i \gamma_i^{*c}}{b_i \gamma_i^{*m}} = \rho_s = \frac{f_i^{*m}}{f_i^{*c}} \Leftrightarrow$$

$$f_i^{*m} = \rho_s f_i^{*c}$$

(330)

ρ_s is the density of the pure solvent at (T,P) equal to the (T,P) at which the f_i^{*c} is found.

A.3 Converting standard properties between standard states

Converting between standard states is performed using (14):

$$\mu_i^{\Theta_2 s} - \mu_i^{\Theta_1 s} = RT \ln \frac{\hat{f}_i^{\Theta_2 s}}{\hat{f}_i^{\Theta_1 s}}$$

(14)

The relations between standard state fugacities, $\hat{f}_i^{\Theta_i s}$, is given by (315), (318) and (321) and the fractions $\hat{f}_i^{\Theta_2 s} / \hat{f}_i^{\Theta_1 s}$ are basically a small rearrangement of the standard state fugacities. :

$$\frac{f_i^{*x}}{f_i^{\circ x}} = \gamma_i^{\infty x}$$

(315)

$$\frac{f_i^{*m}}{f_i^{\circ x}} = M_s \gamma_i^{\infty x}$$

(318)

$$\frac{f_i^{\circ x}}{f_i^{*c}} = \frac{\rho_s}{M_s \gamma_i^{\infty x}}$$

(321)

If we for example had a huge database of standard state data in molal unsymmetrical standard state, f_i^{*m}, at a reference T°, P°, like the NIST database. Take that we want to convert it to rational symmetrical standard state, $f_i^{\circ x}$, at the same T°, P° we would insert (318) in (14)

$$\mu_i^{\circ x} = \mu_i^{*m} + RT \ln \frac{f_i^{\circ x}}{f_i^{*m}}$$

$$= \mu_i^{*m} - RT \ln M_s \gamma_i^{\infty x}$$

(331)

This indicates that by subtract $RT \ln M_s \gamma_i^{\infty x}$ from all our molal unsymmetrical standard state properties will convert those into rational symmetrical standard state. A drawback to this approach is that a model of $\gamma_i^{\infty x}$ at T°, P° is needed.

To convert standard state data to other reference temperatures would require standard state properties.

B. Theory of electrochemistry

B.1 Isolation of net current in equation (171)

Assume:

$$\nu_X = \nu_R = 1$$

Assume also that one reactant and one product is found in (123). This lead to the following net current density of the involved redox reaction from (171):

$$i = i_0\left(\left(1 - \frac{i}{i_R^d}\right)\exp\left(\frac{(1-\alpha)nF\eta}{RT}\right) - \left(1 - \frac{i}{i_X^d}\right)\exp\left(\frac{-\alpha nF\eta}{RT}\right)\right)$$

Isolating of the exchange current density and the limiting current densities gives:

$$\frac{i}{i_0} = \exp\left(\frac{(1-\alpha)nF\eta}{RT}\right) - \frac{i}{i_R^d}\exp\left(\frac{(1-\alpha)nF\eta}{RT}\right) - \exp\left(\frac{-\alpha nF\eta}{RT}\right) + \frac{i}{i_X^d}\exp\left(\frac{-\alpha nF\eta}{RT}\right)$$

Moving the current densities to the left side gives:

$$i\left(\frac{1}{i_0} + \frac{1}{i_R^d}\exp\left(\frac{(1-\alpha)nF\eta}{RT}\right) - \frac{1}{i_X^d}\exp\left(\frac{-\alpha nF\eta}{RT}\right)\right) = \exp\left(\frac{(1-\alpha)nF\eta}{RT}\right) - \exp\left(\frac{-\alpha nF\eta}{RT}\right)$$

The final equation of the net current density as function of the limiting currents and the overpotential:

$$i = \frac{i_0\left(\exp\left(\frac{(1-\alpha)nF\eta}{RT}\right) - \exp\left(\frac{-\alpha nF\eta}{RT}\right)\right)}{1 + i_0\left(\frac{1}{i_R^d}\exp\left(\frac{(1-\alpha)nF\eta}{RT}\right) - \frac{1}{i_X^d}\exp\left(\frac{-\alpha nF\eta}{RT}\right)\right)} \quad (172)$$

B.2 Derivation of equation (163)

It can be shown that the SG theory can be extended to a more general scheme by using the net following net current density instead of (147).

$$i_{net} = i_{01}\left(\exp\left(\frac{(1-\alpha_1)n_1F\eta_1}{RT}\right) - \exp\left(\frac{-\alpha_1 n_1 F\eta_1}{RT}\right)\right)$$

$$+ i_{02}\left(\exp\left(\frac{(1-\alpha_2)n_2F\eta_2}{RT}\right) - \exp\left(\frac{-\alpha_2 n_2 F\eta_2}{RT}\right)\right) \quad (162)$$

which rearranges to:

$$i_{net} = i_{01} \exp\left(\frac{-\alpha_1 n_1 F \eta_1}{RT}\right)\left(\exp\left(\frac{n_1 F \eta_1}{RT}\right) - 1\right)$$
$$+ i_{02} \exp\left(\frac{-\alpha_2 n_2 F \eta_2}{RT}\right)\left(\exp\left(\frac{n_2 F \eta_2}{RT}\right) - 1\right)$$

(332)

at $(\pi - \phi) = (\pi - \phi)^{corr}$ where $i_{net}=0$ and by using definition (164) where $\eta_k^{(\pi-\phi)^{corr}} = (\pi - \phi)^{corr} - (\pi - \phi)^{eq,k}$ result in:

$$i_{net} = i_{net,1} + i_{net,2} = 0 \text{ at } (\pi - \phi) = (\pi - \phi)^{corr} \implies$$

$$i_{corr} \equiv i_{01} \exp\left(\frac{-\alpha_1 n_1 F \eta_1^{(\pi-\phi)^{corr}}}{RT}\right)\left(\exp\left(\frac{n_1 F \eta_1^{(\pi-\phi)^{corr}}}{RT}\right) - 1\right)$$

(333)

$$= -i_{02} \exp\left(\frac{-\alpha_2 n_2 F \eta_2^{(\pi-\phi)^{corr}}}{RT}\right)\left(\exp\left(\frac{n_2 F \eta_2^{(\pi-\phi)^{corr}}}{RT}\right) - 1\right)$$

This rearranges to the following to relations:

$$i_{01} \exp\left(\frac{-\alpha_1 n_1 F \eta_1^{(\pi-\phi)^{corr}}}{RT}\right) = i_{corr} \bigg/ \left(\exp\left(\frac{n_1 F \eta_1^{(\pi-\phi)^{corr}}}{RT}\right) - 1\right)$$

$$-i_{02} \exp\left(\frac{-\alpha_2 n_2 F \eta_2^{(\pi-\phi)^{corr}}}{RT}\right) = i_{corr} \bigg/ \left(\exp\left(\frac{n_2 F \eta_2^{(\pi-\phi)^{corr}}}{RT}\right) - 1\right)$$

(334)

Now differentiating (162) with respect to the potential gives:

$$\left(\frac{di_{net}}{d(\pi - \phi)}\right) = i_{01}\left(\frac{(1-\alpha_1)n_1 F}{RT}\exp\left(\frac{(1-\alpha_1)n_1 F \eta_1}{RT}\right) + \frac{\alpha_1 n_1 F}{RT}\exp\left(\frac{-\alpha_1 n_1 F \eta_1}{RT}\right)\right)$$

$$+ i_{02}\left(\frac{(1-\alpha_2)n_2 F}{RT}\exp\left(\frac{(1-\alpha_2)n_2 F \eta_2}{RT}\right) + \frac{\alpha_2 n_2 F}{RT}\exp\left(\frac{-\alpha_2 n_2 F \eta_2}{RT}\right)\right)$$

(335)

After some rearrangement, this gives:

$$\left(\frac{di_{net}}{d(\pi - \phi)}\right) = i_{01}\frac{\alpha_1 n_1 F}{RT}\exp\left(\frac{-\alpha_1 n_1 F \eta_1}{RT}\right)\left(\exp\left(\frac{n_1 F \eta_1}{RT}\right)\left(\frac{1}{\alpha_1} - 1\right) + 1\right)$$

$$+ i_{02}\frac{\alpha_2 n_2 F}{RT}\exp\left(\frac{-\alpha_2 n_2 F \eta_2}{RT}\right)\left(\exp\left(\frac{n_2 F \eta_2}{RT}\right)\left(\frac{1}{\alpha_2} - 1\right) + 1\right)$$

(336)

At the corrosion potential, the above is:

$$\left(\frac{di_{net}}{d(\pi-\phi)}\right)_{(\pi-\phi)=(\pi-\phi)^{corr}} = i_{01}\frac{\alpha_1 n_1 F}{RT}\exp\left(\frac{-\alpha_1 n_1 F\eta_1^{(\pi-\phi)^{corr}}}{RT}\right)\left(\exp\left(\frac{n_1 F\eta_1^{(\pi-\phi)^{corr}}}{RT}\right)\left(\frac{1}{\alpha_1}-1\right)+1\right)$$
$$+i_{02}\frac{\alpha_2 n_2 F}{RT}\exp\left(\frac{-\alpha_2 n_2 F\eta_2^{(\pi-\phi)^{corr}}}{RT}\right)\left(\exp\left(\frac{n_2 F\eta_2^{(\pi-\phi)^{corr}}}{RT}\right)\left(\frac{1}{\alpha_2}-1\right)+1\right)$$

(337)

And substituting (334) into the above gives:

$$\left(\frac{di_{net}}{d(\pi-\phi)}\right)_{(\pi-\phi)=(\pi-\phi)^{corr}} = i_{corr}\frac{\alpha_1 n_1 F}{RT}\left(\frac{1}{\alpha_1}\exp\left(\frac{n_1 F\eta_1^{(\pi-\phi)^{corr}}}{RT}\right)\right)\bigg/\left(\exp\left(\frac{n_1 F\eta_1^{(\pi-\phi)^{corr}}}{RT}\right)-1\right)-1\right)$$
$$-i_{corr}\frac{\alpha_2 n_2 F}{RT}\left(\frac{1}{\alpha_2}\exp\left(\frac{n_2 F\eta_2^{(\pi-\phi)^{corr}}}{RT}\right)\right)\bigg/\left(\exp\left(\frac{n_2 F\eta_2^{(\pi-\phi)^{corr}}}{RT}\right)-1\right)-1\right)$$

which is the same as:

$$\left(\frac{di_{net}}{d(\pi-\phi)}\right)_{(\pi-\phi)=(\pi-\phi)^{corr}} = i_{corr}\left(-\frac{\alpha_1 n_1 F}{RT}+\frac{n_1 F}{RT}\left(1-\exp\left(\frac{-n_1 F\eta_1^{(\pi-\phi)^{corr}}}{RT}\right)\right)^{-1}\right)$$
$$+i_{corr}\left(\frac{\alpha_2 n_2 F}{RT}-\frac{n_2 F}{RT}\left(1-\exp\left(\frac{-n_2 F\eta_2^{(\pi-\phi)^{corr}}}{RT}\right)\right)^{-1}\right)$$

(338)

Which rearrange to:

$$\left(\frac{di_{net}}{d(\pi-\phi)}\right)_{(\pi-\phi)=(\pi-\phi)^{corr}} = i_{corr}\left(\frac{(1-\alpha_1)n_1 F}{RT}+\frac{n_1 F}{RT}\left(\left(1-\exp\left(\frac{-n_1 F\eta_1^{(\pi-\phi)^{corr}}}{RT}\right)\right)^{-1}-1\right)\right)$$
$$+i_{corr}\left(\frac{\alpha_2 n_2 F}{RT}-\frac{n_2 F}{RT}\left(1-\exp\left(\frac{-n_2 F\eta_2^{(\pi-\phi)^{corr}}}{RT}\right)\right)^{-1}\right)$$

(339)

Which rearrange to:

$$\left(\frac{di_{net}}{d(\pi-\phi)}\right)_{(\pi-\phi)=(\pi-\phi)^{corr}} = i_{corr}\left(\frac{(1-\alpha_1)n_1 F}{RT}+\frac{n_1 F}{RT}\left(\exp\left(\frac{n_1 F\eta_1^{(\pi-\phi)^{corr}}}{RT}\right)-1\right)^{-1}\right)$$
$$+i_{corr}\left(\frac{\alpha_2 n_2 F}{RT}+\frac{n_2 F}{RT}\left(\exp\left(\frac{-n_2 F\eta_2^{(\pi-\phi)^{corr}}}{RT}\right)-1\right)^{-1}\right)$$

(340)

by looking at (152) it is essentially the same plus two correction factors, for the redox':

$$\frac{n_1 F}{RT}\left(\exp\left(\frac{n_1 F \eta_1^{(\pi-\phi)^{corr}}}{RT}\right)-1\right)^{-1} \text{ and } \frac{n_2 F}{RT}\left(\exp\left(\frac{-n_2 F \eta_2^{(\pi-\phi)^{corr}}}{RT}\right)-1\right)^{-1} \tag{341}$$

B.3 Derivation of equation (179)

Assume two redox reactions. Reaction 1 includes only cathodic reaction and reaction 2 only anodic. This way and equation is obtained, which is more precise then (152). The net current of each of the redox reactions are given by (176) and (177). Isolating the net currents, gives:

$$i_{net,1} = \frac{-i_{01}\exp\left(\dfrac{-\alpha_1 n_1 F \eta_1}{RT}\right)}{1-\dfrac{i_{01}}{i_1^d}\exp\left(\dfrac{-\alpha_1 n_1 F \eta_1}{RT}\right)} \tag{342}$$

$$i_{net,2} = \frac{i_{02}\exp\left(\dfrac{(1-\alpha_2)n_2 F \eta_2}{RT}\right)}{1+\dfrac{i_{02}}{i_2^d}\exp\left(\dfrac{(1-\alpha_2)n_2 F \eta_2}{RT}\right)} \tag{343}$$

at $(\pi-\phi)=(\pi-\phi)^{corr}$ the net current is zero and defined, $i_{net}=0$. Therefore i_{corr} becomes $i_{corr}=-i_{net,1}=i_{net,2}$ because only one cathodic and only one anodic reaction occur. From (342) and (343) this gives:

$$i_{net} = i_{net,1} + i_{net,2} = 0 \Rightarrow$$

$$i_{corr} = \frac{i_{01}\exp\left(\dfrac{-\alpha_1 n_1 F\left((\pi-\phi)^{corr}-(\pi-\phi)^{eq1}\right)}{RT}\right)}{1-\dfrac{i_{01}}{i_1^d}\exp\left(\dfrac{\alpha_1 n_1 F\left((\pi-\phi)^{corr}-(\pi-\phi)^{eq1}\right)}{RT}\right)}$$

$$= \frac{i_{02}\exp\left(\dfrac{(1-\alpha_2)n_2 F\left((\pi-\phi)^{corr}-(\pi-\phi)^{eq2}\right)}{RT}\right)}{1+\dfrac{i_{02}}{i_2^d}\exp\left(\dfrac{(1-\alpha_2)n_2 F\left((\pi-\phi)^{corr}-(\pi-\phi)^{eq2}\right)}{RT}\right)} \tag{344}$$

By using (160) and differentiating the net current, (178), gives:

$$\left(\frac{di_{net}}{d(\pi-\phi)}\right) = \frac{i_{01}\dfrac{\alpha_1 n_1 F}{RT}\exp\left(\dfrac{-\alpha_1 n_1 F \eta_1}{RT}\right) - \dfrac{i_{01}}{i_1^d}\dfrac{\alpha_1 n_1 F}{RT}\exp\left(\dfrac{-\alpha_1 n_1 F \eta_1}{RT}\right)i_{net,1}}{1-\dfrac{i_{01}}{i_1^d}\exp\left(\dfrac{-\alpha_1 n_1 F \eta_1}{RT}\right)}$$

$$+\frac{i_{02}\dfrac{(1-\alpha_2)n_2 F}{RT}\exp\left(\dfrac{(1-\alpha_2)n_2 F \eta_2}{RT}\right) - \dfrac{i_{02}}{i_2^d}\dfrac{(1-\alpha_2)n_2 F}{RT}\exp\left(\dfrac{(1-\alpha_2)n_2 F \eta_2}{RT}\right)i_{net,2}}{1+\dfrac{i_{02}}{i_2^d}\exp\left(\dfrac{(1-\alpha_2)n_2 F \eta_2}{RT}\right)} \tag{345}$$

$i_{net,k}$ is given by (342) and (343) and they can easily be substituted into the above equation. At $(\pi-\phi)=(\pi-\phi)^{corr}$ the above gives, where $\eta_k^{(\pi-\phi)^{corr}} =(\pi-\phi)^{corr}-(\pi-\phi)^{eq,k}$:

$$\left(\frac{di_{net}}{d(\pi-\phi)}\right)_{(\pi-\phi)=(\pi-\phi)^{corr}} =$$

$$\frac{i_{01}\dfrac{\alpha_1 n_1 F}{RT}\exp\left(\dfrac{-\alpha_1 n_1 F \eta_1^{(\pi-\phi)^{corr}}}{RT}\right) - \dfrac{i_{01}}{i_1^d}\dfrac{\alpha_1 n_1 F}{RT}\exp\left(\dfrac{-\alpha_1 n_1 F \eta_1^{(\pi-\phi)^{corr}}}{RT}\right)i_{net,1}\left((\pi-\phi)^{corr}\right)}{1-\dfrac{i_{01}}{i_1^d}\exp\left(\dfrac{-\alpha_1 n_1 F \eta_1^{(\pi-\phi)^{corr}}}{RT}\right)}$$

$$+\frac{i_{02}\dfrac{(1-\alpha_2)n_2 F}{RT}\exp\left(\dfrac{(1-\alpha_2)n_2 F \eta_2^{(\pi-\phi)^{corr}}}{RT}\right)}{1+\dfrac{i_{02}}{i_2^d}\exp\left(\dfrac{(1-\alpha_2)n_2 F \eta_2^{(\pi-\phi)^{corr}}}{RT}\right)}$$

$$-\frac{\dfrac{i_{02}}{i_2^d}\dfrac{(1-\alpha_2)n_2 F}{RT}\exp\left(\dfrac{(1-\alpha_2)n_2 F \eta_2^{(\pi-\phi)^{corr}}}{RT}\right)i_{net,2}\left((\pi-\phi)^{corr}\right)}{1+\dfrac{i_{02}}{i_2^d}\exp\left(\dfrac{(1-\alpha_2)n_2 F \eta_2^{(\pi-\phi)^{corr}}}{RT}\right)}$$

$i_{net,k}\left((\pi-\phi)^{corr}\right)$ indicates that (342) and (343) has to be evaluated at $(\pi-\phi)=(\pi-\phi)^{corr}$. Essentially this can easily be done by the use of (344). One can see that $i_{net,1}\left((\pi-\phi)^{corr}\right)=i_{corr}$ and $i_{net,1}\left((\pi-\phi)^{corr}\right)=-i_{corr}$. By substituting (344) into the above, a very simple equation appears:

$$\left(\frac{di_{net}}{d\left(\pi-\phi\right)}\right)_{(\pi-\phi)=(\pi-\phi)^{corr}} = i_{corr}\left(\frac{\alpha_1 n_1 F}{RT}\left(1-\frac{i_{corr}}{i_1^d}\right)+\frac{(1-\alpha_2)n_2 F}{RT}\left(1-\frac{i_{corr}}{i_2^d}\right)\right) \quad (179)$$

B.4 Derivation of equation (180)

Assume the net current density is given by (141) and the *k*'th net current density is given by (172). The derivative of the net current density with respect to potential is:

$$\left(\frac{di_{net,k}}{d\left(\pi-\phi\right)}\right)=\frac{\dfrac{(1-\alpha_k)n_k F}{RT}\exp\left(\dfrac{(1-\alpha_k)n_k F\eta_k}{RT}\right)+\dfrac{\alpha_k n_k F}{RT}\exp\left(\dfrac{-\alpha_k n_k F\eta_k}{RT}\right)}{1/i_{0k}+\dfrac{1}{i_{Rk}^d}\exp\left(\dfrac{(1-\alpha_k)n_k F\eta_k}{RT}\right)-\dfrac{1}{i_{Xk}^d}\exp\left(\dfrac{-\alpha_k n_k F\eta_k}{RT}\right)}$$
$$-\frac{\dfrac{(1-\alpha_k)n_k F}{RT i_{Rk}^d}\exp\left(\dfrac{(1-\alpha_k)n_k F\eta_k}{RT}\right)+\dfrac{\alpha_k n_k F}{RT i_{Xk}^d}\exp\left(\dfrac{-\alpha_k n_k F\eta_k}{RT}\right)}{1/i_{0k}+\dfrac{1}{i_{Rk}^d}\exp\left(\dfrac{(1-\alpha_k)n_k F\eta_k}{RT}\right)-\dfrac{1}{i_{Xk}^d}\exp\left(\dfrac{-\alpha_k n_k F\eta_k}{RT}\right)}\cdot i_{net,k}$$

Which rearrange to:

$$\frac{di_{net,k}}{d\left(\pi-\phi\right)}=\frac{\dfrac{n_k F}{RT}\left((1-\alpha_k)\left(1-\dfrac{i_{net,k}}{i_{Rk}^d}\right)\exp\left(\dfrac{(1-\alpha_k)n_k F\eta_k}{RT}\right)-\alpha_k\left(1-\dfrac{i_{net,k}}{i_{Xk}^d}\right)\exp\left(\dfrac{-\alpha_k n_k F\eta_k}{RT}\right)\right)}{\dfrac{1}{i_{0k}}+\dfrac{1}{i_{Rk}^d}\exp\left(\dfrac{(1-\alpha_k)n_k F\eta_k}{RT}\right)-\dfrac{1}{i_{Xk}^d}\exp\left(\dfrac{-\alpha_k n_k F\eta_k}{RT}\right)}$$
$$(180)$$

C. Theory of diffusion

C.1 Porous media

Diffusion in porous media is like free diffusion. The basic difference is the travel distance from a to b as shown in figure 57. The difference in length is due to the porous structure. In free diffusion the travel distance on a macroscopic level is L. The travel distance in a porous media is higher due to the solid matrix through which the molecules have to travel. This distance is designated L_e, $L_e > L$. The ratio L_e/L is called the tortuosity, τ:

$$\tau \equiv \frac{L_e}{L} > 1 \tag{346}$$

The porosity, ϕ, is the fraction of the total volume of a samples which are voids or occupied by liquid. The porosity is defined by:

$$\phi = \frac{V_{voids}}{V_{total}} \tag{347}$$

A porosity of 0 is a solid sample and a porosity of 1 is a sample without a solid structure, like in free diffusion. The tortuosity is a relative length and the porosity is a relative volume.
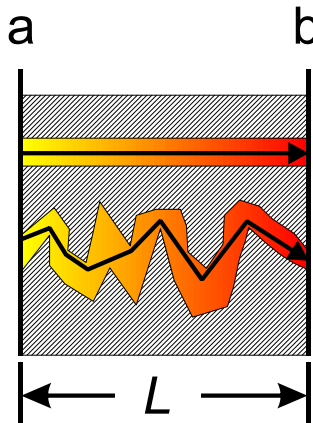
Figure 57: Figure showing the principle of the tortuosity.

The paper by Epstein[1] gives a thorough derivation of the relation between $Đ_{eff}$ and $Đ$:

---

[1] N. Epstein. On tortuosity and the tortuosity factor and diffusion through porous media. Chem Eng. Sci. 44(3), 777, 1989.

$$\text{\DH}_{eff} = \frac{\text{\DH}\phi}{\tau^2} \tag{196}$$

By rearranging this gives:

$$\varepsilon \equiv \frac{\text{\DH}_{eff}}{\text{\DH}} = \frac{\phi}{\tau^2} \tag{348}$$

Where ε is the porosity-tortuosity-factor.

D. Model details of Na₂CO₃-NaHCO₃-MEG-water

D.1 Correlation matrix and confidence intervals

Table 34: Correlation matrix of parameters fitted in parameter set *A*.

| i | | r | q | u_{ij}^0 | | | | | | u_{ij}^t | | | | | |
j		MEG	MEG	MEG H₂O	MEG MEG	MEG CO₂	MEG Na⁺	MEG CO₃²⁻	MEG HCO₃⁻	MEG H₂O	MEG MEG	MEG CO₂	MEG Na⁺	MEG CO₃²⁻	MEG HCO₃⁻
r	MEG	1	0.0493	0.2831	0.3495	0.556	0.3399	0.6746	0.7312	0.0757	0.1204	0.3059	0.1866	0.0501	0.0552
q	MEG	0.0493	1	0.1972	-0.0867	-0.3396	-0.8301	0.1861	0.1487	0.5514	0.4756	-0.0042	-0.8017	0.522	0.5713
u_{ij}^0 MEG	H₂O	0.2831	0.1972	1	0.9538	0.7896	0.0775	0.5038	0.5564	0.3722	0.2302	0.0354	-0.4058	0.2375	0.2019
MEG	MEG	0.3495	-0.0867	0.9538	1	0.9253	0.341	0.5055	0.5716	0.416	0.3014	0.1261	-0.3181	0.2735	0.2445
MEG	CO₂	0.556	-0.3396	0.7896	0.9253	1	0.6081	0.5461	0.6268	-0.3162	-0.271	-0.1406	0.0534	0.0974	0.0658
MEG	Na⁺	0.3399	-0.8301	0.0775	0.341	0.6081	1	-0.0991	0.0112	-0.0562	0.1882	0.432	0.6929	0.0786	0.0863
MEG	CO₃²⁻	0.6746	0.1861	0.5038	0.5055	0.5461	-0.0991	1	0.9496	0.0567	-0.0853	-0.2045	-0.2391	-0.186	-0.1102
MEG	HCO₃⁻	0.7312	0.1487	0.5564	0.5716	0.6268	0.0112	0.9496	1	0.3459	0.1909	0.0004	-0.2909	0.0162	-0.0302
u_{ij}^t MEG	H₂O	0.0757	0.5514	0.3722	0.416	-0.3162	-0.0562	0.0567	0.3459	1	0.9929	0.5199	-0.3567	0.3605	0.6146
MEG	MEG	0.1204	0.4756	0.2302	0.3014	-0.271	0.1882	-0.0853	0.1909	0.9929	1	0.5354	-0.2821	0.3232	0.5936
MEG	CO₂	0.3059	-0.0042	0.0354	0.1261	-0.1406	0.432	-0.2045	0.0004	0.5199	0.5354	1	0.1176	0.1152	0.1361
MEG	Na⁺	0.1866	-0.8017	-0.4058	-0.3181	0.0534	0.6929	-0.2391	-0.2909	-0.3567	-0.2821	0.1176	1	-0.8303	-0.7423
MEG	CO₃²⁻	0.0501	0.522	0.2375	0.2735	0.0974	0.0786	-0.186	0.0162	0.3605	0.3232	0.1152	-0.8303	1	0.8332
MEG	HCO₃⁻	0.0552	0.5713	0.2019	0.2445	0.0658	0.0863	-0.1102	-0.0302	0.6146	0.5936	0.1361	-0.7423	0.8332	1

Table 35: Confidence intervals of parameters fitted in parameter set *A*.

| i | | r | q | u_{ij}^0 | | | | | | u_{ij}^t | | | | | |
j		MEG	MEG	MEG H₂O	MEG MEG	MEG CO₂	MEG Na⁺	MEG CO₃²⁻	MEG HCO₃⁻	MEG H₂O	MEG MEG	MEG CO₂	MEG Na⁺	MEG CO₃²⁻	MEG HCO₃⁻
Par. value		5.4996	7.0797	249.738	339.966	174.558	292.992	671.891	676.577	0.71268	0.56247	5.0355	3.9323	2.1482	-0.50597
conf. %		7.66	7.95	10.65	12.5	19.59	46.08	5.67	3.58	37.6	74.32	5.18	61.8	24.67	-69.17

Table 36: Correlation matrix of parameters fitted in parameter set B.

i	j	r MEG	q MEG	u_{ij}^0 MEG H_2O	u_{ij}^0 MEG MEG	u_{ij}^0 MEG CO_2	u_{ij}^0 MEG Na^+	u_{ij}^0 MEG CO_3^{2-}	u_{ij}^0 MEG HCO_3^-	u_{ij}^t MEG H_2O	u_{ij}^t MEG MEG	u_{ij}^t MEG CO_2	u_{ij}^t MEG Na^+	u_{ij}^t MEG CO_3^{2-}	u_{ij}^t MEG HCO_3^-
r	MEG	1	0.66	0.0953	-0.0108	0.0778	-0.3029	0.2474	0.3309	0.3753	0.3411	0.3356	-0.0964	0.5837	0.3796
q	MEG		1	0.1869	0.0361	-0.1339	-0.6485	-0.2383	-0.1338	0.534	0.4922	0.1112	-0.0639	0.4986	0.4338
u_{ij}^0	MEG H_2O	0.0953	0.1869	1	0.986	0.9127	-0.0782	0.4548	0.4692	0.2784	0.2182	0.1108	-0.3333	-0.0036	0.0299
	MEG MEG	-0.0108	0.0361	0.986	1	0.9475	0.0181	0.4958	0.4933	0.36	0.3099	0.2036	-0.3041	0.0512	0.0796
	MEG CO_2	0.0778	-0.1339	0.9127	0.9475	1	0.1716	0.6623	0.648	-0.5143	-0.5261	-0.4505	-0.042	-0.1109	-0.1082
	MEG Na^+	-0.3029	-0.6485	-0.0782	0.0181	0.1716	1	-0.1722	-0.2182	0.1376	0.1501	0.1355	-0.5934	0.5878	0.5559
	MEG CO_3^{2-}	0.2474	-0.2383	0.4548	0.4958	0.6623	-0.1722	1	0.9545	0.0078	-0.0631	-0.0612	0.078	-0.2974	-0.2164
	MEG HCO_3^-	0.3309	-0.1338	0.4692	0.4933	0.648	-0.2182	0.9545	1	0.2527	0.2	0.1443	0.1273	-0.2635	-0.3119
u_{ij}^t	MEG H_2O	0.3753	0.534	0.2784	0.36	-0.5143	0.1376	0.0078	0.2527	1	0.9932	0.5509	0.0595	0.4525	0.5654
	MEG MEG	0.3411	0.4922	0.2182	0.3099	-0.5261	0.1501	-0.0631	0.2	0.9932	1	0.4956	0.0757	0.4244	0.5647
	MEG CO_2	0.3356	0.1112	0.1108	0.2036	-0.4505	0.1355	-0.0612	0.1443	0.5509	0.4956	1	-0.0538	0.375	0.2465
	MEG Na^+	-0.0964	-0.0639	-0.3333	-0.3041	-0.042	-0.5934	0.078	0.1273	0.0595	0.0757	-0.0538	1	-0.7296	-0.6377
	MEG CO_3^{2-}	0.5837	0.4986	-0.0036	0.0512	-0.1109	0.5878	-0.2974	-0.2635	0.4525	0.4244	0.375	-0.7296	1	0.8308
	MEG HCO_3^-	0.3796	0.4338	0.0299	0.0796	-0.1082	0.5559	-0.2164	-0.3119	0.5654	0.5647	0.2465	-0.6377	0.8308	1

Table 37: Confidence intervals of parameters fitted in parameter set B.

i	j	r MEG	q MEG	u_{ij}^0 MEG H_2O	u_{ij}^0 MEG MEG	u_{ij}^0 MEG CO_2	u_{ij}^0 MEG Na^+	u_{ij}^0 MEG CO_3^{2-}	u_{ij}^0 MEG HCO_3^-	u_{ij}^t MEG H_2O	u_{ij}^t MEG MEG	u_{ij}^t MEG CO_2	u_{ij}^t MEG Na^+	u_{ij}^t MEG CO_3^{2-}	u_{ij}^t MEG HCO_3^-
Par. value		4.006	5.461	241.245	350.404	173.276	496.39	566.661	616.879	0.18095	-0.21916	4.4442	-3.5685	4.2392	0.65204
conf. %		5.77	6.76	11.03	11.62	15.7	17.47	5.68	3.71	133.74	-176.58	6.14	-28.58	10.9	49.23

D.2   The extended UNIQUAC model

The gibbs excess, G^E, is defined by difference between the total gibbs energy in the standard state, $G^{t\Theta s,id}$, and the total Gibbs energy of the system, G^t:

$$G^{t\Theta s,E} \equiv G^t - G^{t\Theta s,id} \tag{349}$$

$G^{t\Theta s,E}$ is therefore a function of the chosen standard state and concentration scale, Θs. It can be shown that

$$RT \ln \gamma_i^{\Theta s} = \left(\frac{\partial \left(G^{t\Theta s,E} \right)}{\partial n_i} \right)_{P,T,n_j} \tag{350}$$

the log. of the activity coefficient is a partial derivative of the total Gibbs excess energy of compound i with respect to constant T,P, and the j'th compound.
The extended UNIQUAC model describes the Gibbs excess property by the following contributions to a Gibbs-excess energy:

$$G^{t\circ x,E} = G^{\circ x,C} + G^{\circ x,R} + G^{\circ x,DH} \tag{351}$$

$G^{\circ x,C}$, $G^{\circ x,R}$, and $G^{\circ x,DH}$ are the Gibbs combinatorial, residual and Debye-Hückel contributions respectively. Which are given by:

$$\frac{G^{\circ x,C}}{RT} = \sum_i x_i \ln \left(\frac{\phi_i}{x_i} \right) - \frac{z}{2} \sum_i q_i x_i \ln \left(\frac{\phi_i}{\theta_i} \right) \tag{352}$$

$$\frac{G^{\circ x,R}}{RT} = -\sum_i q_i x_i \ln \left(\sum_k \theta_k \psi_k \right) \tag{353}$$

$$\frac{G^{\circ x,DH}}{RT} = -x_w M_w \frac{4A}{b^3} \left(\ln \left(1 + b\sqrt{I} \right) - b\sqrt{I} + \frac{b^2 I}{2} \right) \tag{354}$$

The variables are explained in the text below. The rational symmetrical activity coefficient of water, $\gamma_w^{\circ x}$, denoted by subscript w is calculated using (350):

$$\ln \left(\gamma_w^{\circ x} \right) = \ln \gamma_w^{\circ x,C} + \ln \gamma_w^{\circ x,R} + \ln \gamma_w^{\circ x,DH} \tag{355}$$

$\gamma_w^{\circ x,C}$, $\gamma_w^{\circ x,R}$ and $\gamma_w^{\circ x,DH}$ are the combinatorial, residual and Debey-Hückel rational symmetrical activity coefficients of water respectively. The rational unsymmetrical activity coefficient of the ions, γ_i^{*x}, is:

$$\begin{aligned} \ln \gamma_i^{*x} &= \ln \gamma_i^{*x,C} + \ln \gamma_i^{*x,R} + \ln \gamma_i^{*x,DH} \\ &= \ln \gamma_i^{\circ x,C} - \ln \gamma_i^{\infty x,C} + \ln \gamma_i^{\circ x,R} - \ln \gamma_i^{\infty x,R} + \ln \gamma_i^{*x,DH} \end{aligned} \tag{356}$$

Which is calculated from the rational symmetric activity coefficient using the rational symmetrical activity coefficients at infinite dilution, $\gamma_w^{\infty x, C}$, $\gamma_w^{\infty x, R}$. $\gamma_i^{*x, DH}$ is the rational unsymmetrical Debye-Hückel activity coefficient of ion i. The rational symmetrical combinatorial activity coefficient is expressed from (352) using (350):

$$\ln \gamma_i^{\circ x, C} = \ln\left(\frac{\phi_i}{x_i}\right) + 1 - \frac{\phi_i}{x_i} + \frac{z}{2} q_i \left(\ln\left(\frac{\phi_i}{\theta_i}\right) + 1 - \frac{\phi_i}{\theta_i} \right)$$

$$= \ln\left(\frac{r_i}{\sum_k^N (x_k r_k)}\right) + 1 - \frac{r_i}{\sum_k^N (x_k r_k)} + \frac{z}{2} q_i \left(\ln\left(\frac{r_i \sum_k^N (x_k q_k)}{q_i \sum_k^N (x_k r_k)}\right) + 1 - \frac{r_i \sum_k^N (x_k q_k)}{q_i \sum_k^N (x_k r_k)} \right) \quad (357)$$

x_i is the mole fraction of component i, z is the combinatorial number, $z=10$.

ϕ_i and θ_i are defined as:

$$\phi_i = \frac{x_i r_i}{\sum_k^N x_k q_k} \quad (358)$$

$$\theta_i = \frac{x_i q_i}{\sum_k^N x_k q_k} \quad (359)$$

where r_i is the volume parameter and q_i is the surface parameter of component i with a total of N liquid components. The rational symmetrical residual activity coefficient is expressed from (353) using (350):

$$\ln \gamma_i^{\circ x, R} = q_i \left(1 - \ln\left(\sum_k^N \theta_k \psi_{ki}\right) - \sum_k^N \frac{\theta_k \psi_{ik}}{\sum_l^N \theta_l \psi_{lk}} \right) \quad (360)$$

where the energy interaction parameters, u_{kl}, are used in the ψ_i as:

$$\psi_{kl} = \exp\left(-\frac{u_{kl} - u_{ll}}{T}\right) = \exp\left(-\frac{u_{kl}}{T}\right) \exp\left(\frac{u_{ll}}{T}\right) = \frac{\tau_{kl}}{\tau_{ll}} \quad (361)$$

$$\tau_{kl} = \exp\left(-\frac{u_{kl}}{T}\right) \quad (362)$$

T is the temperature in Kelvin. There are two interaction parameters, u_{kl}^0 and u_{kl}^t, for every component pair since u_{kl} is expressed by the linear temperature relationship as:

$$u_{kl} = u_{kl}^0 + u_{kl}^t \left(T - 298.15K \right) \tag{363}$$

The binary interaction between component *A* and *B* are assumed to be the same as the interaction between *B* and *A* therefore:

$$u_{kl}^0 = u_{lk}^0 \tag{364}$$

$$u_{kl}^t = u_{lk}^t \tag{365}$$

The rational symmetrical combinatorial and residual activity coefficient are found by setting $x_w = 1$, and letting composition of others species be zero.

$$\ln \gamma_i^{\infty x, C} = \ln \frac{r_i}{r_w} + 1 - \frac{r_i}{r_w} + \frac{z}{2} q_i \left(\ln \left(\frac{r_i q_w}{r_w q_i} \right) + 1 - \frac{r_i q_w}{r_w q_i} \right) \tag{366}$$

$$\ln \gamma_i^{\infty x, R} = q_i \left(1 - \ln \psi_{wi} - \psi_{iw} \right) \tag{367}$$

the rational symmetrical Debye-Hückel activity coefficient of water is:

$$\ln \gamma_w^{\circ x, DH} = M_w \frac{2A}{b^3} \left(1 + b\sqrt{I} - \frac{1}{1+b\sqrt{I}} - 2\ln\left(1+b\sqrt{I}\right) \right) \tag{368}$$

and the rational unsymmetrical Debye-Hückel activity coefficient for ions are:

$$\ln \gamma_i^{*x, DH} = -z_i^2 \frac{A\sqrt{I}}{1+b\sqrt{I}} \tag{369}$$

A is assumed temperature dependent by:

$$A = \left(1.131 + 1.335 \cdot 10^{-3} \left(T - 273.15 \right) + 1.164 \cdot 10^{-5} \left(T - 273.15 \right) \right) \sqrt{kg/mol} \tag{370}$$

A is valid in the temperature range: 273.15K<*T*<383.15K and typically also used down to 230K. *b* is $b = 1,5\sqrt{kg/mol}$. M_w is the molecular weight of water in kg/mol and z_i is the charge of ion *i* including sign. *I* is the molal ionic strength of the compounds in *mol/kg H₂O*:

$$I = \frac{1}{2} \sum_1^N b_i z_i^2 = \frac{1}{2} \sum_1^N x_i z_i^2 / \left(x_w M_w \right) \tag{371}$$

b_i is the molal concentration in mol compound/kg water of component *i*.

D.3 The extended UNIQUAC parameters

The core parameters of the UNIQUAC model are r_i, q_i, u_{kl}^0 and u_{kl}^t. r_i and q_i of non-ionic species are typically calculated from their geometry as given by the theory of Abrams and Prausnitz[2] and Bondi[3]. The r_i and q_i of water were originally fitted[4] to experimental VLE data of water and should be regarded as constants. In the extended UNIQUAC model other r_i and q_i are fitted as parameters in the model. The r_i, q_i and interaction parameters of the solids are not known, since they are not present in the liquid phase.

It is not possible to measure the thermodynamic properties of an ion independently of other ions, because electro neutrality has to be fulfilled. By convention the ions are measured relative to the hydrogen ion. The interaction parameters are defined by (363) to (365). u_{kl}^0 for H^+ and ion are defined as 10^9 and u_{kl}^t for H^+ and ions are defined as 0. H_2O-H^+ interaction is 10^4. u_{kl}^0 and u_{kl}^t of H_2O-H_2O are set to zero. The equivalent parameter for other solvents is not set to zero but fitted.

The Gibbs energy of H^+ of formation, enthalpy of formation and heat capacity is set to 0 in the molal unsymmetrical standard state at all *T,P* as defined by NIST:

$$\mu_{H^+}^{*m}(T,P) \equiv 0 \tag{372}$$

By assuming that the contribution of H^+ to the excess enthalpy is zero, then the surface parameter becomes:

$$q_{H^+} \approx 0 \tag{373}$$

This result in $\ln\gamma_{H^+}^{\infty x,R} = 0$ by insertion of (373) in (367). Assuming that the rational symmetrical activity coefficient of H^+ at infinite dilution is 1, then $\ln\gamma_{H^+}^{\infty x} = 0$. These assumptions results in $\ln\gamma_{H^+}^{\infty x,C} = 0$ from (356) since $\ln\gamma_i^{\circ x,C} + \ln\gamma_i^{\circ x,R} + \ln\gamma_i^{*x,DH} = 0$ at infinite dilution. r_{H^+} is then calculated from (366) by:

$$\ln\gamma_i^{\infty x,C} = \ln\frac{r_{H^+}}{r_w} + 1 - \frac{r_{H^+}}{r_w} = 0 \Rightarrow$$
$$r_{H^+} = 0.13779 \tag{374}$$

Therefore r_{H^+} and q_{H^+} are known by convention. For numerical reasons $r_{H^+} = 10^{-14}$. The reason why the above assumptions are made, is to *anchor* the ion parameters to the H^+ ion or else an infinite number of interaction parameters could be found. The

---

[2] Abrams, D. S; Prausnitz J. M. Statistical Thermodynamics of liquid mixtures: a new expression for the Gibbs energy of partly of completely miscible system; AIChE J. 21(1), 116, 1975.
[3] Bondi, A. Physical Properties of Molecular Crystals, Liquids and Glasses. Wiley, New York, 1968.
[4] Prausnitz, J. M; Anderson, T. F.; Grens, E. A.; Eckert, C. A.; Hsieh, R.; O'Connel, J. P. Computer calculations for multicomponent vapour-liquid and liquid-liquid equilibria. Prentice-Hall, Inc., New Jersey, p. 42, 1980.

above "*anchor-scheme*" is used in the extended UNIQUAC model. Other schemes may be used, as presented by Thomsen[5].

Anion-anion interaction is determined from the equivalent acid. For example Cl^--Cl^- interaction is fitted to the properties of *HCl*. The cation-cation interaction is set to zero, which is equivalent to fitting the interaction parameters relative to the anions. For example in the *NaCl-H$_2$O* system the Na^+-Na^+ interaction is zero and the Na^+-Cl^- interaction is relative to the Cl^--Cl^- interaction.

The total number of interaction parameters are $2N^2$ for the *N* liquid component system.

From the rules given above the number of fitted interaction parameters, N_u, are :

$$N_u = \underset{\#tables}{2} \left(\underset{table \div diagonal}{\tfrac{1}{2}\left(N^2 - N\right)} - \underset{H^+}{\left(N-1\right)} + \underset{neutral \div water}{\left(N_{netutral} - 1\right)} + N_{anions} \right) \qquad (375)$$

N is the number of all liquid species in the system, water, solvent, and ions. $N_{neutral}$ is the number of neutral species, including water. N_{anions} is the number of anions. N_u is calculated from (375). The first term is obtained from N^2 interaction parameters minus the diagonal, N^2-N, since the diagonal is described by the remaining terms. The factor ½ is observed, since $u_{ij}=u_{ji}$. The second term, *N-1,* are the number of interaction parameters predefined in relation to H^+. The -1 is observed since the diagonal has already been subtracted. The third term, $N_{neutral}$-1, is the number of parameters for neutral species, except water which is predefined. The fourth term, N_{anions}, refers to the number of anion-anion interaction parameters. The above rearranges to:

$$N_u = N^2 - 3N + 2N_{neutral} + 2N_{anions} \qquad (376)$$

Typical values are given in the table 38.

Table 38: Number of interaction parameters for example systems.

N	Example	$N_{neutral}$	N_{anions}	N_u
4	*NaOH-H$_2$O*	1 (*water*)	1 (i.e. OH^-)	8
5	*NaCl-H$_2$O*	1 (*water*)	2 (i.e. OH^-, Cl^-)	16
6	*Na-K-Cl-H$_2$O*	1 (*water*)	2 (i.e. OH^-, Cl^-)	24
8	The system in section 7	3 (*water, MEG, CO$_2$*)	3 (i.e. OH^-, CO_3^{2-}, HCO_3^-)	52

The number of interaction parameters shown in table 38 is of cause the maximum number of parameters which will be fitted. Some of the parameters are arbitrarily defined to a low interaction. For example it is very unlikely that $CO_2(aq)$ and CO_3^{2-} will ever "meet" each other in the same carbon dioxide system. One of the compounds will be extremely low in concentration at a given *pH* due to dissociation to HCO_3^-. This kind of interaction is set arbitrarily to "no interaction", which is u_{kl}^0=2500 and u_{kl}^t=0.

---

[5] Thomsen, K. Aqueous Electrolytes, model parameters and process simulation. Ph.D. Thesis, IVC-SEP, Technical University of Denmark, 1997.

14 Index

The focus of this study is carbon dioxide corrosion. CO_2 corrosion is observed in offshore natural gas transportation pipelines. A general overview of the problem is presented. The chemical system in the pipelines consists of CO_2-Na_2CO_3-$NaHCO_3$-MEG-H_2O. Sodium is injected as aqueous NaOH or $NaHCO_3$ in order to pH-stabilize and avoid corrosion and MEG is injected in order to prevent gas hydrates.

There are a great number of models available in the literature which may predict CO_2 corrosion. These models are not accurate and assume ideality in the main part of the equations. This thesis deals with aspect of improving the models to account for the non-ideality.

Theories on electrolyte thermodynamics, electrolyte mass transport, and electrochemical kinetics are presented. A literature overview of CO_2 corrosion is given and possible extensions of existing models are discussed.

A literature review presented in this work shows that $FeCO_3$ plays a main part in the protection of steel. Especially the solubility of $FeCO_3$ is an important factor. The thermodynamic properties of $FeCO_3$ are discussed and validated. A consistent set of $FeCO_3$ properties are given.

A mixed solvent electrolyte model is regressed for the CO_2-Na_2CO_3-$NaHCO_3$-MEG-H_2O system. Parameters of the extended UNIQUAC model is fitted to literature data of VLE, SLE, heat excess, and validated against heat capacity data. The model is also fitted to experimental data produced in this work for SLE in the Na_2CO_3-$NaHCO_3$-MEG-H_2O system.

The application of the above model is shown. It demonstrates the calculated thermodynamic correction factors. These show how the diffusion process in CO_2 corrosion models deviate from the ideal case.

Department of Chemical
and Biochemical Engineering
DTU Building 229
Søltofts Plads
DK-2800 Kgs. Lyngby
www.kt.dtu.dk